PNNL-13818

Results of Tank-Leak Detection Demonstration Using Geophysical Techniques at the Hanford Mock Tank Site—Fiscal Year 2001

D. B. Barnett
G. W. Gee
M. D. Sweeney

March 2002

Prepared for the U.S. Department of Energy
under Contract DE-AC06-76RL01830

DISCLAIMER

This report was prepared as an account of work sponsored by an agency of the United States Government. Neither the United States Government nor any agency thereof, nor Battelle Memorial Institute, nor any of their employees, makes **any warranty, express or implied, or assumes any legal liability or responsibility for the accuracy, completeness, or usefulness of any information, apparatus, product, or process disclosed, or represents that its use would not infringe privately owned rights**. Reference herein to any specific commercial product, process, or service by trade name, trademark, manufacturer, or otherwise does not necessarily constitute or imply its endorsement, recommendation, or favoring by the United States Government or any agency thereof, or Battelle Memorial Institute. The views and opinions of authors expressed herein do not necessarily state or reflect those of the United States Government or any agency thereof.

PACIFIC NORTHWEST NATIONAL LABORATORY
operated by
BATTELLE
for the
UNITED STATES DEPARTMENT OF ENERGY
under Contract DE-ACO6-76RLO183O

Printed in the United States of America

Available to DOE and DOE contractors from the
Office of Scientific and Technical Information,
P.O. Box 62, Oak Ridge, TN 37831-0062;
ph: (865) 576-8401
fax: (865) 576-5728
email: reports@adonis.osti.gov

Available to the public from the National Technical Information Service,
U.S. Department of Commerce, 5285 Port Royal Rd., Springfield, VA 22161
ph: (800) 553-6847
fax: (703) 605-6900
email: orders@ntis.fedworld.gov
online ordering: http://www.ntis.gov/ordering.htm

This document was printed on recycled paper.
(8/00)

PNNL-13818

Results of Tank-Leak Detection Demonstration Using Geophysical Techniques at the Hanford Mock Tank Site--Fiscal Year 2001

D. B. Barnett
G. W. Gee
M. D. Sweeney

March 2002

Prepared for the U.S. Department of Energy
under Contract DE-AC06-76RL01830

Pacific Northwest National Laboratory
Richland, Washington 99352

Summary

During July and August of 2001, Pacific Northwest National Laboratory (PNNL), hosted researchers from Lawrence Livermore National Laboratory (LLNL) and Lawrence Berkeley National laboratory (LBNL), and a private contractor, HydroGEOPHYSICS, Inc., for deployment of the following five geophysical leak-detection technologies at the Hanford Site Mock Tank in a Tank Leak Detection Demonstration (TLDD):

- Electrical Resistivity Tomography (ERT)
- Cross-Borehole Electromagnetic Induction (CEMI)
- High-Resolution Resistivity-Steel Casing Resistivity Technology (HRR-SCRT)
- Cross-Borehole Radar (XBR)
- Cross-Borehole Seismic Tomography (XBS).

Under the Tri-party Agreement with federal and Washington State regulators, the U.S. Department of Energy will remove wastes from single-shell tanks (SSTs) and other miscellaneous underground tanks for storage in the double-shell tank system. Waste retrieval methods are being considered that use minimal amounts of liquid to dislodge, mobilize, and remove the wastes. As additional assurance of protection of the vadose zone beneath the SSTs, tank wastes and tank conditions will be monitored aggressively during retrieval operations, possibly by methods that are deployed outside the SSTs in the vadose zone.

The FY 2001 TLDD was conducted at the Mock Tank Site in the 200 East Area of the Hanford Site. The 15.24-m (50-ft)-diameter Mock Tank structure was constructed in 1994–1995 for testing the applicability and effectiveness of ERT imaging of simulated fluid leaks beneath a steel-lined tank. A 36-wt% solution of sodium thiosulfate pentahydrate (benign waste surrogate) was released to a central leak point in the Mock Tank at different discharge rates during five leak periods. A total of ~15,100 L (~4,000 gal) of solution was released during the two-week test period. All geophysical methods required the monitoring of background and noise conditions before the solution (leak) detection portions of the test. Two of the five solution releases were "blind" in that none of the operators knew the solution release volumes/flowrates. ERT and HRR-SCRT were the only geophysical methods of the five tested that produced estimates of volumes leaked during these releases. The XBR method was able to detect a leak after ~378 L (~100 gal) were released but did not produce leak-volume estimates.

Qualitative estimates based on the FY 2001 results of the ERT method indicate that the minimum detectable leak for the most robust configuration of the method (16 vertical electrode arrays around the tank with tomographic imaging) is in the range of hundreds of gallons. The three-dimensional (3-D) tomographic method also allowed approximations of leak location, size, and movement.

Results of CEMI deployment were only marginally successful in identifying a developing leak beneath the tank. Changes in soil resistivity between background conditions and post-solution release periods of August 13–15 suggest that leaks were detected, but other conditions (such as unplanned leaks in peripheral wells) distorted the data. The large inductive influence of the metal tank significantly degraded the effectiveness of the method, as did the minimal separation (~21 m [~70 ft] of the transmitter and receiver boreholes. It was concluded that CEMI would not be effective in the steel-cased wells that

surround SSTs at the Hanford Site because of the combination of low frequencies needed to penetrate the casings and the high soil resistivities of the tank settings.

Four electrode configurations (central-leak-point electrode to surface electrodes, steel well casing to surface electrodes, tank to pseudo-casings ["short-circuited" ERT arrays], and surface electrode to pseudo-casings) deployed using the HRR-SCRT methods detected leakage from the Mock Tank. Measurements conducted using the steel casings around the periphery of the tank as transmitters, and an array of 61 surface electrodes as receivers, appeared to have produced the least-sensitive configuration for detecting a leak at tank center. The most sensitive configurations used the center leak point of the tank as the transmitter of current with the surface electrodes or steel casings as receivers. It was estimated that the minimum leak volume detectable using the most robust configuration (SCRT, *mise-a-la-masse* [excitation of mass] configuration) is less than 40 L (10 gal) at the nearby Sisson and Lu site and ~1,890 L (500 gal) for measurements between steel casings and surface electrodes (HRR method) at the Mock Tank. Leak volume estimates using the tank-to-steel casing measurements proved strikingly comparable to the actual volumes released, with departures ranging from -11% to almost 0% (no difference between estimate and actual release). Discontinuities in the leak releases, probably the result of flowmeter malfunction, were also observable using perturbation analysis.

The XBR and XBS techniques were deployed as complementary methods to evaluate different aspects of the subsurface from the same vantage points. A signal of 100 to 300 Hz was used for the seismic source, with water-immersed hydrophone receivers. XBR used 50- and 100-MHz antennas. Both were deployed alternately in nine boreholes opposed diametrically across the tank. Because of the potential of leaking borehole casings interfering with other methods, the XBS method was not adequately tested but still provided structural (stratigraphic, textural) constraints and appeared to respond to the introduction of the leak (qualitatively). The XBR method was apparently capable of detecting relatively small releases ~378 L (100 gal), and extraneous electrical wires in the PVC boreholes did not degrade the signal where it was deployed.

In January 2002, a "down-selection" workshop was conducted to determine which methods or technologies were of sufficient maturity and overall applicability to be considered for more advanced testing in FY 2002 and beyond. Of the six methods evaluated (including one non-geophysical method), the ERT and HRR-SCRT methods were selected for further testing and demonstration. The testing scheduled to begin in FY 2002 will include a performance evaluation to determine the rates of false alarm and probabilities of detection, as well as a possible deployability test inside a tank farm.

Acknowledgments

The authors extend their appreciation and recognition to the principal researchers whose knowledge and experience are at the heart of the testing represented by this report. Their expertise, cooperation, and diligence allowed for the success of the FY 2001 demonstrations.

The principal investigators for each of the geophysical methods for the FY 2001 project are as follows:

ERT Method:	Dr. William Daily and Dr. Abe Ramirez of Lawrence Livermore National Laboratory; Dr. Andrew Binley, Lancaster University, U.K.
XBS and XBR Methods:	Dr. Ernest Major, Dr. Ken Williams, Dr. T. M. Daley, and Dr. J. E. Peterson, Lawrence Berkeley National Laboratory.
CEMI Method:	Dr. Mike Hoversten of Lawrence Berkeley National Laboratory, and Dr. Barry Kirkendall of Lawrence Livermore National Laboratory.
HRR-SCRT Method:	Dr. Jim Fink and Marc T. Levitt of HydroGEOPHYSICS, Inc.

Appreciation is also extended to Mr. Jerry Cammann, CH2M HILL Hanford Group, and Mr. R. M. (Mike) Boger, Numatec Hanford Corporation, for programmatic support.

The entire project is indebted to Dr. Wes Bratton and Dr. Joe Maresca, Vista Engineering Technologies, L.L.C., for their special contributions, guidance and insight in technical specifications for the project, and for providing evaluation guidelines for the outcome of the testing. Much of the discussion in this report is based upon their work.

Sincere thanks are also extended to Mr. Michael Johnson, Pacific Northwest National Laboratory, for providing peer review, and Mr. Joe Brothers, Pacific Northwest National Laboratory, for unflagging program support and logistical support in planning.

Duratek Federal Services, Inc. drilled, surveyed, and installed casings; CH2M HILL, Inc. surveyed the Mock Tank Site with ground-penetrating radar, and Applied Research Associates provided cone penetrometer services. The authors gratefully acknowledge the high-quality work of these contractors in preparing the site for the FY 2001 testing.

Acronyms

3-D	three-dimensional
CEMI	Cross-Borehole Electromagnetic Induction
CHG	CH2M HILL Hanford Group, Inc.
CPT	Cone Penetrometer Technology
ERT	Electrical Resistivity Tomography
FY	fiscal year
HRR-SCRT	High-Resolution Resistivity-Steel Casing Resistivity Technology
I.D.	inside diameter
LBNL	Lawrence Berkeley National Laboratory
LDMM	Leak Detection, Monitoring and Mitigation
LLNL	Lawrence Livermore National Laboratory
LOW	liquid observation well
PNNL	Pacific Northwest National Laboratory
PVC	polyvinyl chloride
RPE	retrieval performance evaluation
SAFE	subsurface air flow and extraction
SDA	SAFE Development Area
SST	single-shell tank
TLDD	Tank Leak Detection Demonstration
ULF	ultra low frequency
VEA	vertical electrode array
VZTFS	Vadose-Zone Transport Field Study
XBR	Cross-Borehole Radar
XBS	Cross-Borehole Seismic Tomography

Contents

Summary iii

Acknowledgments v

Acronyms vii

1.0 Introduction 1

1.1 Purpose of the TLDD 1

1.2 Specific Objectives 2

1.3 Relationship to Other Projects 3

2.0 Test Site Description 5

2.1 Existing Infrastructure and Historical Studies at the Mock Tank Site 5

2.1.1 Construction Details of the Mock Tank Structure 5

2.1.2 Previous Work and Installations at Mock Tank Site 7

2.2 FY 2001 Modifications to the Mock Tank Site 9

2.2.1 Drilling 11

2.2.2 Cone Penetrometer and Preliminary Tests 13

2.3 Stratigraphy and Hydrogeology 14

2.4 Instrumentation and Ancillary Equipment 14

2.4.1 Geophysical Installations 14

2.4.2 Well Placement 15

2.4.3 SAFE Installations 15

2.4.4 Solution and Solution Delivery System 15

3.0 Summary of FY 2001 Tests 19

3.1 Background Measurements 19

3.2 Solution Release Measurements 19

3.3 Summary of Geophysical Methods 20

3.3.1 Electrical Resistance Tomography—Method Description 21

3.3.2 Cross-Borehole Radar—Method Description 24

3.3.3 Cross-Borehole Seismic—Method Description 27

3.3.4 Cross-Borehole Electromagnetic Induction—Method Description 27

3.3.5 High-Resolution Resistivity-Steel Casing Resistivity Technology—Method Description 29

4.0 Conclusions 33

4.1 Results of Down-Selection Workshop 33

4.2 Comparison of the Mock Tank with SSTs 33

5.0 References 37

Appendix A – Tank Leak Experiment at the Mock Tank Site, 200 East Area: Electrical Resistance Tomography—Final Results A.1

Appendix B – Mock Tank High-Resolution Seismic and Radar Measurements B.1

Appendix C – Cross-Well Electromagnetic Surveys at Hanford Mock Tank Site C.1

Appendix D – Electrical HRR-SCRT Measurements Completed for the 2001 LDMM Study, Mock Tank Site D.1

Appendix E – Lithologic and Cone Penetrometer Data from the Mock Tank Site 1996, 2001 ..... E.1

Appendix F – Log of Physical Parameters for Sodium Thiosulfate Solution During the FY 2001 TLDD F.1

Figures

1. Location of the Mock Tank Site and the FY 2001 TLDD Project 4

2. The Mock Tank Site Before Start of FY 2001 Activities 6

3. Details of the Mock Tank Construction in Relation to One of the 1995 ERT Installations 7

4. Layout of the Mock Tank Site and Adjoining SDA, Showing Old Installations and New Infrastructure for FY 2001 Testing 8

5. View Looking East at the Mock Tank During the FY 2001 TLDD Activities 10

6. Interior of the Mobile Geophysics Laboratory Used for Workspace and Housing of Recording Equipment 10

7. Interior Access to the Mock Tank 11

8. Drilling of the Mock Tank Wells for FY 2001 Using Hollow-Stem Auger Methods 12

9. PVC Sealed Well Installed During FY 2001 with Liner Installed to Prevent Water Leakage 13

10. View of the SAFE Infrastructure Around the Mock Tank, and Gas Monitoring and Sampling Lines Entering the SAFE Field Laboratory 16

11. The Digital Flowmeter System Connected Directly to the 15,140 L Sodium Thiosulfate Storage Tank; Existing Manifold System Used Initially to Deliver the Solution to the Central Leak Point in the Tank 17

12. Test Schedule for the FY 2001 TLDD 20

13. Configuration and Operating Principle of the ERT Method at the Mock Tank 22

14. ERT Patch Panel Located Near the Edge of the Mock Tank Used to Control Connections Between Recording Instrumentation and the 16 Electrode Arrays Surrounding the Tank 23
15. Principles of Operation for XBS and XBR Methods 25
16. Antenna Configuration for XBR Measurements at the Mock Tank..... 26
17. Lowering of Hydrophones into a Steel Case-Lined Well at the Mock Tank 26
18. Configuration and Principles of CEMI Operation..... 28
19. Receiving Coil for the CEMI Method Being Lowered into a Well..... 28
20. Schematic Illustration of HRR-SCRT Deployment 31
21. Representation of a 100 Series SST, Showing Ancillary Instrumentation and Construction Features 34

Table

1 Solution Release Details for the FY 2001 TLDD..... 20

1.0 Introduction

During July and August of 2001, CH2M HILL Hanford Group, Inc. (CHG) engaged Pacific Northwest National Laboratory (PNNL) to deploy six "ex-tank" leak-detection technologies at the Hanford Site Mock Tank Site in a Tank Leak Detection Demonstration (TLDD). These technologies consist of five geophysical methods and a subsurface air flow and extraction (SAFE) method. The following describes the background and basic elements of the FY 2001 testing and a summary of results for the geophysical methods. A separate report (Cameron et al. 2002) describes the deployment and results of the SAFE technology at the Mock Tank Site.

The body of this report describes test conditions and the Mock Tank Site, historical information related to the testing, and a summary of results for the geophysical method demonstrations. The full technical reports for each geophysical method are presented in Appendixes A through D. Results of the SAFE technology are summarized below only insofar as they relate to the test-site layout or results of geophysical techniques. Barnett et al. (2001) described the test plan that guided the FY 2001 demonstration of geophysical methods. Vista Engineering Technologies (Vista 2001) provided the test specifications for the FY 2001 TLDD.

1.1 Purpose of the TLDD

In accordance with the M-45 series of milestones under the Hanford Federal Facility Agreement and Consent Order (Tri-Party Agreement; Ecology et al. 1998), CHG will remove wastes from single-shell tanks (SSTs) and other miscellaneous underground tanks for storage in the double-shell tank system. Under the Tri-Party Agreement, CHG is demonstrating several retrieval methods as alternatives to past practice sluicing that use minimal amounts of liquid to dislodge, mobilize, and remove the wastes. As additional assurance of protection of the vadose zone beneath the SSTs, tank wastes and tank conditions will be monitored aggressively during retrieval operations. Hence, significant effort is aimed at detecting, monitoring, and devising mitigation techniques for tank leakage. In addressing this effort, CHG and their subcontractors have been evaluating a variety of potential in-tank and ex-tank (monitoring conducted from outside a tank) technologies in support of the development of a leak detection, monitoring and mitigation (LDMM) system for use during waste-retrieval operations.

The ex-tank technologies are being evaluated in phases, beginning with small field-scale tests during fiscal year (FY) 2001 to demonstrate proof-of-concept under vadose-zone conditions approaching those actually found beneath an SST farm site. Hence, the initial phase described in this report was conducted at the Mock Tank, which was constructed to approximately simulate an SST setting. Additional Mock Tank site demonstrations are planned for FY 2002 for the most promising leak-detection techniques (ERT and HRR-SCRT). This testing will determine the range(s) of sensitivity and reliability of the technology(ies) in support of possible consideration in the retrieval technology demonstration (including LDMM design) for Tri-Party Agreement milestone series M-45.

The TLDD was designed to provide data to determine the lower limits of sensitivity, including both minimum detectable effluent volume and time-to-detection of methods described below. The TLDD also provided an early assessment of the interference with the methods of infrastructural features (e.g., transfer

lines, pipes, electrical noise, etc.) likely to be present in SST environments. The overall performance (see Section 4.0) also allowed for a "downselection" process to select methods for further evaluation.

1.2 Specific Objectives

The five geophysical techniques selected for demonstration included (1) Electrical Resistance Tomography (ERT), (2) Cross-Borehole Electromagnetic Induction (CEMI), (3) High-Resolution Resistivity-Steel Casing Resistivity Technology (HRR-SCRT), (4) Cross-Borehole Radar (XBR), and (5) Cross-Borehole Seismic Tomography (XBS). Although the work constituted an experimental, preliminary phase of method evaluation, specific objectives included:

- Acquiring a better understanding of each leak-detection technology's sensitivity to leaks (on a total volume basis)
- Determining minimum response time for leak detection by each method
- Estimating a rough, order-of-magnitude cost of deployment for installing an operating system around an SST
- Determining an optimum system configuration for best performance (borehole placement, electrode placement)
- Selecting the method(s) that offers most promise for eventual deployment in a tank farm.

While FY 2001 leak quantification efforts focused on *detection*, and secondarily on total volume determination, subsequent work on down-selected geophysical methods will require determination of leak *rates* to fully support retrieval performance evaluation (RPE) criteria. The follow-on work in FY 2002 and beyond will involve quantification of leak volumes. More specific criteria that will be considered in the ultimate selection of methods for further development include:

- *Accuracy*: Is a solution release (leak) detectable by the method; if so, how does the (test) volume released compare with the volume indicated by the method?
- *Precision (reliability)*: Can the method consistently detect a leak with acceptable probabilities of false detection?
- *Engineered Practicality*: What are the logistical and practical constraints to deploying a system derived from the method within an SST farm (e.g., can existing infrastructure and wells be used successfully, or are more invasive procedures needed to install an effective system)?
- *Status of Development*: What level of effort will be required to develop the method into an effective monitoring system?

- *Versatility*: What scenarios of tank leakage will the method be likely to address successfully (e.g., will the engineered system be capable of detecting multiple leak points or recurrent leaks superimposed over previous leaks in the soil or operate with variable levels of noise)?

Although FY 2001 testing provided insight to these objectives and performance criteria, significant refinement of these is planned for the selected methods (ERT and HRR-SCRT) during FY 2002 testing.

1.3 Relationship to Other Projects

Recent and ongoing experimentation with several subsurface vadose-zone plume-detection techniques, including the geophysical methods considered in this plan, is the subject of work at the Vadose-Zone Transport Field Study (VZTFS) site (Sisson and Lu site; Figure 1) as reported by Gee and Ward (2001). The VZTFS site is approximately 1200 m (3937 ft) south of the Mock Tank Site in the 200 East Area (see http://vadose.pnl.gov/tldd.asp).

The prime focus of VZTFS is to evaluate mass balance and migration characteristics of a simulated tank leak in the subsurface for vadose-zone transport modeling purposes. A secondary objective is to evaluate emerging measurement techniques for noninvasive or semi-invasive vadose-zone characterization (Ward and Gee 2000, 2001; Gee and Ward 2001). These techniques include isotopic tracers, neutron probe, advanced tensiometers, core sampling, and the five geophysical techniques (ERT, XBR, XBS, CEMI, and HRR-SCRT). Although mutually supporting, objectives of the work at this site differ from TLDD testing at the Mock Tank Site. The VZTFS project seeks to identify dominant transport mechanisms on a detailed scale in typical Hanford soils under hydrologic constraints that are typical of tank farm situations. In contrast, the TLDD testing is focused primarily on geophysical methods for detecting leaks and estimating waste volumes lost to the subsurface.

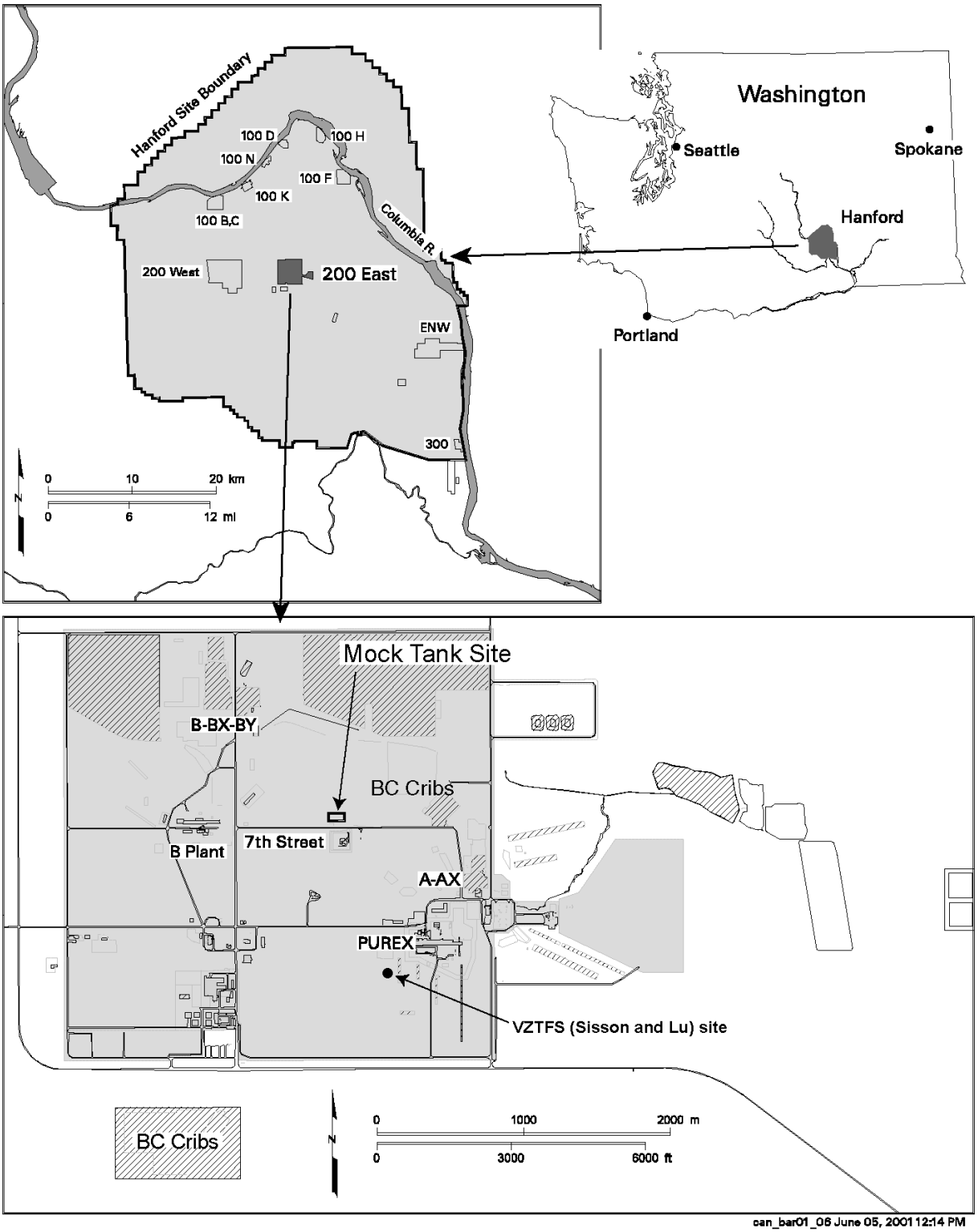

Figure 1. Location of the Mock Tank Site and the FY 2001 TLDD Project

2.0 Test Site Description

The TLDD was conducted at the Mock Tank Site in the 200 East Area of the Hanford Site (Figures 1 and 2). The Mock Tank was constructed in 1994–1995 and previously used for testing the applicability and effectiveness of an array of electrical resistivity sensors in providing tomographic imaging of simulated fluid leaks beneath the tank. Leak-detection studies at the Mock Tank Site were conducted from 1994 through 1996 (Ramirez et al. 1995, 1996; Narbutovski et al. 1996a, 1996b). In 1994 and 1995, vertical electrode arrays (VEAs) installed in 16 boreholes around the Mock Tank were used to evaluate the performance of ERT as a leak detection method using injections of saline solution through the tank leak points. An example of one of these 16 arrays in relation to a profile of Mock Tank construction is shown in Figure 3. A more detailed description of the test site as it was before the 2001 activities can be viewed at http://vadose.pnl.gov/files/contrepts/pnnl-13598.pdf.

2.1 Existing Infrastructure and Historical Studies at the Mock Tank Site

Since the Mock Tank was used for extensive testing from 1994–1996, much of the infrastructure created for those tests has been left in place. Boreholes and ERT installations put in place in 1995 are still serviceable, and some of these were used during the 2001 TLDD. This section describes the existing features of the site that were used during the FY 2001 work and are of continuing importance to future use of the Mock Tank Site.

2.1.1 Construction Details of the Mock Tank Structure

Primary design features of the Mock Tank structure are illustrated schematically in Figure 3. The main function of the Mock Tank was to simulate leaks at various points around an SST. Thus, it was constructed with a distribution manifold of pipes that directed water or solutions to five separate leak-simulation ports. The interior leak points are short sections of steel casing protruding through the floor of the tank, with PVC plumbing leading to the distribution manifold on the outside of the tank (see Section 2.2.4). Two interior leak points, one central and one off-center (Figures 3 and 4), are plumbed from the manifold. Three exterior leak-simulation outlets were also installed to simulate a blanket leak, a point leak, and a closely spaced group of leaks. In addition to the interior leak points, 12 additional soil access ports (differing from the interior leak points only by the absence of plumbing to the manifold) are distributed around the floor of the tank (Figure 4). Only the interior, central leak point was used during FY 2001 testing.

The 0.32-cm (0.125-in.) steel wall of the tank is 15.24 m (50 ft) in diameter and rests on a 15.24-cm (6-in.) thick, 45.72-cm (18-in.) wide concrete footer that is approximately 1.5 m (5 ft) below grade. Some distortions (flat areas) of the sidewalls of the tank occur near the steel wall-footer junction. The tops of the tank walls are held true (kept in round) by an ~10-cm (~4-in.) steel ring welded to the top of the tank walls along the entire tank circumference. A layer of shotcrete and geofabric coats the lower portion of the tank wall and contains the plumbing for the exterior leak points.

Figure 2. Top: The Mock Tank Site Before Start of FY 2001 Activities. Shown are the sixteen 1995 ERT arrays, the previous field laboratory, and two 9,464-L (2500-gal) tanks used in the 1995–96 experiments. Bottom: Oblique aerial view of the Mock Tank from the northwest following FY 2001 testing, showing the mobile geophysics laboratory (bus lower left of tank) and SAFE Development Area (SDA) (upper left of mock tank). A 15,140-L (4,000-gal) tank, which contained the sodium thiosulfate solution for the FY 2001 testing, had already been removed at the time of the photograph (see Section 2.4.4).

Because the ERT method was the first to be considered for leak detection testing at the Mock Tank, many of the tank's features were designed with that technology in mind. Most notably, the 0.32-cm (0.125-in.) steel floor of the tank was tack welded together to provide electrical continuity, and a 10-to-15-cm (4-to-6-in.) gravel layer was spread over the steel bottom to ensure contact with the compacted soil

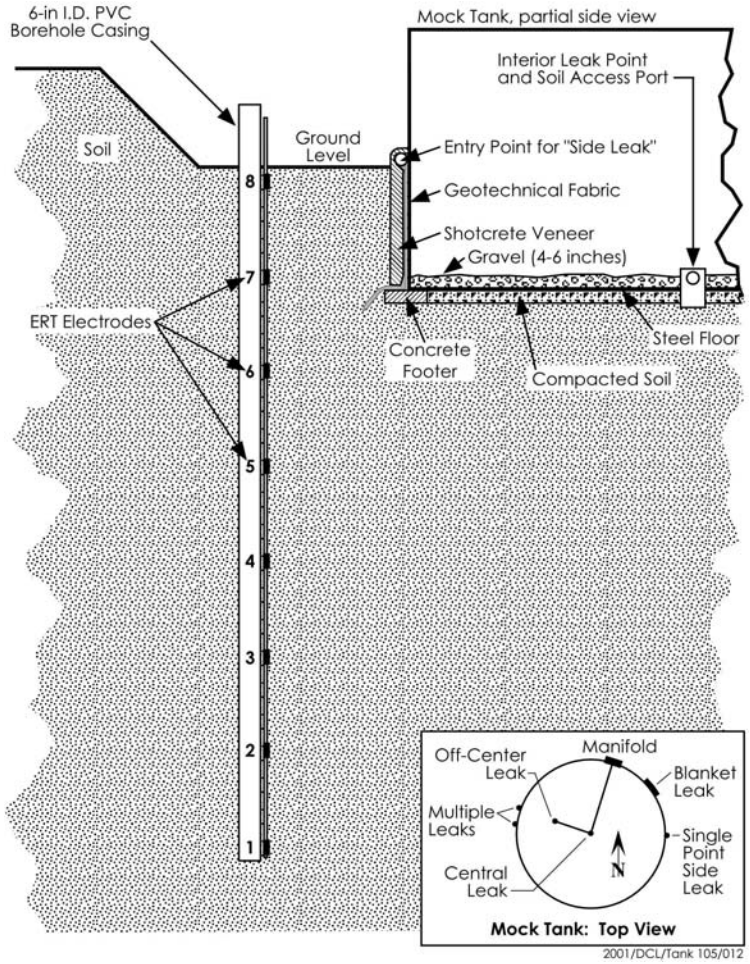

Figure 3. Details of the Mock Tank Construction in Relation to One of the 1995 ERT Installations. The Mock Tank is approximately 15.2 m (50 ft) in diameter; the ERT array extends to ~10.6 m (35 ft) below ground level, with an electrode every 1.52 m (5 ft).

underneath. Also, a leveled, backfilled surface was provided around the periphery of the tank to allow installation of the 16 ERT electrode arrays. The presence of the conductive tank embedded in the relatively resistive soils results in a resistivity contrast of 10 orders of magnitude (Ramirez et al. 1995), resulting in a pronounced shunting of current through the tank. Experimental work with scale models of buried tanks (Daily et al. 1992) indicated that ERT methods would still be able to detect fluid leakage in the presence of these contrasting materials, and, in part, helped guide the construction details of the tank. A simplified description of an actual SST is included in Section 4.2 to provide comparison with the Mock Tank.

2.1.2 Previous Work and Installations at the Mock Tank Site

Leak-detection studies at the Mock Tank site were conducted from 1995 through 1996 (Ramirez et al. 1995, 1996; Narbutovski et al. 1996a, 1996b). In 1995 and 1996, VEAs installed in sixteen boreholes

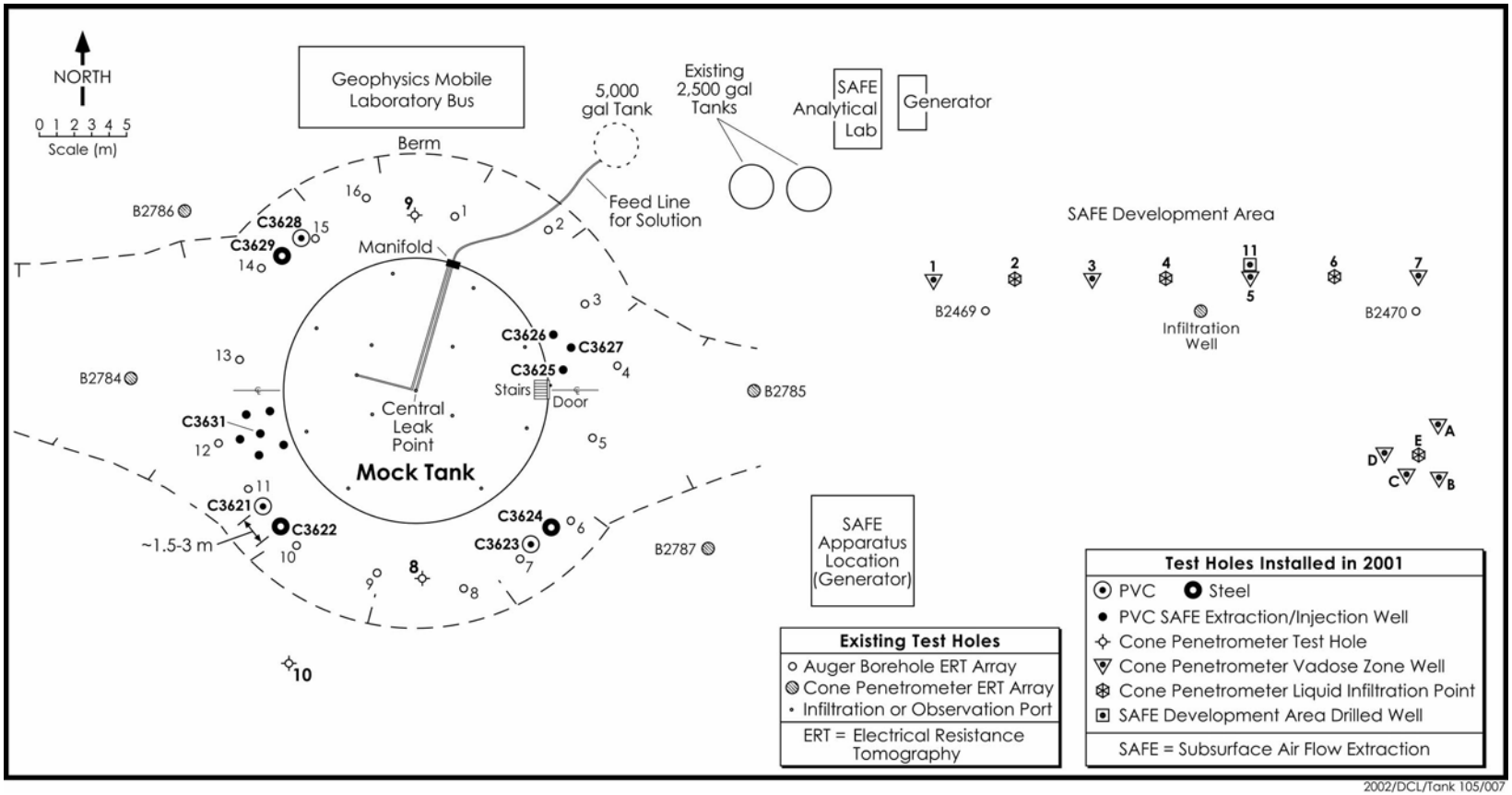

Figure 4. Layout of the Mock Tank Site and Adjoining SDA Showing Old Installations and New Infrastructure for FY 2001 Testing

around the Mock Tank (see Figure 4) were used to evaluate the performance of ERT as a leak detection method using injections of saline solution through the tank leak points. An example of one of these sixteen arrays in relation to the Mock Tank is shown in Figure 3. Both the 1995 and 1996 studies consisted of releases of 0.08 molar saline (NaCl) solutions at different leak points within the Mock Tank.

The ERT (VEA) array installed in 1995 consists of 16 boreholes, each completed with 15.24-cm-(6-in.-) inside-diameter (I.D.) polyvinyl chloride (PVC) casings to a depth of 10.7 m (35 ft). The casings were sealed at the bottom so they are isolated from the soil environment. On the outside of the 15.24-cm (6-in.) casings was strapped a smaller tube, upon which were mounted eight electrodes (see Figure 3). This array was found to be in serviceable condition and was used in the FY 2001 TLDD. In the 1995 study (Ramirez et al. 1995), three release/monitoring events were staged. The first consisted of 3,800 L (1,004 gal) of solution released at a rate of 26 L/hr (9.5 gal/hr) at the side leak location at the northeast portion of the tank (see inset in Figure 3). The second release of 1,900 L (502 gal) was conducted at the center release point at a rate of 3.2 L/hr (0.85 gal/hr). A third release was discharged at the off-center leak location but was aborted because of difficulties with the release system. The leaks were imaged using the 16 auger-hole ERT array shown in Figure 4.

Approximately 25 m (82 ft) east of the Mock Tank are two drilled boreholes with a central infiltration well installed in 1996. These installations (B2469 and B2470 in Figure 4) are within the SDA and consist of a VEA in each well to a depth of approximately 49 m (160 ft). These were completed with a 9.65 cm (3.8 in.) PVC casing and fitted with an array of electrodes at intervals of 3 m (10 ft). This testing was aimed at determining the effectiveness of ERT in mapping vadose-zone plume-migration monitoring apart from tank leak scenarios. Some success was achieved in imaging the downward migration of a saline plume with ERT at this site.

Later in 1996, an additional four VEAs were installed east and west of the tank (wells B2784 through B2787 in Figure 4) outside of the original 16 installations. These were used not only to perform additional ERT evaluation but also as a technology transfer using the cone penetrometer (CPT) as an installation method. The arrays were installed to a depth of 30.5 m (100 ft) and have eight electrodes equally spaced on each array (Narbutovskih et al. 1996b). The blanket leak point on the northeast portion of the tank (see Figure 3) was used in the 1996 study (Narbutovskih et al. 1996a) to receive 11,500 L (3,000 gal) of saline solution over a period of 12 days at rates between 30 and 40 L/hr (8 and 10 gal/hr). For this study, the four CPT-emplaced electrode arrays (wells B-2784 through B2787 in Figure 4) were used for generating two-dimensional tomographic images of the leak.

2.2 FY 2001 Modifications to the Mock Tank Site

Figure 5 is an overview of the Mock Tank Site following the installation of new infrastructure for the FY 2001 TLDD tests. The figure shows the vacuum lines (PVC) for the SAFE system leading around the south side of the Mock Tank to the extraction wells on the west side (foreground) of the tank. The mobile geophysics laboratory, a refitted bus, was located on the north side of the Mock Tank and contained workspace and recording instrumentation for the geophysical methods (Figure 6).

A doorway was cut into the east side of the tank to permit safe access to the interior (Figure 7). This was necessary to allow installation of instrumentation, to monitor fluid levels in access ports, and to seal the tank floor to ensure airtight coverage for SAFE operation. Several batteries of lights were deployed

Figure 5. View Looking East at the Mock Tank During the FY 2001 TLDD Activities. Large PVC pipes are SAFE air-extraction lines. The bus at left is the mobile geophysics laboratory. The large black storage tank contains the sodium thiosulfate solution used to simulate a tank leak (see Section 2.4.4). The trailer and the RV to the right of the storage tank are the SAFE field laboratory.

Figure 6. Interior of the Mobile Geophysics Laboratory Used for Workspace and Housing of Recording Equipment

Figure 7. Interior Access to the Mock Tank. A door was cut in the east side of the tank and stairs installed to the floor of the tank (~0.9 m [~3 ft] below exterior grade). This allowed installation of instruments and monitoring of soil conditions beneath the tank floor. The covering on the floor prevents air leakage during SAFE operations. Three of the 12 soil access ports are shown protruding from the floor covering.

around the tank perimeter to allow safe nighttime operations. The pit area around the Mock Tank was cordoned off, and only investigators were allowed into the working area. Wires leading to control panels and instruments from electrodes around the tank were bundled where possible to limit tripping hazards.

Because of the drilling and CPT pushes planned for the site (see below), ground-penetrating radar surveys were conducted over the entire area of study, around the tank and at the SDA that adjoins the Mock Tank Site to the east. Figure 4 shows the layout of the work areas with the locations of test holes and wells from FY 2001 and previous years.

2.2.1 Drilling

All drilling was done by hollow-stem auger methods. Twelve PVC wells and three steel-cased wells were emplaced to a depth of 12 m (40 ft) (Figure 8). Nine of the wells were emplaced for the SAFE tests around the tank. These were screened at depth to allow air injection/withdrawal. To allow access by the drill rig and CPT truck, the 16 ERT casings installed in 1995 were cut to near-ground level.

The six new holes used for geophysical methods were completed with PVC or carbon steel casing (wells labeled C3621-C3624 and C3628-C3629 in Figure 4). These six "wells" were actually sealed from the environment by capping the bottoms of the casings. The intent was to provide fluid (water) containment to allow deployment of seismic techniques. Some of the casings (well no. C3628 in Figure 4 and all the ERT array casings) did not hold water efficiently, so attempts were made to install flexible plastic

Figure 8. Drilling of the Mock Tank Wells for FY 2001 Using Hollow-Stem Auger Methods. Access to locations around the tank for drilling was difficult due to pre-existing well casings and limited maneuvering space. The preexisting casings were cut to near ground level to improve access.

liners in the wells that leaked (Figure 9). The liners reduced the rate of water loss to the soil but did not completely stop the leakage. The wells were filled with raw water just before the seismic hydrophones were deployed and pumped out immediately after the seismic data were collected to avoid introducing significant water to the test area, which might interfere with the electrical methods.

Figure 9. PVC Sealed Well Installed During FY 2001 with Liner Installed to Prevent Water Leakage. Seismic techniques require a water-filled well to provide sufficient coupling with the geologic formation and allow signal propagation.

2.2.2 Cone Penetrometer and Preliminary Tests

In preparation for geophysical testing and SAFE deployment at the Mock Tank, several CPT and other tests were performed around the tank and in the adjacent SDA. These tests provided baseline information on soil moisture, density (lithology), electrical resistivity, and air permeability as ground-truth information for geophysical and SAFE tests. Specific tests included:

- Tip and sleeve pressure (CPT test)
- Pore pressure (CPT test)
- Air permeability (in CPT-constructed boreholes)
- Electrical resistance at 2.54-cm (1-in.) resolution (CPT test)
- Capacitance soil moisture content (CPT test)
- Neutron moisture logging (in CPT-constructed boreholes).

Graphic results of these tests for specific holes (numbers 1 and 7 in Figure 4) near the Mock Tank and in the SDA are presented in Appendix E. Five CPT holes were emplaced in the southeast portion of the SAFE (Figure 4) to characterize stratigraphy and measure infiltration rates and depths of penetration of the solution used for the FY 2001 testing (sodium thiosulfate).

At the SDA, seven CPT wells (four vadose zone wells and three liquid infiltration points) in a linear array were the site of SAFE development activities; five CPT wells (four vadose-zone wells and one

liquid infiltration point) comprise the Infiltration Gallery at the southeast corner of the SDA. These were used in an infiltration experiment to help predict solution infiltration parameters at the Mock Tank Site. Three additional CPT boreholes were emplaced around the Mock Tank (Numbers 8, 9, 10 in Figure 4) for characterization purposes, along with a drilled borehole in the linear array in the SDA (Number 11 in Figure 4).

Sediment core was collected from CPT hole number 8, just south of the Mock Tank before the beginning of the FY 2001 TLDD, and this core is described in Appendix E. Although no direct measurements of salt concentrations were made from the sediments, CPT logs (Appendix E) do not indicate any prior incursions of salt outside the perimeter of the tank from earlier tests (1995-1996). So far, no data have been obtained to verify distribution of the FY 2001 releases of sodium thiosulfate in sediments underlying the Mock Tank or outside the perimeter of the tank.

2.3 Stratigraphy and Hydrogeology

The details of the stratigraphy and hydrogeology of the 200 East Area have been described by numerous authors over the years of Hanford Site operations, with the most recent and authoritative including Reidel et al. (1992), Lindsey et al. (1992), and Williams et al. (2000). Site-specific lithologic data for the Mock Tank area were collected from drilled boreholes (B2469 and B2470 in Figure 4) and included in the report by Narbutovskih et al. (1996b).

Surficial sediments at the Mock Tank consist of a thin veneer of dune sand up to 1 m (3 ft) thick. Fluvial (catastrophic floods) sand and gravel of the Pleistocene Hanford formation extend from about 1 m (3.3 ft) below ground surface (bgs) to greater than 120 m (400 ft) bgs. Lindsey described some of this section as Pliocene/Miocene Ringold formation sand and gravel, but Williams et al. (2000) interpret this area to be scoured by Pleistocene flood events and thus the entire section to be underlain by the less-consolidated Hanford formation sediments. The sediments, in turn, overlie the basalt flows of the Miocene Columbia River Basalt Group.

The only detailed lithologic records of the subsurface at the Mock Tank Site are those derived from borehole drilling for the ERT investigation by Narbutovskih et al. (1996b). These borings each extended to approximately 49 m (160 ft) bgs, with the nearest (B2469) located approximately 24 m (80 ft) from the eastern edge of the Mock Tank. The lithologic descriptions and interpretations were also supported by neutron and natural gamma logging. Figure E-1, Appendix E, illustrates the lithologies encountered in this borehole, which are considered generally representative of strata beneath the Mock Tank.

2.4 Instrumentation and Ancillary Equipment

2.4.1 Geophysical Installations

Geophysical equipment and sensors were installed at the surface for the HRR-SCRT and ERT methods. Surface electrodes for the HRR-SCRT measurements were installed as radial arrays at intervals around the tank and at extreme distance from the tank to account for baseline conditions. Measurements for the CEMI and XBR methods were made within existing and newly installed PVC casings (wells) around the Mock Tank. XBS data were collected from within water-filled PVC and steel-cased wells.

2.4.2 Well Placement

Sealed wells were emplaced to allow downhole operation of the XBS, XBR, and CEMI methods, and screened wells were installed for SAFE operation. Horizontal configurations of the wells (spacing and angles between wells with respect to the tank center) were important for XBR, XBS, and CEMI methods. New steel-cased wells were installed as close as possible to the new PVC wells to allow us to compare the results of the geophysical methods. Well depths were selected to match the pre-existing ERT array depths of 10.67 m (~35 ft).

2.4.3 SAFE Installations

Application of the SAFE technology at the Mock Tank required the installation of a significant array of piping and tubing to allow air injection/extraction and gas analyses/monitoring. Gas samples were conveyed to analytical equipment housed in the SAFE field laboratory (Figure 10). No sources of interference between the SAFE technology operations and the geophysical methods were identified during the FY 2001 testing. Although the SAFE operations removed an estimated 376 gal of water from sediments beneath the tank during tracer tests (Cameron et al. 2002), this removal was not detected or resolved by the geophysical methods. Because this change in water content (~0.5% by volume) occurred over a large volume of sediment (swept by the SAFE method), the contrasts between this change and the more pronounced dielectric signature introduced by the leaking solution are extreme. The electrical geophysical methods have the potential of detecting a much smaller volume of fluid because of the large change in effective dielectric when high-salt liquids leak from a tank and are discharged into the soil.

2.4.4 Solution and Solution Delivery System

The solution selected for injection in the FY 2001 tests is concentrated (36% by atomic weight) sodium thiosulfate pentahydrate ($Na_2S_2O_3 \cdot 5\ H_2O$). Important properties of the sodium thiosulfate solution are as follows:

Atomic weight percent:	36.0
Solution weight percent:	56.51
Specific gravity:	1.3406
Concentration (g/L):	481.8
Relative Viscosity:	4.350
Conductivity (μmhos/cm):	128

The tabulated data and experience garnered from the Sisson and Lu site (Ward and Gee 2001) suggest that concentrated sodium thiosulfate solution is a good surrogate for tank waste in terms of density and electrical properties. This is substantiated by studies of waste characteristics from process information (e.g., WHC 1992). The viscosity of the solution is approximately three times greater than some estimates of tank-waste viscosity. Gee and Ward (2001) report that the sodium thiosulfate solution infiltrated approximately as rapidly as water, in spite of the higher viscosity. During injection of the fluids (water and 36% by wt. sodium thiosulfate) there was comparable infiltration rates and the spreading was quite similar to water injection. Although most salt wastes are various metals complexed with nitrate ligands, sodium thiosulfate is a reasonable surrogate with virtually no risk to the environment and human health or safety.

Figure 10. View of the SAFE Infrastructure Around the Mock Tank (top left and right), and Gas Monitoring and Sampling Lines Entering the SAFE Field Laboratory (bottom). Samples were analyzed by gas chromatography inside the laboratory. The SAFE experiments were conducted concurrently with the geophysical demonstrations.

Sodium thiosulfate ($Na_2S_2O_3 \cdot 5\ H_2O$), when prepared as a concentrated solution (at 36% atomic weight), has a specific gravity of 1.34. When such a dense solution is applied to unsaturated Hanford sediments, the solution moves at rates different than those of water. Preliminary bench-scale tests, including permeameter and capillary-rise experiments, were conducted to evaluate the movement of saturated sodium thiosulfate in Hanford sediments (Ward and Gee 2001). Use of the solution in March 2001 at the Sisson and Lu site indicated that a 40% (by weight) thiosulfate solution would crystallize if the solution temperature fell below 10°C (Gee and Ward 2001). For this reason, the concentration was reduced to 36 wt% for the purposes of the Mock Tank simulations. Ambient air and solution temperatures were monitored with a thermocouple array on and near the solution storage tank and at the solution release point in the Mock Tank.

Selected properties (e.g., the conductivity and density) of samples of the solution were evaluated periodically during the test by lab analyses to confirm the stability of the solution (Appendix F). The density varied between 1.34 and 1.27; conductivity was also fairly stable, varying between 84,000 and

88,000 µS/cm. Analyses also indicated that during the testing the concentration of the solution ranged from about 33 to 38 wt% sodium thiosulfate, with the average around 37 wt%.

For the FY 2001 TLDD testing, the sodium thiosulfate solution was delivered to the Mock Tank center leak point (Figure 3) via a digitally controlled flowmeter from the 15,140-L (4000-gal) storage tank. Some difficulty occurred with the pre-existing manifold at the tank (Figure 11), apparently blocking flow intermittently, and with operation of the flowmeter. These problems were circumvented by rerouting the delivery line directly to the infiltration point at the tank center through the access bar (bypassing the manifold) and by having a spare flowmeter on hand.

Figure 11. (Top and Middle) The Digital Flowmeter System Connected Directly to the 15,140-L (4000-gal) Sodium Thiosulfate Storage Tank; (Bottom) Existing Manifold System Used Initially to Deliver the Solution to the Central Leak Point in the Tank. This manifold was abandoned late in the test to circumvent suspected clogging.

3.0 Summary of FY 2001 Tests

This section summarizes the primary activities involving the deployment of the geophysical methods at the Mock Tank during July and August 2001. Results of each method are also summarized, along with special circumstances encountered during the tests. Details of each method, its performance, and conclusions are presented fully in Appendixes A through D.

3.1 Background Measurements

Baseline (background) measurements for all methods were conducted during most of July 2001. Drilling and completion of wells around the Mock Tank were not completed until mid-July because of a general work stand down on the Hanford Site and various difficulties resulting from simultaneous deployment of several technologies at one site. Thus, some methods were required to forestall or accelerate background measurements to meet the anticipated schedule for solution-release (leak-simulation) measurements. The background measurements were necessary for all methods to determine "noise" levels and to provide a baseline condition to which later measurements would be compared. This comparison is part of the basis for determining the appearance of a leak. More specific details on background measurements are provided in the individual reports in Appendixes A through D.

3.2 Solution Release Measurements

The first release of sodium thiosulfate began on August 9, 2001. Figure 12 shows the schedule of method measurements and solution releases. All geophysical methods conducted multiple measurement episodes during the leak release period (August 9 to August 29, 2001), except the CEMI method, which conducted only one prolonged measurement following the first leak, extending through leaks 2A and 2B. Although Figure 12 indicates simultaneous measurements by several methods, data collection periods for some, such as ERT and HRR-SCRT, had to be alternated to avoid interference between these methods. Thus, ERT would collect data for two hours, then stand down for HRR-SCRT to collect a data set. By this approach, both methods were able to obtain data from approximately the same time frames. Table 1 indicates the volumes (in gallons) and timing for the five solution releases. The volumes of the first and fourth releases were unknown to the investigators (blind) and were made known only after all analyses were final. Release rates range from approximately 38 L (10 gal) per hour (#2A) to about 90 L (23.5 gal) per hour (#4). The releases were scheduled so as to determine if the methods could detect initial releases and total discharged volumes, and to demonstrate sensitivity to superimposition of releases.

All 12 soil access ports in the bottom of the Mock Tank were monitored periodically during the solution releases. No evidence of solution encroachment was observed at any time during the testing, although condensation was seen in some ports. These ports were kept sealed during the tests to avoid air leakage and hindrance of the SAFE operation. The temperatures of the soil at the center release point and of the solution itself were recorded manually and by a data logger during the testing. The maximum solution temperature of 40.5°C was recorded on the afternoon of August 10; the lowest (28.3°C) occurred on the morning of that same day. Soil temperatures at the central release point ranged from ~28°C to almost 36°C.

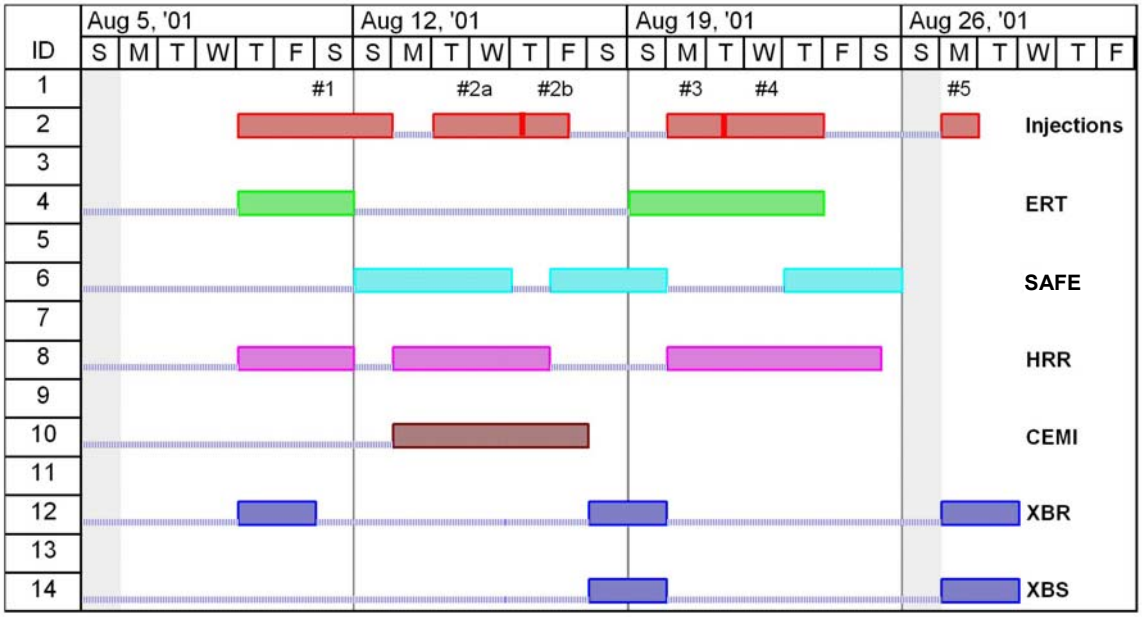

Figure 12. Test Schedule for the FY 2001 TLDD (after Vista Engineering 2001)

Table 1. Solution Release Details for the FY 2001 TLDD (after Vista Engineering 2001)*

	Volume (gal)	Start	Stop
Release #1	1,122 (blind)	8/9/2001 8:30	8/13/2001 8:50
Release #2A	468	8/14/2001 11:45	8/16/2001 11:00
Release #2B	464.9	8/16/2001 15:13	8/17/2001 11:50
Release #3	360	8/20/2001 12:04	8/21/2001 11:37
Release #4	1,080 (blind)	8/21/2001 14:45	8/23/2001 12:04
Release #5	379	8/27/2001 13:08	8/29/2001 8:38
*All releases were through the central leak point in the Mock Tank interior.			

Rain fell at the Mock Tank site (0.02 in. on August 22 at Hanford Meteorological Station) on August 22 and 23, but had no discernable effect on the testing operations or subsequent results. A high air temperature of 40°C (104°F) was recorded outside the mobile geophysics laboratory bus on August 22. This high temperature had no identifiable effect on operations.

3.3 Summary of Geophysical Methods

Geophysical methods that were selected for testing in FY 2001 are based on proven technologies that have been used, in one form or another, for many years and within many industries. These methods also have recent application history at the Hanford Site (e.g., Ward and Gee 2001). Adaptations of these technologies have produced specific approaches that offer even greater promise for detecting leaks,

potentially of very limited volumes and within short time frames. The Vadose Zone Advanced Characterization Workshop held in January 2000 addressed numerous potential methods for external tank leak detection, including the geophysical methods discussed below (see http://vadose.pnl.gov/workshops.stm).

Electrical and electromagnetic geophysical methods have long been used as mineral and groundwater exploration techniques, being deployed both in boreholes and as large surface arrays or moving surveys to define ore bodies or aquifer characteristics. Similarly, numerous seismic methods have been used for decades in defining subsurface conditions. Advances in data processing/computing capabilities and electronics have allowed these methods to be refined and new instrument configurations to evolve. More recent methods involve deployment in conjunction with vertical borehole arrays around specific targets of more limited size (such as underground tanks) and tomographic processing and display of results. These developments allow three-dimensional, volume-integrating representations of subsurface features, specifically, contaminant plumes in the case of tank leaks. When applied over time intervals, the methods allow depiction of transient features, such as developing and migrating contaminant plumes. The characteristics of these advanced methods are described in Barnett et al. (2001) and in the individual reports of Appendixes A through D.

Ward and Gee (2000) described the process of selecting and eliminating geophysical monitoring technologies that have application to problems at Hanford. Despite the logistical/operational difficulties involved, the simultaneous deployment of multiple methods during the testing at the Mock Tank does allow comparisons of methods to provide verification of results. The summary descriptions of the techniques discussed below are adapted from Ward and Gee (2000, 2001), and descriptions provided by the geophysical researchers. Full descriptions of the methods and configurations used in the FY 2001 TLDD at the Mock Tank are provided in Appendixes A through D.

3.3.1 Electrical Resistance Tomography (ERT)—Method Description

ERT has been demonstrated to be a useful characterization tool, providing details of the lithostratigraphy between wells (e.g., Newmark et al. 1994), subsurface processes such as fluid infiltration (Daily et al. 1992), and steam injection and ohmic heating (Ramirez et al. 1993) by mapping the spatial and temporal changes in soil resistivity resulting from changes in liquid saturation and temperature. Because tank wastes at Hanford are generally rich in high-ionic-strength electrolytes, resistivity is an ideal surrogate for locating difficult-to-detect contaminants. Typical electrode installations involve multiple electrodes strung on nonconductive casing (e.g., plastic or fiberglass) in conventionally installed boreholes, or as instrumentation strings installed using CPT. Both designs have been effective in shallow to moderate depths (most recently >395 m [1,296 ft]), but deeper installations require significant and more costly modifications. The ERT sensors consist of the 16 existing borehole electrode arrays surrounding the Mock Tank, with eight electrodes spaced 1.5 m (5 ft) apart vertically within each array (see Figures 3 and 4). The main components of the data collection and recording system are as follows: Zonge Engineering transmitter, multichannel receiver, multiplexer, isolation amplifier, a Hewlett Packard current monitor, and a DC power supply. A schematic representation of the ERT configuration and principle is illustrated in Figure 13. Connections to the 16 arrays are controlled manually via a patch panel (Figure 14).

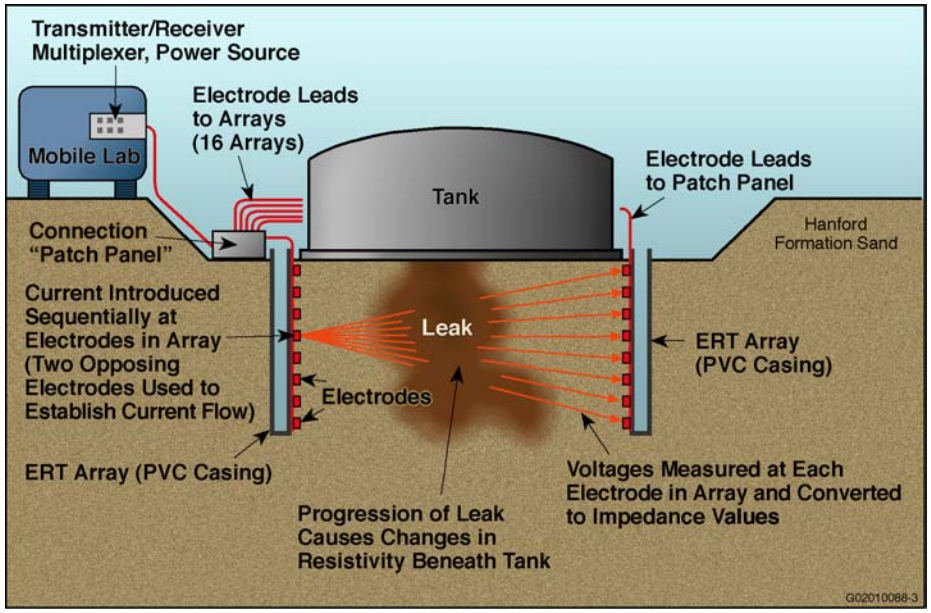

Figure 13. Configuration and Operating Principle of the ERT Method at the Mock Tank. Only one current electrode and one potential array (with eight electrodes) are shown activated in the figure, but 1,620 combinations using all 16 arrays are made during a full suite of measurements, requiring approximately 2 hours.

In general, ERT has been conducted using a cross-borehole geometry that makes use of multiple electrically isolated electrodes placed in vertical arrays. This geometry has the potential to produce relatively high-quality, high-resolution images when the aspect ratio of vertical (length of array) to horizontal spacing is equal to or greater than 1.5:1.0. This ratio, also referred to as the method aspect ratio, represents an optimal volume of interrogation in the subsurface. For the Mock Tank, this ratio was not optimized in that the vertical plane of interrogation (35 ft) was not greater than the horizontal plane (50 ft). The aspect ratio for the Mock Tank is calculated as 0.7:1. Had the 1.5:1 aspect ratio been maintained at the Mock Tank Site, the influence of the highly conductive tank bottom could have been reduced, enabling greater sensitivity to leak volume and the resulting plume geometry.

The capability to obtain ERT images using existing conventional steel casings would increase the applicability of the technique and make it particularly useful for deployment in tank farms. Recent simulations of ERT with vertical casings as electrodes show that there is a distinct signature indicative of the changing resistivity across the field, which is well above the noise level in the simulations. However, vertical resolution may be limited (Newmark et al. 1994).

Although steel well casings create serious electrical short circuits that affect the sensitivity of all electromagnetic methods, especially in the vertical plane, ERT has been determined to work satisfactorily at a site when the effects of the steel casings are properly modeled. The steel casings can also be used as long electrodes to produce images of coarse resolution. At the VZTFS site (Ward and Gee 2001), ERT results produced by a combination of electrode arrays and long electrodes (steel casings) compared reasonably well with neutron probe studies to show tracer plumes. Also, the location and general size of

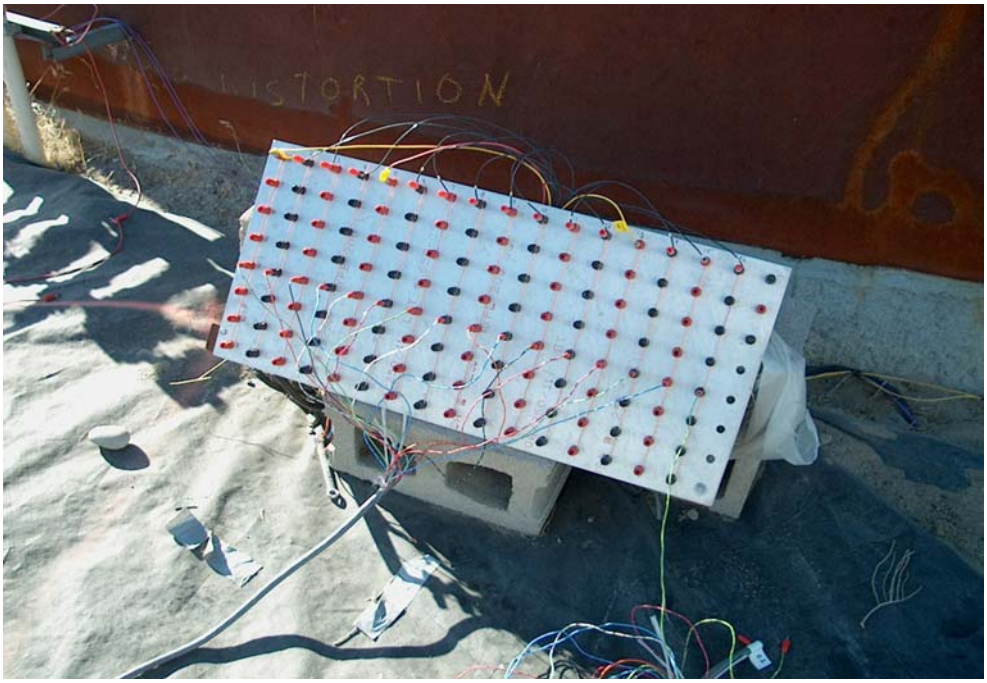

Figure 14. ERT Patch Panel Located Near the Edge of the Mock Tank Used to Control Connections Between Recording Instrumentation and the 16 Electrode Arrays Surrounding the Tank. Each column of connectors represents one of the 16 electrode arrays around the tank. The cable extending off the left bottom of the photograph leads to recording instrumentation in the geophysics mobile lab (bus).

the plume(s), as determined by ERT and neutron data, generally agreed, as did mass-balance calculations from both, which appear to be based realistic on previous experience with fluid migration in the vadose zone at the Hanford Site.

ERT deployment in a tank farm would be simplified if the dry wells could be used as "long electrodes." These wells could be supplemented with additional electrode arrays located outside the tank farm boundary to allow ERT leak detection underneath the tanks. Thus, the method might not require new drilling inside the farms. This "long-electrode" approach was one of the more successful configurations for leak detection that did not require the entire 16 ERT arrays.

Summary of FY 2001 ERT Results

Two separate survey periods were conducted for ERT (Appendix A). The baseline data were collected before injection on August 8, 2001, and the first survey was completed near the end of the first injection on August 11, 2001. The second survey was performed near the end of the injection schedule, beginning on August 19th and ending on August 23, 2001.

The ERT method, refined by investigators from Lawrence Livermore National Laboratory (LLNL), used the existing electrode arrays around the Mock Tank Site to develop a three-tiered surveying strategy for leak detection. The results suggest that a "triggering" system detecting an increase in moisture

content can be developed with few or no changes to the existing tank farm infrastructure. The results also show that a low-resolution imaging system can be constructed using the current inventory of steel-cased wells surrounding the SSTs. The investigators from LLNL have also shown that a more enhanced electrical resistivity network could generate high-resolution tomographic images capable of defining plume geometry as well as establishing fluid travel time and direction. Such a network would require installing VEAs or "point electrodes." The results of the ERT measurements (Appendix A) indicate that detection of a leak of "a few hundred gallons" is possible with confidence at the Mock Tank. The tomographic analysis also indicated that the leak moved in a northeast direction during the course of the tests. Estimates of the blind releases were in good agreement with actual release volumes. The estimate for the release beginning on August 9 was 1,260 gallons, and that of August 21 was estimated at 1,550 gallons. These estimates are within +11% and +30%, respectively, of the actual released volumes (see Section 3.2, Table1).

3.3.2 Cross-Borehole Radar (XBR) — Method Description

XBR measurements provide information about the porous medium (sediments) between two boreholes. Radar is analogous to the seismic reflection technique, except that radar (electromagnetic energy) is used rather than acoustic waves. The basic principles of operation and deployment configuration for both of these methods are shown schematically in Figure 15. A more complete description of the method and application to the Mock Tank tests is provided in Appendix B. The primary information obtained by XBR is the variation of dielectric properties of the subsurface. Because of the large contrast in the dielectric constant between water ($\kappa = 80$) and most earth materials ($\kappa = 3$ to 5), volumetric water contents can be easily inferred from radar data (Hubbard et al. 1997). Also inferred are the lithology and distribution of different soil types. Media with strong discontinuities (e.g., fracture zones) delay pulse arrival times and attenuate the transmitted radar pulse. The late arrivals and reduced-pulse amplitudes are measured and analyzed using tomographic processing. Even later arrivals from reflectors are analyzed. The velocity and amplitude of the data are recorded as a function of time, resulting in a series of data in the time domain. However, the data are often reduced to the frequency domain to infer attributes of the data indicative of various subsurface properties. Normally, numerous rays are measured, and the data are usually collected in a tomographic mode, which is then inverted to provide a tomogram of either velocity or attenuation properties. The data can also be collected in a more rapid fashion in a limited crosshole configuration. The data can also be processed to give reflection images in stratigraphic sequences.

Of particular significance is the reinforcing nature of the XBR and XBS methods when used in combination. XBR is primarily sensitive to moisture content of the soils, and XBS is sensitive to porosity. One of the objectives of the combined evaluation is to merge and jointly interpret the XBS method's high resolution of the lithology with the XBR high resolution of moisture changes.

The downhole components of the XBR system consist of a dipole antenna(s) (transmitter in one borehole, receiver in another [Figure 16]) with lengths of 0.5 to 2.0 m (1.6 to 6.6 ft) depending on the frequencies used. The frequencies used in the Mock Tank study were 50, 100, and 200 MHz. The borehole selected for XBR deployment and ray-path geometry are presented in Appendix B, Figure 2. Measurement intervals in the boreholes are from 0.25 to 2.0 m (0.8 to 6.6 ft). Both antennas were moved down the boreholes incrementally and in multiple configurations to provide numerous receiver/transmitter ray paths. Deployment is limited to PVC-cased wells or open holes (cannot be used in metal casings).

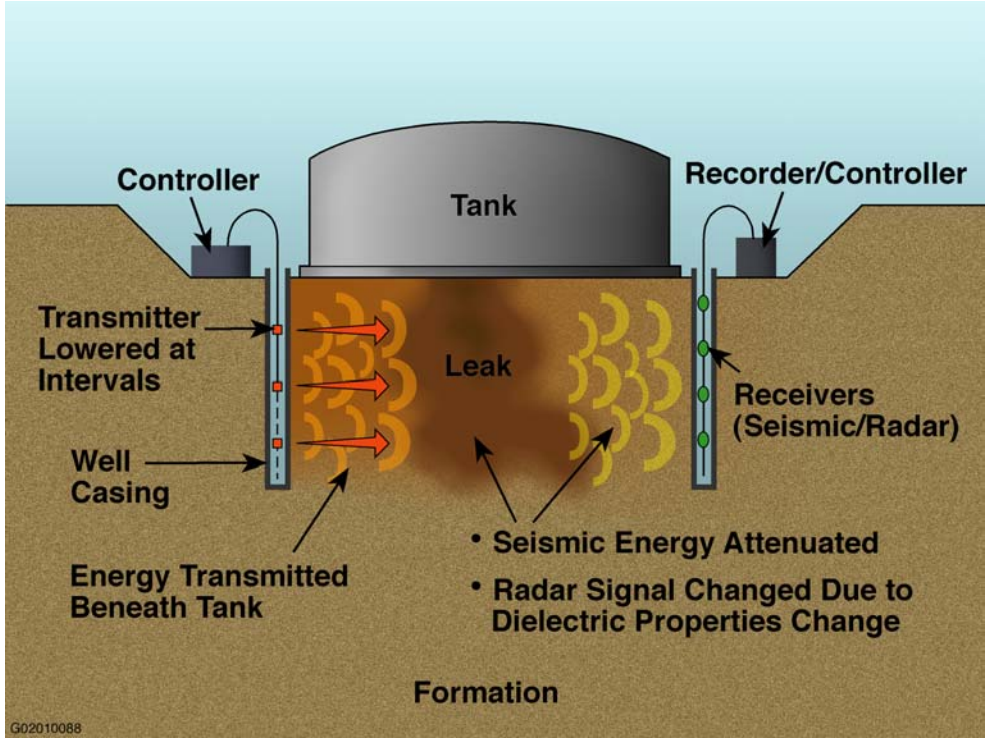

Figure 15. Principles of Operation for XBS and XBR Methods. The XBR receiving antenna (see Figure 16) is raised from the bottom of the borehole in parallel with the transmitting antenna located on the opposite side of the tank to interrogate multiple levels beneath the tank. For XBS, a string of hydrophones (Figure 17) is emplaced in the receiving borehole, and a vibrating energy source is raised incrementally in a borehole on the opposite side of the tank.

Summary of FY 2001 XBR Results

Six individual cross-well radar measurement sets were obtained by Lawrence Berkeley National Laboratory (LBNL) from July 18 to August 28, 2001. The radar sets included a baseline measurement against which the subsequent measurements are evaluated.

The plots of differential first arrivals show a more pronounced sensitivity to the changes in moisture content in the subsurface compared with the seismic data (see Appendix B). The analyses indicate that changes in first-arrival amplitude show the greatest change within the first 2 to 3 hours after the injection started. All subsequent changes in amplitude indicate that the radar first arrivals were tracking a horizontal spread of the thiosulphate solution, mostly to the southwest, without any obvious vertical migration. The radar output indicated changes beneath the tank, assumed to be caused by the leak, when approximately 378 L (100 gal) had been released. Processing of data collected from August 9 and 10 indicated that the leak that was started on August 9 moved mainly downward but somewhat to the southeast of the central leak point.

Figure 16. Antenna Configuration for XBR Measurements at the Mock Tank. Both transmitter and receiver are equipped with centralizers.

Figure 17. Lowering of Hydrophones (seismic receiver sensors) into a Steel Case-Lined Well at the Mock Tank. Wells were filled with water to perform the measurements, then pumped out after the measurements were finished (pump reel next to well)

3.3.3 Cross-Borehole Seismic (XBS)—Method Description

The XBS tomography method involves measuring the travel time of seismic energy transmitted between two or more boreholes to derive information on the dynamic elastic properties of the intervening porous medium (Majer et al. 1997). Such data can then be used to infer lithology, bed geometry and continuity, fracture and fault properties, porosity, and in some cases, interstitial fluid distribution. A transmitter (an oscillatory vibrator to produce the seismic energy) is deployed in one hole, and multiple receivers (hydrophones) in an adjacent hole or holes (Figures 13 and 17). Energy is transmitted at multiple positions in the transmitter well and received in the hydrophones in the receiver well(s). In practice, a directional downhole seismic energy source and the string of hydrophones are initially lowered to the bottom of two boreholes. The energy source is a 3.8-cm x 10-cm (1.5-in. x 4-in.) piezoelectric cylinder. An OYO DAS-2[(a)] recorder is used for data collection. The source is moved up the hole in increments so that a near-horizontal ray path is maintained between it and the hydrophone at the corresponding level (see Figure 2, Appendix B). Average shear (S) and compressional (P) wave velocity values are obtained by calculating wave travel times between the source and receiver boreholes.

To ensure the accuracy of the data, the boreholes must be installed as vertically as possible and be cased with steel or PVC. The technique requires that the boreholes be sealed at the bottom so they can be filled with water, providing acoustic coupling with the formation. In the case of existing steel wells (such as at the tank farms), inflatable packers that can be removed after the test could be used to seal the boreholes. Measurements were made of background conditions before solution release at the Mock Tank Site and after the final release.

Summary of FY 2001 XBS Results

Seismic (XBS) measurements were made at the Mock Tank Site by investigators from LBNL in FY 2001. The measurements were obtained from three boreholes constructed especially for this exercise. Four cross-well measurements were gathered—one as a baseline before fluid injection and three during separate injections of the sodium thiosulfate solution.

Early results from cross-well seismic measurements are inconclusive regarding the capability of this method to detect changes in moisture or fluid content. The change in fluid density was most pronounced at approximately 4 m (13 ft) bgs. This horizon appears in raw data plots from the August 28, 2001, survey as a distinct change in amplitude in the first arrivals at approximately 40 to 45 milliseconds. The entire seismic survey effort, however, was plagued by well seal failures and the necessity of preventing leakage of water from the wells that could hamper the electrical and electromagnetic methods.

3.3.4 Cross-Borehole Electromagnetic Induction (CEMI)—Method Description

CEMI uses the principle of induction to measure the electrical conductivity of the subsurface between two boreholes (Figure 18 and 19). The technique can provide high-resolution images of the subsurface between existing wells up to 1,000 m (3,280 ft) apart. The CEMI system consists of a transmitter

---

(a) Trademark of OYO, Inc.

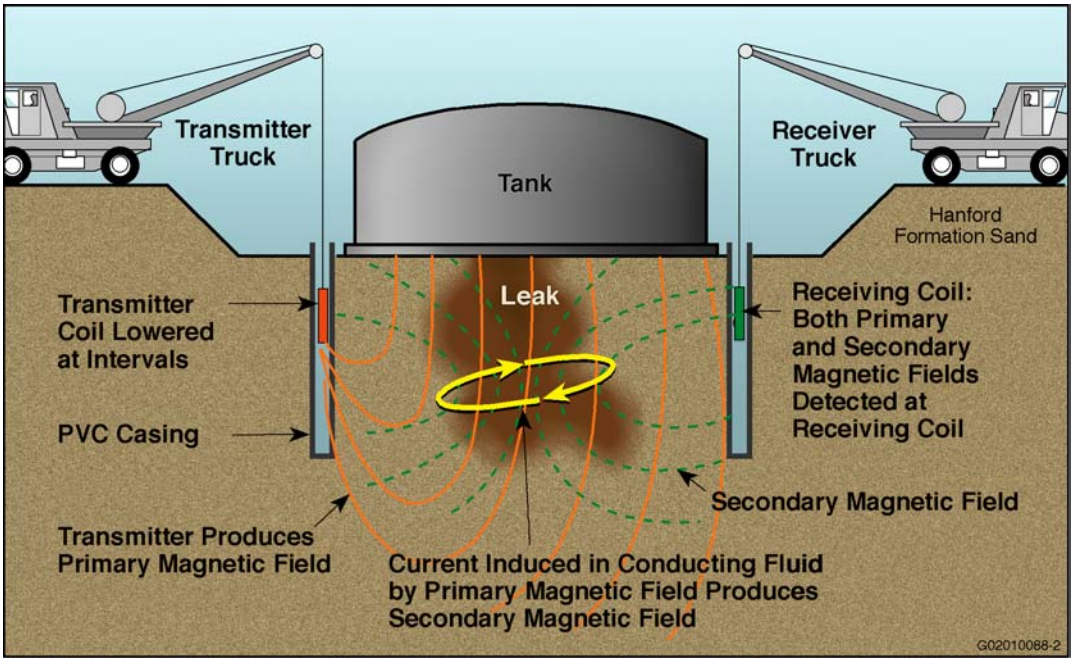

Figure 18. Configuration and Principles of CEMI Operation

Figure 19. Receiving Coil for the CEMI Method Being Lowered into a Well. The transmitter is placed in a well opposite from the tank off the left side of the photograph. The truck housing the recording equipment and generator is seen in the background.

in one well and a receiver in a second well. The transmitter uses a vertical-axis coil wrapped with 100 to 300 turns of wire tuned to emit a single low-frequency sinusoidal signal that induces currents to flow in the surrounding soil. The optimum operating frequency depends on borehole separation and background resistivity, but generally the frequency ranges from 40 to 100 kHz. A frequency that is too low limits the resolution, while one too high limits the range of the measurement. At the receiver borehole, a custom-designed coil detects the total magnetic field, consisting of the magnetic field from the induced currents in the medium as well as the primary magnetic field generated by the transmitter. The receiver section consists of a magnetic field sensor and a commercial lock-in amplifier located at the surface. The lock-in amplifier operates like a radio by measuring only those signals that are coherent with the transmitted signal while rejecting incoherent background noise.

By positioning both the transmitter and receiver tools at various levels in the boreholes spanning the zone of interest, images of the resistivity distribution in the region beneath the Mock Tank can be generated (see Appendix C, Figures A-1 and B-1). The data are interpreted by inverse modeling to produce a tomogram. The main sensor components are a vertical magnetic field transmitter and magnetic field sensors. The transmitter generates a time-varying magnetic field that produces secondary magnetic fields in the soil. The secondary field signal in combination with the transmitter field (measured at the receivers) is used for nonlinear inversion techniques to develop the three-dimensional tomogram of the media conductivity.

Summary of FY 2001 CEMI Results

Electromagnetic (CEMI) surveys were conducted twice during the scheduled releases at the Mock Tank Site in FY 2001 by investigators representing LBNL and LLNL. One set of baseline measurements was made before releasing the sodium thiosulphate solution (July 23 to July 25, 2001) and spanning releases 2a and 2b (from August 13 through August 17, 2001).

Preliminary results for the CEMI survey roughly coincide with those obtained from the seismic method, but several of the responses remain problematic. A pronounced conductivity change was identified approximately 6 m (19.7 ft) beneath the tank. No explanation was determined for the presence of the discontinuity. Also, time-lapse results from August 14 indicated rapid movement of solution to the east-southeast. This is in contrast to imaging by ERT on August 20-23, which clearly indicated movement of the leak to the northeast. Although the injected solution was not specifically imaged during a preliminary phase, a leak from a PVC casing used for seismic measurements was identified, and its distribution was apparently detected.

The CEMI deployment was complicated by infrastructure from other methods (subsurface conductors), inadvertent leakage of water in CEMI wells from XBS deployment, and very rigorous data processing requirements (still incomplete). The CEMI method as a leak detection method in this setting was relatively ineffective and would require further development to be useful as such.

3.3.5 High-Resolution Resistivity-Steel Casing Resistivity Technology (HRR-SCRT)—Method Description

Electrical surveys made by a direct current (DC) resistivity device involved placement of electrodes in the ground. There are various geometries for the electrode layout, but most have all four electrodes in

line. The familiar Wenner and Schlumberger arrays are the most popular. The two outer electrodes are the current source and sink; self-contained batteries (DC source) produce the current. The two inner potential electrodes sense the electrical potential at the surface while current is flowing between the outer electrodes. The measured potential varies with electrode spacing in a predictable way and also changes as the strata and contained fluids vary laterally and vertically. In general, two modes of operation are common, depth sounding and profiling. In the depth-sounding mode, all four electrodes are placed in the ground initially with very short spacing between adjacent electrodes. A reading is taken, and then the array is reset with an incremental increase in spacing. Another reading is taken, and the array is, in turn, progressively expanded in this manner until the maximum depth to be investigated is reached. The current and potential sense progressively deeper layers as the array is expanded. In the profiling mode, a constant electrode spacing is selected that senses the subsurface geology to the depth of interest, and this constant array is "leap frogged" along a profile line to measure lateral variations that have geologic meaning. Adaptations of these configurations were applied at the Mock Tank site using existing ERT installations, surface electrodes, and newly installed steel-cased wells.

High-Resolution Resistivity (HRR) is an evolutionary development in DC electrical resistivity differing from conventional, industry-standard approaches by modifying the field-data acquisition procedures (Fink 1980, 1994) and subsequent data processing (Fink 2000). HRR has proven itself in extremely rugged terrain by incorporating the topography into the volume calculations. HRR is particularly useful in mapping the distribution and time-dependent changes of moisture in the subsurface. Steel Casing Resistivity Technology (SCRT) refers to the use of existing steel casings as transmitters or receivers in various combinations with surface electrodes or other conductors (e.g., metallic tank structures). When used with steel well casings or with electrodes (including the steel tank and attached structures) in direct contact with the conductive solution, this method is called excitation of mass. The combined term "HRR-SCRT " is used herein to simplify discussion of general or common elements involved in the deployment of both of these configurations. HRR-SCRT is optimally based on the pole-pole electrode geometry but, as noted, may be derived from any array of electrical sensors, including steel well casings. A detailed description of HRR-SCRT configurations and deployment is described in Appendix D.

Although the power source for the HRR-SCRT methods is nominally 12 V DC, the signal is modified to an alternating-polarity square wave in the ultra low frequency (ULF) range. The period of the wave is sufficiently long (one to four seconds) that DC measurements of each polarity are possible. These measurements are averaged to derive a DC value upon which calculations are based. The purpose of this approach is to eliminate interference by extraneous DC sources such as metal corrosion, telluric currents, or poorly isolated electrical equipment.

During the FY 2001 TLDD at the Mock Tank, several configurations of surface electrodes, steel casings, "fused" ERT arrays (all electrodes in an array are connected together), and connections to the leak point or steel tank were used to detect leak releases (Figure 20). The most effective of these, particularly where immediate detection is concerned, was the excitation-of-mass technique. Excitation-of-mass techniques have also been used successfully for saturated groundwater plume detection (Osiensky and Donaldson 1994; Osiensky and Williams 1996) and have been proposed for use in waste management facilities at the Hanford Site (Sweeney 1999).

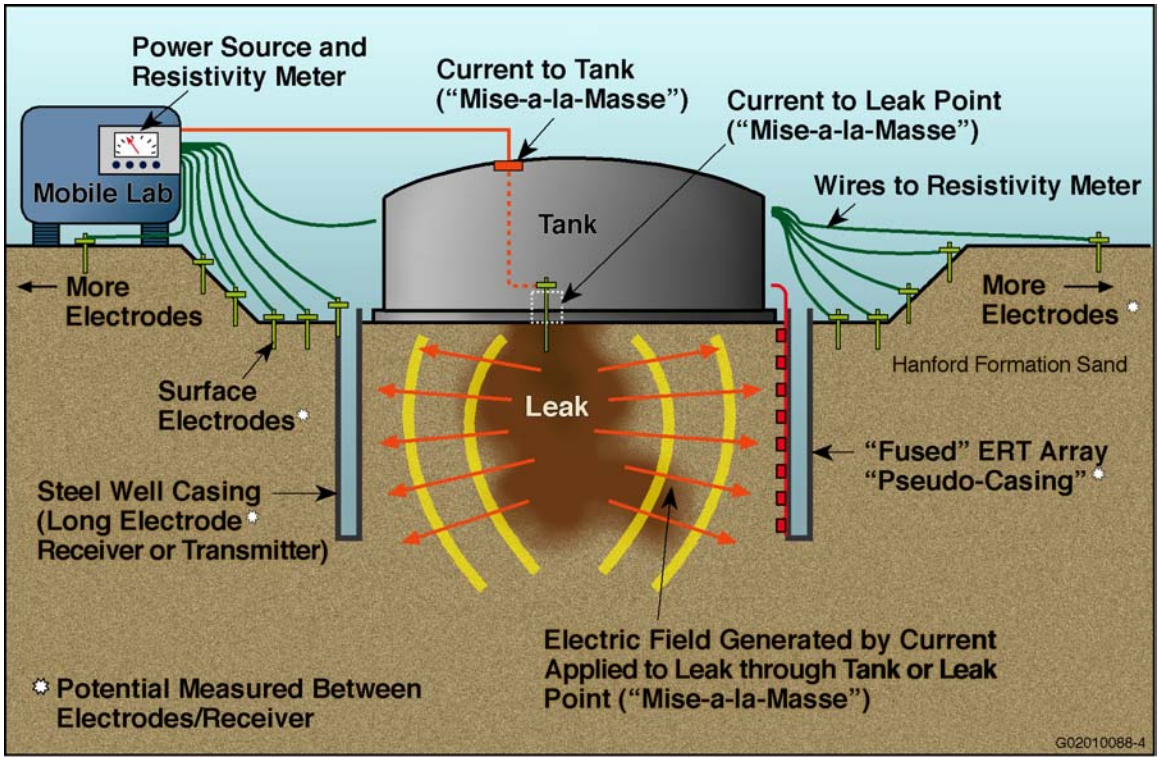

Figure 20. Schematic Illustration of HRR-SCRT Deployment. Several combinations of surface electrodes (61 of these), steel casings, fused ERT arrays, and connections to the Mock Tank itself were used to detect and image leaks. The most successful of these, Steel Casing Resistivity Technology (SCRT) or excitation of mass is emphasized in the figure.

Summary of FY 2001 Results

Results of the HRR-SCRT deployment at the Mock Tank FY 2001 TLDD are presented in Appendix D. This resistivity method developed by hydroGEOPHYSICS, Inc. was deployed in and around the Mock Tank Site for the FY 2001 exercise. The investigation team installed 61 surface electrodes to enhance the three steel-cased wells installed adjacent to the Mock Tank. The hydroGEOPHYSICS team also used the existing electrical resistivity array (ERT) to increase the sampling density and improve electrical measurement resolution.

Data were collected and preprocessed using the Advanced Geosciences, Inc. SuperSting[(b)] R8 IP memory earth resistivity meter (see Photo 3 in Appendix D). Four types of electrodes were used for HRR-SCRT deployment at the Mock Tank: the 61 surface electrodes were used as receivers; the tank itself (including the central leak point which was nominally in direct contact with the solution and tank) was used as transmitter/receiver; the carbon steel well casings were used as transmitters; and the ERT arrays were "shorted" or "fused" to simulate a metal casing. Eight combinations of these electrodes were used to make measurements in pole-to-pole arrays.

(b) Trademark of Advanced Geosciences, Inc., Austin Texas.

Measurements were conducted throughout the discharge schedule, beginning on August 7, 2001 (prior to release) and ending on August 25, 2001. In spite of some equipment failures that destroyed two sample sets, a nearly continuous set of measurements was obtained during the injection. The results of the HRR-SCRT survey show that simple plume geometry and volume estimates can be obtained using this method. At the Mock Tank, the minimum detectable leak was estimated at ~1,890 L (500 gal) for the HRR method (steel casing transmitters with surface electrode receivers), but the excitation-of-mass approach produced leak detections at less than 40 L (10 gal) at the Sisson and Lu site. This lower detection limit is based on the observed changes in potential (or resistance) that occur when the leak solution bridges the interface between the anionic components of the soil interstices (groundwater) and the steel container (whether casing or tank).

4.0 Conclusions

Results of the FY 2001 geophysical TLDD demonstrated that all methods detected solution release beneath the Mock Tank. CEMI and XBS methods were problematic in detecting capabilities, but both were hampered by deployment and/or data-processing problems. It is also likely that all methods (with the possible exception of CEMI) would perform considerably better if interferences resulting from simultaneous testing of multiple methods were removed, and other logistical problems (such as scheduling) were resolved. Of the five geophysical methods, ERT and HRR-SCRT appear to hold the most promise for leak detection on a tank scale.

4.1 Results of Down-Selection Workshop

On January 29, 2002 a "down-selection" workshop was held to formally evaluate and select the most promising methods for further evaluation as tank-external, leak-detection methods. During the workshop, a set of primary criteria was derived to provide a basis for this selection. These were:

- Safety in application
- Detection capabilities (performance)
- Technical maturity (pedigree)
- Sensitivity to leak quantification (volume determination)
- Cost
- Schedule (how quickly the method will be ready to deploy).

Based on these criteria, the HRR-SCRT and ERT methods emerged as clear choices for further evaluation of geophysical leak detection. The evaluation also suggested that XBR and XBS offered some potential with further development but would not be considered for FY 2002 continuation of the TLDD.

4.2 Comparison of the Mock Tank with SSTs

Although the Mock Tank was constructed to simulate the electrical profile of an actual SST, some differences are especially noteworthy. The "100"-Series SSTs are 22 m (75 ft) in diameter and 10 to 13 m (30 to 40 ft) in height (Figure 21). The steel interiors of the tanks are encased in concrete, with a layer of asphaltum apparently separating the steel liner and concrete in some tanks. The additional insulating effect of the asphalt layer could enhance the detectability of a leak by electrical methods. The SSTs are covered by concrete domes and are completely buried beneath 2 to 3 m (6 to 10 ft) of fill soil (WHC 1992). In contrast, the steel walls of the Mock Tank are exposed to the soil and are almost completely above ground level. Also, the SSTs contain varying amounts of waste, and in other respects (proximity to adjacent tanks, infrastructural details of the farms, etc.) are unique structures that will probably present unique monitoring challenges for electrical geophysical technologies. In particular, the connection of some SSTs with adjacent SSTs by "cascade lines" (steel piping allowing waste transfer) could affect electrical measurements from all configurations (ERT and HRR-SCRT). The proximity of adjacent SSTs may also hinder deployment of surface and subsurface sensors.

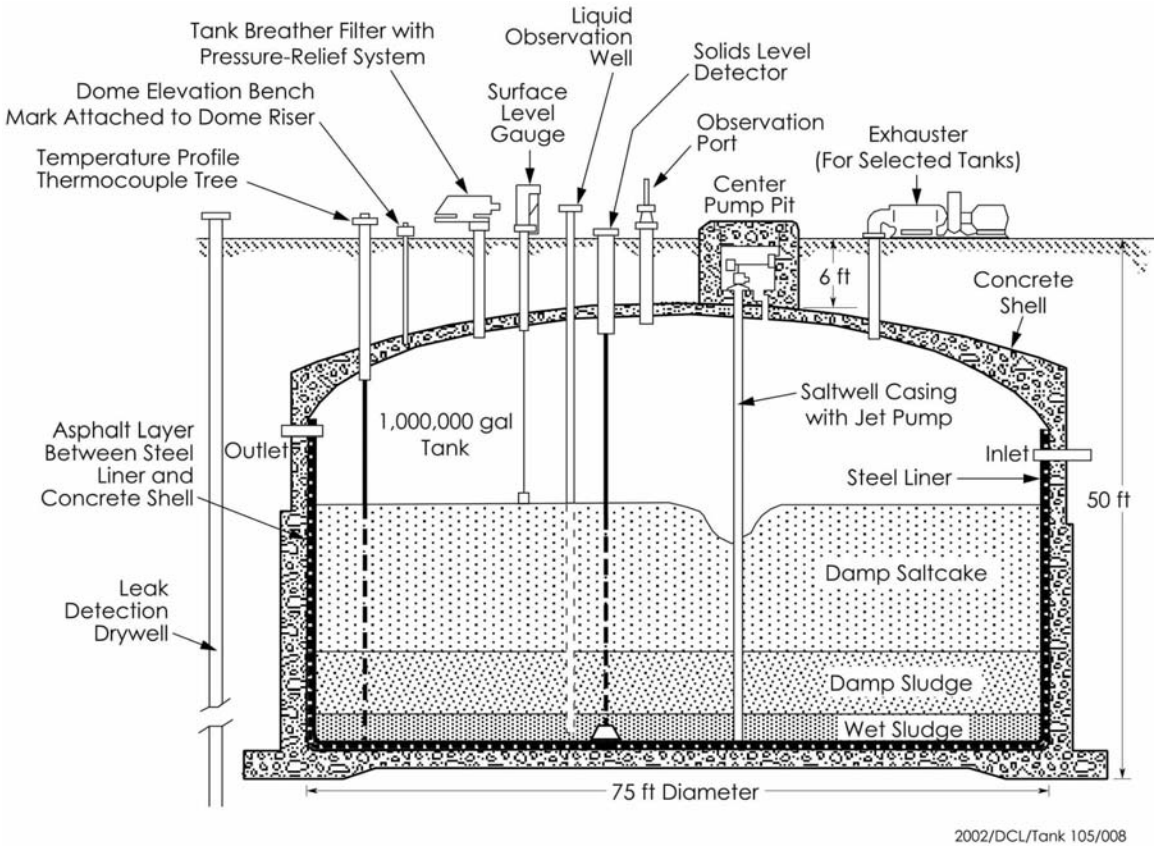

Figure 21. Representation of a 100 Series Single-Shell Tank, Showing Ancillary Instrumentation and Construction Features

Conversely, some SST features offer a potential opportunity for electrical measurements. For instance, it is possible that SCRT measurements may be made via the liquid observation well (LOW). These wells are nominally in contact with the conductive tank waste and hence the steel liner of the tank. Energizing a LOW while monitoring the subsurface beneath the SST would allow a leak to be observed electrically as long as the circuit from LOW through the waste to the leak is complete. Additional electrical monitoring is also possible using the leak-detection drywells located outside of the SST as long electrodes (see ERT and HRR-SCRT discussions in Appendixes A and D, respectively).

Hence, while the primary difference between actual SSTs and the Mock Tank may be that of scale where the responses of geophysical methods are concerned, other differences are at present non-quantifiable and may require modeling and/or further testing in more realistic settings. In general, these are the following:

- Larger size of the SSTs (scaling factors)
- Greater depth of leak detection required because of the subsurface locations of the tanks (aspect ratios)
- Complex infrastructure within a tank farm (including adjacent tanks)

- More complex electrical “circuit” between tank waste and the soil environment

- Limitations to emplacement of additional infrastructure.

These factors may create greater challenges for electrical methods compared with the Mock Tank. However, other SST features such as the LOWs may present opportunities for more effective leak monitoring.

5.0 References

Barnett DB, GW Gee, and MD Sweeney. 2001. *Test Plan for the Demonstration of Geophysical Techniques for Single Shell Tank Leak Detection at the Hanford Mock Tank Site—Fiscal Year 2001*. PNNL-13598, Pacific Northwest National Laboratory, Richland, Washington.

Cameron RJ, JC Evans, MD Johnson, and TL. Liikala. 2002. *Summary of Hanford Subsurface Air Flow and Extraction (SAFE) Activities for FY 2001*. PNNL-13820, Pacific Northwest National Laboratory, Richland, Washington.

Daily W, A Ramirez, DJ LaBrecque, and J Nitao. 1992. "Electrical Resistivity Tomography of Vadose Water Movement." *Water Resour. Res.* 28:1429-1442.

Ecology - see Washington State Department of Ecology.

Fink JB. 1980. "Logarithmic Pseudosections for IP and Resistivity." Presented at the *50th Ann. Internat. Mtg., Soc. Expl. Geophys*.

Fink JB. 1994. "A Unified Method of Plotting DC Resistivity and Induced Polarization Data." Presented at the *John S. Sumner Memorial International Workshop on Induced Polarization (IP) in Mining and the Environment*, Tucson, Arizona.

Fink JB. 2000. "High Resolution Resistivity: Applications and Case Histories." Presented at the *Advanced Vadose Zone Characterization Workshop*, Richland, Washington.

Gee GW and AL Ward. 2001. *Vadose Zone Transport Field Study: Status Report*. PNNL-13679, Pacific Northwest National Laboratory. Richland, Washington.

Hubbard S, Y Rubin, and E Majer. 1997. "Ground-Penetrating Radar-Assisted Saturation and Permeability Estimation." *Water Resour. Res*. 33:971-990.

Lindsey KA, BN Bjornstad, JW Lindberg, and KM Hoffman. 1992. *Geologic Setting of the 200 East Area; An Update*. WHC-SD-EN-TI-012 Rev. 0, Westinghouse Hanford Company, Richland, Washington.

Majer EL, JE Peterson, T Daley, B Kaelen, L Myer, J Queen, P Donfro, and W Rizer. 1997. "Fracture Detection Using Crosswell and Single Well Surveys." *Geophysics* 62(2):495-504.

Narbutovskih SM, TD Halter, MD Sweeney, W Daily, and AL Ramirez. 1996a. *Electrical Resistivity Tomography at the DOE Hanford Site*. WHC-SA-3035-VA, Westinghouse Hanford Company, Richland, Washington.

Narbutovskih SM, DF Iwatate, MD Sweeney, AL Ramirez, W Daily, RM Morey, and L Christensen. 1996b. *Feasibility of CPT-Deployed Vertical Electrode Array in Single-Shell Tank Farms*. WHC-SD-EN-TA-004 Rev. 0, Westinghouse Hanford Company, Richland, Washington.

Newmark RL, S Boyd, W Daily, R Goldman, R Hunter, D Kayes, K Kenneally, A Ramirez, K Udell, and M Wilt. March 1994. "Using Geophysical Techniques to Control In Situ Thermal Remediation." *Proceedings of the Symposium on the Application of Geophysics to Engineering and Environmental Problems (SAGEEP)* '94. Boston, pp. 195-211.

Osiensky JL and PR Donaldson. 1994. "A Modified Mise-a-La-Masse Method for Contaminant Plume Delineation." *Groundwater* 32(3):448-457. National Groundwater Association, Delaware, Ohio.

Osiensky JL and RE Williams. 1996. "A Two-Dimensional MODFLOW Numerical Approximation of Mise-a-La-Masse Electrical Flow Through Porous Media." *Groundwater* 34(4):727-733. National Groundwater Association, Delaware, Ohio.

Ramirez A, W Daily, DJ LaBrecque, E Owen, and D Chestnut. 1993. "Monitoring an Underground Steam Injection Process Using Electrical Resistance Tomography." *Water Resour. Res.* 29:73-87.

Ramirez A, W Daily, A Binley, D LaBrecque, and D Roelant. 1995. *Detection of Leaks in Underground Storage Tanks Using Electrical Resistance Methods*. UCRL-JC-122180, Lawrence Livermore National Laboratory, Livermore, California.

Ramirez A, W Daily, A Binley, and D LaBrecque. April 1996. *Tank Leak Detection Using Electrical Resistance Methods*. UCRL-JC-122875, Preprint prepared for the Symposium on the Application of Geophysics to Engineering and Environment, Keystone, Colorado, Lawrence Livermore National Laboratory, Livermore, California.

Reidel SP, KA Lindsey, and KR Fecht. 1992. *Field Trip Guide to the Hanford Site*. WHC-MR-0391, Westinghouse Hanford Company, Richland, Washington.

Sweeney MD. 1999. *Environmental Monitoring Alternatives for the Liquid Effluent Retention Facility*. PNNL-12024, Pacific Northwest National Laboratory, Richland, Washington.

Vista. June 2001. *Test Specification for FY 2001 Demonstrations at the 105A Mock Tank Site*, Rev. 0. Vista Engineering Technologies, L.L.C., Richland, Washington.

Ward AL and GW Gee. 2000. *Vadose Zone Transport Field Study: Detailed Test Plan for Simulated Leak Tests*. PNNL 13263, Pacific Northwest National Laboratory, Richland, Washington.

Ward AL and GW Gee. 2001. *Vadose Zone Transport Field Study: FY 2001 Test Plan*. PNNL-13451, Rev. 1, Pacific Northwest National Laboratory, Richland, Washington.

Washington State Department of Ecology, U.S. Environmental Protection Agency, and U.S. Department of Energy (Ecology). 1998. *Hanford Federal Facility Agreement and Consent Order*. Document No. 89-10, Rev. 5 (The Tri-Party Agreement), Olympia, Washington.

Westinghouse Hanford Company (WHC). 1992. *Work Plan for Drilling and Sampling Activities Near Single-Shell Tank 241-T-106 in Response to GAO/RCED-89-157*. WHC-SD-EN-AP-078, Rev 1, Westinghouse Hanford Company, Richland, Washington.

Williams BA, BN Bjornstad, R Schalla, and WD Webber. 2000. *Revised Hydrogeology for the Suprabasalt Aquifer System, 200 East Area and Vicinity, Hanford Site, Washington*. PNNL-12261, Pacific Northwest National Laboratory, Richland, Washington.

Appendix A

Tank Leak Experiment at the Mock Tank Site, 200 East Area: Electrical Resistance Tomography—Final Results

Appendix A

Tank Leak Experiment at the Mock Tank Site, 200 East Area:

Electrical Resistance Tomography Results

Submitted by

Lawrence Livermore National Laboratory

Livermore, CA 94550

Abelardo L. Ramirez, William D. Daily and Andrew Binley*

[*Lancaster University, Lancaster, UK]

January 18, 2002

Summary

Electrical resistance measurements were used to monitor several releases of brine from the Mock Tank Test site at the 200 East Area. Three different methods were used to analyze the data: 1) a simple average of the raw data was used as an indicator of the presence/absence of a leak, 2) tomography of the region beneath the tank using data from steel-cased borehole, and 3) tomography of the region beneath the tank using data from vertical electrode arrays. Each of these methods was able to detect the presence of what appeared to be conductive plumes forming beneath the tank. The results suggest the following: 1) The minimum detectable leak volume is of the order of a few hundred gallons. 2) A procedure involving the use of reciprocal data can be used to evaluate the reliability of the results and minimize the potential for false-positive and false-negative conclusions. 3) The dry wells may be used as long electrodes to obtain 2D images of the plume under the tank. 4) 3D electrical resistance tomography (ERT) images provide information that can be used to determine the released volume, the speed and direction of plume movement, the regions of the soil that are being contaminated, and the approximate location of the hole in the tank. 5) It may be possible to map pre-existing plumes when no pre-spill data exists. 6) A "quick look" calculation that can be used in the field can reliably detect the occurrence of a leak.

Work performed under the auspices of the U.S. Department of Energy by the Lawrence Livermore National Laboratory under Contract W-7405-Eng-48.

Introduction

This report covers the electrical resistance tomography (ERT) work performed at the Mock Tank site, 200 East Area, Hanford Reservation, during the months of July and August, 2001.

The goals of the ERT work were to:

1- determine if there was a simple, non-imaging electrical measurement, which could detect the presence of a leak of fluid from a single shell tank.

2- determine if electrical measurements could be made using dry wells (steel cased boreholes) to detect the presence of a leak and make a rough determination of its magnitude and location.

3- determine if electrical measurements could be made using ERT electrode arrays installed around a tank to detect a leak and image the resulting plume in order to estimate its origin, size and movement.

Electrical resistance tomography (ERT) is a method that calculates subsurface images of electrical properties from a large number of impedance measurements. Arrays of electrodes are placed on or beneath the surface. A low frequency (typically 0.125 to 1.0 Hz) current is driven between two electrodes. As this current flows through the ground, it establishes voltages at the other electrodes that are measured and recorded. Two other electrodes are then used to drive current, and voltages are again measured on all other electrodes. This process is repeated until all linearly independent combinations of current and voltage measurements are made. For 30 electrodes, there are 405 such measurements (n[n-3]/2 where n is the number of electrodes). Based on our field experience, we suggest that measurement errors are best determined by a reciprocity test. Two measurements are reciprocal when the transmitter dipole and the receiver dipole are interchanged. The ratio of voltage to current for both the normal and reciprocal

measurements will be identical if the process is linear (i.e., obey Ohm's law) and there are no measurement errors.

The raw data are inverted to produce tomographic images of electrical properties in the ground. For the simple case where the impedance is adequately described by the resistance, the method is called electrical resistance tomography (ERT). In this case, there are no phase differences (between the current and voltage). ERT data has been described by Daily and Owen (1991), Oldenburg and Li (1994), Sasaki (1992), and LaBrecque *et al*. (1996). Early adaptations of the technique to the field of geophysics were by Pelton *et al.,* (1978), Dines and Lytle (1981), Tripp *et al.* (1984), Wexler *et al.,* (1985). Adaptations for medical diagnostics can be found in Isaacson (1986), Barber and Seager (1987), and Yorkey *et al.* (1987).

LaBrecque et al. (1999) describe a three-dimensional inversion algorithm that calculates electrical resistivity; this algorithm is used for the work described herein. A two dimensional algorithm is also used in this work, as described in Ramirez *et al.* (1996).

Here we only summarize the general structure of the algorithms used for this work. First, a numerical model of the subsurface electrical resistivity is assumed, and the voltage field is calculated. These calculated voltages are compared to those measured; they will be different because the computer model of the subsurface is only an initial guess. The model is then changed in such a way as to make the voltages calculated for the new model closer to those measured. The algorithm continues making changes to the numerical model, improving agreement between calculated and measured voltages. This iterative process is continued until the agreement is within some specified value that is related to the accuracy of the measured values.

Site Description

The field experiments were performed under a 15.2 m diameter steel tank mockup located at the Hanford Reservation (200 East Area). Figure 1 shows the tank's location and the electrode layout at the leak detection experiment site. This empty steel tank contained several built-in spill points. Sixteen boreholes with eight electrodes in each surrounded the tank. The electrodes were

located in 10.7 m deep boreholes starting at the ground surface and spaced every 1.52 m. The diametrical distance between boreholes was 20.3 m.

This report describes the results obtained during a brine release experiment conducted during July and August, 2001. Sodium thiosulfate solution was released several times at the center of the tank. ERT was used to monitor the first release and two of the last three releases.

Experimental Approach

ERT data surveys were collected before, during and after a brine release in each of the 16 electrode arrays. The data were used in three different ways:

1- Develop a fast and simple 'yes/no' indication of a leak. This approach can be performed in the field immediately after the data is collected, and the results are available in seconds. Each transfer resistance measurement is multiplied by an appropriate geometrical factor to generate an apparent resistivity and the geometric mean of these values for a given data set represent a single value, $R_{\square}$, that is representative of the electrical bulk or average resistivity beneath the tank. As conductive fluid accumulates beneath the tank, reducing the bulk resistivity, $R_{\square}$ is a single number representing subtank conditions that can be used as a simple metric of the presence or absence of a leak. It would be used only by comparing conditions during sluicing to conditions before sluicing (baseline) when the tank was presumed not to be leaking. This means that any leak present at the time of the baseline would not be detectable but leakage subsequent to the baseline would be detectable. This method would yield no information about the location or movement of a plume but will reliably identify the presence of a leak.

2- To get a high resolution image of plumes formed by leakage and use this image to estimate leakage volume and monitor plume migration: All measured values of transfer resistances (1620 in all) are used to reconstruct a three-dimensional tomographic image of the soil's electrical resistivity. This approach allows us to delineate the changes in resistivity created by the salt-water release. The tomograph anomalies will reveal the presence or absence of a leak as well as indicate the position and size of the plume. We realize that this approach requires considerable additional infrastructure around a tank. This approach offers the most information: leak detection by the presence of a

statistically significant conductive anomaly, leak location by the position of the plume, approximate leaked volume from the size of the anomaly, and information about the speed and direction of the plume movement, and the flowpath(s) that it follows.

3- Develop low-resolution 2D images of a plume using steel case boreholes (i.e., dry wells): All of the electrodes in each vertical array are connected together at the surface to form an electrical short circuit. As a result, each vertical array behaves electrically like a steel-cased well in a tank farm. With this methodology, a series of dry wells could be used to produce a low resolution, two-dimensional tomographic image of subtank electrical resistivity. Such an image could be used to detect the presence or absence of a leak and provide only a rough estimate of the plume size and horizontal position. This approach would require little or no additional infrastructure for tank monitoring.

For cases 2 and 3 above we calculate the changes in the soil's electrical resistivity by comparing two data sets: 1) one for the case where a plume caused by a tank release is present, and 2) a corresponding data set for the case where there is no plume. This comparison was accomplished by subtracting, pixel by pixel, images of a baseline and some later condition.

Results and Discussion

Leak Detection

Electrical resistivity methods may be used in several ways to detect tank leaks. In this section, we will discuss three methods that we have tried during this study. The first is a very simple, non-imaging method to produce a leak alarm using the raw ERT data. The second is a method using only dry wells located near the tank to detect the presence of and produce a low-resolution image of a plume forming under the tank. The third method is a 3 dimensional reconstruction of data from the ERT arrays to produce high-resolution images of plume formation and migration. At the end of this section we will discuss the issues of detecting a new leak after other leaks have occurred.

A Very Simple Leak Alarm-- Geometric Mean Apparent Resistivity

External tank leak detection methods rely on changes in the soil under the tank caused by the release of tank fluids. These fluids are very conductive and small quantities will change the electrical properties of the soil in measurable ways. However, it is not necessary to reconstruct an image of the plume to detect its presence. Each measurement of resistivity under the tank contains a portion of the total information and it is possible to calculate a weighted average of these data to obtain a single number (apparent resistivity) representing the bulk conductivity under the tank at any single time. To do this, we weight each resistance measurement by a geometrical factor, transforming it into the resistivity that would be necessary to produce the measurement if the soil were entirely uniform. This weighting factor is only a function of the geometrical arrangement of the electrodes. It is found by solving the forward electrostatic problem, for a homogeneously resistive half space.

$$\rho = GR_t$$

Here ρ is the resistivity, R_t is the measured transfer resistance and G is the geometrical or weighting factor (see Keller and Frischknecht, 1966, or Hearst et al., 2000). It can be shown that:

$$G = 2\pi\left(\frac{1}{C_1P_1} - \frac{1}{C_1P_2} - \frac{1}{C_2P_1} + \frac{1}{C_2P_2}\right)$$

where C_1P_1 is the distance between the positive current pole and the positive potential pole, C_1P_2 is the distance between the positive current pole and the negative potential pole, C_2P_1 is the distance between the negative current pole and the positive potential pole, and C_2P_2 is the distance between the negative current pole and the negative potential pole.

Using these equations, we calculate the geometric mean of these normalized data. As the soil becomes more conductive this number will decrease in value.

Figure 2 shows the geometric mean apparent resistivities during the first and last release. The values show a decrease from August 8th (baseline, before the first release) to August 11th (in the morning, near the end of the first release). We interpret this steady decrease as evidence for a developing plume of salt water beneath the tank.

We did not acquire data between August 12th and 18th. For the last release, between August 19th and 23rd, the data show a similar behavior as before. Here again we interpret this data as evidence for additional salt-water release. In this sequence, however, the last point implies an increase in bulk electrical resistivity under the tank at the end of the release. The cause for this increase is unknown although we speculate that part of the plume may be moving so that our assumption of uniform resistivity produces inconsistent conditions for the last two points.

This simple analysis yields no quantitative information about plume volume or location. On the other hand, it is simple and quick--a mean can be calculated within moments of data collection. This approach might be useful for signaling the need for more extensive leak detection such as ERT imaging using either the dry wells or using ERT electrode arrays.

Approximate Plume Images Using Dry Wells

Using dry wells as electrodes, it is possible to reconstruct approximate 2 dimensional images under a tank and use these to detect the presence of a leak. To demonstrate how this is done, we used the ERT electrode arrays with all eight electrodes in each array connected together (forming an electrical short circuit) to make 16 long electrodes. The electrical equivalent of this arrangement is shown in Figure 3. Connecting all electrodes together in an array formed an electrical approximation to a continuous steel pipe or dry well. Although this approximation might seem crude, it is actually quite good—an array with point electrodes separated by 8 feet but connected together, and a continuous steel pipe, will look very similar at a distance of 15 or 20 feet. This configuration is entirely adequate to demonstrate the point that dry wells can be used for crude imaging.

Figure 4 shows the results for the release conducted between 0747 hrs on August 20th and 0742 hrs on the 21st. These difference images, relative to the baseline on the 19th, constitute maps of the 3D volume under the tank projected unto a horizontal 2D plane. Only this two dimensional reconstruction is meaningful because the electrodes are 35 feet long.

There is a clear progression of conductivity changes with time during the experiment. The first difference image is for a no-change condition and it is therefore blank because the data were taken about 8 a.m. on the 20th, before the release started at noon. Then at 1233 hrs, just after the release started, there is a weak anomaly extending from the release point at the center toward the Northeast. That anomaly becomes stronger by 1320 hrs. By 1422 hrs, the anomaly all but disappears, implying that the water was shut off for a short time and the plume drained out of the image volume. Since such fast drainage is unlikely, even with no inflow, we don't have a good explanation why the plume anomaly weakened at 1422 hrs. A similar effect is observed at 1621 hrs on that day. Notice that the strongest anomaly is at 1658 hrs on the 20th. The next morning the anomaly was much weaker, implying a lower flow rate during the night of the 20th.

A possible explanation for the occasional disappearance of the anomaly is that the signal measured by the long electrodes is weak. In the appendix, we show the results of numerical modeling for the long electrodes case. The modeling shows that when long electrodes are used most of the current flows through the tank shell and only a small fraction flows through the soil. This means that there is relatively little sensitivity to the soil properties. The diminished sensitivity may be a reason why the image anomalies in Figure 4 behave in the manner shown.

The same analysis that we have described above for the case of August 19th baseline was repeated using an August 10th (at 1036 hrs) baseline. This data was taken during, not before, the initial release but it is the first usable data acquired during the experiment (earlier data, including the intended baseline, was taken with a saturated current monitor amplifier, and thus is untrustworthy). Although the baseline on August 10th is not ideal, it was taken approximately 24 hours after the release started and therefore can be used to show changes *after* the first day of the release.

Figure 4a shows the entire sequence of long electrode ERT using the August 10th baseline. Resistivity changes from the first release are first detected by the data taken early on August 11. It appears that the plume is forming near the center of the tank. By August 20th at 1230 hrs, a little over one day into the second release, the plume is in the same place but now presents a much stronger conductivity contrast. Subsequent images show a persistent anomaly from the plume but with some variations in strength and size from the combined effects of added brine and drainage.

The same analysis shown in Figure 4a was repeated using data from only 8 of the long electrodes; these results are shown in Figure 4b. The full data set was decimated to include every other electrode in the array to simulate the case for long electrode ERT from only 8 dry wells. We note here that this decimated data set contains only 20 linearly independent measurements, 25% of data for the previous case, which severely limits its ability to constrain the solution. We should, therefore, expect to see results of reduced contrast, sensitivity and resolution. Recognizing this limitation, we see that the results are consistent with those of Figure 4a. Now the plume from the first release is not detected. With this reduced sensitivity, the plume first appears on August 20th (note that no measurements were made between 8/11 and 8/19/01 because the site was being used by other investigators), more diffuse but still offset from the tank center. Subsequent images show a persistent anomaly but most detail of variations in strength, size, and location are lost.

High Resolution Images of Plumes—Using ERT Electrode Arrays

<u>Differences in resistivity relative to baseline surveys:</u>

We now shift our attention to the resistivity changes mapped using the point electrode arrays. For these images, 128 electrodes located in 16 boreholes were used to survey the subsurface. We consider these to be the best results of all the approaches discussed so far in terms of accuracy, sensitivity, and resolution.

We will first discuss the changes caused by the first release as well as the first three combined (shown in Figure 5) and then discuss the changes caused by fourth and fifth releases (Figure 6).

The images in Figure 5 show the changes relative to a reference image collected on 8/8/01, just prior to the start of the first release. The size of the image block shown is 20.3 m wide by 20.3 m deep and 10.7 m tall. The red dots on top of the block indicate the location of the electrode arrays used. The results are shown in the form of log10 resistivity ratios (i.e., $\log_{10}(\frac{\rho_{s,a}}{\rho_{s,b}})$) where $\rho_{s,a}$ is the resistivity after the release started and $\rho_{s,b}$ is the resistivity of the baseline. The top 2 rows of images display the same results displayed using different transparency levels. The white bar across the color bar indicates the range of values that are rendered transparent. Note that when the change relative to the baseline is 0, the ratio is 1.0 and the log10 of the ratio is 0. Decreases in resistivity (expected to be associated with the plume) are indicated by ratios below 1.0 (log10 of the ratio below 0.0). The bottom row of images in the figure shows a vertical slice below the release point (marked by vertical arrow pointed downward).

The first four columns of images in Figure 5 show the changes observed by the first release, which ended sometime after the 8/11/01 data was collected. The fifth column (dated 8/19/01) shows the cumulative changes caused by the first three releases. The figure suggests that a plume, represented by resistivity decreases, develops as the volume of released fluid increases. The plume migration grows primarily downward and to the Northeast. Approximately 8 hours after the start of the first release (afternoon of 8/9/01), clear indications of a plume can be observed on the second row of images. At the time of writing, the total volume released to this point is unknown, but it is expected to be of the order of a several hundred gallons. These results illustrate the ability of the ERT method to detect released volumes within this range. Also, the results suggest that the images may be useful in determining the approximate location of the hole in the tank, speed, flow direction and volume of the plume, and identify the soil regions that are being contaminated.

Now we consider the changes caused by the last two releases; these changes are shown in Figure 6. The baseline tomograph used to calculate the change is for 8/20/01, collected before the fourth release started. The fourth release occurred between noon on 8/20/01 and 11:37 AM on 8/21/01; approximately 360 gallons were released. The first two columns in Figure 6 show the resistivity changes caused by this release. The first column shows changes where most of the 360 gallons

have been released because the data was collected around 9 AM on the 21st. The images indicate that, by the end of the release, a plume is forming below and to the NE of the release point. This result confirms our earlier claim (Ramirez et al., 1996): that plumes of the order of a few hundred gallons are detectable with this approach.

The next release started on 8/21/01 at around 2:40 PM and lasted until noon on 8/23/01. The images on the third and fourth columns show the cumulative effects of the 8/20-21/01 and 8/21-23/01 (the 4th and 5th) releases. The finger continues to grow towards the NE. When compared to the plume created by the first release (Figure 5), these images seem to suggest that the plume is moving sideways more (to the NE) and less downward.

The same analysis that is shown in Figure 5 was repeated using data from only 4-point electrode arrays. The full data set was decimated to include every fourth of the 16 electrode arrays to simulate the case for 3D ERT from only 4 arrays. Just as for the decimation of the long electrode data discussed above, decimation of the point electrode data leaves us with about 25% of the original data, thereby decreasing the information that constrains the parameters in a 3D inversion. As a result we should expect results of reduced sensitivity, contrast and resolution.

Figure 5b shows the results of this analysis. The images in Fig. 5b have a "blocky" look to them because we chose to use larger parameter blocks in order to reduce the number of unknowns in the inversion problem. The first row of images in Fig. 5b is shown using the same color scale and transparency as the images in the second row of Figure 5. It is clear that we see changes earlier (lower released volume) in Figure 5 than in Figure 6. This means that using a larger number of arrays increases the sensitivity to the plume.

For the 8/20/01 results, the volume observed in Figure 5 is smaller than in Fig. 5b because the larger number of arrays allows better resolution of the image.

The images show similar trends to those observed for the 16 array images in Figure 5. Both image sets show anomalies that increase in volume as the volume of released brine kept increasing. Both also show significant changes located directly below the release point. From these comparisons we conclude that it is possible to produce useful images of the plume using only four vertical electrode arrays. However, fewer arrays produce fewer data with which to constrain the inversion and decreased sensitivity and resolution.

The discussion so far has centered on resistivity differences relative to a baseline tomograph. We now explore the question of whether it is possible to map pre--existing plumes without the benefit of baseline surveys. Figure 7 shows the absolute values of resistivity measured during the course of the releases. The figure at the top shows the resistivity values corresponding to 8/8/01 before all the releases. The bottom row of images show the resistivity measured as more solution is released. Note the region of high conductivity (low resistivity) corresponding to the tank metal. Below the tank's bottom one can clearly see regions of low resistivity that emanate from the tank. These regions are approximately vertical and become less resistive with time. We believe that these results raise the possibility that pre-existing plumes under tanks may be detectable without the need of baseline data. This capability may make possible the detection of pre-existing plumes under the tanks at Hanford.

Detection Limits and False Alarms

Establishing the limits of any leak detection system is very important because of the consequences of a detection error. A false negative result would mean a lack of sensitivity in the method, so that a significant leak might be present but not detected. For this case, it is important to determine the minimum leak volume that can be reliably detected in the presence of all its associated errors and uncertainties. A false positive result would mean that the method is detecting leaks that are not real (giving false alarms) because it is sensitive to conditions not related to a leak and there is no way to differentiate between them and a leak.

Our interpretation approach assumes that all detected changes in soil resistivity are due to a tank leak or to data error. False alarms as well as tomograph sensitivity can be addressed by

performing an analysis of the effects of measurement error on the images. Error analysis will indicate a threshold (in terms of released volume) above which the results are reliable. We define the minimum detection volume as this threshold.

Tank managers may also choose to add a “factor of safety” to this threshold. If the goal is to minimize disruption to a sluicing operation and only act when large leaks are likely to be present, one may chose to define an alarm threshold that is several times larger than this sensitivity threshold. This means that a leakage prediction would be issued only after the analysis showed changes equal to the alarm threshold. Setting the alarm threshold at a given number may be based on the detection limits of the method and the operational goals of the tank managers. We mention this arbitrary criterion here to demonstrate how the analysis might be done to set an alarm threshold that might be useful for actual tank operations.

For the geometric mean analysis, we determine the sensitivity threshold and the alarm threshold by generating the mean using only the normal data and then again using only reciprocal data for a given time. The difference between these two means is considered the sensitivity threshold. If the geometric mean at two different times differs by more than this amount, we conclude that a statistically significant change in subtank soil resistivity has occurred and we interpret that as a developing leak for the time interval. This is our sensitivity threshold. Analysis of the data displayed in Figure 2 yields sensitivity threshold of +-0.2 ohm m, as indicated by the scatter of the points around the diagonal line shown. Points that plot along the diagonal line indicate a perfect match between the normal and reciprocal. The distance between any point and the diagonal (along a line perpendicular to the diagonal) indicates the degree of mismatch between the results.

Of special interest to tank operations is the false alarm rate of a leak detection method. To determine the false alarm rate, we would compare our alarm rate to the history of water injected (or not injected) during the test. At the time of writing, we do not have injection rates for this test so cannot determine a false alarm rate at this time.

The geometric mean data satisfy not only the sensitivity threshold test but also satisfy our *ad hoc* alarm threshold test. The very first mean value at 580.8 ohm m which represents a baseline and the second mean value at 572.4 ohm m are different by more than 3 times 0.2 ohm m, implying that the difference is statistically significant for a leak alarm—not a false alarm.

We could produce a similar threshold analysis from an error analysis on the long electrode reconstructions (see Figure 4). Now, however, the analysis requires a quantitative comparison of reconstructed images instead of two numbers.

However, a qualitative comparison will demonstrate the principles involved and probably leads to the same conclusion. Figure 8 shows the same sequence of long electrode data as shown in Figure 4 except that the top row uses only the normal data and the bottom row uses only reciprocal data. For each time given, there are noticeable differences between the two reconstructions. However, comparing Figures 4 and 8 it is also clear that the anomalies detected during the leak are clearly larger in magnitude than the differences seen in the threshold analysis. We therefore conclude that the anomalies in Figure 4 are above the threshold limit and thus statistically significant. These anomalies would then be considered as reliable indicators of leakage.

Now we turn our attention to sensitivity limits for the 3D ERT analysis. As discussed previously, our strategy in determining the trustworthiness of the detected electrical resistivity changes is based on the concept of reciprocity. Each data set collected contained data that is fully reciprocal; i.e., for each measurement, its reciprocal measurement was collected. When one compares images calculated using reciprocal data sets, an estimate of how closely the data obeys Ohm's law is obtained. This approach also quantifies how measurement errors propagate through the data inversion process, and provides an estimate for the threshold of changes in the images that are likely to be reliable.

Figure 9 shows the results of our reciprocal analysis for the 3D images. The figure quantitatively compares the resistivity in the "normal" tomograph (tomograph calculated using only the first measurement in a pair of reciprocal measurements) and in the "reciprocal" tomograph (tomograph calculated using the second measurement in a pair of reciprocal measurements where the transmitter and receiver dipoles have been switched). Specifically, the values plotted along the X and Y axes are of the form $\log_{10}(\frac{\rho_{s,a,n}}{\rho_{s,b,n}})$ and $\log_{10}(\frac{\rho_{s,a,r}}{\rho_{s,b,r}})$, where $\rho_{s,a,n}$, $\rho_{s,b,n}$ are the tomograph resistivities using the normal data, and $\rho_{s,a,r}$, $\rho_{s,b,r}$ are the tomograph resistivities based on the reciprocal data. All voxel values in the region between the boreholes are shown. A perfect match between these two tomographs would be indicated if all symbols plotted along the central dashed line shown. Values that plot away form this line indicate an imperfect match between voxel values and give a measure of the degree of the mismatch. The two lines on either side of the central dashed line indicate the range of values in which there is a mismatch. We will use this mismatch as an estimator of the reliability of the ERT results.

Figure 9 shows the results of this analysis for the changes early during the fourth release ($\rho_{s,a}$ corresponds to the tomograph for 8/21/01, and $\rho_{s,b}$ corresponds to the tomograph for 8/20/01). This plot suggests that that the vast majority of voxel values agree within $10^{+/-\ 0.2}$ (resistivity ratios between 0.63 and 1.58). We believe this is the sensitivity threshold for these images.

We will now use the results of this analysis to evaluate the ability to reliably detect the plumes. The approach we have followed is to render transparent any voxel values that fall within the range of values defined above. Referring to Figures 5 and 6, we can now justify the levels of transparencies chosen. The top row of images shows as transparent all ratio values greater than $10^{-0.2}$; this value is based on the $10^{+/-\ 0.2}$ threshold determined from the fourth release tomographs—the sensitivity threshold. The second row of images in the figures shows as transparent all ratio values greater than $10^{-0.1}$ –a level arbitrarily chosen at half the expected error.

During the first release (Figure 5), the top row of images shows that reliable anomalies are observed for images corresponding to 8/10/01 AM and later times. On the other hand, if we choose the second row of images (half the sensitivity threshold), all images (including the 8/9/01 PM image show changes that are considered reliable. Because the released volume is unknown we cannot determine the sensitivity threshold for the leak volume.

We can do a similar assessment for the images corresponding to the fourth and fifth releases (Figure 6). The image corresponding to 8/21/01 (around 9AM) represents the case where roughly 300 gallons had been released (this is a rough estimate since all we know at the time of writing is that 360 gallons were released between noon 8/20/01 and 11:30 AM, 8/21/01). All images in the top and middle rows of images in Figure 6 show credible changes. Therefore, the minimum detectable volume is about 300 gallons; it could be less than that because the estimate depends on how often the surveys were repeated.

In summary, an analysis of image reliability suggests a minimum detectable volume for 3D ERT of approximately 300 gallons (possibly less). When the minimum detectable volume has been released, a false negative interpretation becomes very unlikely. The reciprocity analysis described also minimizes the possibility of false-positive (false alarm) interpretations because it provides an estimate of reliability on the observed changes and minimizes the possibility that resistivity changes caused by measurement error are interpreted as leaks.

Estimates of Release Volume and Flow Rate

Estimating the volume of the plume (i.e., the volume of soil invaded by the released solution) is relatively easy. One simply sums the volume of all voxels that exhibit a level of change that is determined to be credible. However, tank managers are not interested in the plume volume; they are very interested in knowing the released volume (i.e., the volume of liquid tank wastes that have leaked). Estimates of released volume require that we use the volume of the plume together with a petrophysical model to estimate released volume.

The petrophysical model we chose is widely accepted and is known as 'Archie's' equation (Hearst *et al.,* 2000). This model relates the soil's resistivity (ρ_s) to the soil's saturation (S), porosity (ϕ), and pore fluid conductivity (ρ_w) as follows:

$$\frac{\rho_s}{\rho_w \phi^{-m}} = S^{-n} \qquad (1)$$

The exponents m and n are empirically derived constants. Given that we are primarily interested in changes and that porosity is unlikely to change, we can derive the following equation:

$$\frac{S_a^{-n}}{S_b^{-n}} = \frac{\rho_{w,b}}{\rho_{w,a}} \frac{\rho_{s,a}}{\rho_{s,b}} \qquad (2)$$

The subscripts b and a indicate conditions before and after the soil's property change due to fluid invasion. Hearst *et al.* indicate that the exponent n is generally determined based on laboratory data and when such data is unavailable, an acceptable value is about 2.0 +/- 0.5. Once the change in change in saturation is established, the change in pore water volume can be calculated as follows:

$$\Delta V_w = (\frac{S_a}{S_b} - 1) S_b \phi V_v$$

where ΔV_w is the change in the volume of water in each tomograph voxel and V_v is the volume of the voxel. Then, we sum ΔV_w over all voxels that exhibit $\frac{\rho_{s,a}}{\rho_{s,b}}$ that have been determined to be credible. In most cases, good estimates of S_b and ϕ can be obtained from geophysical well logs (neutron) and /or laboratory measurements made on core.

Equation 2 says that in order to calculate $\frac{S_a}{S_b}$ (change in saturation), we need to know $\frac{\rho_{w,b}}{\rho_{w,a}}$ (the change in pore water conductivity) and the changes in soil resistivity ($\frac{\rho_{s,a}}{\rho_{s,b}}$). This implies that

from one known value ($\frac{\rho_{s,a}}{\rho_{s,b}}$), we need to estimate two unknown values. Clearly, this calculation cannot be performed unless one assumes the value for $\frac{\rho_{w,b}}{\rho_{w,a}}$.

We will use equations 2 and 3 to estimate ΔV_w. An estimate of $\frac{\rho_{w,b}}{\rho_{w,a}}$ will be obtained for one release where the volume released was known; this estimate will be the average change in pore water conductivity over the whole tomograph volume. We will assume that for the other releases where an unknown volume of solution was used, the same value of $\frac{\rho_{w,b}}{\rho_{w,a}}$ applies. For the release that started on 8/20/01 and ended on 8/21/01, a total of about 360 gallons were released.

When the following assumptions are made:

Porosity, ϕ	0.25
"before" water resistivity, $\rho_{w,b}$	30 ohm-m
"after" water resistivity, $\rho_{w,a}$	21 ohm-m
Exponent, n	2
initial saturation, S_b	0.25

the estimated volume released is 290 gallons. This estimate is in reasonable agreement with the true volume. We will assume the same values apply to other releases.

We will next provide volume estimates for two "blind releases" were volume released is unknown at the time of writing. For the release that started on 8/09/01, the estimated released volume on 8/11/01 at around 9:00 AM is 1260 gallons. For the release that started during the afternoon of 8/21/01, the estimated released volume on 8/23/01 at around 9:00 AM is 1550 gallons.

We consider the above estimates as coarse approximations due to the large number of assumptions that are required and due to distortions to the plume size caused by the inverse solution.

The ERT methods discussed here are not directly capable of estimating the leak flow rate. Neither Archie's equation (equation 2) nor any other petrophysical model that we are aware of indicates that soil resistivity is a direct function of flow rate. Indirectly, it is possible to get a qualitative flow rate estimate by looking at the increases in released fluid volume (as determined the analysis above) as function of time. From this simple approach we estimate an average flow rate of 50.4 gal/hour for the 1st release (average flow rate between 8/9/01 and 8/11/01 in the morning) and 46.3 gal/hour for the 5th release (average flow rate between the afternoon of 8/21/01 and morning of 8/23/).

Conclusions and Recommendations:

We have demonstrated that electrical resistance measurements can be used in three quite different ways to detect changes in electrical conductivity under the test tank. Without knowing details of the released volumes, the results support the conclusion that the conductivity changes we detect arise from released fluids and from this we infer that these methods are good candidates for leak detection at single shell tanks. We have also shown how statistical limits can be set on sensitivity (minimum detectable volume) and how these limits can be used to evaluate the possibility of false positives and false negatives. In addition, ERT images have been used to estimate total released volume and flow rates for two "blind tests". The results presented here indicate that ERT provides useful information about tank leaks.

These results point to one possible operational strategy for ERT use in tank farm operations: the geometric mean of the apparent resistivity can be measured quickly and often (using either the dry wells or point electrode arrays installed for ERT) as a 'quick look', non-imaging capability. When this analysis suggests that observed changes are above the sensitivity threshold, more detailed electrical data could be taken, and this additional data could be used for imaging. From dry wells, one could obtain low-resolution 2D images that may be useful to yield the leak

location. From ERT arrays, one could get higher resolution 3D images that may be useful for leak location and plume size (which could be used to estimate leak volume).

We have shown that ERT can be used in two ways. The first approach involves the use of dry well casings as long electrodes. We have shown results using 8 and 16 long electrodes. Both show reliable evidence of the brine releases, but the 16 electrode results offer substantially higher sensitivity and resolution. It may be possible to perform similar surveys with as few as 6 dry wells; however, this scenario is likely to be quite challenging and needs to be properly investigated before it is selected.

The second approach involves the use of vertical electrode arrays around a tank. These arrays could be deployed using CPT or standard drilling technology. We have evaluated the case where 4 and 16 electrode arrays are used. Both of these provide much better resolution than dry well survey scenarios. The results based on data from 4 arrays yield useful plume images. Comparisons with the 16 array images indicate that the 4 array images offer substantially less resolution and sensitivity. We believe that better sensitivity and resolution can be achieved when the 4 electrode arrays cover a substantially longer vertical distance than the 10.7 m length of the existing arrays at the site. This allows the use of a higher number of electrodes, and the encirclement of the target region with electrodes thereby increasing the information available about the plume.

Recent work we have done on a different but related project has lead us to believe that it may be possible to detect leaks using ERT from measurements taken entirely outside of a tank farm. This method would have reduced sensitivity and resolution compared to the 3D ERT in this report, but it would require no additional infrastructure inside the tank farm fence-line Figure 10 shows the ERT image of a tank sitting on the surface, leaking jet fuel (kerosene). The data were collected on electrodes arranged around the periphery of the tank in such a manner that currents were made to flow under the tank. An electrically similar strategy would be to use electrodes arranged around the periphery of a tank farm (outside the fence) so that current is made to flow under the buried tanks. We believe that this method, or simple variations, could be used to

detect large (thousand gallons) tank leaks. In addition, such a leak detection system could be used to monitor long term the changes in soil properties under of a tank farm.

Points pertaining to possible FY2002 work:

We have been requested to address the following points.

1) Reasons why the method should (or should not) be further investigated.

We believe that the ERT method is ideally suited to detect leaks under tanks and that it should be investigated further for the following reasons.

The method can be adapted to use existing infrastructure (dry wells) thereby reducing deployment costs.

ERT is a mature technology that has been demonstrated in a variety of geologic environments (including the Hanford site) and for a variety of applications. The capability to detect leaks under tanks at Hanford has been demonstrated in 3 separate trials at the Hanford site (Ramirez et al., 1996; Narbutovskih et al., 1996; Ramirez and Daily: this report). The method can detect leaks of the order of several hundred gallons of brine.

Under routine operating conditions, one person can operate the system. Once the system is permanently connected to electrodes within the farm, the operator remains outside the tank farm fence. The ERT data collection process does not require the movement of sensors or probes and so can easily be automated, thereby reducing the need for field personnel.

2) Next steps in deployment.

The performance envelope of the technology with respect to false-positive and false negative detection needs to be investigated.

We need to fully investigate the technique's performance under "low data" conditions. These conditions are expected when few electrode arrays (<=6) are available or when few dry well casings are available. In these situations, relatively little linearly independent data can be collected, thereby reducing the technique's robustness, sensitivity and resolution. The effects of "low data" need to be evaluated using numerical models as wells as field trials.

The technology can be evolved to allow full autonomous/remote operation where the data collection system can be operated without the need for on-site personnel. The system requirements and preliminary costs for such a system need to be developed.

We believe the ERT method can be adapted to detect large leaks (1000+ gallons) using electrodes located outside the fence of tank farm. In this scenario, the cost of deploying borehole electrode arrays should be substantially lower. This scenario needs to be properly evaluated using numerical simulations, physical models and field trials.

3) Estimated costs of further studies relating to deployment.

We estimate these costs to be approximately $350,000 over the next calendar year. The work scope includes activities described in "Next steps in deployment' as well as in participation in field trials planned for FY02. We assume that the field trails will require monitoring over a 5-7 month period at a simulated leaking tank.

As per B. Barnett email request (1/16/02) for estimated costs of deployment in a tank farm, we have assumed that a test lasting 20 days will be conducted. There will be 4 vertical electrode arrays available around the tank that will be provided and installed by PNNL. We have assumed that this test will be concurrent with other tests at the Mock Tank site. LLNL will provide the measurement electronics and personnel for data acquisition, data processing and analysis, and reporting. The estimate for this work is an additional $70,000.00.

4) Estimated (order of magnitude) cost of a permanent operating system.

We estimate the cost of a permanent data acquisition system to range between $50000 and $150000. The costs of deploying electrodes (if any), the costs of the wiring between the electrodes and data acquisition system, and the costs of data processing hardware and software are not included in this estimate.

5) Anticipated problems with deployment in culturally "noisy" areas such as a tank farm.

One issue that needs to be investigated is the interaction between the cathodic protection system used to mitigate tank corrosion and ERT data acquisition. Cathodic protection generates a DC field that may influence the validity of the measurements. Most state of the art data acquisition systems have the capability of correcting for DC signals of a few volts. If the DC field generated by cathodic protection exceeds the measurement system limit, this issue will have to be addressed.

Another possible problem may be the presence of water leaks unrelated to a tank. Normal operations may inadvertently release water into the subsurface that may create electrical resistivity changes similar to released tank waste. Subsurface water mains in the area may release large amounts of water that may create similar changes.

6) Requirements for development of a remotely activated detection system, so as to minimize on site personnel.

We believe that a typical ERT system will minimize on site personnel because the system will be located and operated from outside a tank farm. Wires will connect the electrodes within the farm to the measurement system outside. For tank remediation monitoring, a single ERT operator can easily perform surveys with the all needed equipment located in an equipment trailer or office located outside the farm's perimeter. This means that current ERT systems already achieve the goal of minimal on-site personnel.

A remotely activated system makes sense to be considered for the case of long term monitoring of a tank farm. In this case, the soil under the tanks would be monitored for unexpected changes for periods of many of years. A remotely activated system would eliminate the need for onsite visits to perform surveys thereby reducing personnel costs.

We believe that it is technically and economically feasible to develop an autonomous ERT system that would monitor electrical properties around an active tank(s). While the development of this field-monitoring capability is new, it constitutes an extension of already-proven technology, and has a high expectation for success. This method could also be used with either vertical electrode arrays or long electrodes (casings) that may already be present or those that may be added around a tank(s). Data

interpretation is accomplished using existing computer codes that treat the fully 3D case (the codes have been tested for over 5 years under a variety of conditions). The products will be time dependent maps of the changes in formation resistivity caused by tank waste released. The relatively inexpensive data acquisition system (permanently installed in the field) can be designed to operate autonomously. When information is desired, the operator can call the system up, initiating an acquisition sequence. The system will acquire data in an unattended mode, store and transmit the data stream and shut itself down. Alternatively, the system can be programmed to obtain data periodically on its own.

References

Daily, W. and E. Owen, 1991, Cross-borehole resistivity tomography, *Geophysics, 56,* 1228-1235.

Dines, K. A. and R. J. Lytle, 1981, Analysis of electrical conductivity imaging, *Geophysics, 46,* 1025-1036.

Hearst, J., P. H. Nelson, and F. L. Paillet, 2000, *Well Logging for Physical Properties*, Second Edition, John Wiley & Sons, Chicester, England

LaBrecque, D., Morelli, G., Daily, W., Ramirez, A., and P. Lundegard, 1999, Occam's Inversion of 3D Electrical Resistivity Tomography", *in Three Dimensional Electromagnetics*, eds. M. Oristaglio, and B. Spies, Soc. Expl. Geophys.

Narbutovskih, S., D. Iwatate, M Sweeney, A. Ramirez, W. Daily, R. Morey, L. Christensen, 1996, Feasibility of CPT deployed Vertical Electrode Array in Single Shell Tank Farms, Westinghouse Hanford Co., WHC-SD-EN-TA-004, Rev. 0, Richland, WA.

Ramirez, A., W. Daily, A. Binley, D. LaBrecque and D. Roelant, Detection of Leaks in Underground Storage Tanks Using Electrical Resistance Methods, (UCRL-JC-122180, October, 1995), *J. Engineering and Environmental Geophysics*, *1*, 189-203, 1996.

Oldernberg, D. W. and Y. Li, 1994, Inversion of induced polarization data, *Geophysics, 59,* 1327-1341.

Pelton, W. H., L. Rijo and C. M. Swift, Jr., 1978, Inversion of two-dimensional resistivity and induced-polarization data, *Geophysics, 43,* no. 4, 788-803, June.

Ramirez, A., W. Daily, A. Binley and D. LaBrecque, 1999, Electrical impedance tomography of known targets, *J. Env. Eng. Geoph., 4,* 11-26.

Ramirez, A., W. Daily, A. Binley, D. LaBrecque and D. Roelant, Detection of Leaks in Underground Storage Tanks Using Electrical Resistance Methods, (UCRL-JC-122180, October, 1995), *J. Engineering and Environmental Geophysics*, *1*, 189-203, 1996.

Sasaki, Y., 1992, Resolution of resistivity tomography inferred from numerical simulation, *Geophysical Prospecting, 40,* 453-463.

Tripp, A. C., G. W. Hohmann and C. M. Swift, 1984, Two dimensional resistivity inversion, *Geophysics, 49*, 1708-1717.

Weller, A., M. Seichter, and A. Kampke, 1996, Induced polarization modeling using complex electrical conductivities*, Geophysical Journal International*, 127, 387-398.

Wexler, A., B. Fry and M. R. Neuman, 1985, Impedance-computed tomography algorithm and system, *Applied Optics, 24,* no. 23, 3985-3992, December.

Yorkey, T. J., J. G. Webster and W. J. Tompkins, 1987, Comparing reconstruction algorithms for electrical impedance tomography, *IEEE Trans Biomedical Engineering, BME-34,* no. 11, 843-852, November.

Yuval, and D. W. Oldenberg, 1997, Computation of Cole-Cole parameters using IP data, *Geophysics*, 62, no. 2, 436-448.

Appendix A1

Estimates of changes in soil resistivity caused by plume infiltration

Infiltration of the sodium thio-sulfate solution caused increases in pore fluid salinity and increases in saturation. We have used Archie's (Hearst, *et al.,* 2000) equation to estimate soil resistivity as a function of saturation and the pore fluid's resistivity. The results of this simple model are shown in Figure A.1. We calibrated the model to produce a bulk resistivity of 1000 ohm-m based on the resistivity logs measured by Applied Research Assoc. prior to the start of the FY 00 work at the Sisson and Lu site. The model assumed that the ambient properties were as follows: saturation was 0.4, porosity was 0.3 and the resistivity of the ambient pore fluid was 30 ohm-m (a factor of 2.5 smaller than river water). Measurements of the resistivities for the various fluids considered are shown in Figure A.1.

The curves in Figure A.1 help illustrate that the primary mechanism affecting the measured changes in resistivity is the change in fluid salinity created by the highly conducting, sodium thio-sulfate brine. If we assume that the brine causes the fluid conductivity to change from 30 ohm-m to 0.1 ohm-m ands there is 0.0 saturation change, the bulk resistivity changes a factor of 100. Conversely, if the salinity remains fixed while the saturation changes from 0.4 to 1.0, the bulk resistivity changes a factor of about 5. This suggests that, for the case of sodium thio-sulfate infiltration, the tomographs of resistivity change are 20 times more sensitive to salinity changes than to saturation changes.

Appendix A2

Numerical modeling of current density – indicator of sensitivity

It is important to understand how the sensitivity of the measurements varies within the region of interest to properly interpret images of electrical resistivity under a steel tank. The steel shell of the tank has electrical properties that are vastly different than those of the surrounding soil. These differences have a large effect on measurement sensitivity to changes occurring in the soil beneath the tank. We have performed numerical simulations to provide a qualitative understanding of measurement sensitivity to regions below the tank. We have used current density as an indicator of measurement sensitivity. Simply stated, the electrical measurements are most sensitive to regions in which current preferentially flows, i.e., regions of high current density.

Figure B.1 shows the results of the modeling. The drawings on the left column of the figure indicate the various electrode configurations considered. The modeling assumes that each electrode is injecting one ampere of current. Note that cases with and without the tanks are included (middle and rightmost columns of images). The top row of images in the figure shows the current density when two steel cased wells are used as long electrodes. The highest current densities occur along the steel shell and in the near vicinity of the steel casings. Relatively high current densities are also observed along the soil next to the tank's perimeter. The region of lowest current density occurs directly below the tank's center.

These results suggest that measurements made with long electrodes have the lowest sensitivity in the soil just below the center of the tank. The release point for the field experiment was located near the center of the tank. This means that the long electrode measurements had the least amount of sensitivity to the soil region invaded by the plume. This helps explain the relatively small changes measured with the long electrodes. Substantially higher sensitivity is expected for leaks that develop along the tank's perimeter.

The second and third rows of images depict the current densities for short electrodes located close to and away from the tank. These images also suggest that a most of the current is channeled through the steel shell and that the lowest current density is in the soil just below the tank's center. However, because the electrodes are short, current flow is much more focused than for the long electrodes. Therefore, short electrodes yield higher current densities in localized regions, including the soil beneath the tank's center. This may be the reason why the 3D ERT tomographs show much larger resistivity changes than the long electrode tomographs.

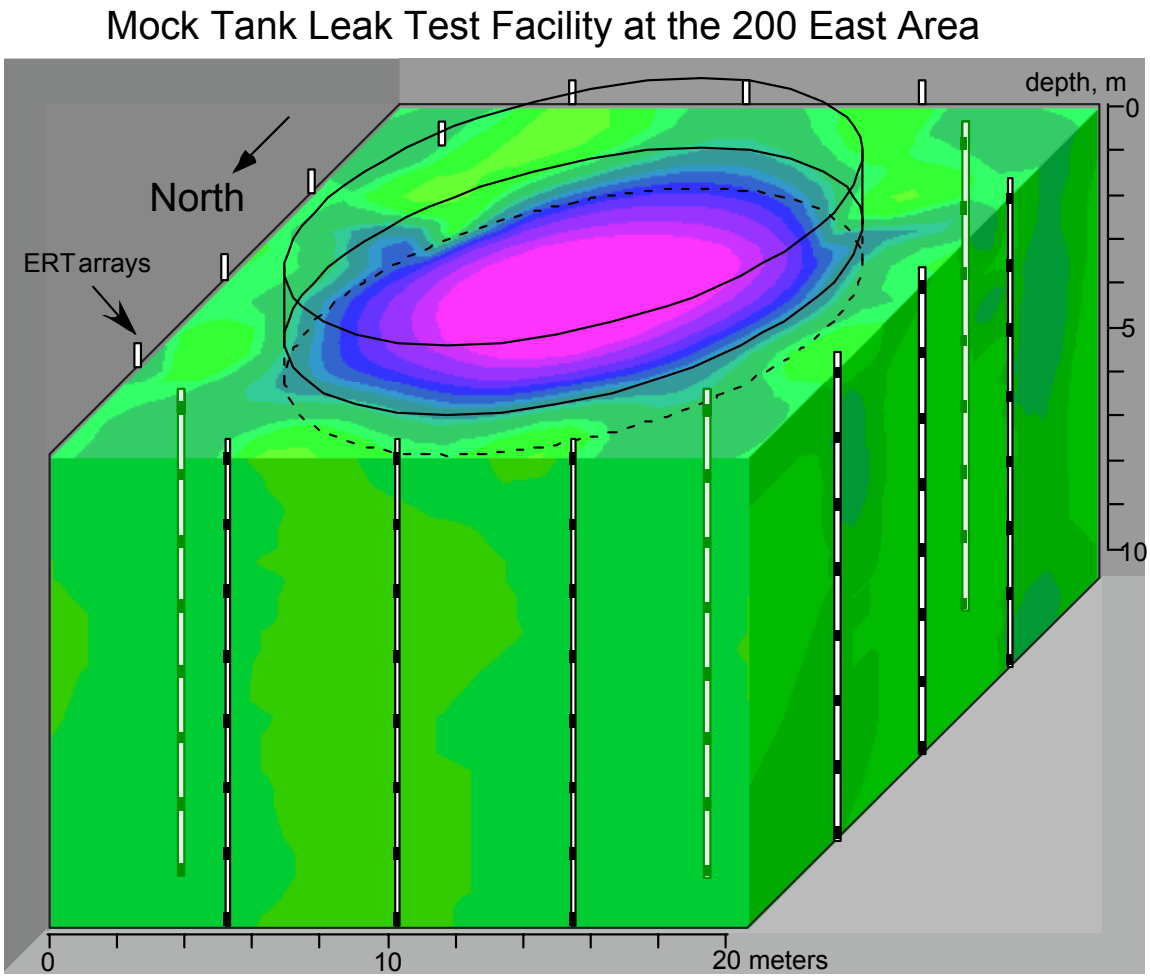

Figure 1. The point electrode model for the mock test site. The image shown is a 3D reconstruction of baseline conditions.

Geometric Mean of Apparent Resistivity-Simple Leak Detection Approach

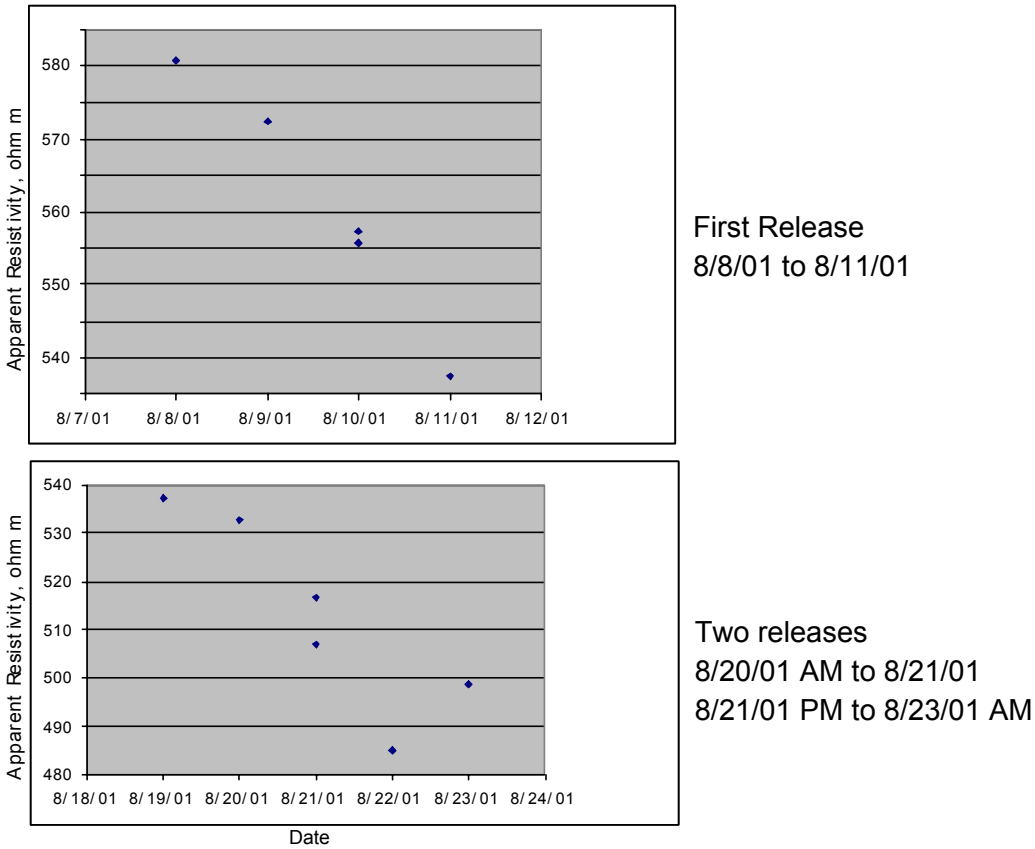

Figure 2. The figure shows the geometric mean of apparent resistivity beneath the Mock Tank during the two separate releases.

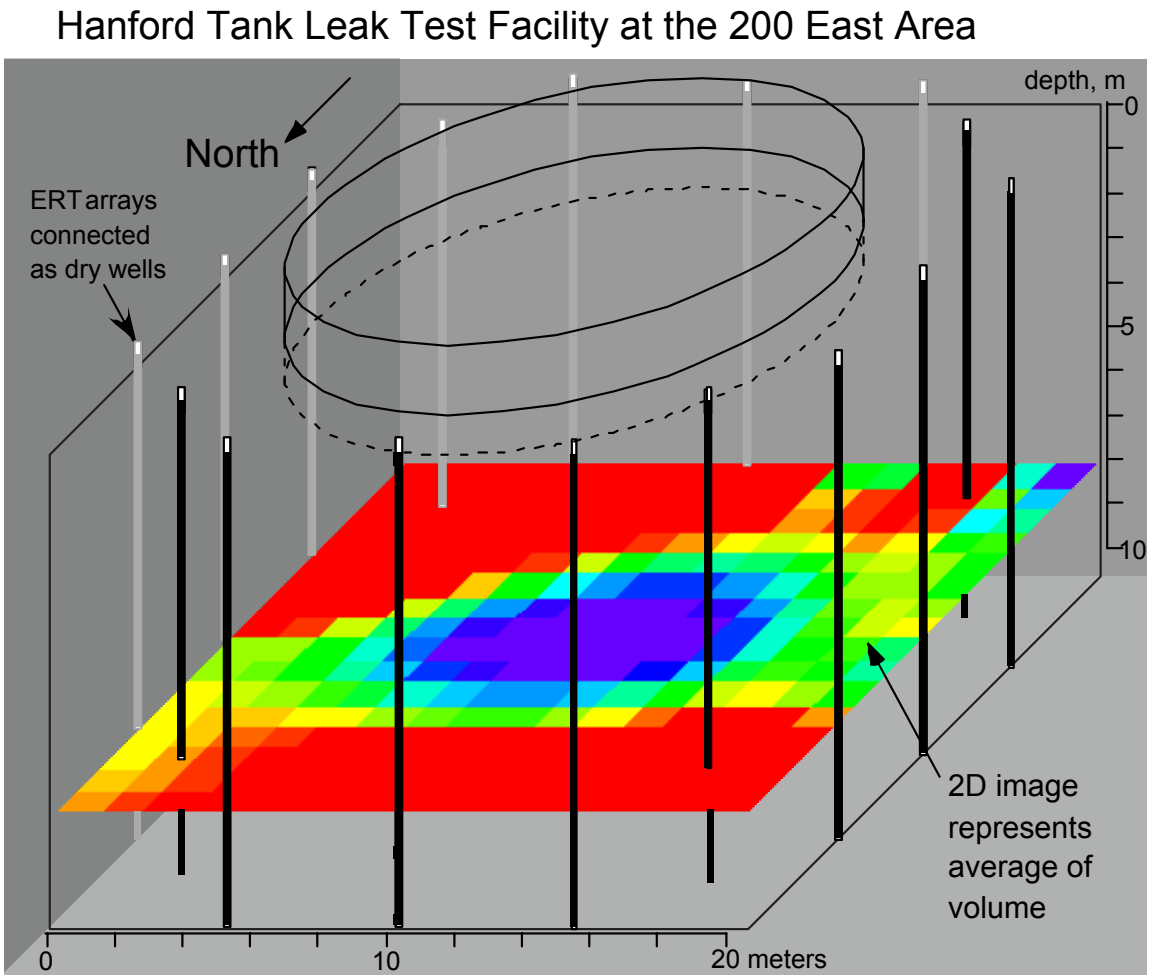

Figure 3. The dry well model for the mock tank test site. The image is shown as a plane but is actually an average of volumetric resistivity.

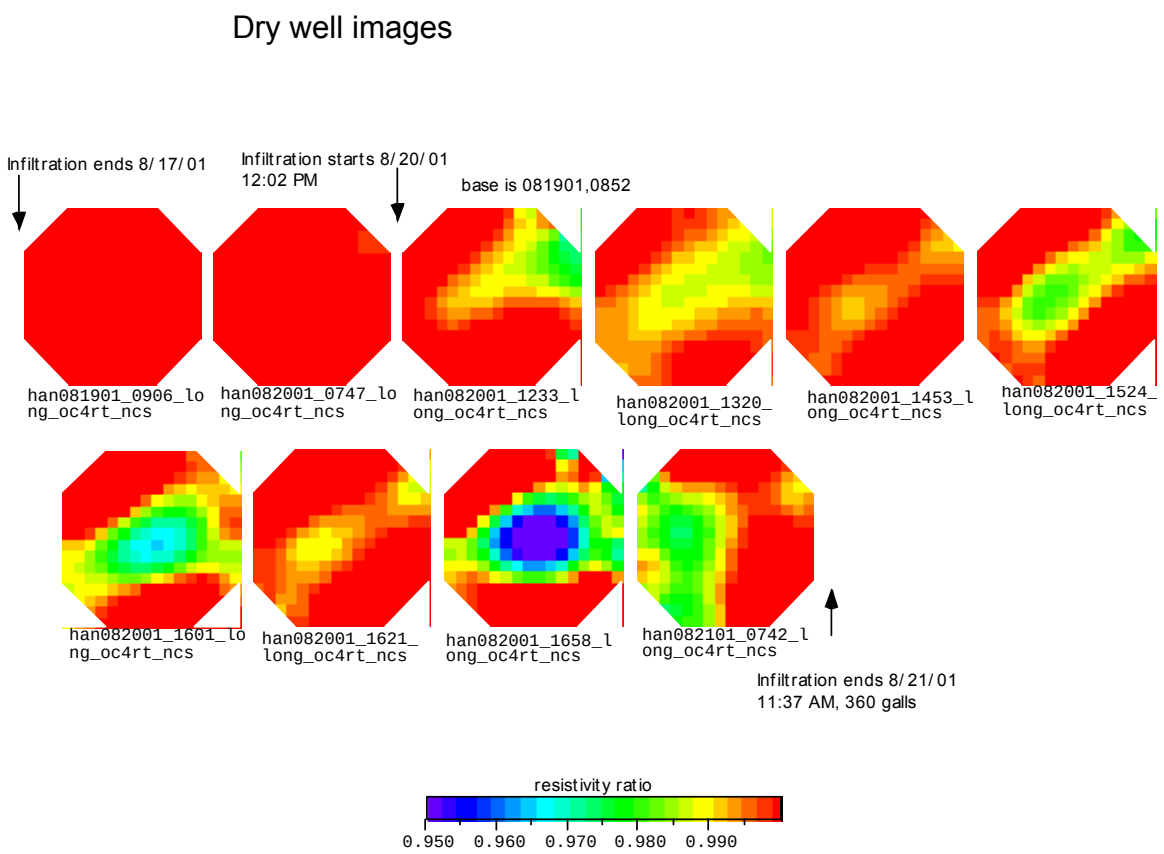

Figure 4. Sequence of 2D images using sixteen long electrodes during the final release.

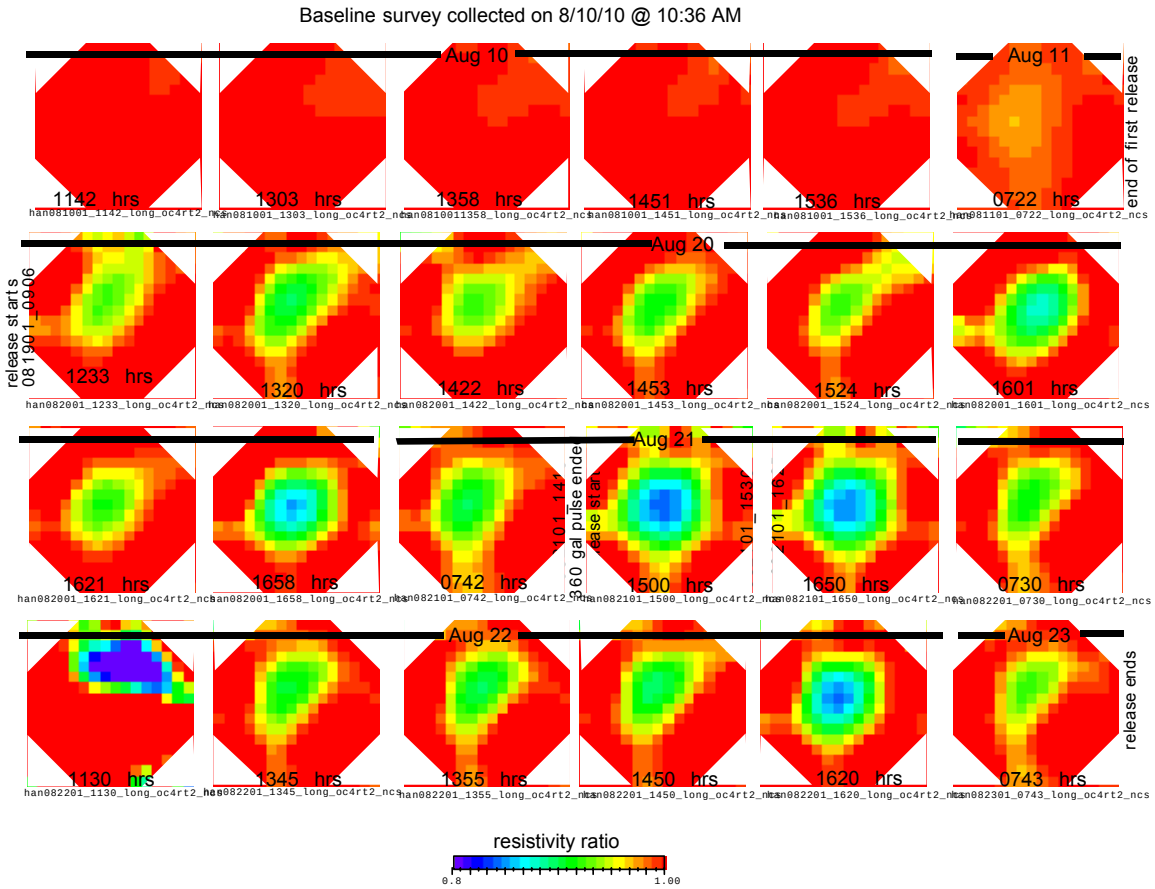

Figure 4a. Sequence of 2D images using sixteen long electrodes. All images calculated relative to a common baseline survey collected on 8/10/01, 10:36 AM.

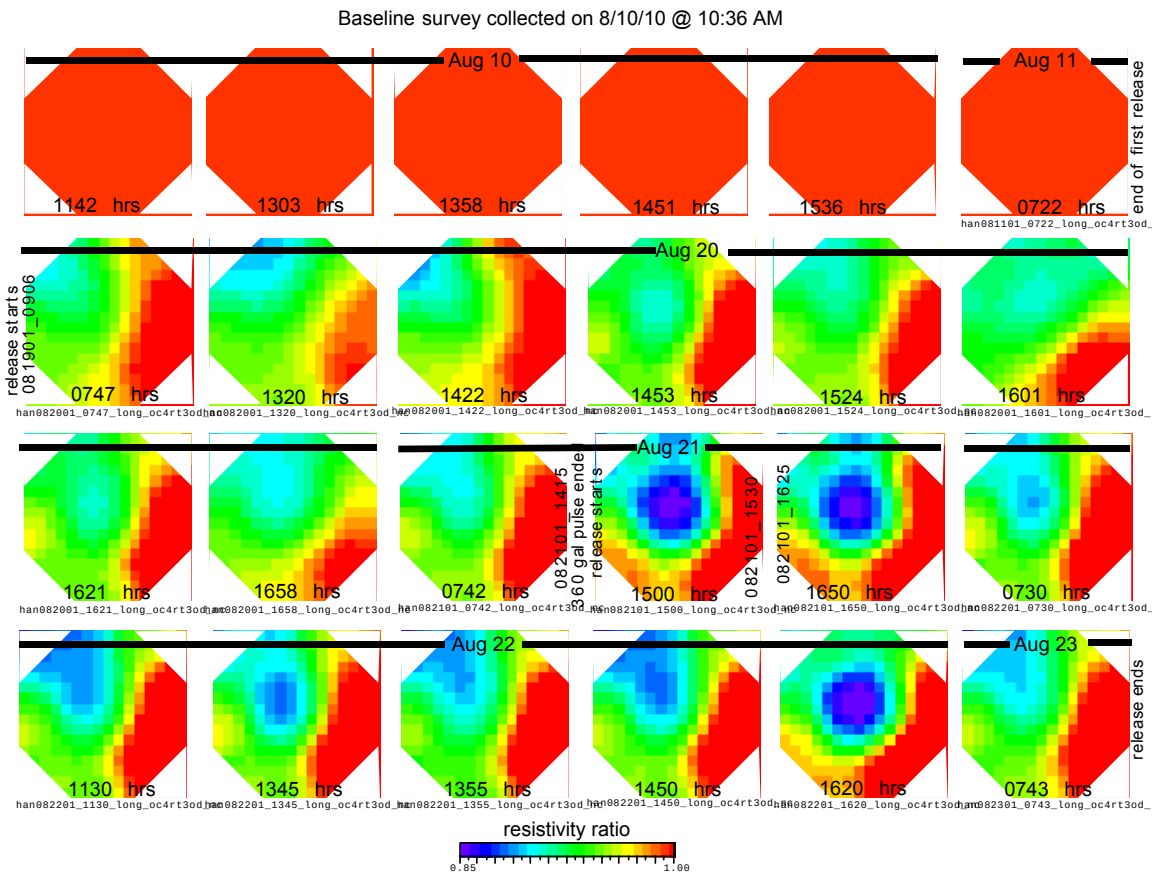

Figure 4b. Sequence of 2D images using only eight long electrodes. All images calculated relative to a common baseline survey collected on 8/10/01, 10:36 AM.

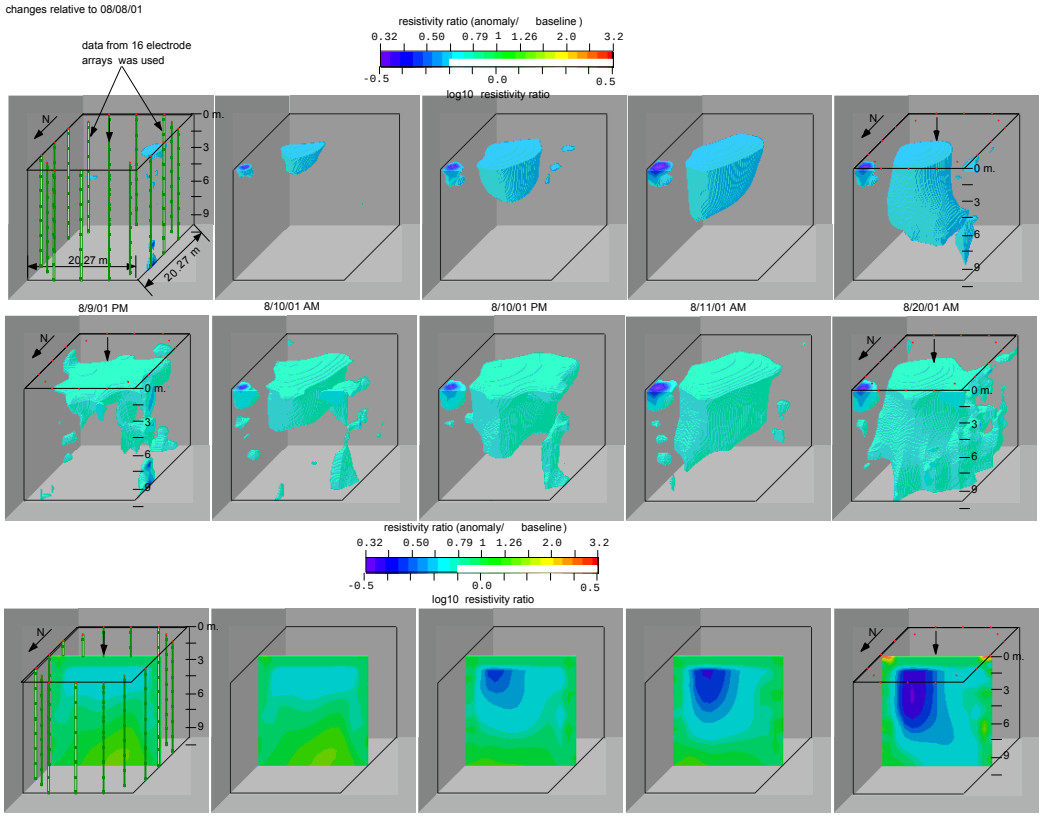

Figure 5. Three-dimensional ERT showing a history of the first three releases. Sixteen electrode arrays were used to collect the data. The first row uses a transparency (sensitivity) threshold of 0.2 to depict changes in resistivity while the second row uses a threshold of 0.1. The bottom row shows a single vertical section through the same 3 D reconstruction.

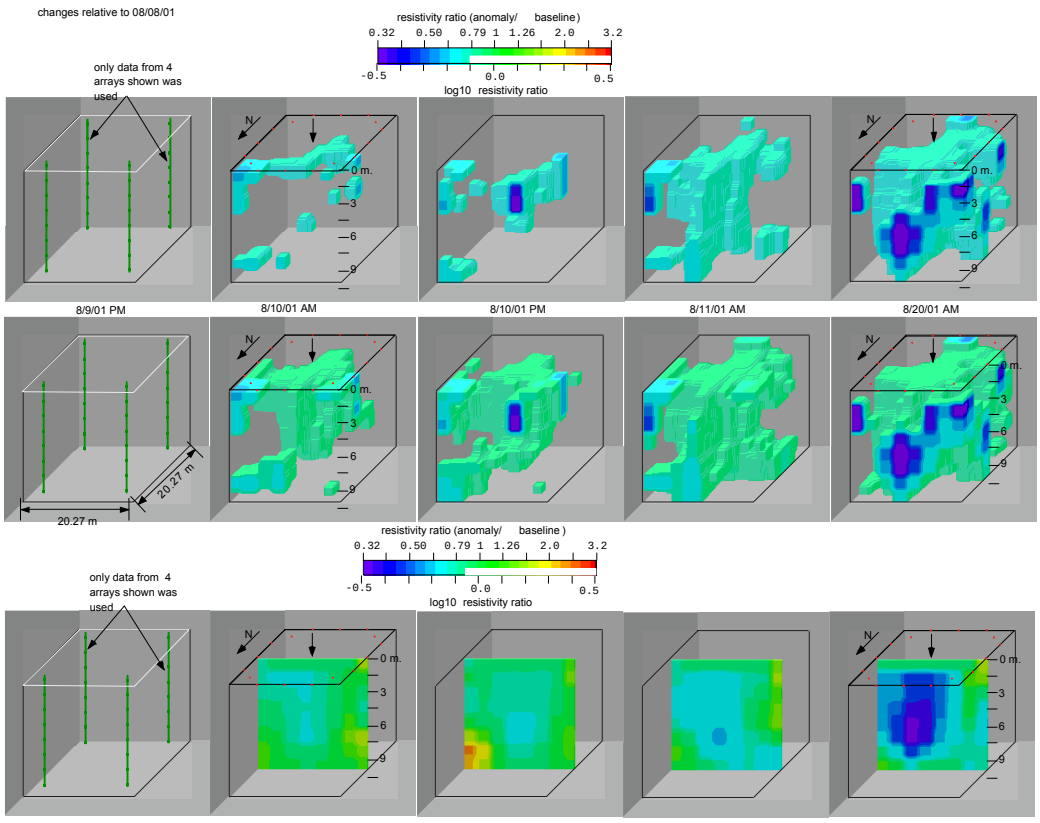

Figure 5a. Three-dimensional ERT showing a history of the first three releases. Only four electrode arrays were used to collect the data. The first row uses a transparency (sensitivity) threshold of 0.1 to depict changes in resistivity while the second row uses a threshold of 0.05. The bottom row shows a single vertical section through the same 3 D reconstruction.

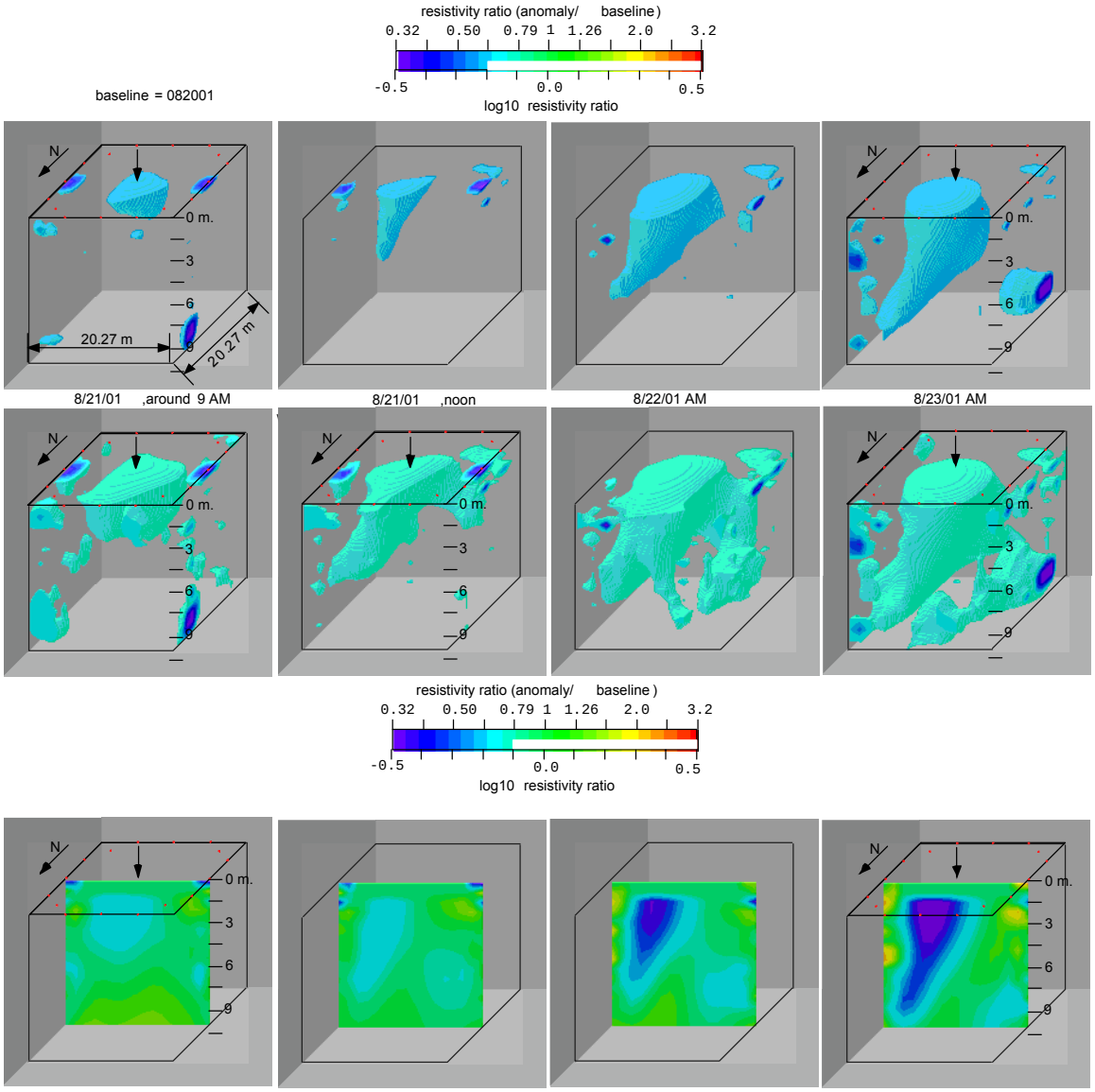

Figure 6. Three-dimensional ERT showing a history of the fifth release. The data was collected using 16 arrays of point electrodes. The format is the same as in Figure 5.

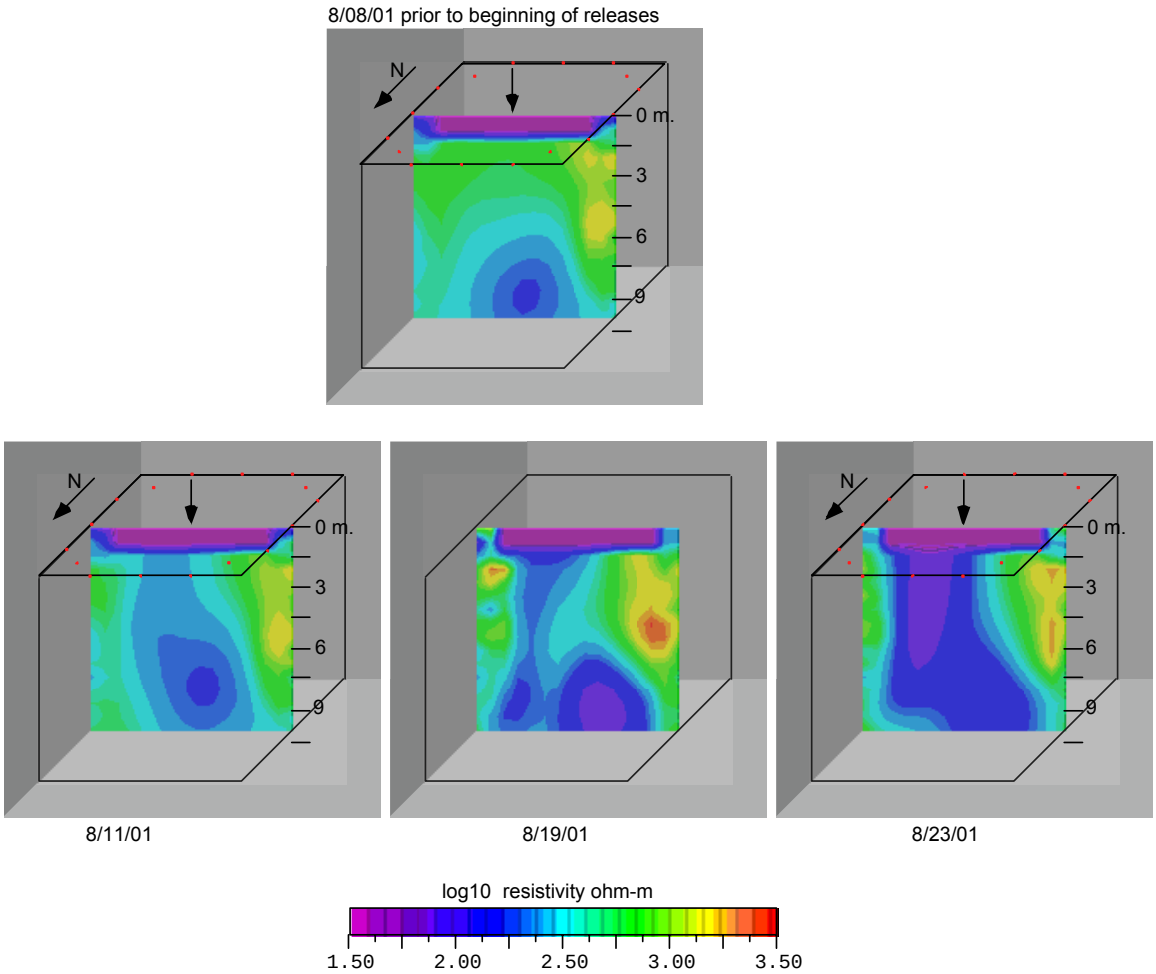

Figure 7. Three-dimensional ERT showing a history of all releases during the experiment. The data was collected using 16 arrays of point electrodes. These reconstructions are **not** of changes in resistivity but rather show the actual values of resistivity beneath the tank at selected times. Only a single slice through the 3 D volume is shown here.

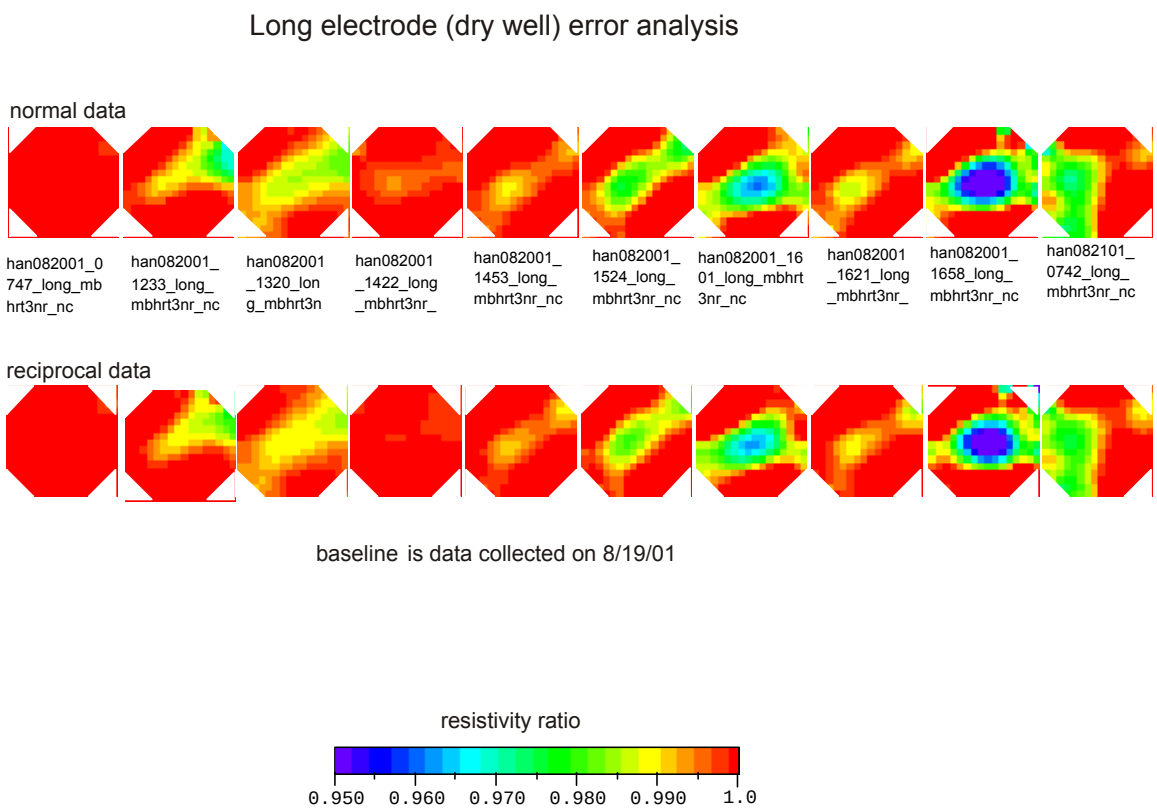

Figure 8. Error analysis for the long electrode ERT approach. The data was collected using 16 long electrodes.

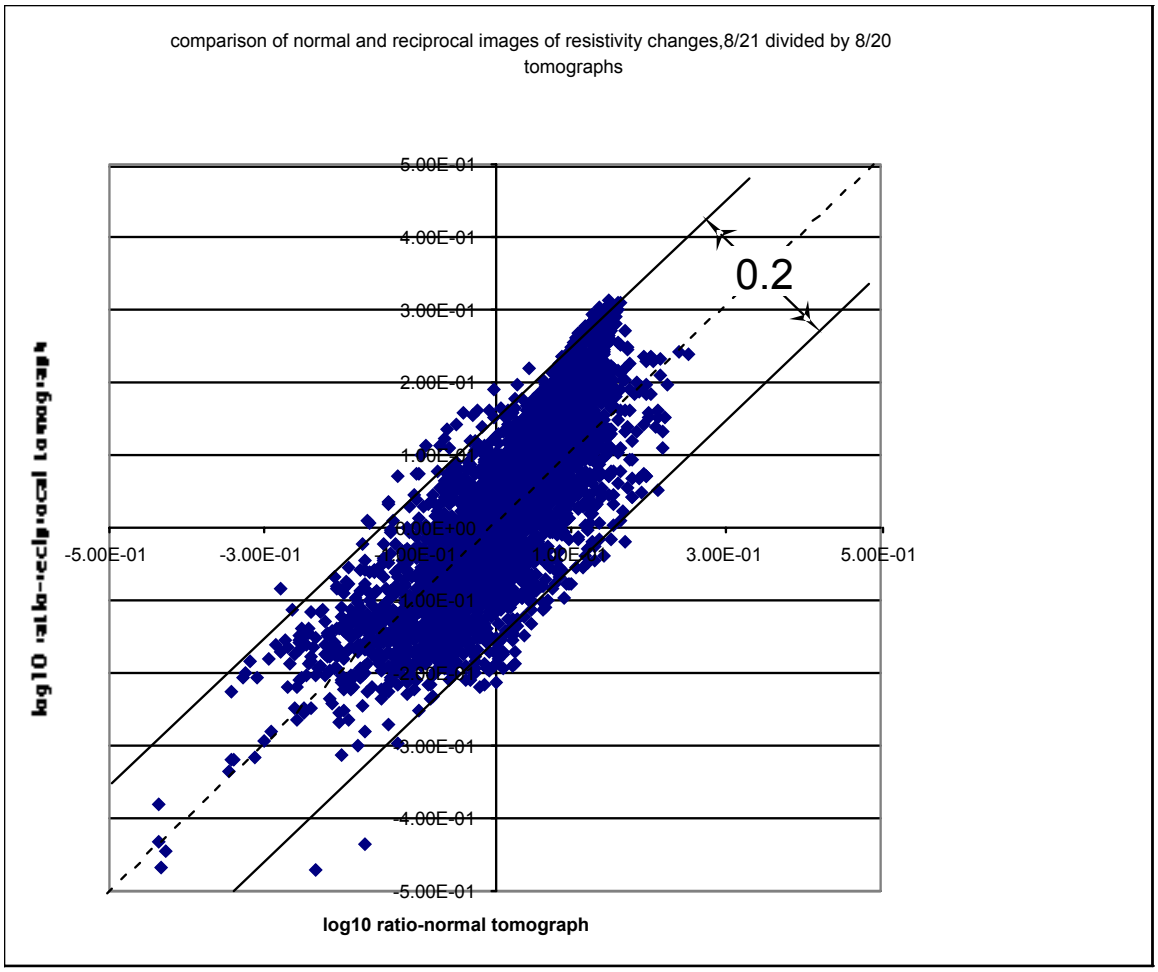

Figure 9. Error analysis for the 3D ERT reconstructions. Axes are the reconstructed ratios for the normal and reciprocal data. A reasonable error in the logarithm of the resistivity ratio is about +/- 0.1 (0.2).

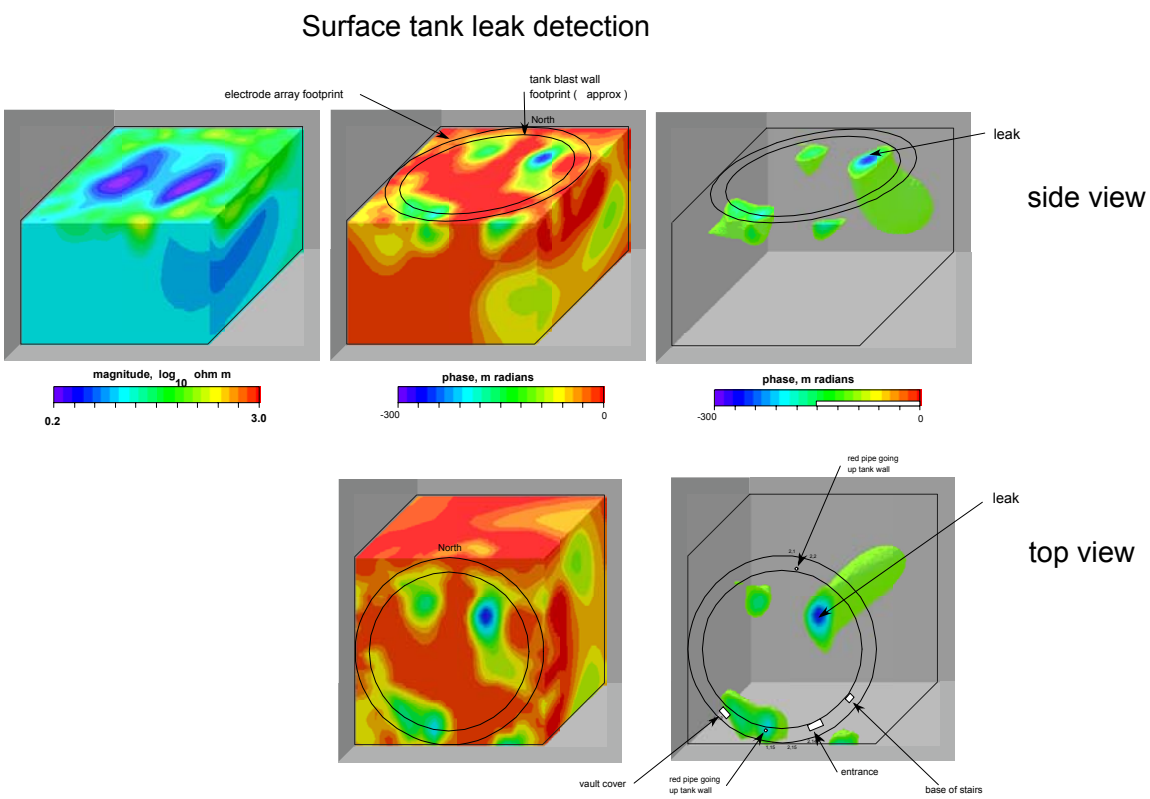

Figure 10. ERT image under a surface fuel storage tank using a ring of electrodes on the ground surface around the tank.

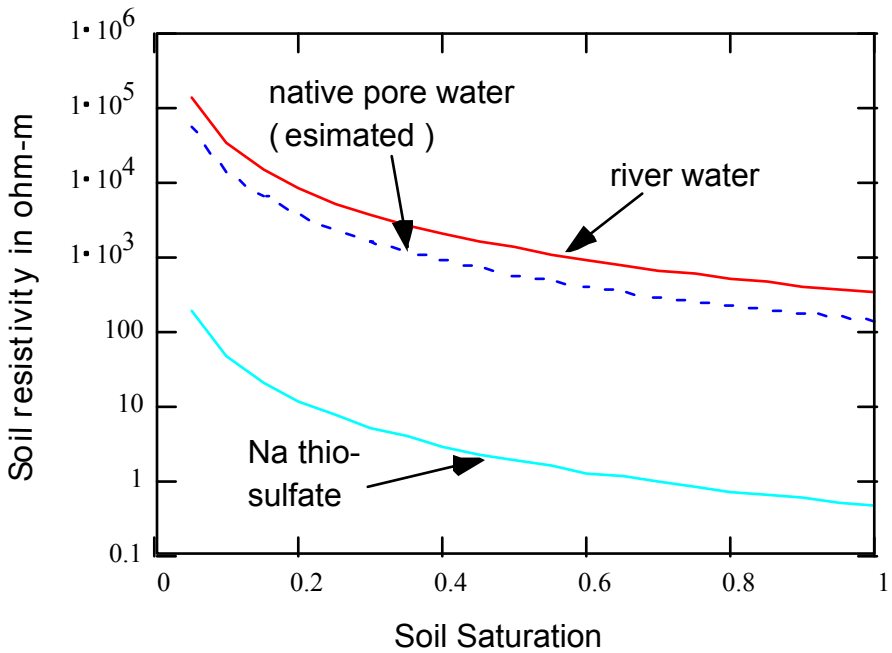

<u>assumptions</u> :

1) mimimal surface conductance
2) porosity = 0.3
3)saturation exponent = 2.0
4)cementation exponent =1.3
5)river water = 70 ohm-m (measured)
6)natural pore water = 30 ohm-m(assumed)
7) sodium thio-sulfate solution = 0.1 ohm-m (measured)

Figure 11. Archie's equation for soil saturation and soil water resistivity expected at the mock tank site.

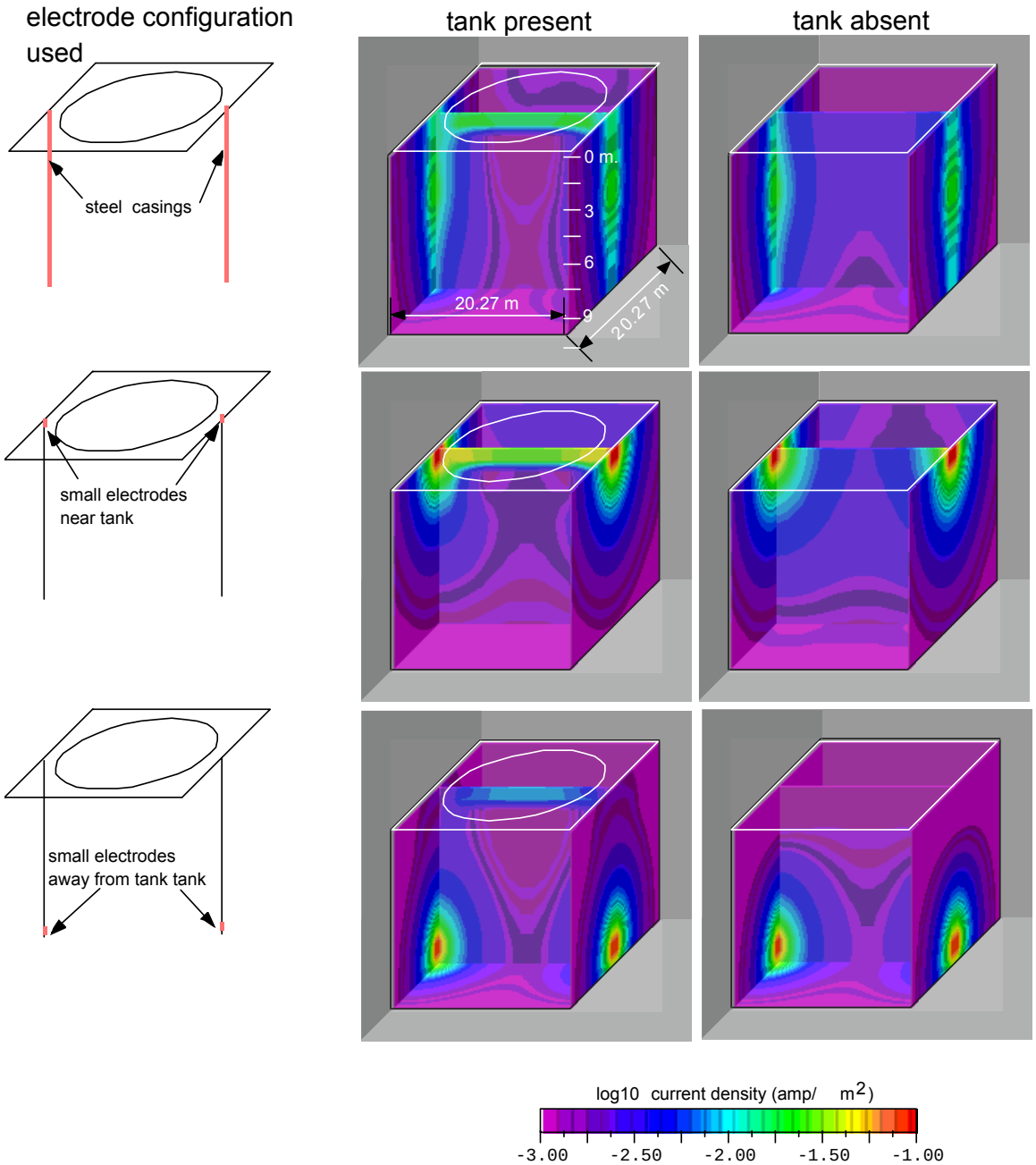

Figure 12. Numerical modeling results showing the current densities associated with three different electrodes configuration. Scenarios with and without the tank are considered. Regions of high current density (shown in the warmer colors) indicate regions to which the measurements have the highest sensitivity.

Appendix B

Mock Tank High-Resolution Seismic and Radar Measurements

Appendix B

Mock Tank High-Resolution Seismic and Radar Measurements:

Final Report Feb 28, 2001

E. L. Majer, K. H. Williams. T. M. Daley and J. E Peterson

Lawrence Berkeley National Laboratory

To test the applicability of radar and seismic methods for tank leak detection measurements were made before, during, and after the mock tank injection in July and August of 2001. Tests at the Sisson and Lu sites in FY 2000 and mid 2001 indicated that radar was sensitive to water influx and even more sensitive to the saturated sodium thiosulfate solution. For example, Figure 1 shows radar cross sections at the Sisson and Lu site for the 2000 injection (river water only) and the 2001 injection (sodium thiosulfate). This cross section was taken after 500 gallons had been injected. As can be seen the fluid was imaged very well. The white area in the 2001 data means that the radar signal was attenuated too much to be used. In addition to the radar tests the seismic tests at the Sisson and Lu site indicated that porosity definition and possibly water content could also be measured. The seismic tests, however, were not as extensive as the radar tests, in that only one set of measurements were made at the end of each set of injections, therefore no time lapse difference images could be made as in the case of the radar.

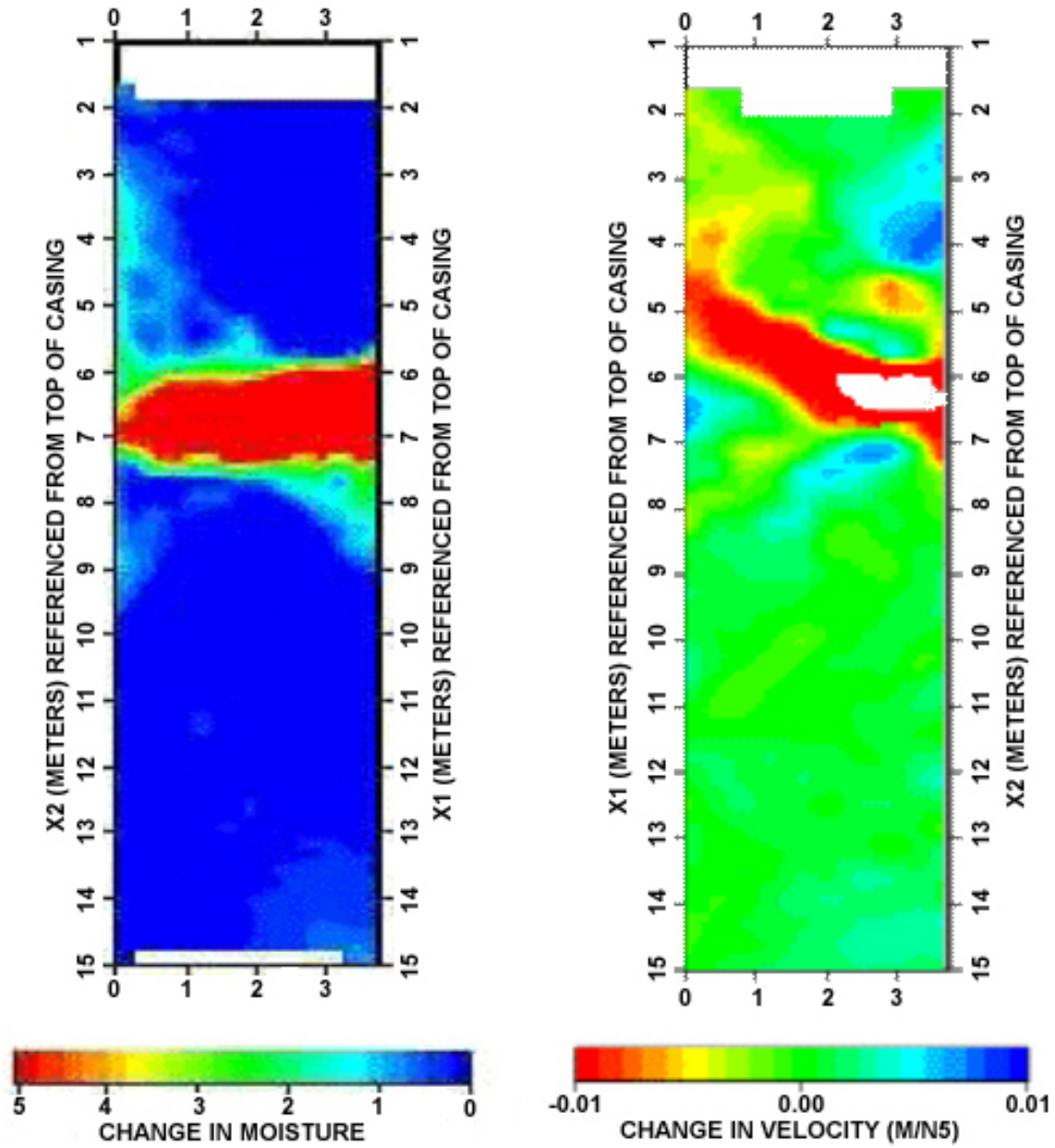

Figure 1. The 2000 and 2001 radar results after 500 gallons of water (2000) and sodium thiosulfate (2001) were injected approximately 1 meter behind the plane of the well pairs The objective of this effort was to test the sensitivity of the two methods at a scale larger than the Sisson and Lu scale, rather than do a comprehensive mapping of the release of the sodium thiosulfate beneath the mock tank. In any "real" application of the method it is unrealistic to expect to have a large number of boreholes available to perform cross well tests. In fact, the number of boreholes available to the seismic test at the mock tank site was even less (3) than the radar, (6) making the lack of holes a particular constraint in the seismic tests.

Radar

100-Mhz radar measurements were carried out at the mock tank. 50 Mhz was also tried in one cross section (8 to 16) to determine how far radar would propagate here, but since 100 Mhz gave good results we used it for all of the cross sections. Six wells were used for the radar measurements, ERT wells 15, 16, 1, 9, 8, and 7. The 100-MHz radar transmitter was placed in wells 7, 8, and 9 while the radar receiver antenna was placed in wells 15, 16, and 1. Therefore in total nine different cross-well sections were obtained, i.e. 9 to 15, 9 to 16, 9 to 1, 8 to 15, 8 to 16, 8 to 1, 7 to 15, 7 to 16, and 7 to 1, using the 100 MHz antenna (see Figure 2). The cross well zero offset data were obtained from the bottom of each well (approximately 10.25 meters from the top of each ERT well) at ¼ meter intervals to within one meter of the top of the ERT wells. In addition to the 100 MHz data, a single cross section of 50 MHz data was obtained at ¼ meter intervals between well pair 7 to 15. The 50 Mhz data was acquired to test the difference in sensitivity between the 50 and 100 Mhz systems, rather than obtain two entirely different data sets.

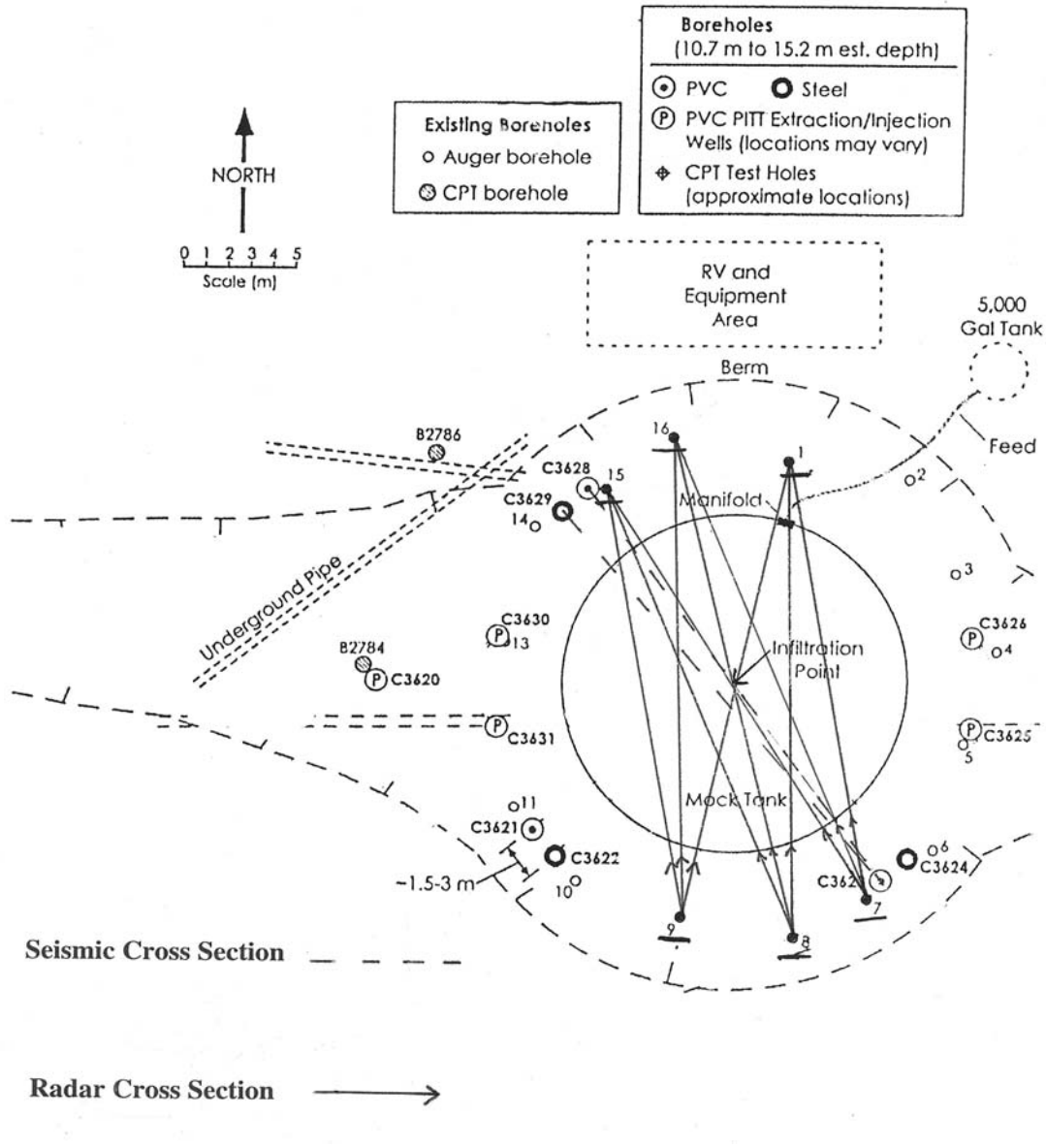

Figure 2. Map view of the crosswell paths used in the radar and seismic tests. Notice the lack of holes compared to the 16 ERT holes.

In total six different radar sets were obtained. The first measurement set was the background data set obtained on July 18, 2001. This data was intended to serve as a reference baseline to which all others could be compared. The next four sets of data were obtained on the first and second day of the spill (August 9 and 10). Set two in the morning (at 11:00 AM) of the onset of the spill. Set three the afternoon (at 4:00 PM) of August 9. Set four in the morning of August 10 (9:00 AM), and set 5 in the late afternoon (at 5:00 PM) on August 10 of the spill.

The last data set was obtained the morning of the first day after the last spill on August 28. There was an attempt to measure an intermediate time period on August 18, but unfortunately the radar equipment malfunctioned and no data was recorded.

Seismic

The experience at Sisson and Lu indicated that by using a relatively powerful seismic source (AC orbital source, 50 Hz to 400 Hz) data could be propagated through the Vadose zone at long enough distances to be of use at the tank scale. To perform a relatively low cost test of the seismic method, a 24 level hydrophone array (½ meter spacing) was used as a receiver string and the orbital vibrator was used as a source. Both the source and receiver requires acoustic coupling to the soil. This can be achieved by clamping or "cementing" the sources and receiver in place, or less optionally, using fluid filled holes. Because these instruments were not dedicated to this project, we chose to use fluid coupling of the sources and receivers, even though it did not provide the most optimal signal. This presented some logistical problems because it was assumed that if the holes we used leaked water, it could interfere with the electrical measurements. Therefore, we were restricted to use relatively few holes compared to other methods (only those holes that did not leak, were lined with a plastic liner to prevent leakage, or only had minimal leakage). Thus only holes C3623 (PVC cased hole) and C3629 (steel cased well) and C3628 (PVC) holes were allowed to be used for the seismic tests. As stated in the introduction of this report this severely limited the testing of the seismic methods. Another unique restriction was that at the time of the background seismic measurements (July 18, 2001) the steel cased wells were not in place so only C3623 and C3628 (the two new PVC cased 6 inch wells) were available.

The approach was to place the 24 level ½ meter spacing hydrophone in the plastic lined, water-filled well C3628. The source was placed in well C3623 (not plastic lined because it held water without leaking) and activated ever ½ meter. This was done on July 18, 2001. Due to leakage concerns we were not allowed to make measurements at the beginning of the spill on August 8th. Therefore, on August 18 when one of the steel cased was made available (C3628) this well was used as a receiver hole for the 24 element, ½ meter hydrophone receiver string while using well C3623 as the source well. Thus two cross sections were obtained on August 18. The last set of seismic data was collected on August 28 using well pair C3623 and C3629. Well C3628 could not be used due to the liner blocking access to the well. Overall the seismic tests were minimal and not deemed representative of the method. In addition to the above problems the wells used were new with loose packing around the well. It was noticed that during the seismic measurements the backfill around the source well settled a few feet! Thus indicating poor contact to the rest of the formation. This would not be the case for wells that had been cemented in place or for wells over several months old.

Results

Seismic

Figures 3, 4, 5, and 6 are representative data sets from each of the data gathering sessions. Figure 3 is a common receiver gather (same receiver but all the different source positions) from the July 17 session for the two PVC wells used by the seismic with the source at a depth of 5 meters in the source well. Figures 4, 5 and 6 are the same data sets for the PVC to PVC seismic on Aug 18, the Steel to PVC on Aug 18, and the PVC to Steel on Aug 28 respectively.

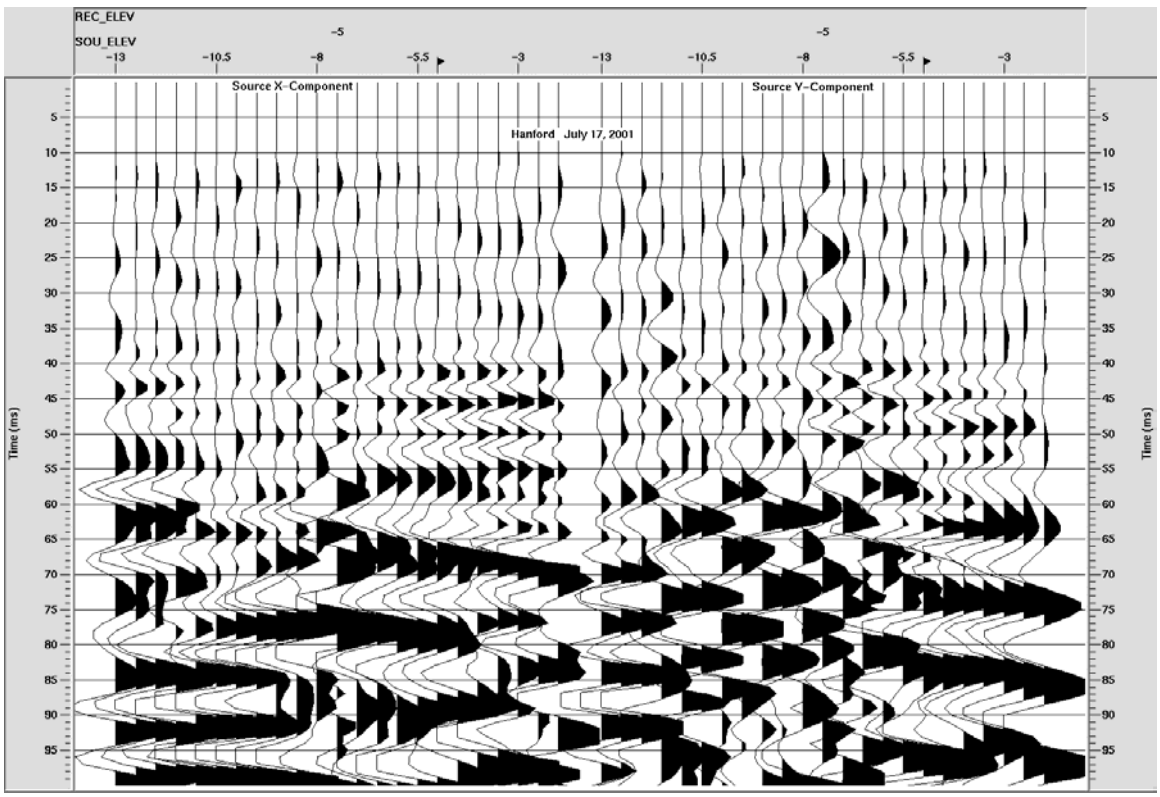

Figure 3. Seismic data on July 17, 2001. Common receiver data for source at 5 meters depth in the PVC source well. The arrival of interest is the one between 40 and 45 milliseconds (P-wave)

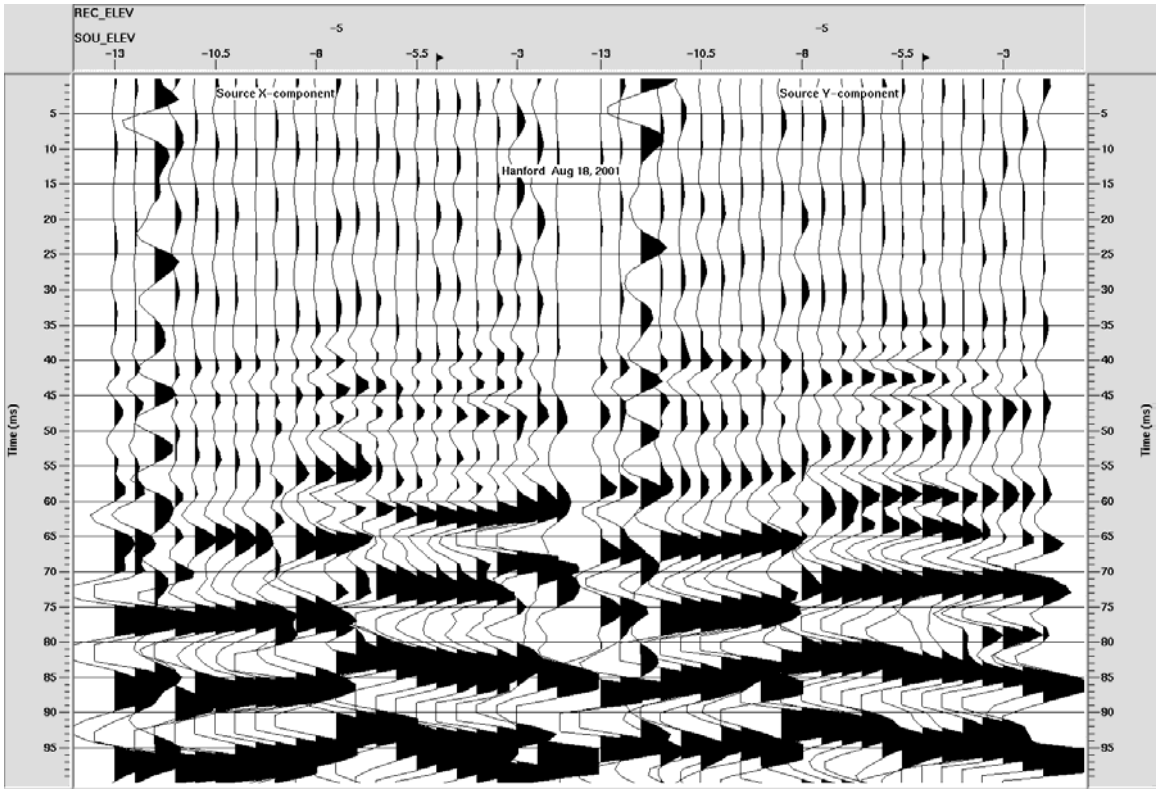

Figure 4. Seismic data on August 18, 2001. (PVC to PVC) Common receiver data for source at 5 meters depth in the PVC source well. The arrival of interest is the one between 40 and 45 milliseconds (P-wave)

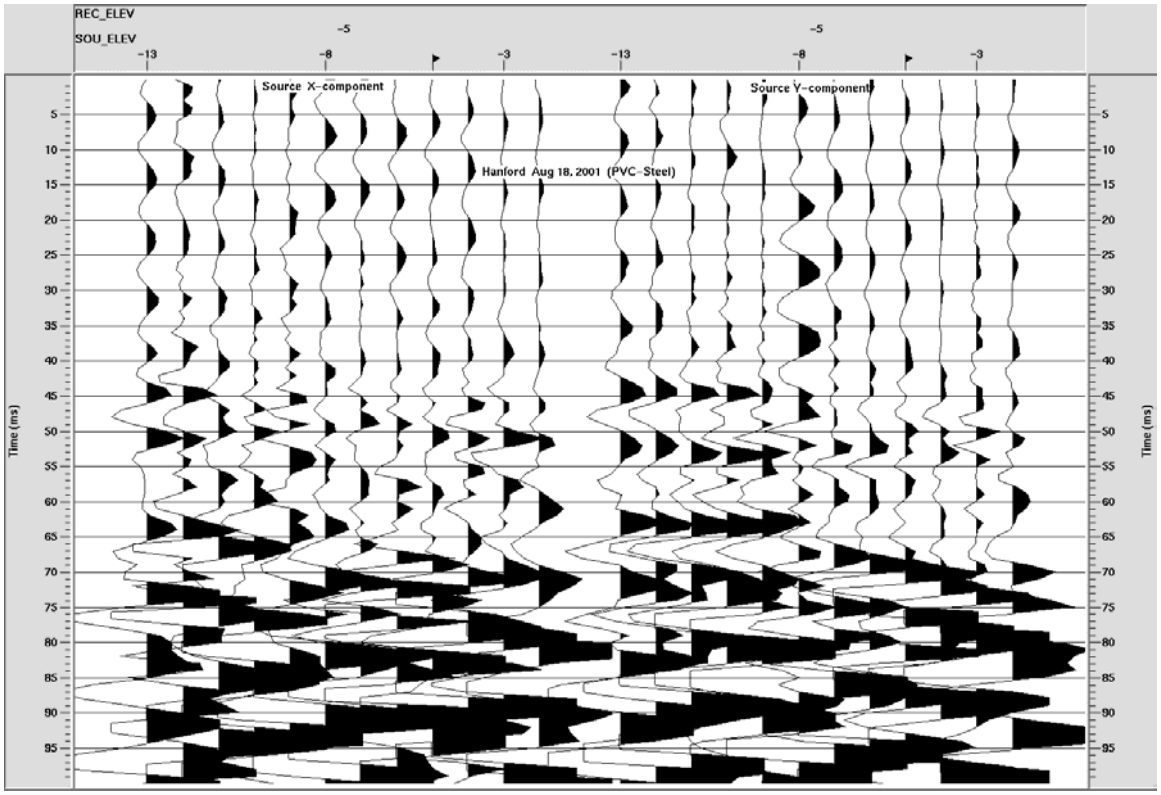

Figure 5. Seismic data on August 18, 2001, (PVC to Steel) Common receiver data for source at 5 meters depth in the PVC source well. The arrival of interest is the one between 40 and 45 milliseconds (P-wave)

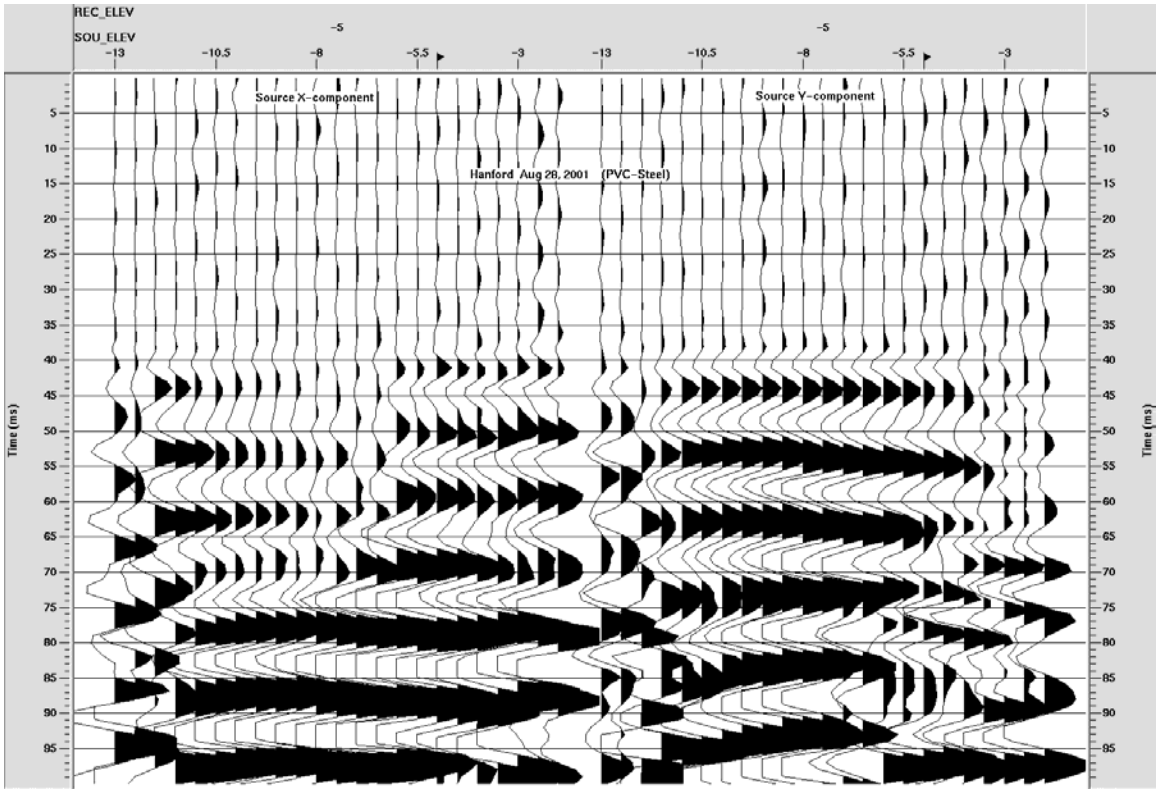

Figure 6. Seismic data on August 28, 2001, (PVC to Steel) Common receiver data for source at 5 meters depth in the PVC source well. The arrival of interest is the one between 40 and 45 milliseconds (P-wave)

.

Of note is the difference between the data plots. The seismic data, if it is sensing the fluid, should improve with time, opposite to the radar data. Seismic is very sensitive to detecting the difference between near and fully saturated sediments (95 to 100 percent saturation). Figure 6 shows the greatest change (increase in amplitude) from the base line data set (Figure 3), i.e., note the increase in amplitude in the 40 to 50-millisecond time window. The data set in Figure 6 was taken immediately after the last spill of fluid. This data set indicates that the fluid is distributed from a few meters (2 to 2.5 meters below the ground surface) meters below the tank (where the large amplitudes in the 40 to 50 millisecond window appear) to a depth of at least the borehole length. In the Aug 18th set there does not seem to be much of a change from the background. This may be due to the fact that enough fluid had gone by to fall below the saturation detection level or the fluid had not intersected the plane of the fairly limited seismic data.

Radar

The radar data are of much higher quality than the seismic, also of much higher quantity. Figures 7 through 15 are time lapse plots the log of the amplitude difference between the data set collected on the morning of August 9 and the data sets collected on the afternoon of August 10 (post2), the data collected on the afternoon of August 10 (post4), and the last data set collected with radar after the completion of the spill (post5). Displayed in these figures are the amplitude differences along each crosswell radar time series trace. Note that the horizontal axis is time not distance. Red means a large change from the first reading on August 8; blue means no change.

As can be seen from these figures the greatest change (most red) is in cross sections 7-15, 7-16 and 8-1 (Figures 13, 10, and 8, respectively). (Note however, that in all sections the changes in the shallow part of the wells should be ignored; i.e., the changes shallower than 2 meters (¼ left hand side of all figures) these are due to surface noise and tank interference. In these three sections the change is along the total depth of the well. In section 7-1 there is a change at depth only. In some sections there is little or no change, i.e., 8-15, 9-15 and 9-16 (Figures 14, 15, and 12, respectively). There are some changes in 9-1 and 8-16 and 8-15 (Figures 8, 11, and 14, respectively). Referring to ray paths in Figure 2 we interpret this to mean that initially the fluid went relatively straight down beneath the injection point. Therefore it appears that the "plume"was drifting to the southeast of the injection point, but mainly down. The north-south extent is constrained by the 9-1 and 7-15 paths. The 9-1 path detected it slightly, while the 7-15 path detected it shallow and deep. There are not enough ray paths to perform a true tomography on these data (more ray paths would allow this), but the results indicate that the radar was very sensitive to the fluids at small volumes. From these data, it seems that the leak solution went straight down, then to the southeast.

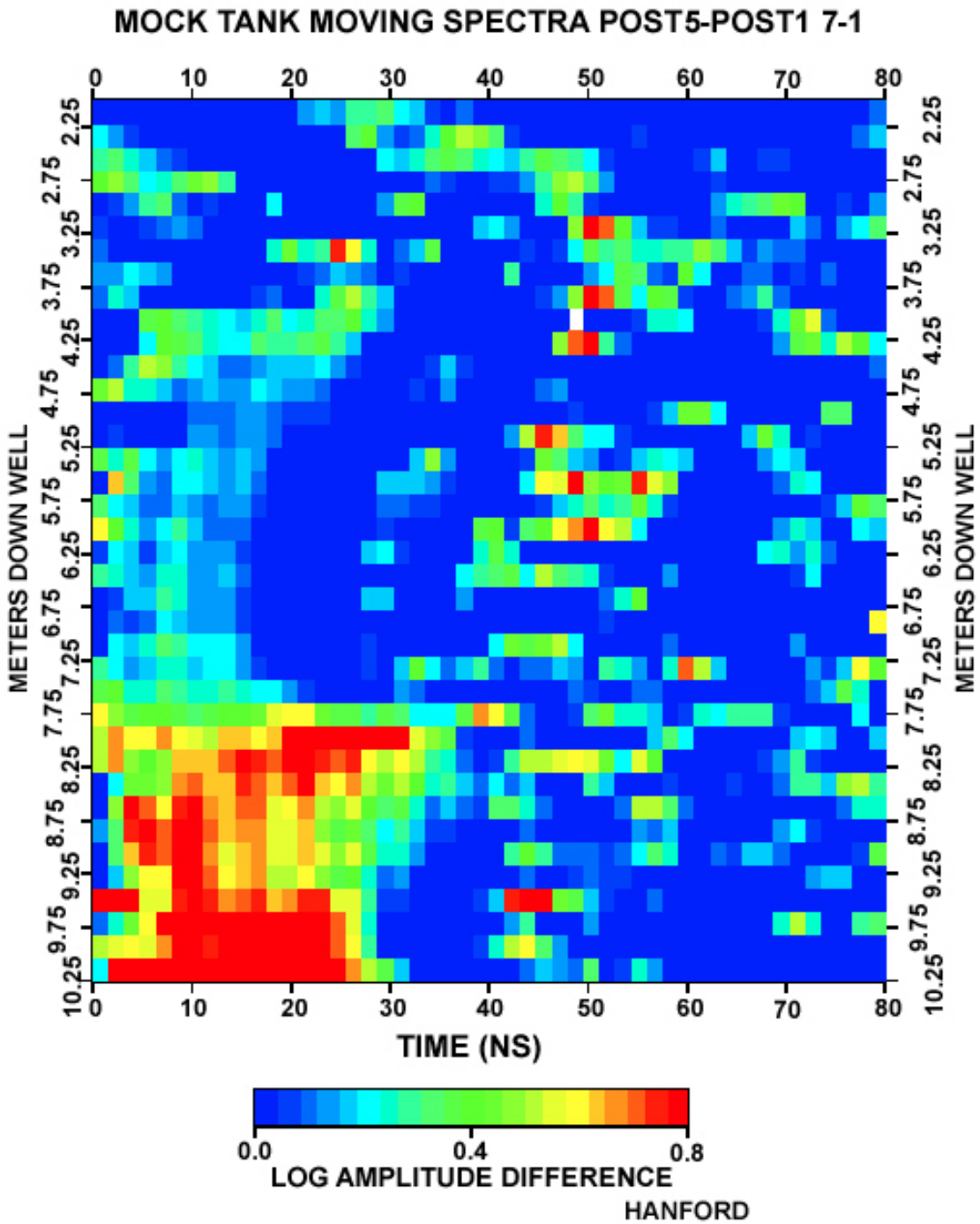

Figure 7. Time lapse of the change in radar amplitude as a function Of depth for wells 7 and 1

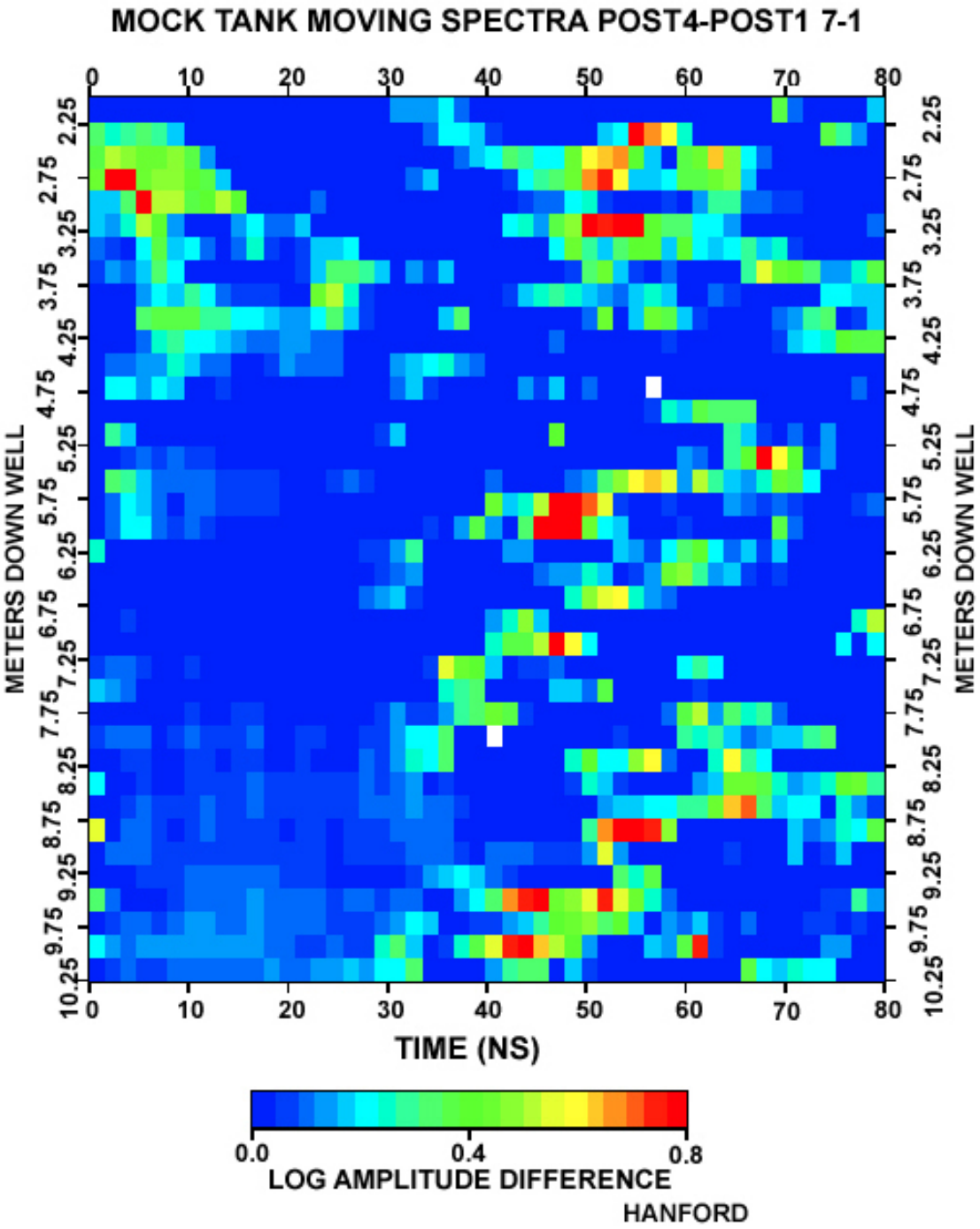

Figure 7 (Contd)

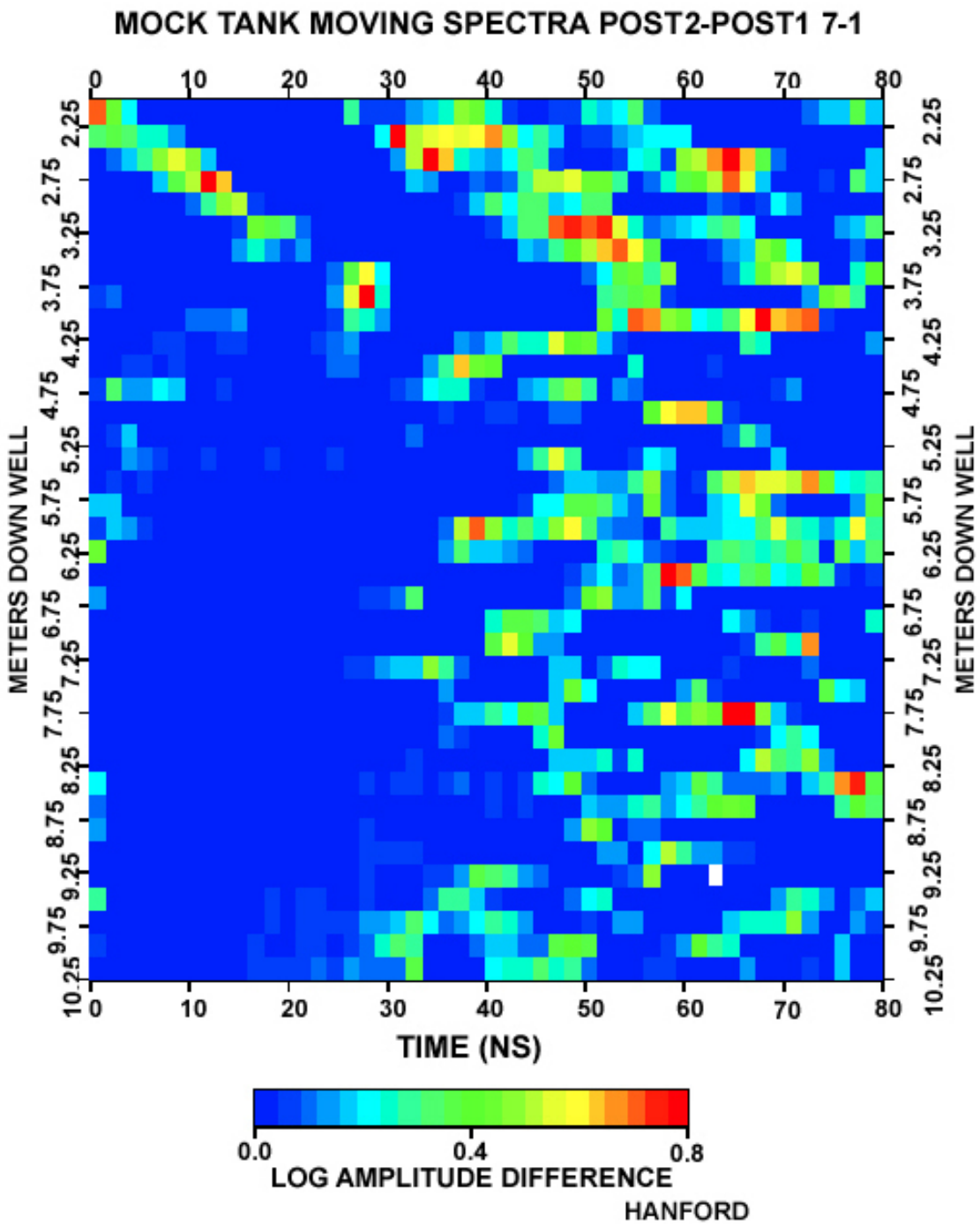

Figure 7 (Contd)

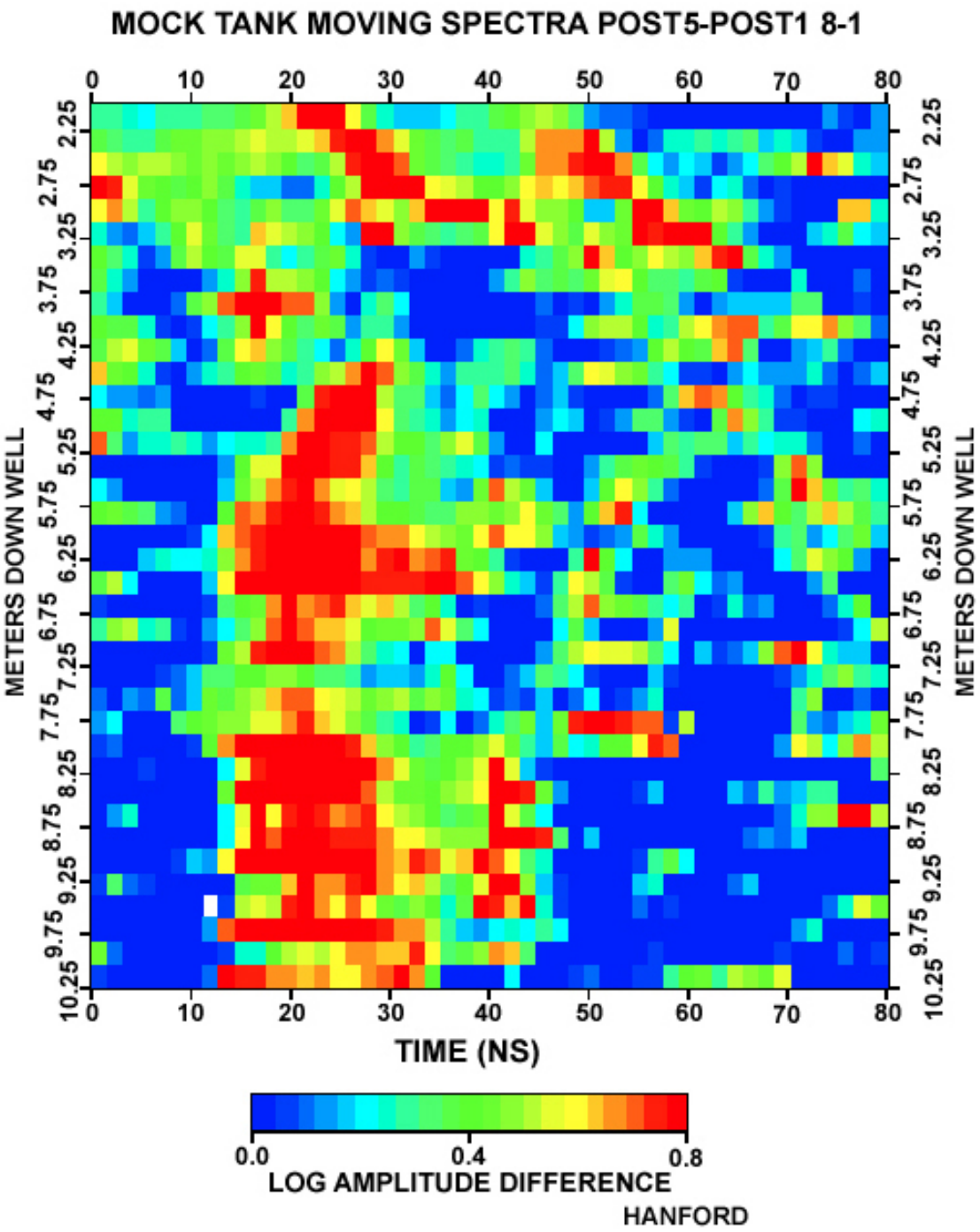

Figure 8. Time lapse of the change in radar amplitude as a function of depth for wells 8 and 1.

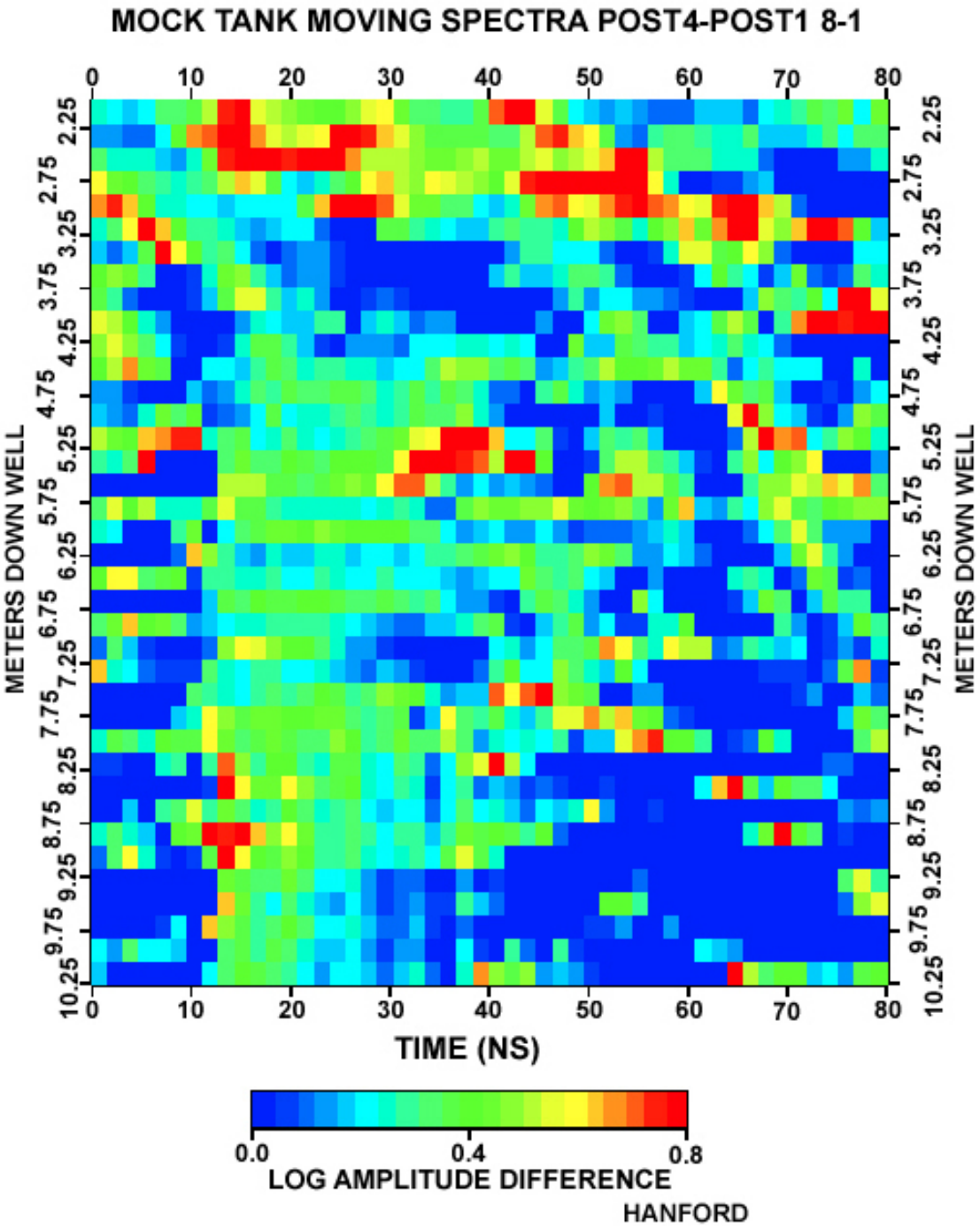

Figure 8 (Contd)

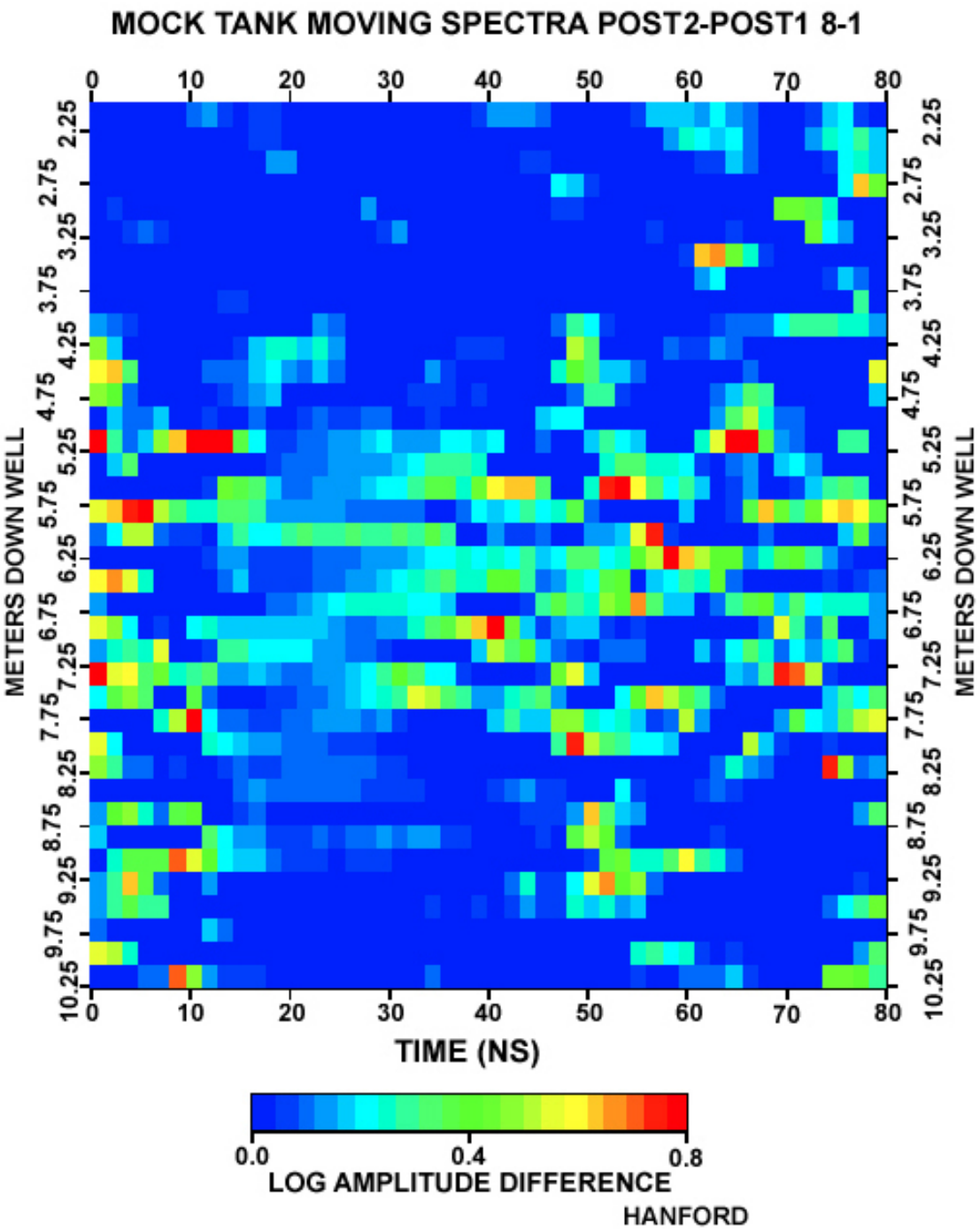

Figure 8 (Contd)

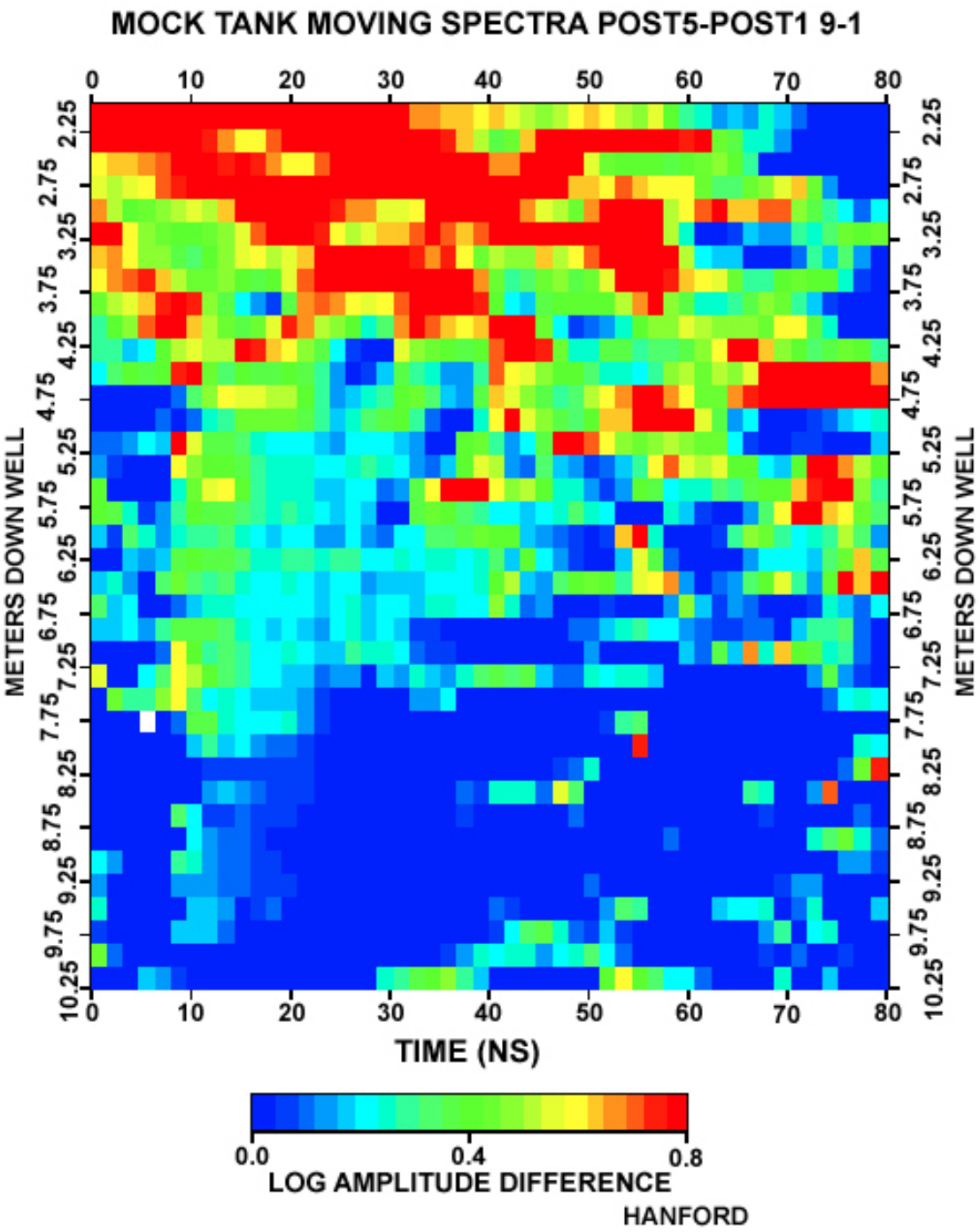

Figure 9. Time lapse of the change in radar amplitude as a function of depth for wells 9 and 1.

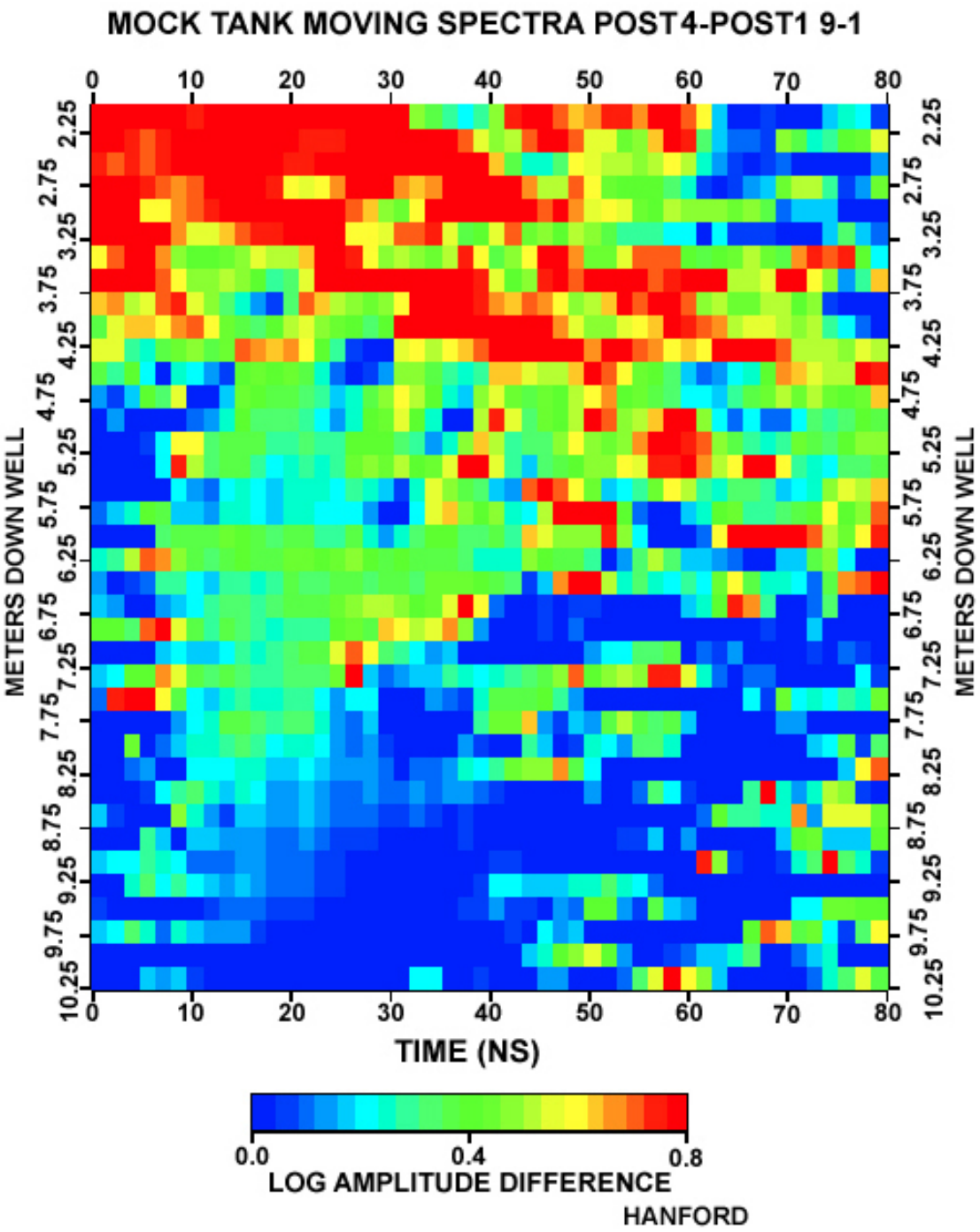

Figure 9 (Contd)

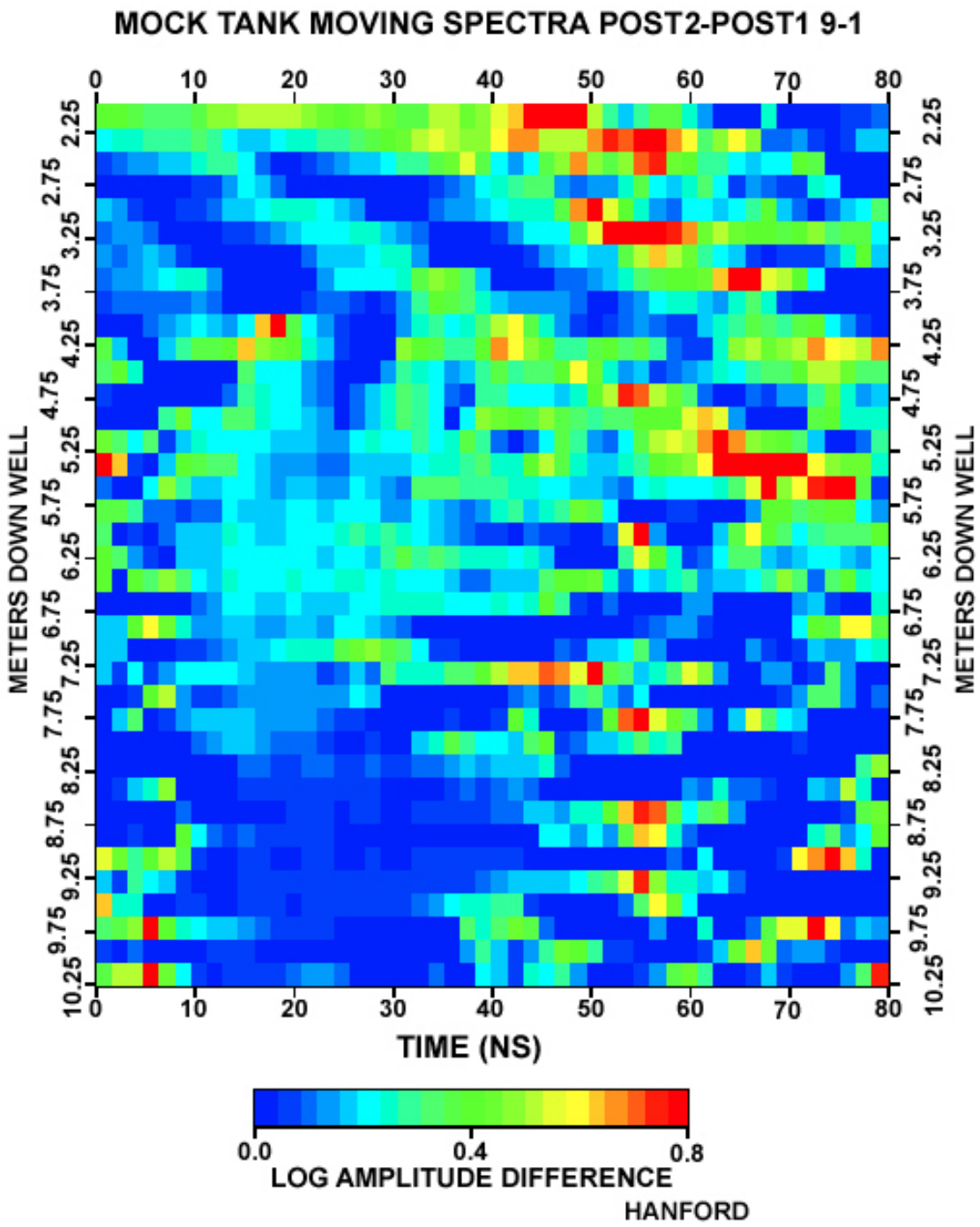

Figure 9 (Contd)

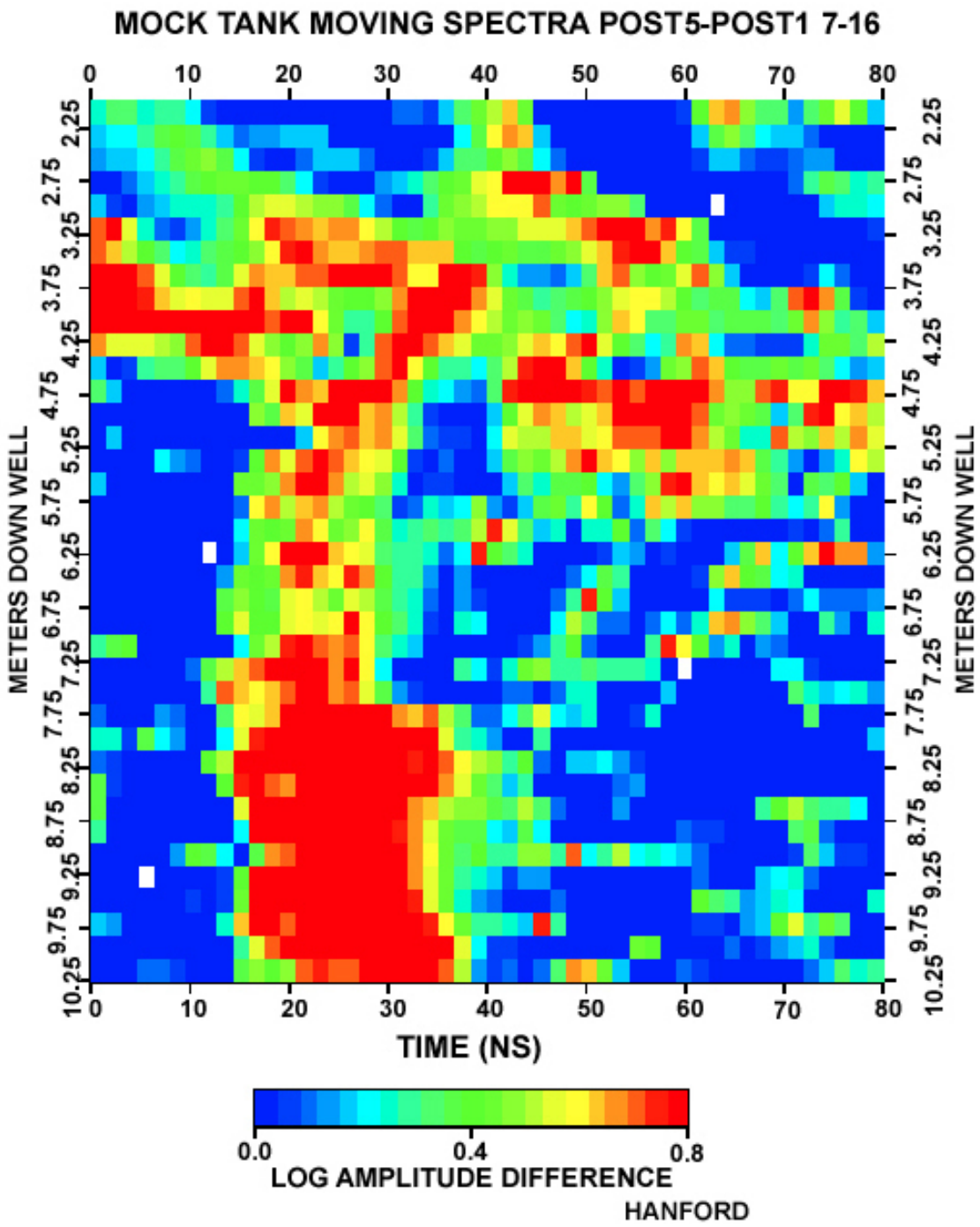

Figure 10. Time lapse of the change in radar amplitude as a function of depth for wells 7 and 16.

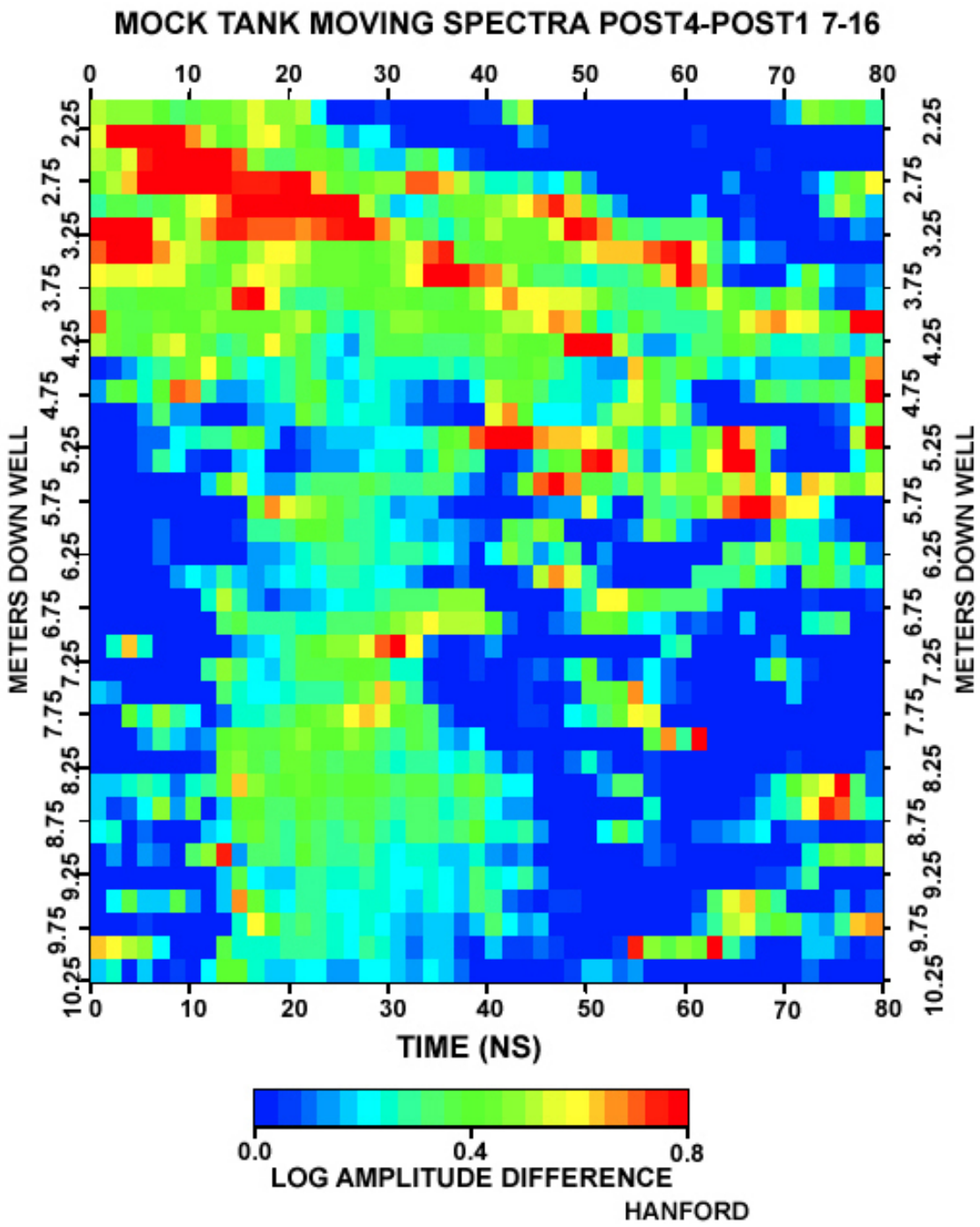

Figure 10 (Contd)

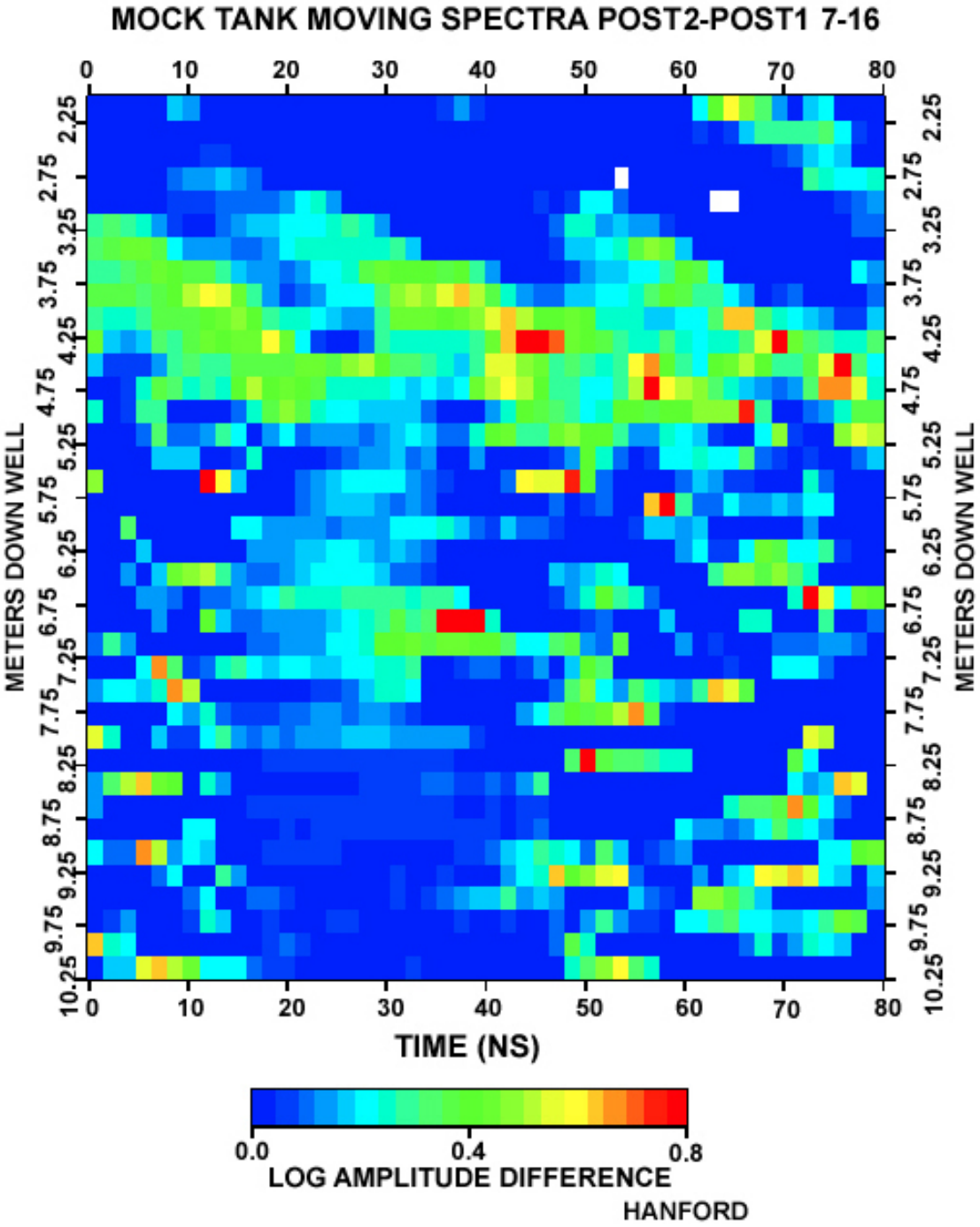

Figure 10 (Contd)

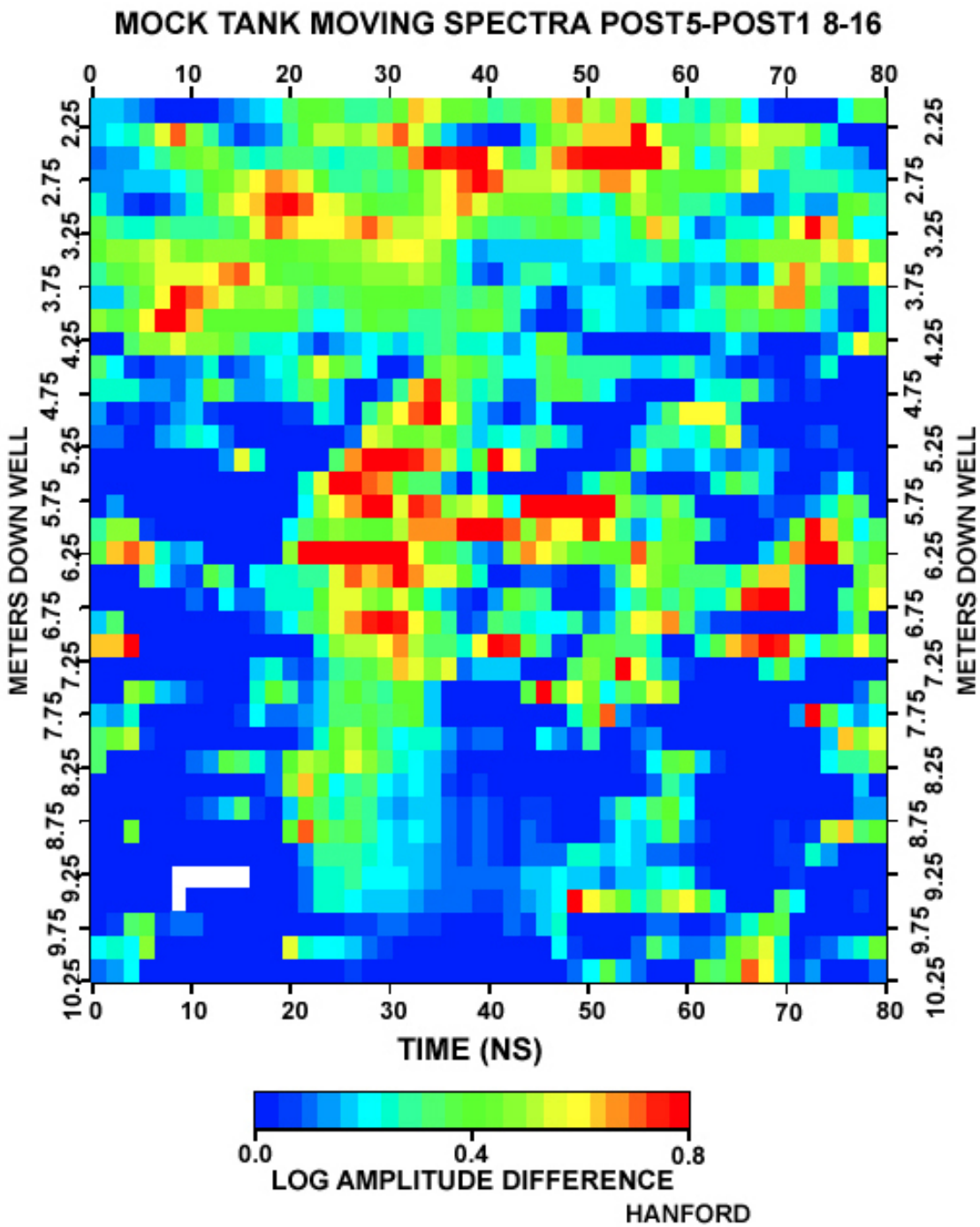

Figure 11. Time lapse of the change in radar amplitude as a function of depth for wells 8 and 16.

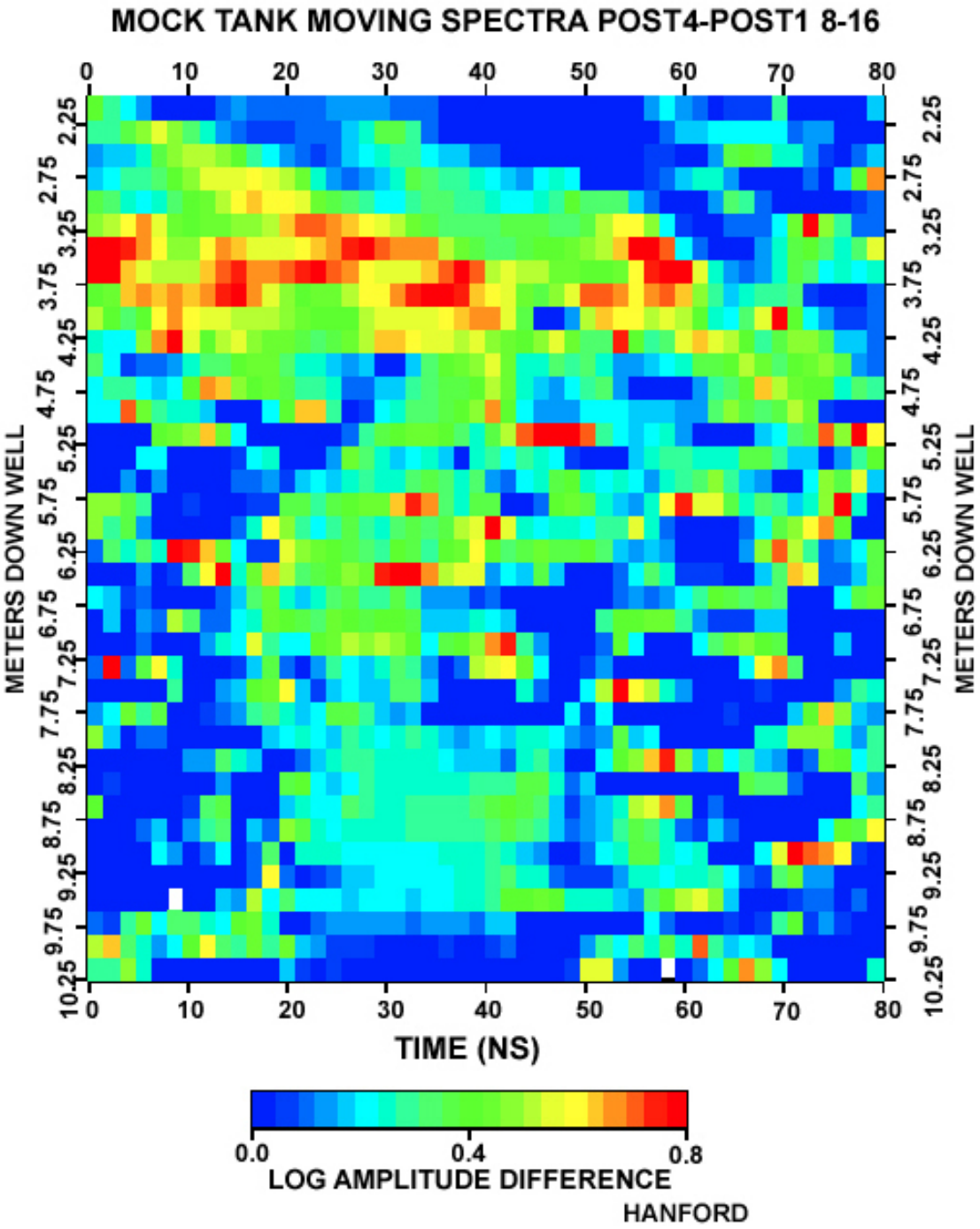

Figure 11 (Contd)

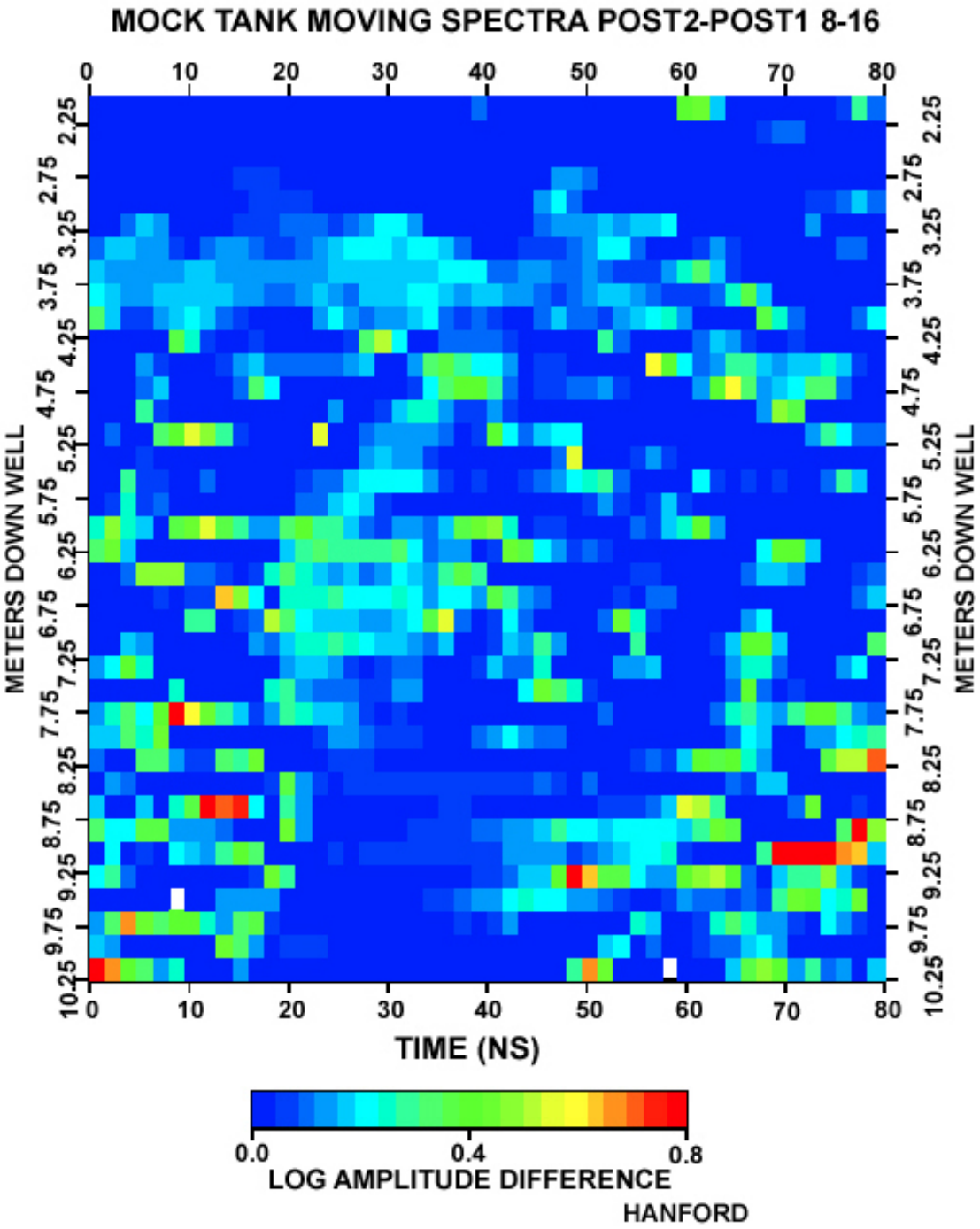

Figure 11 (Contd)

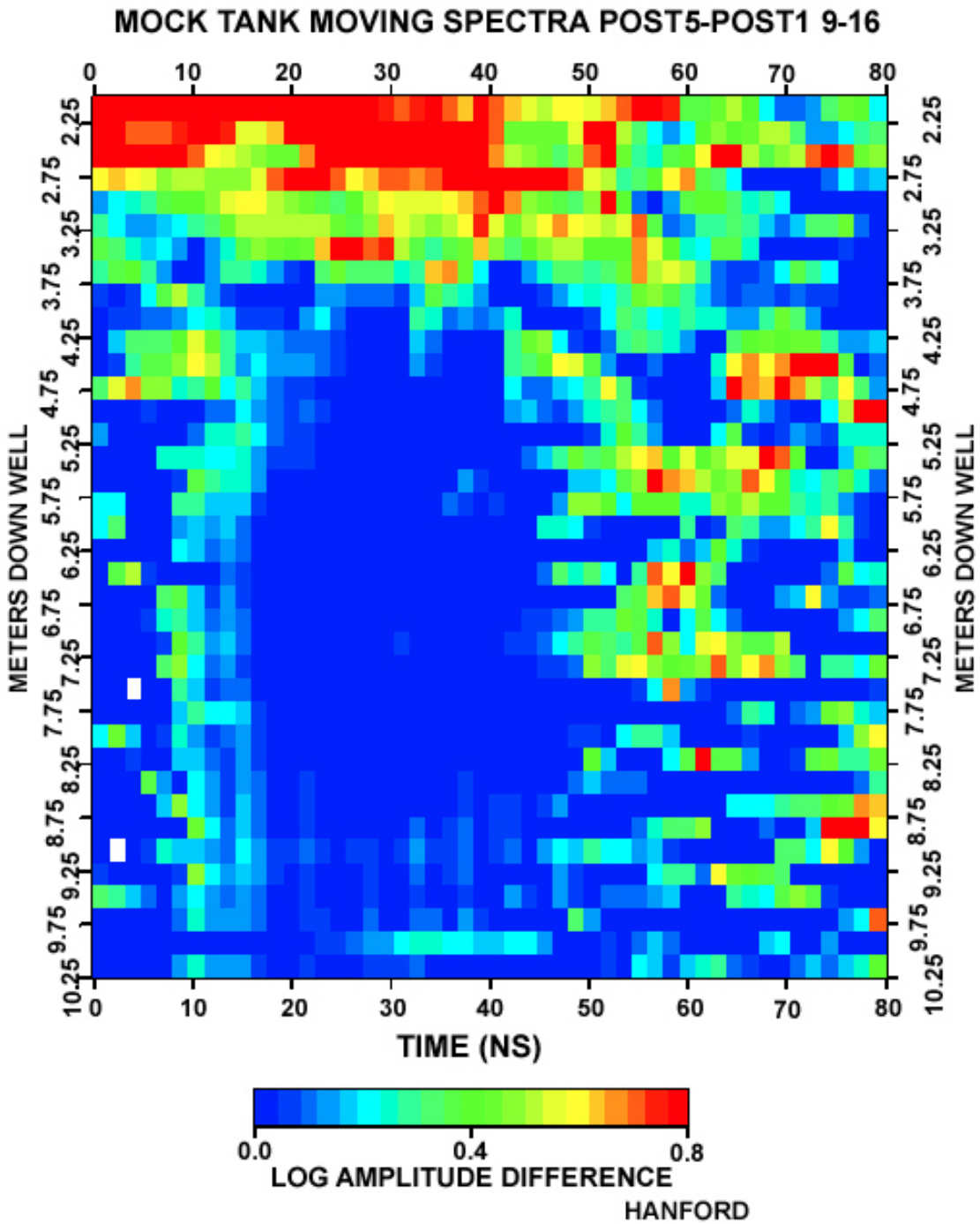

Figure 12. Time lapse of the change in radar amplitude as a function of depth for wells 9 and 16.

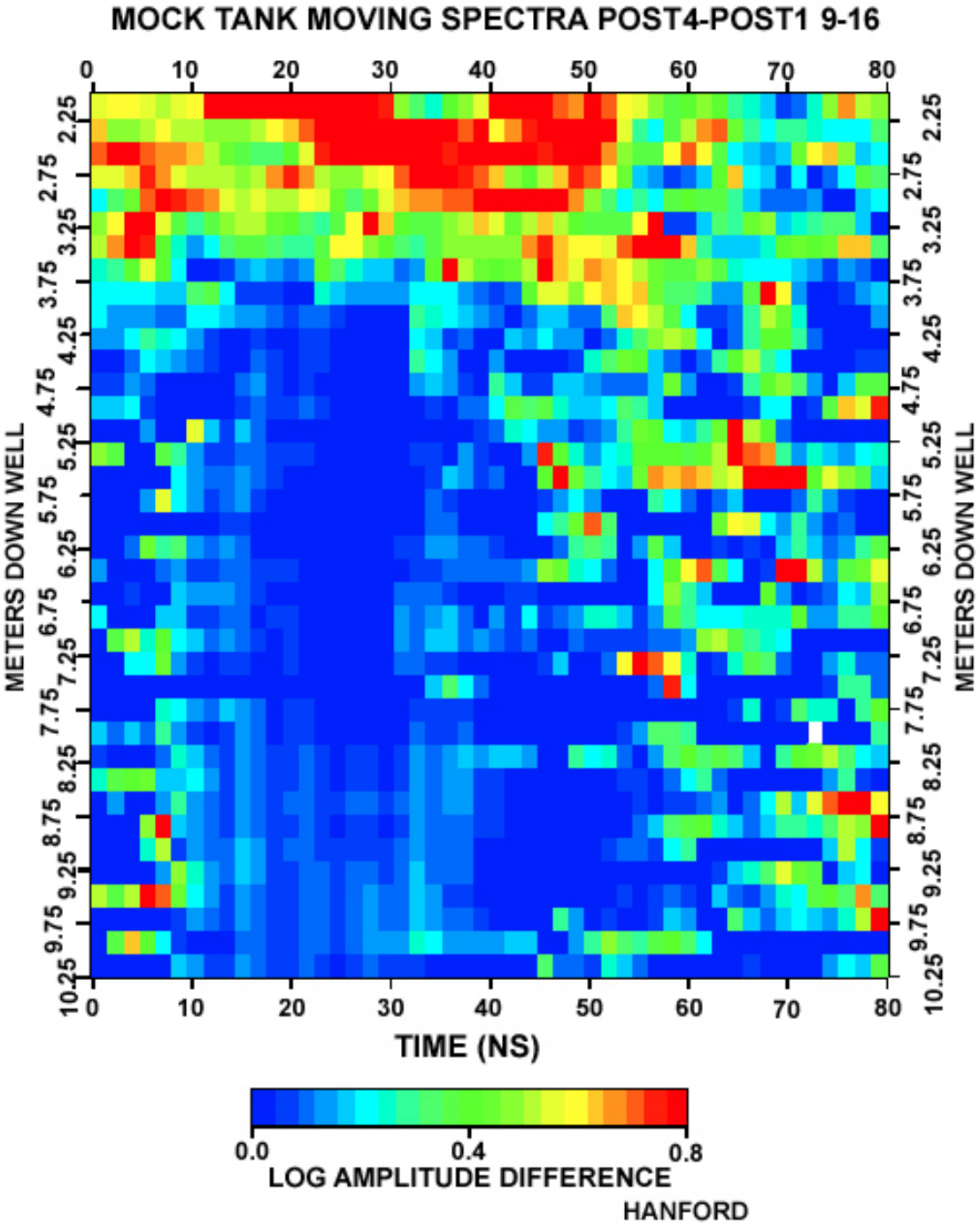

Figure 12 (Contd)

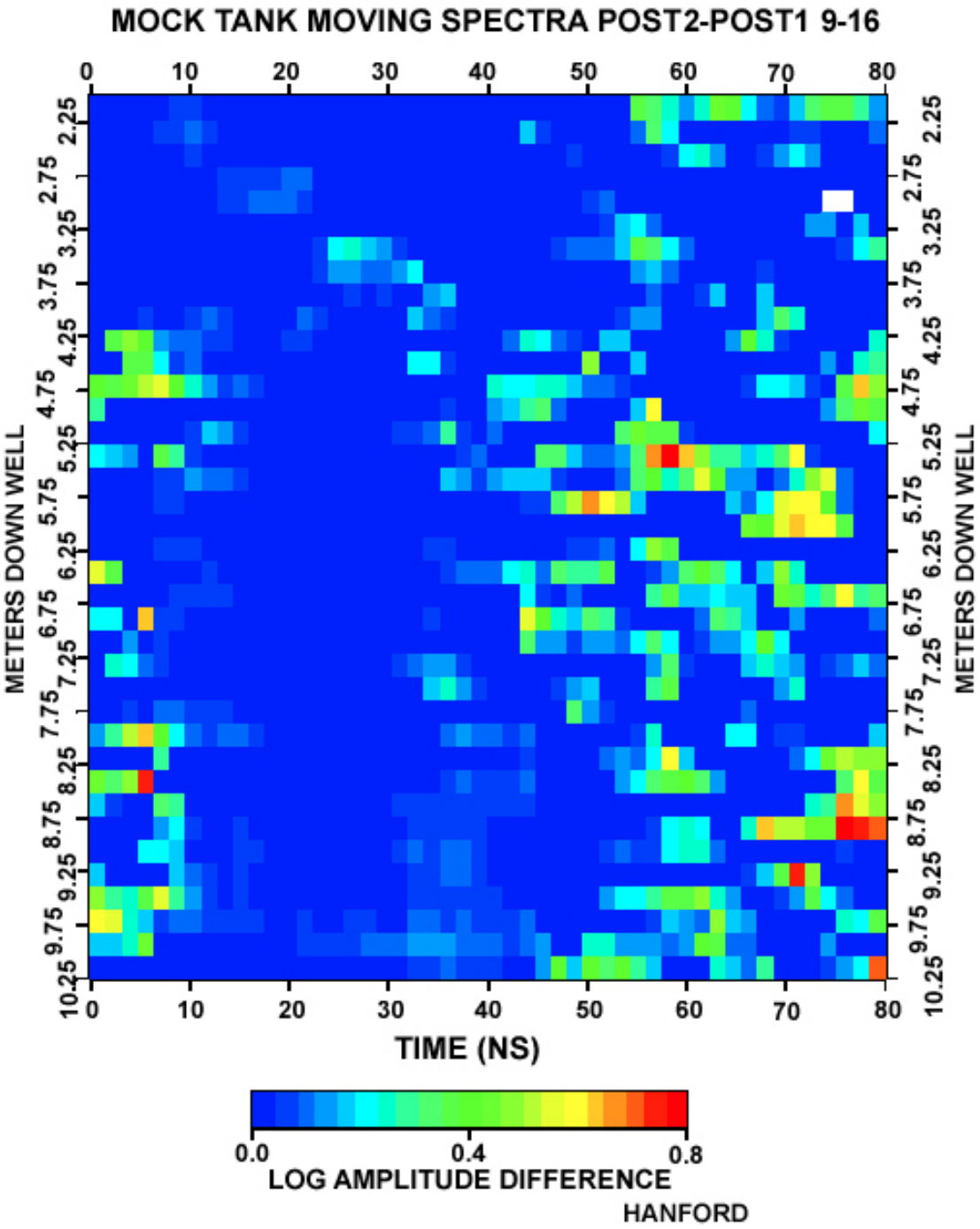

Figure 12 (Contd)

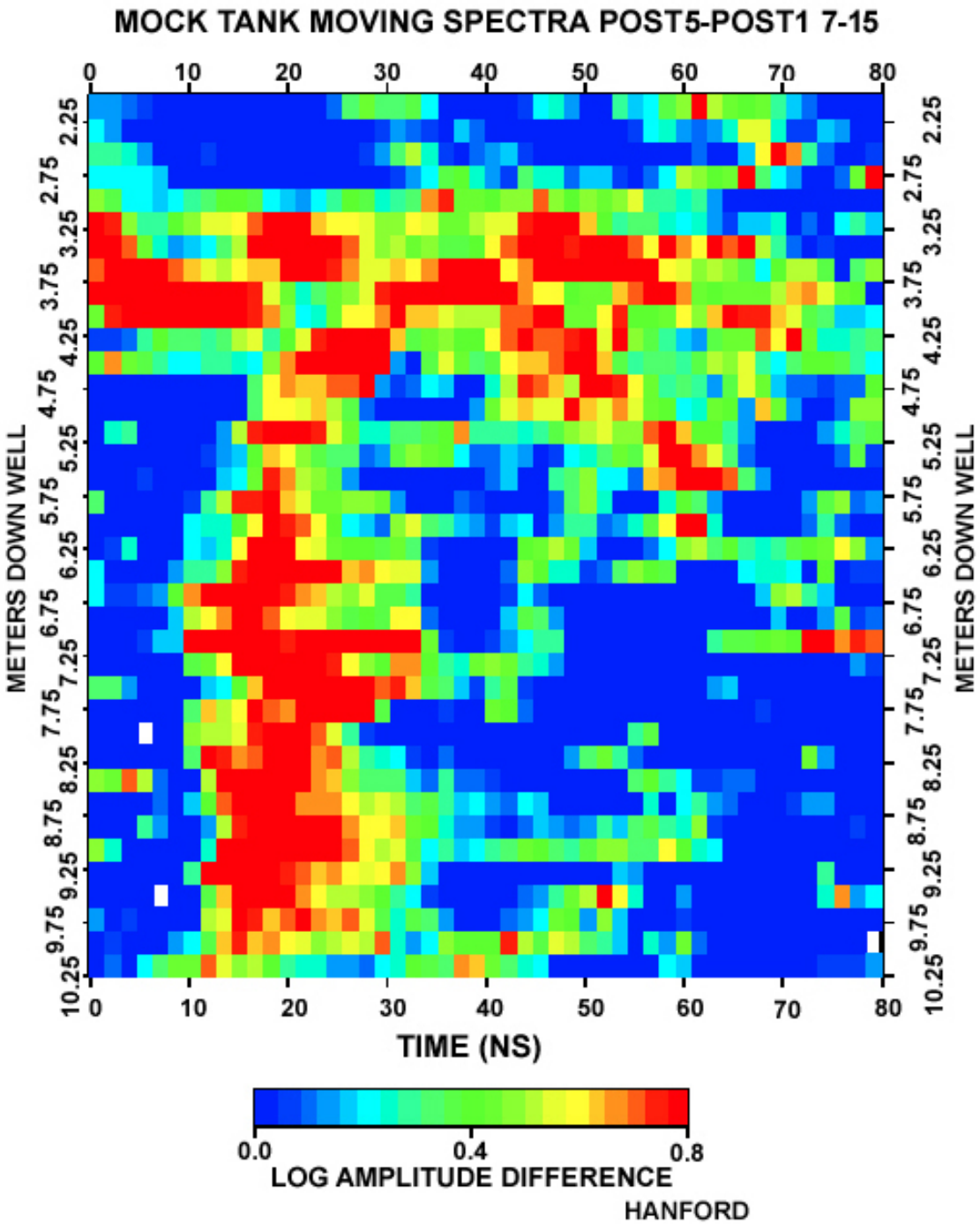

Figure 13. Time lapse of the change in radar amplitude as a function of depth for wells 7 and 15.

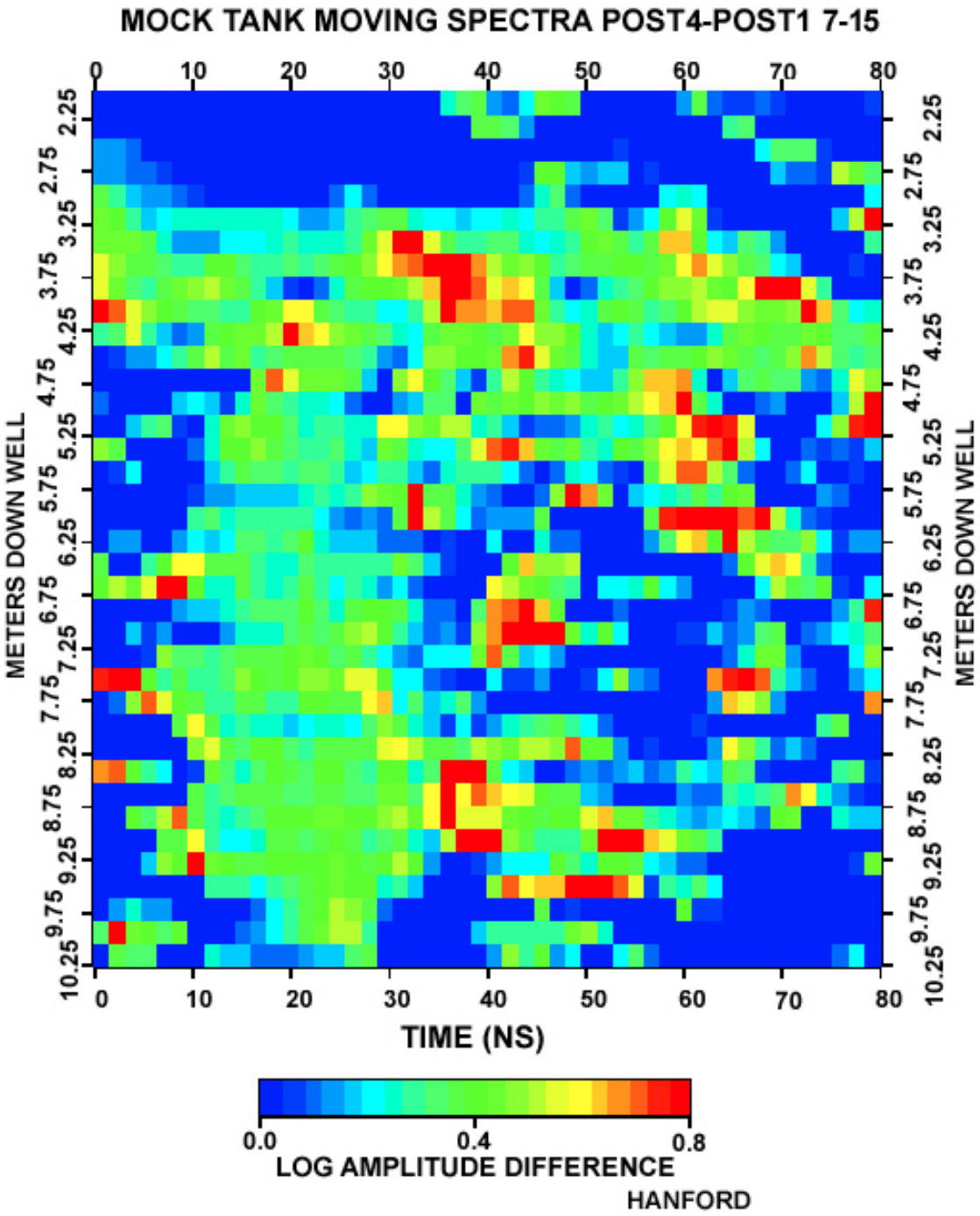

Figure 13 (Contd)

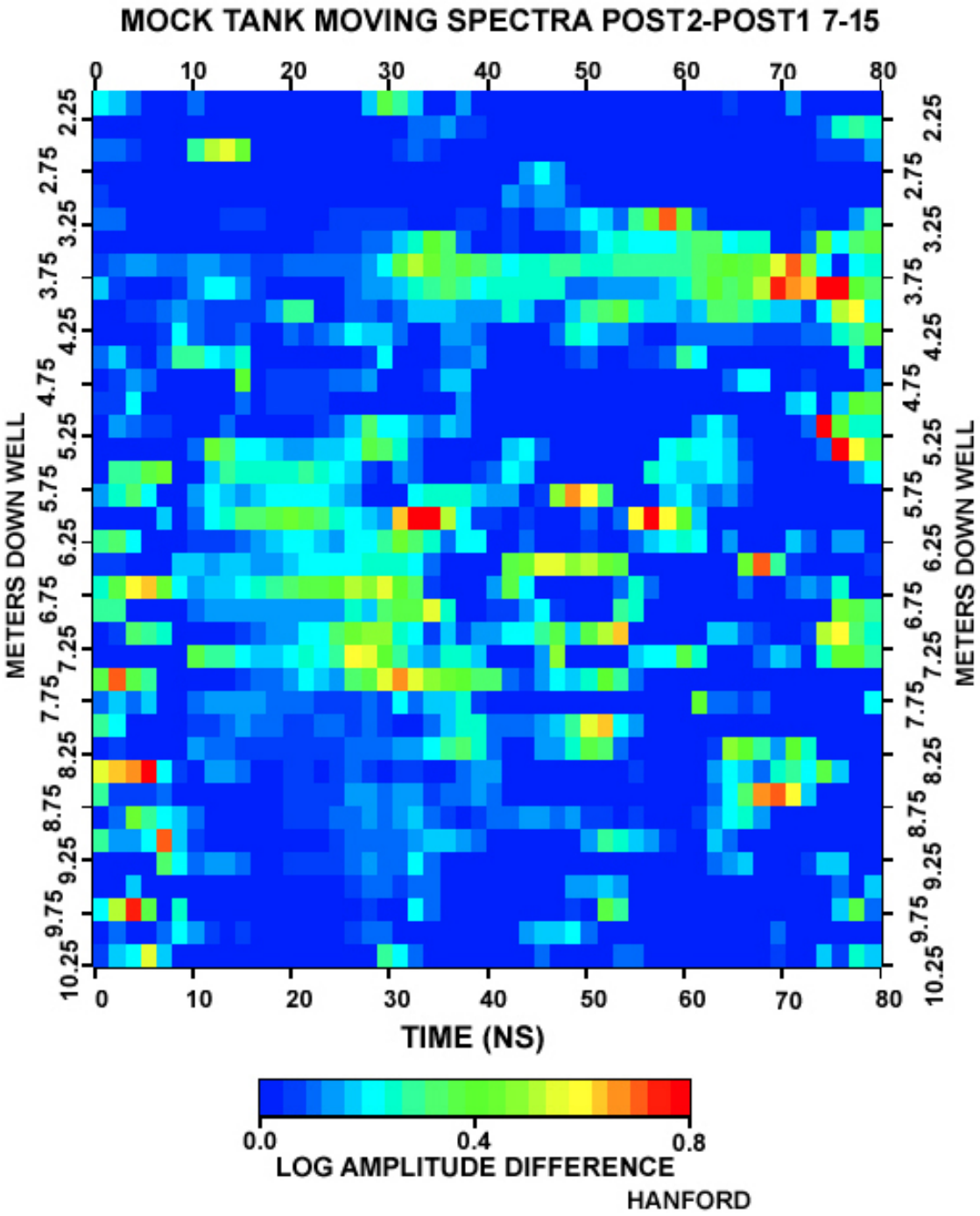

Figure 13 (Contd)

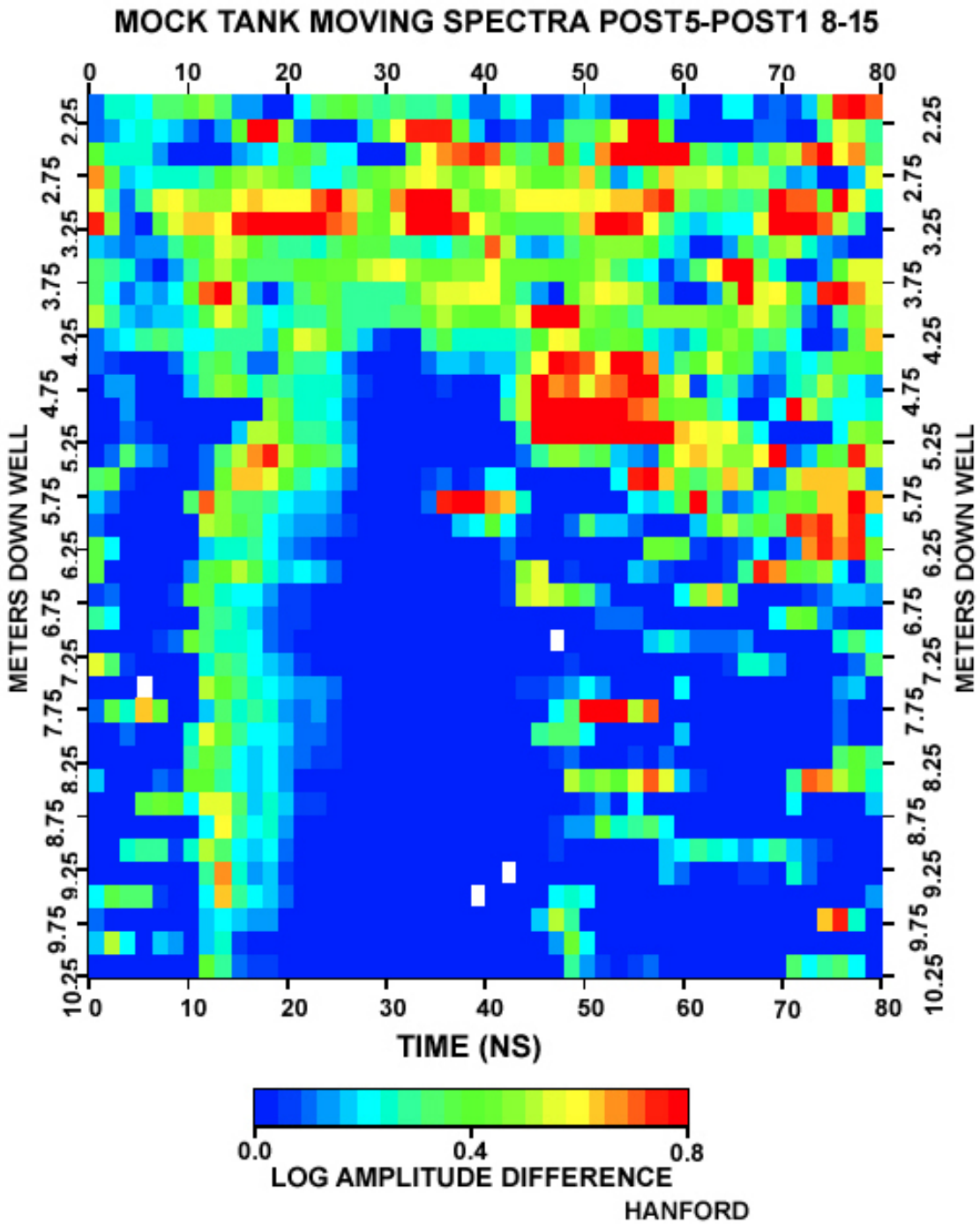

Figure 14. Time lapse of the change in radar amplitude as a function of depth for wells 8 and 15.

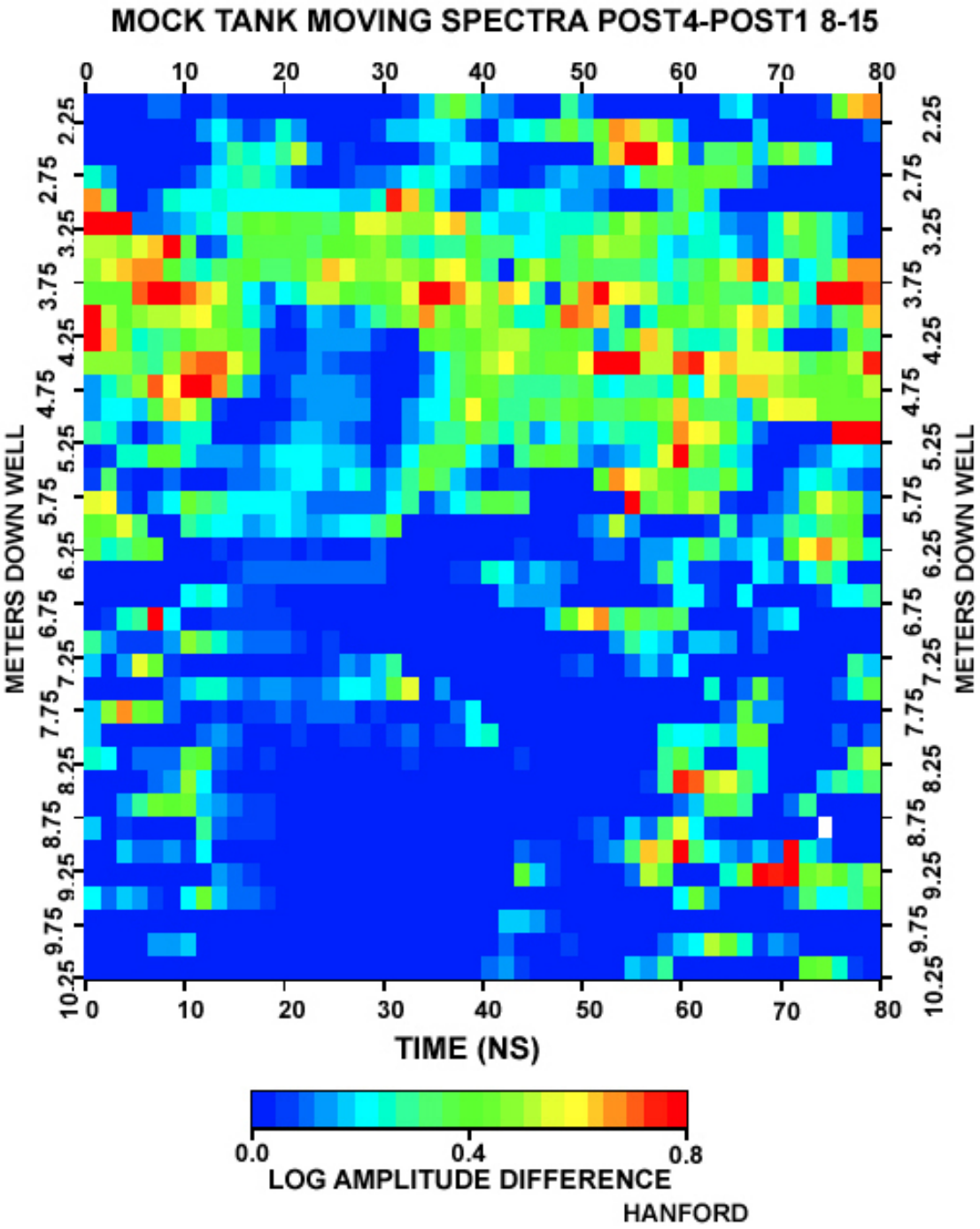

Figure 14 (Contd)

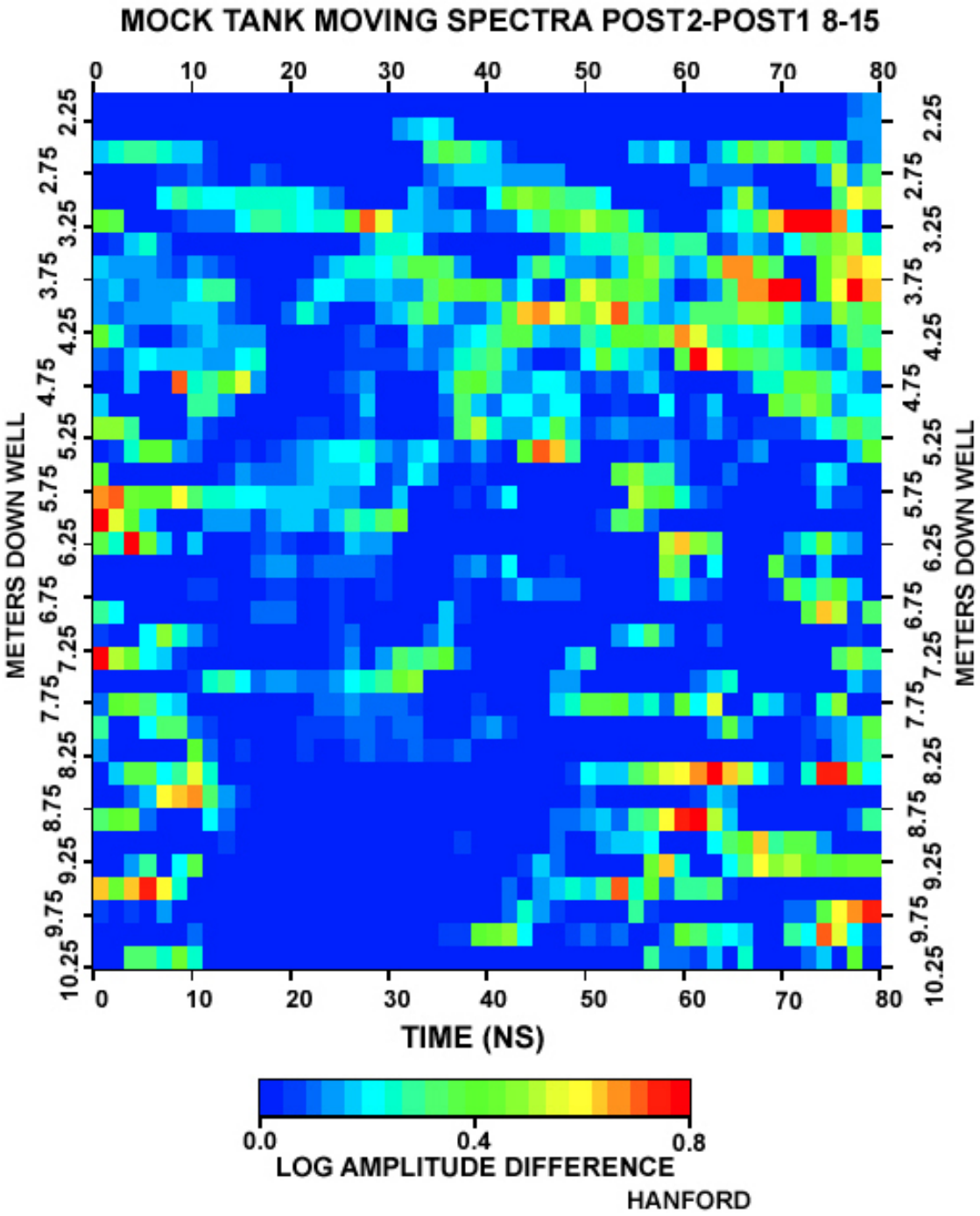

Figure 14 (Contd)

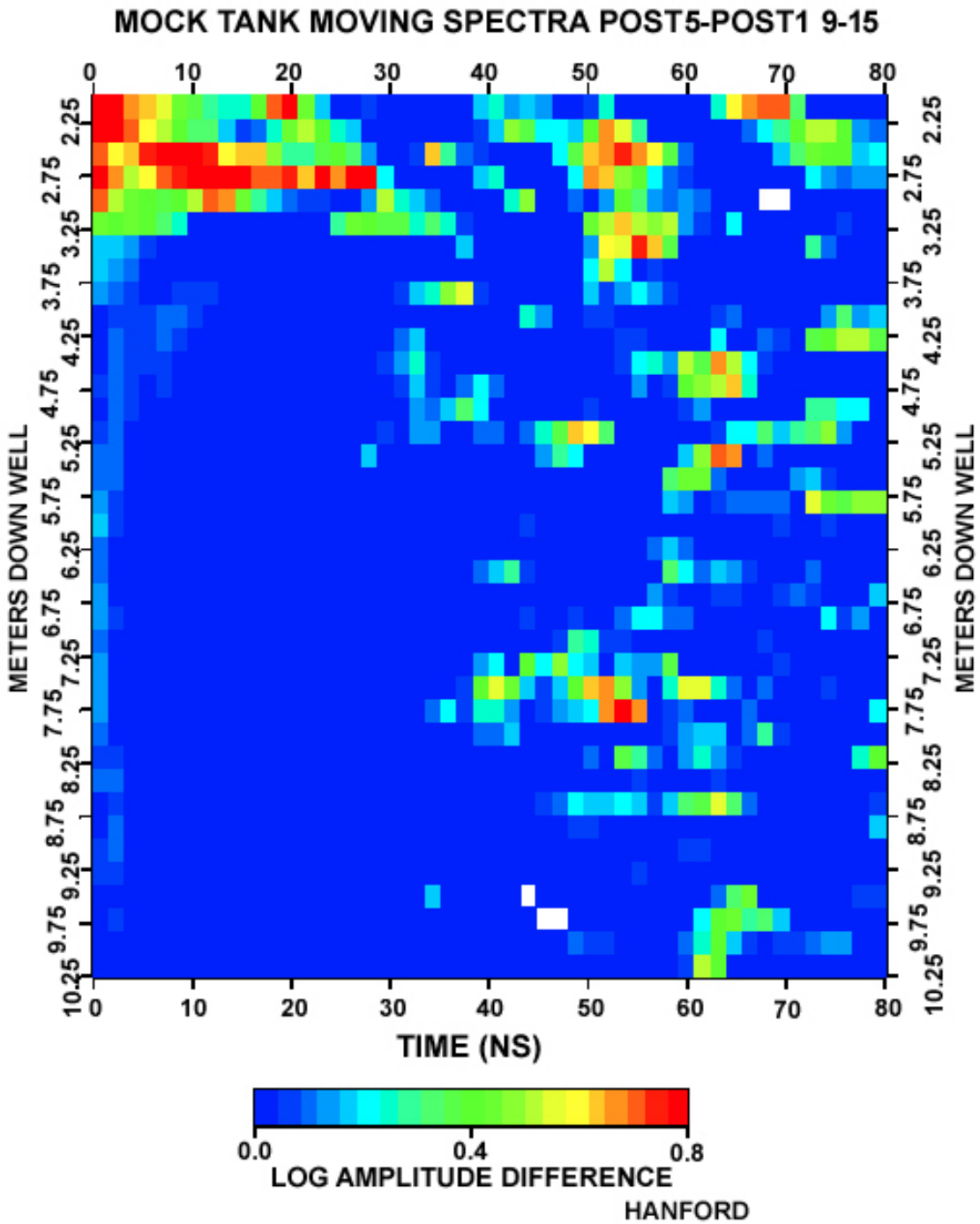

Figure 15. Time lapse of the change in radar amplitude as a function of depth for wells 9 and 15.

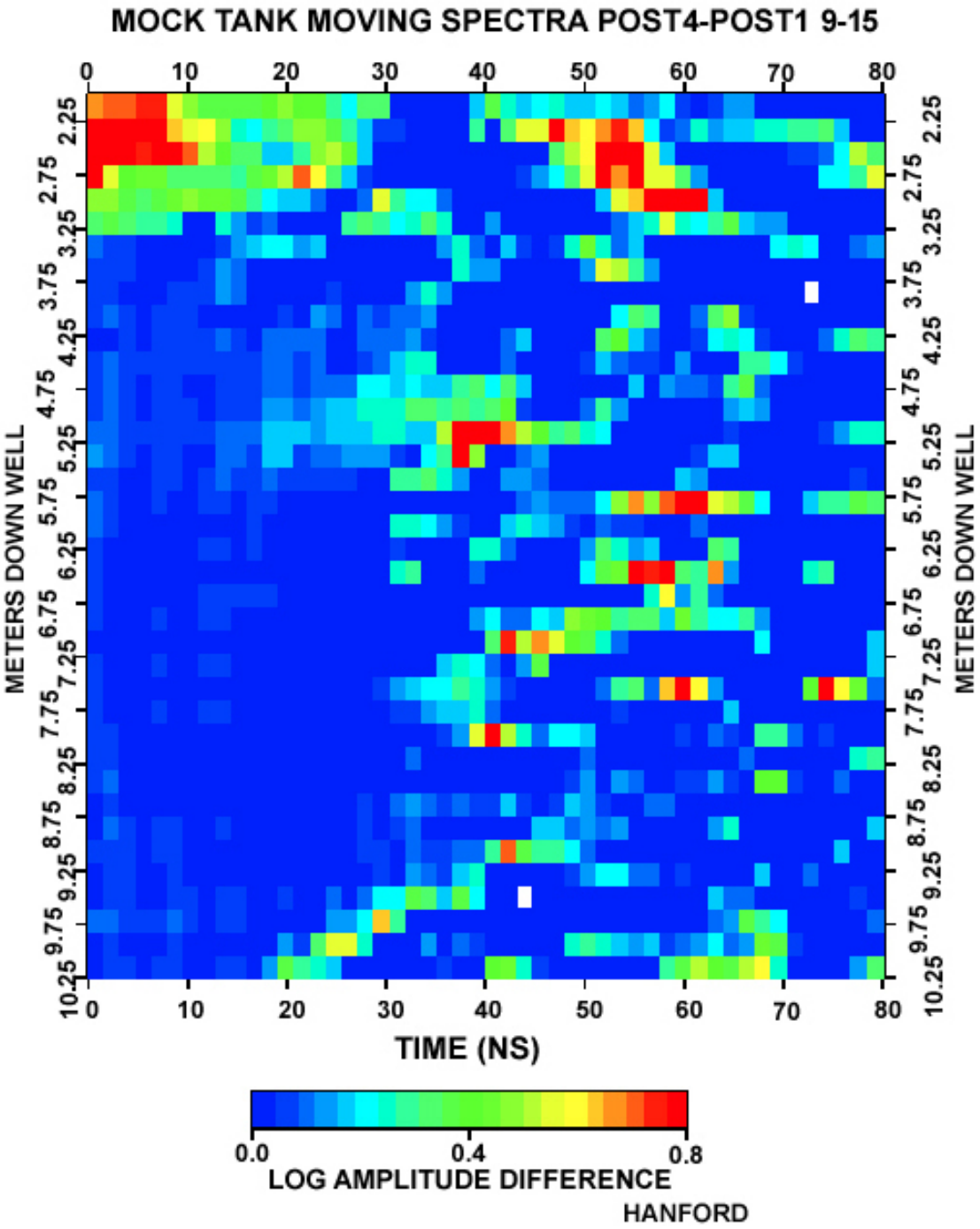

Figure 15 (Contd)

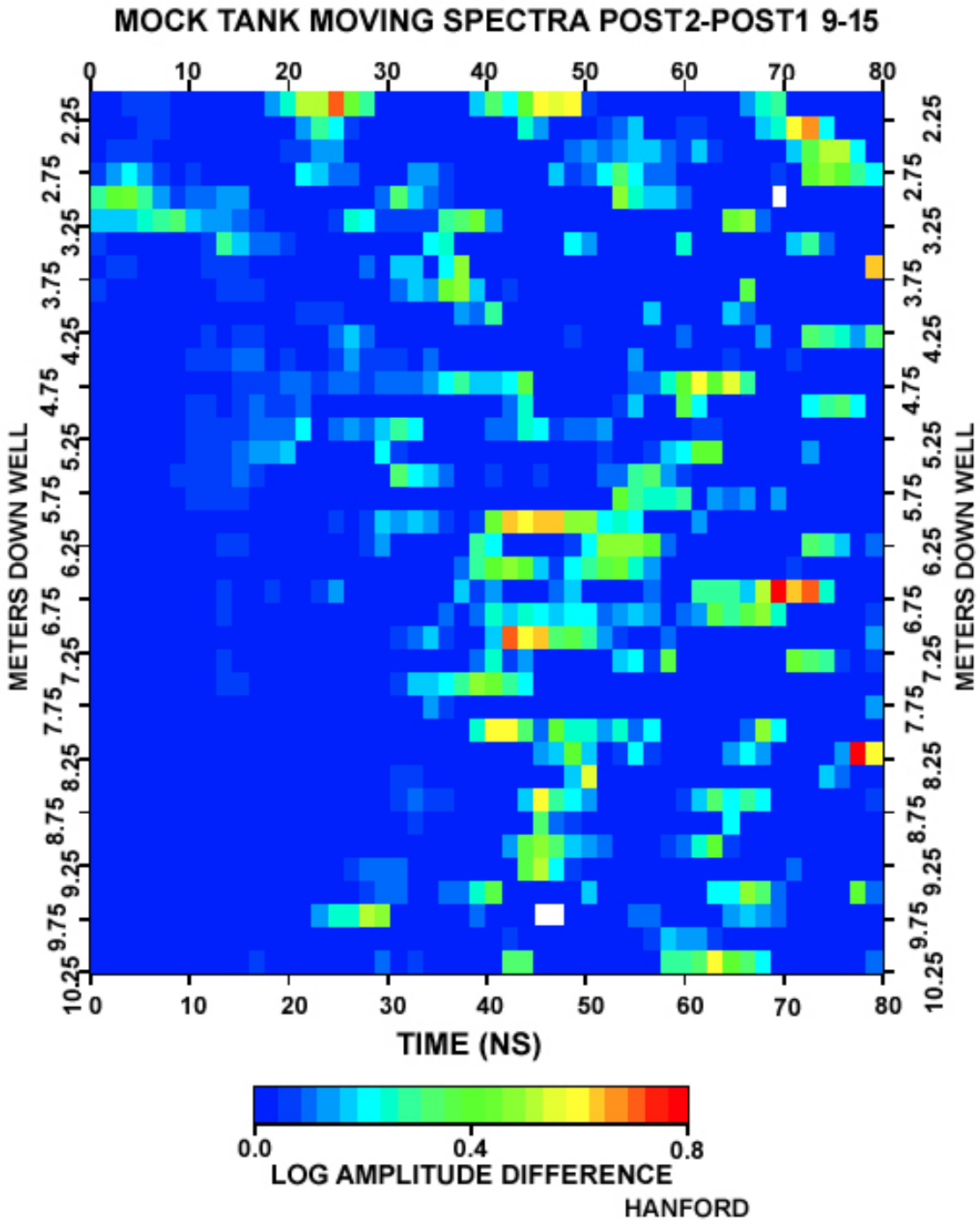

Figure 15 (Contd)

Summary and Recommendations

All radar and seismic data have been examined and processed.
Overall it was clear that radar at 100 Mhz and most definitely at 50 Mhz is easily and quickly capable of detecting any influx of the sodium thiosulfate solution at a tank scale. Figure 16 shows the difference in data quality between the 50 and 100 Mhz data. There is a factor of 10 in signal to noise ratio between the 50 and 100 Mhz data. As stated earlier because of the short spacing of the sampling intervals (1/4 meter) and short distances between transmitter and receiver (20 to 25 meters) we used the highest resolution data we could, i.e. the 100 Mhz data for the measurements. Assuming that the geology will be similar to this site the 50 Mhz should be capable of a range of 40 to 50 meters (geometric spreading will cut the signal by a factor of three, and the attenuation another 1.5). In this case also, (compared to the Sisson and Lu site) speed was sacrificed for detail in spatial mapping, but even under these circumstances the "plume" was delineated at a meter or less resolution. Radar signals almost immediately changed (within 100 gallons or less) as the injection proceeded. Even with limited coverage by the end of the injection radar was capable of detecting the location of the plume and tracing the direction of flow.

Seismic imaging was severely hampered by not having the anticipated boreholes and by having poor coupling of the boreholes to the formation and by having the makeshift liners to prevent fluid from leaking into the formation. Even then seismic did detect a change in character due to the fluid injection, but not to the accuracy or resolution of the radar. Seismic should be re-evaluated under more realistic conditions, especially since seismic is such a developed technology and can be used in any type of borehole, steel, open or PVC. Radar is clearly sensitive enough and easily deployed, the drawback as with all the electrical methods, is the need for PVC or open holes. The high-resolution crosswell method of joint seismic and radar is attractive because two independent properties are measured and fluid content has opposite effects on each (increases seismic amplitudes and velocity and decreases radar amplitudes and velocities) thus decreasing the chance of false positives.

Therefore the main conclusions are: The radar (50 Mhz) has a maximum penetration of about 50 meters (164 feet). This could be possibly extended by increasing the strength of the radar signal by using cable with less line loss and a higher transmitter power. The radar has excellent sensitivity to the fluid. The drier the formation the better the radar will work. The radar signal is sensitive to the change in dielectric properties of the pore space, i.e., the signal is being slowed and attenuated (velocity change) by the increase in the fluid content and salinity in the pores, and being attenuated by the increase in the resistivity of the pore fluids (signal amplitude change). In actual application the resolution and detectability will depend upon the number of wells that one has access to or has available to place sensors in. This is true of any method. The radar and especially the seismic were under sampled compared to the other techniques used (except for the EM). The next phase of evaluation should compare the methods on an equal sampling basis.

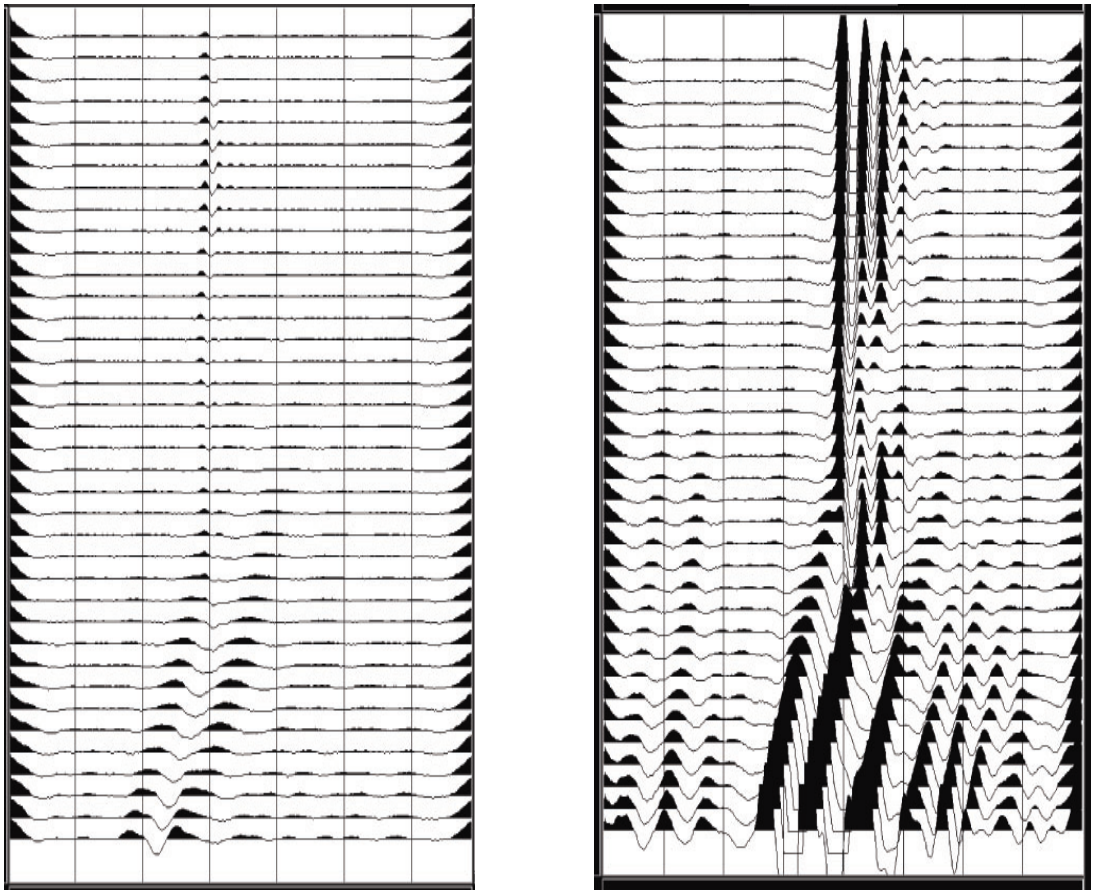

Figure 16. Crosswell data for the 100 Mhz. (left panel) and the 50 Mhz. radar (right panel) data for the well pair 8 to 16. The amplitude difference (and signal to noise ratio difference) is about 10 to 1. Shown are the true amplitude sections with no automatic gain control applied. The top of the hole is the bottom of the figure.

Appendix C

Cross Well Electromagnetic Surveys at Hanford Mock Tank Site

Final Report

February 12, 2002

G. M. Hoversten [1], B. Kirkendall [2]

1 Lawrence Berkeley National Laboratory
2 Lawrence Livermore National Laboratory

Introduction 3

Figure 1. *Diagram of LDMM PITT well field (left) and Pitt-10 resistivity log (right). PITT CPT wells marked in red; liquid infiltration points marked in blue; drilled wells now being installed marked in green. Wells 1-16 around mock tank (black) are ERT wells from previous experiment.* 3

Figure 2*: Magnetic and electric fields associated with a time-varying magnetic dipole source in a crosswell configuration within the earth.* 4

The role of the steel tank 4

Figure 4: *Real (left) and quadrature (right) vertical magnetic field in the ERT-14 well from transmitter well Tx-1 for mock tank bottom in a 300 ohm-m halfspace.* 5

Building the Tank into the 3D Finite Difference Mesh 6

Figure 5: *Central portion of finite difference mesh used to simulate steel tank bottom in a 300 ohm-m ground.* 6

Figure 6: *The integral equation solutions for a thin steel sheet in a 300 ohm-m ground are shown for the shallow transmitter (left panel) and deep transmitter (right panel). The integral equation results are filled boxes the finite difference solution is small open circles.* 7

Figure 7: *Cross section at y=0 through the 3D FD mesh for full tank simulation.* 7

Figure 8: *Finite Difference calculations of the full tank compared to integral equation solution for the tank bottom only. Left panel: shallow transmitter, Right panel: deep transmitter. The integral equation solutions are filled squares and FD calculations are open circles.* 8

Pre-Injection Data 8

Figure 9: *Real (left) and Quadrature (right) vertical magnetic field from Transmitter Tx1 and receiver well ERT-14.* 9

Figure 10: *Real (left) and Quadrature (right) vertical magnetic field from Transmitter Tx3 and receiver well ERT-6.* 9

Figure 11: *Real and quadrature magnetic field strengths. Upper set of curves is the real component and lower set is the quadrature component. Horizontal axis is depth in the receiver well that is directly opposite to the transmitter well. Upper left panel is on August 13 between tx1 and the opposite ERT-14, upper right panel is August 14 between tx1 and ERT14, lower left panel is August 16 between tx1 and ERT14 and lower right panel is August 17 between tx2 and ERT10.* 11

Time Lapse Data differences 10

Figure 11: *Time-lapse changes in real (left) and quadrature (right) vertical magnetic field for transmitter Tx2 and receiver well ERT-10between July 23 (pre-injection) and August 13. Largest changes occur for transmitter and receivers near the surface, with peaks in change at 3.6, 5.2, 6 and 8 m depth for the receivers.* 15

Figure 12: *Time-lapse changes in real (left) and quadrature (right) vertical magnetic field for transmitter Tx2 and receiver well ERT-10 between August 14 and August 13.* 15

Parameters controlling the EM signal 16

Release & measurement schedule 16

Figure 13: *Leak release schedule and EM measurement times. Each red cross represents measurements from a separate EM transmitter well.* 16

Time-lapse conductivity changes from inversion 16

Figure 14: *Time-lapse conductivity difference between August 14 and 13. a) depth 1.2m, b) depth 3.6m, c) depth 7.0m, d) depth 10m. Red= +0.001 S/m, Blue = -0.001S/m. Note the large increase in* σ *to the east and southeast. The horizontal scales are from –10 to +10 meters, with the tank centered on (0,0).* 17

Figure 15: *Vertical cross section at Y=0m through the conductivity difference model for August 14 – August 13. The zones of maximum change at 7 and 9.5 m correspond to low resistivity (high permeability) layers in the Pitt-10 log.* 18

Discussion 19

Continuing Work 20

Conclusions 20

Appendix A 22

Pre-injection crosswell EM data acquisition 22

Figure A-1: *Transmitter-receiver well location map* 22

Appendix B 24

Post-injection crosswell EM data acquisition summary 24

Data Acquisition Schedule 24

Figure B-1: *Post injection crosswell EM survey configurations. Each combination of transmitter and receiver wells is shown by a distinct color.* 25

Introduction

This report describes the crosswell electromagnetic (EM) data acquisition and interpretation at the Hanford Mock Tank site. The crosswell EM data was acquired using the Lawrence Livermore National Laboratory crosswell EM system in collaboration with Barry Kirkendall of LLNL. Pre-injection data acquisition took place between July 23 and July 25 2001 at the site. The data acquisition and data file naming conventions is summarized in Appendix A. A second data acquisition period covered the dates August 13 through August 17 and is summarized in Appendix B.

To date the data has been processed and calibrated and checked for consistency with layered numerical models based on the Pitt-10 CPT resistivity log (pitt10 resistivity log and location shown in Figure 1).

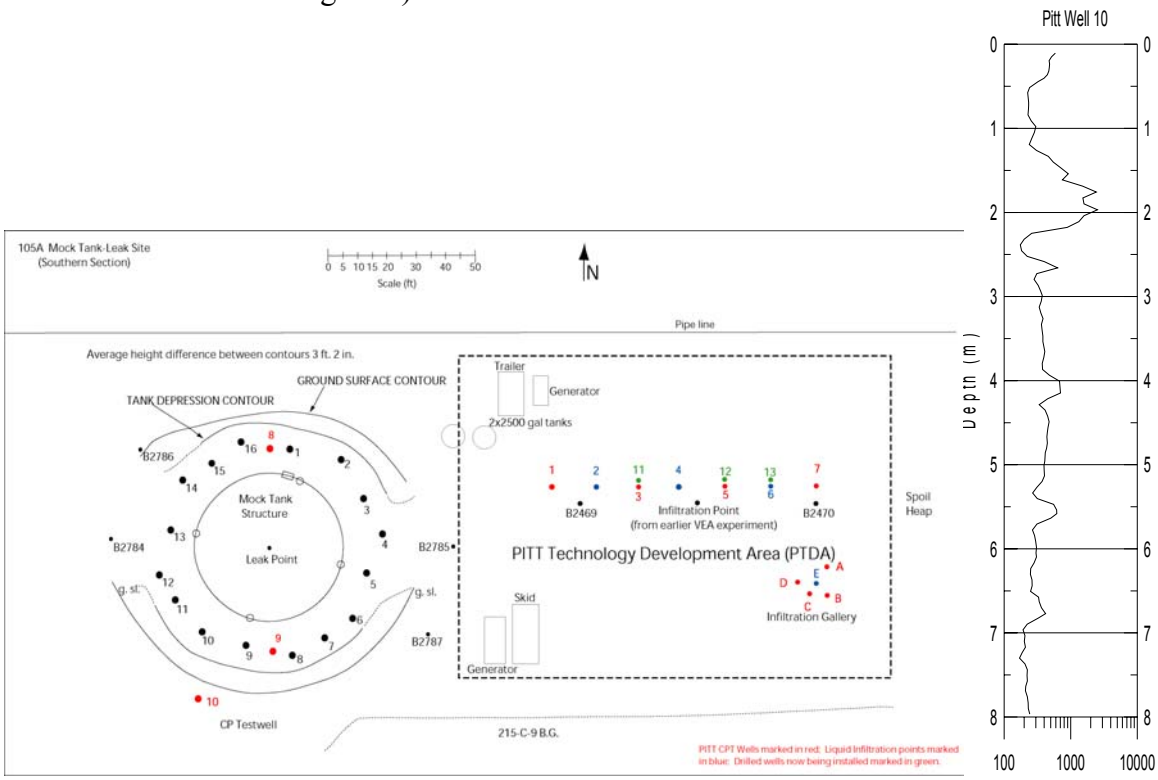

Figure 1. *Diagram of LDMM PITT well field (left) and Pitt-10 resistivity log (right). PITT CPT wells marked in red; liquid infiltration points marked in blue; drilled wells now being installed marked in green. Wells 1-16 around mock tank (black) are ERT wells from previous experiment.*

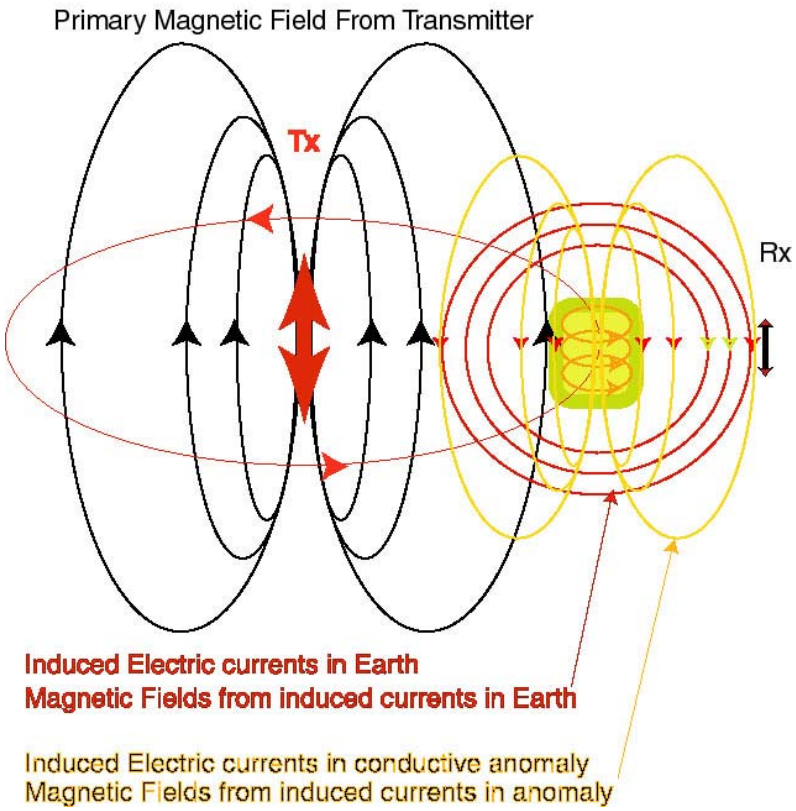

Figure 2*: Magnetic and electric fields associated with a time-varying magnetic dipole source in a crosswell configuration within the earth.*

Crosswell EM uses a magnetic dipole transmitter (wire wound around a magnetic permeable core) to generate a time-varying magnetic field that permeates the earth. Figure 2 shows the operation of the system in schematic fashion. The time-varying magnetic field induces currents to flow in the earth. In addition any conductive areas of the earth, such as areas where fluids have leaked, will have eddy currents induced, which also create secondary magnetic fields. The secondary magnetic fields produced in the earth are measured in the presence of the primary magnetic field (the field that would exist in free space) at receivers in an adjacent borehole. The measured magnetic fields are used to infer an electrical conductivity distribution of the earth by means of inversion of the measure data.

The role of the steel tank

The steel tank in proximity to the crosswell EM survey contributes a considerable signal. To access the tanks effect a model of a 10^{+10} S/m sheet of equal area to the tank bottom embedded at 1m depth in a 300 ohm-m halfspace was run with the transmitter and receiver well coordinates for the Tx1 to ERT-14 crosswell configuration. The 300 ohm-m layered response (crosswell data without the tank bottom) are shown in Figure 3 and the response with the steel tank bottom present is shown in Figure 4.

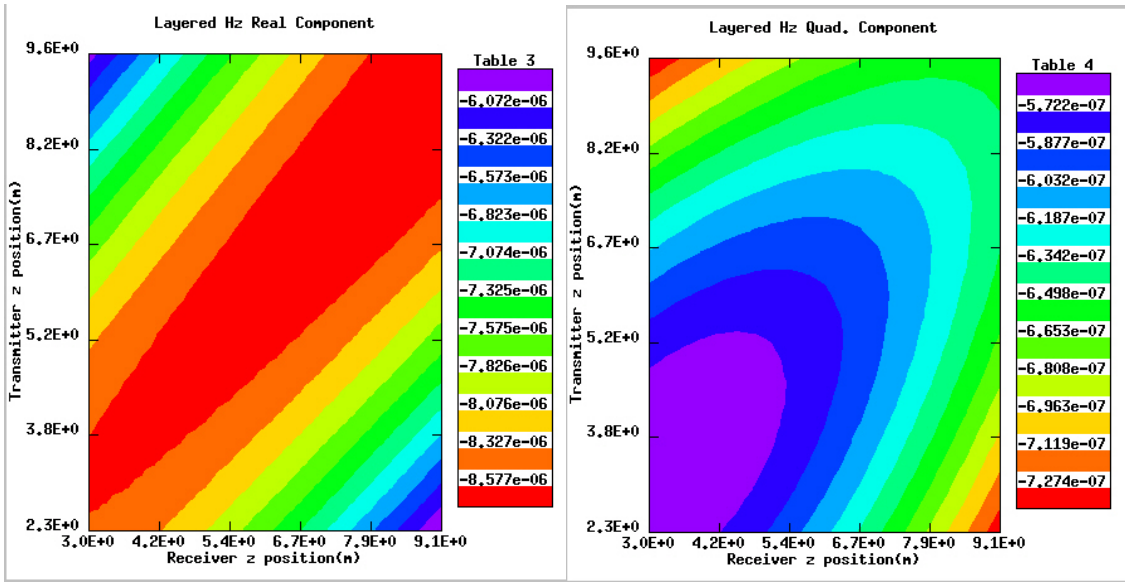

Figure 3: *Real (left) and quadrature (right) vertical magnetic field in ERT-14 from transmitter well Tx1 for a 300 ohm-m halfspace.*

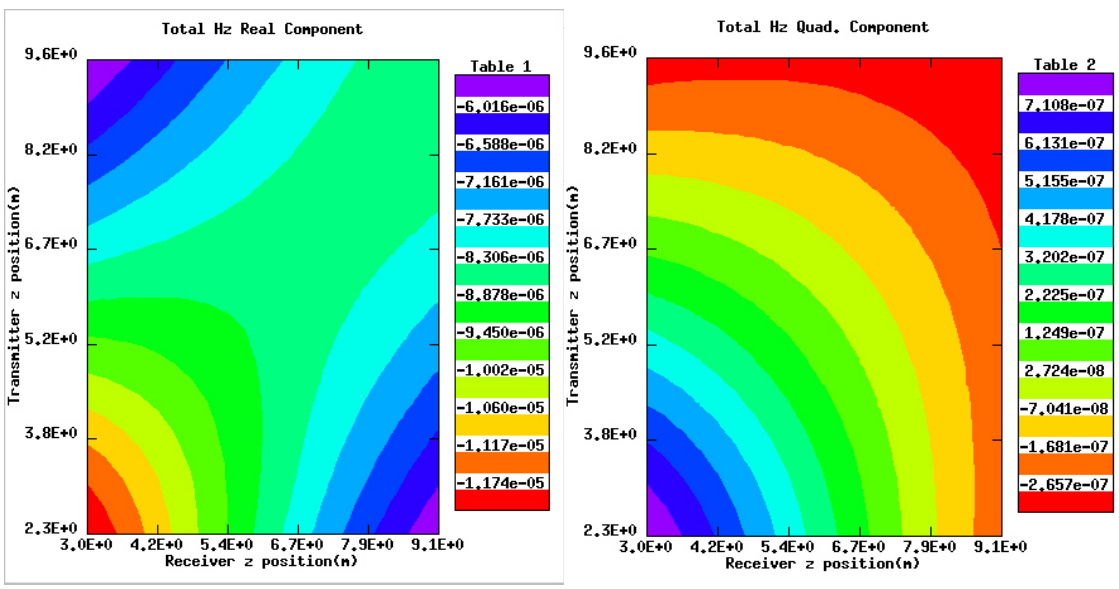

Figure 4: *Real (left) and quadrature (right) vertical magnetic field in the ERT-14 well from transmitter well Tx-1 for mock tank bottom in a 300 ohm-m halfspace.*

Comparing Figure 3 and 4 it is evident that the tank bottom has a large over-print on the data. For the proper imaging of the data the highly conductive tank may have to be accommodated in the inverse models. Two approaches will be investigated. One approach is to let the inversion place conductive material near the surface to accommodate the tank effects. Since we are interested in time-lapse effects and the tank is not changing the difference images should represent the change in conductivity beneath the tank even if the tank itself is not correctly imaged. A second approach is to try to build the tank (bottom and possibly sides) into the finite-difference mesh used for the inverse models and hold it fixed only allowing the region below the tank to vary in the

inversion. This approach has been investigated but represents a considerable numerical challenge since the contrast between the tank and the surrounding sediments is over 10 orders of magnitude.

Building the Tank into the 3D Finite Difference Mesh

In order to build a finite difference (FD) mesh to accurately model the effects of the steel tank on our crosswell EM data a model of only the bottom of the tank was first built. This FD solution can be checked against an integral equations code that models thin conductive sheets in a layered background. Figure 5 shows the portion of the FD mesh around the simulated tank bottom, with a shallow and a deep transmitter location opposite a well with a number of receivers. The bottom of the tank is simulated by a 0.2 m thick layer of cells (red in the figure) at a depth of 1m below the ground surface. This is thicker than the actual tank bottom but matches our integral equation results well. The comparison is shown in Figure 6 for the shallow (left panel) and deep transmitters (right panel).

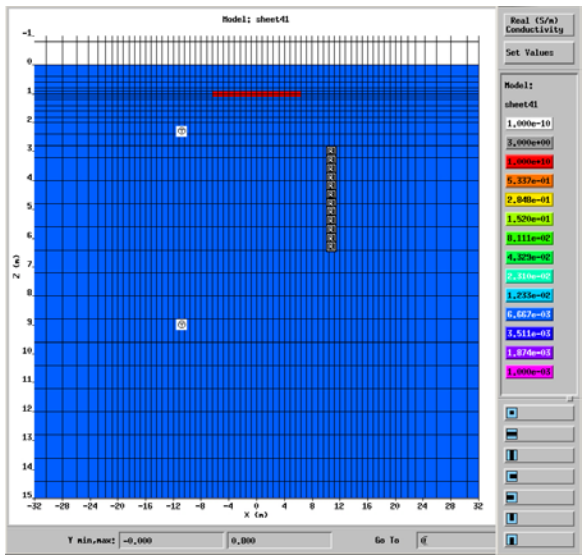

Figure 5: *Central portion of finite difference mesh used to simulate steel tank bottom in a 300 ohm-m ground.*

The area of the conductive plate is equal to the surveyed area of the tank bottom, 188.7 m^2.

A second model was built that includes the tank sides. Figure 7 shows this FD mesh. In this model we have gone to a course mesh where the tank walls are modeled as 0.5 m thick but with a conductivity such that the conductivity time the thickness of the walls are equal to that of the steel tank. In addition the center of the tank is now air filled.

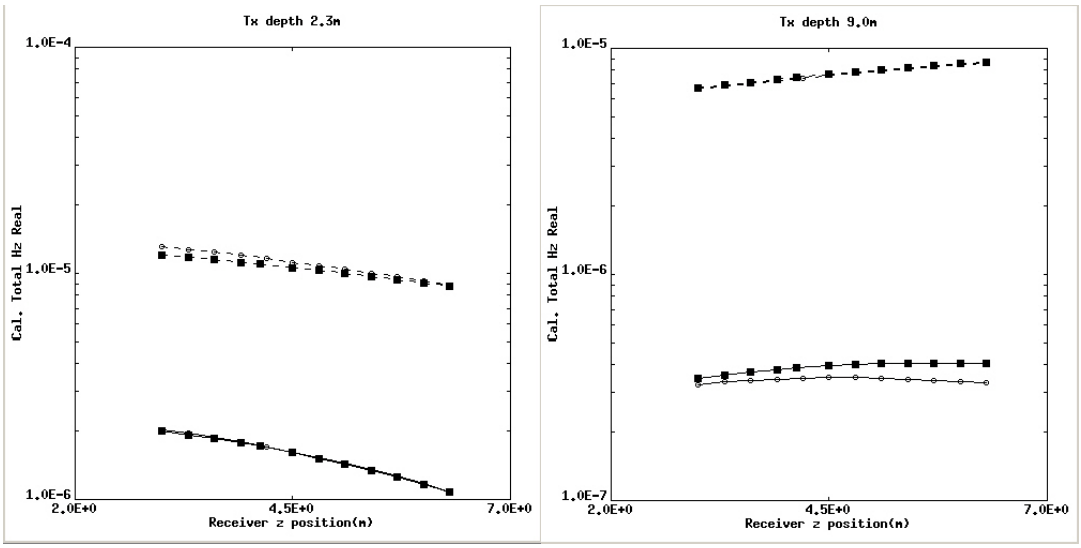

Figure 6: *The integral equation solutions for a thin steel sheet in a 300 ohm-m ground are shown for the shallow transmitter (left panel) and deep transmitter (right panel). The integral equation results are filled boxes the finite difference solution is small open circles.*

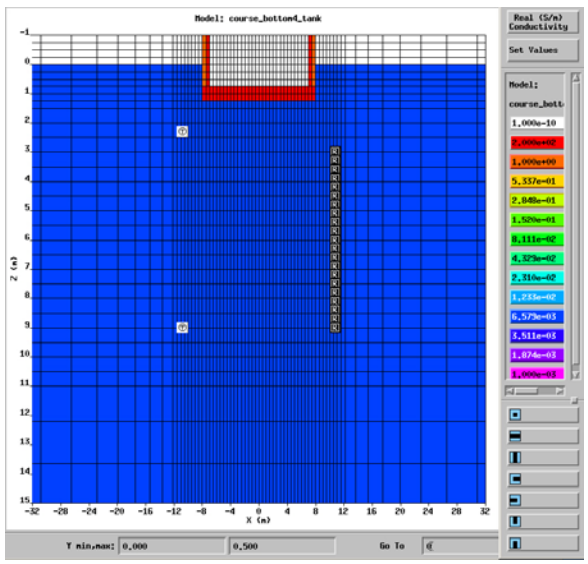

Figure 7: *Cross section at y=0 through the 3D FD mesh for full tank simulation.*

Figure 8 shows the comparison of this FD solution to the integral equation solutions of the tank bottom only. Thicker cells are used to simulate the tank in this model because this reduces the total number of mesh cells required as well as improving the stability of the numerical solution. These two facts result in a model that runs faster in less memory while still accurately representing the tank effects.

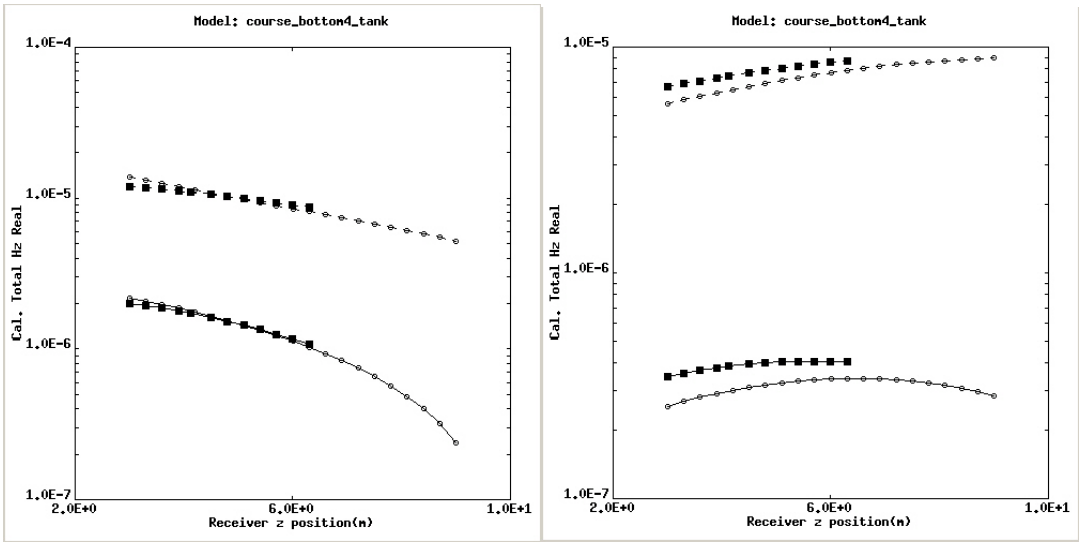

Figure 8: *Finite Difference calculations of the full tank compared to integral equation solution for the tank bottom only. Left panel: shallow transmitter, Right panel: deep transmitter. The integral equation solutions are filled squares and FD calculations are open circles.*

Figure 8 shows that the full tank as opposed to the bottom only does not affect the results for the shallow transmitter but does contribute to the solution for the deep transmitter.

At this time we have not determined if modeling the tank explicitly is required for accurate imaging beneath the tank. Additional forward models will be generated to simulate leaks beneath the tank and these results will be inverted and compared to the forward model that generated the data. This process requires considerable computation resources at this time both to do the inversions and to verify that the forward tank model solutions are accurate. This work will continue.

Pre-Injection Data

The pre-injection data showed evidence of anomalous behavior from the Tx1 transmitter (Figure A-1). Figure 9 shows the real and quadrature vertical magnetic fields from Tx1 to ERT-14 wells.

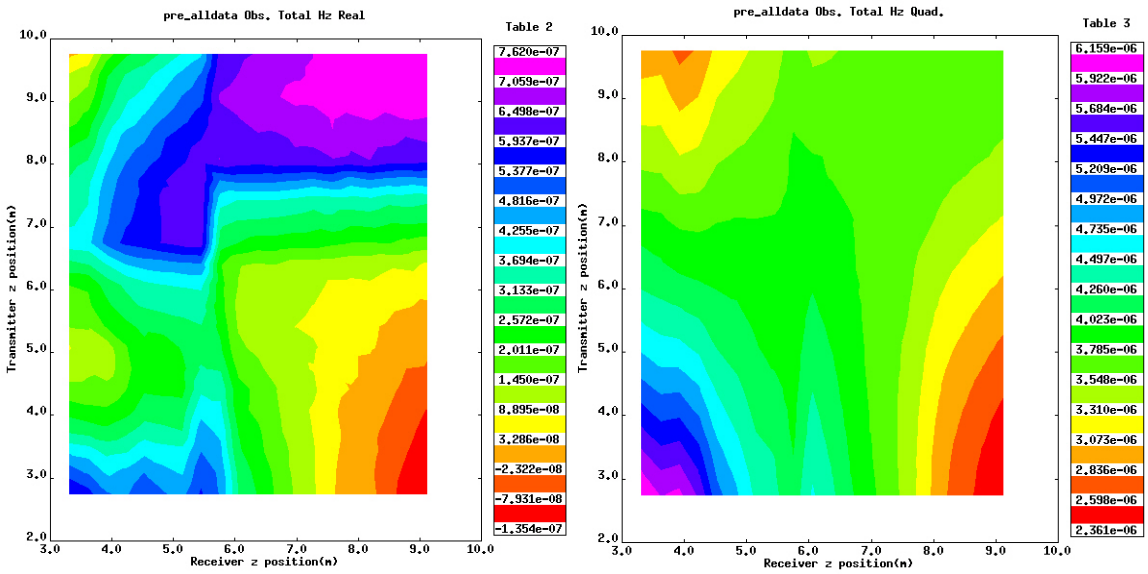

Figure 9: *Real (left) and Quadrature (right) vertical magnetic field from Transmitter Tx1 and receiver well ERT-14.*

Note the sharp discontinuity that occurs at a receiver depth of 6m.

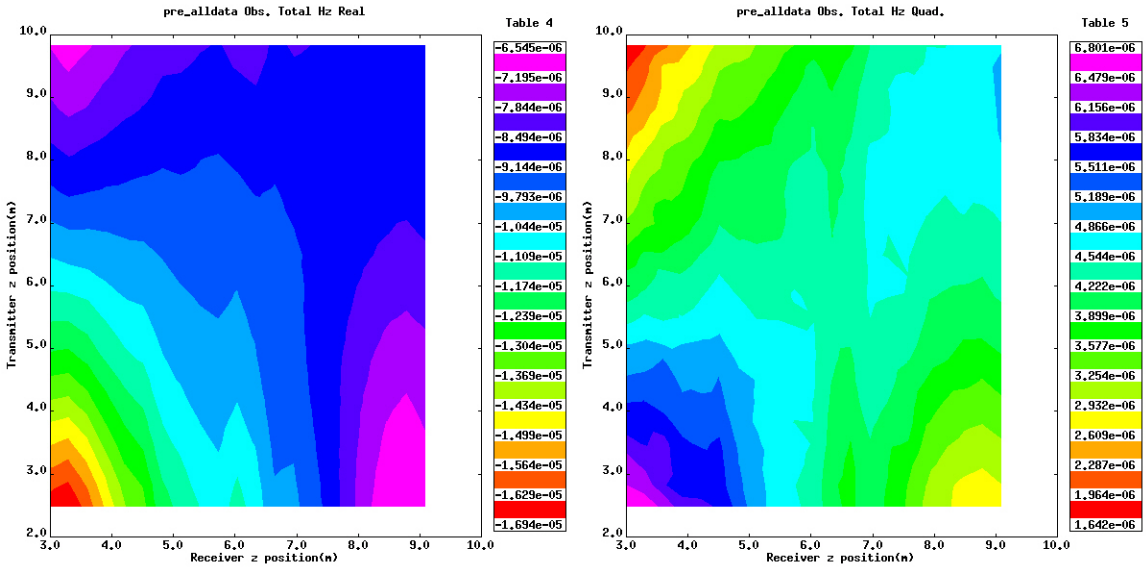

Figure 10: *Real (left) and Quadrature (right) vertical magnetic field from Transmitter Tx3 and receiver well ERT-6.*

In contrast Figure 10 shows the real and quadrature data for Tx3 into ERT-6 (Figure A1). This configuration should be almost reciprocal since the transmitter and receiver wells are nearly co-located. However, there are considerable differences in the real component. These differences persist over the entire time-lapse survey. We suspect that this is due to water that leaked from the Tx1 well during and after the seismic experiment was conducted. Prior to our arrival the Tx1 and Tx3 PVC wells were filled with fresh water (approximately 54 gallons). When we arrived on August 23 the Tx3 well was still full

(we had it pumped out) but the Tx1 only had 5 ft of water remaining in the bottom. The movement of the leak water around the Tx1 well caused the conductivity structure to be different for Tx1 acquisition compared to Tx3 acquisition (5 hours later).

Since the Tx1 well surroundings were contaminated by the water leak we have concentrated our interpretation on the data from the week of August 13. Figure 11 shows the raw data for some of the transmitter receiver combinations. The data is presented as real (in-phase with the transmitter current) and quadrature (out-of-phase with the transmitter current) as a function of depth in the receiver well.

In the upper left panel of Figure 11 we see that the quadrature component has a sharp break at a depth of 6m. This break is gone in for the same well pair on the next day, August 14 (upper right panel Figure 11). Numerical modeling shows that a sharp break like the one observed in our data is caused by a conductive feature extending across the receiver borehole at the depth of the break. The rapid change in response in one day indicates that the leaked fluids are moving across our receiver wells and away within 24 hours. By August 16 small discontinuities are again present in the tx1 to ERT14 pair at depths of 4.5 and 7 meters in the ERT14 well (lower left panel Figure 11). On August 17 (lower right panel Figure 11) we see the first indication that fluid has moved across the ERT10 well to the east.

From these observations of the raw data we conclude that the fluid moves vertically until reaching certain aqua-tards, which then cause the fluid to move laterally beyond the boundaries of the tank quite rapidly.

Time Lapse Data differences

To look at changes in the data at different dates caused by the leaked fluids we have produced data difference plots. Figure 12 shows the difference in real and quadrature vertical magnetic field from the Tx2 to ERT-10 wells between August 13 and July 23. The largest changes in the real component occur at depth intervals that correspond to relatively low resistivity zones in the Pitt-10 resistivity log (Figure 1).

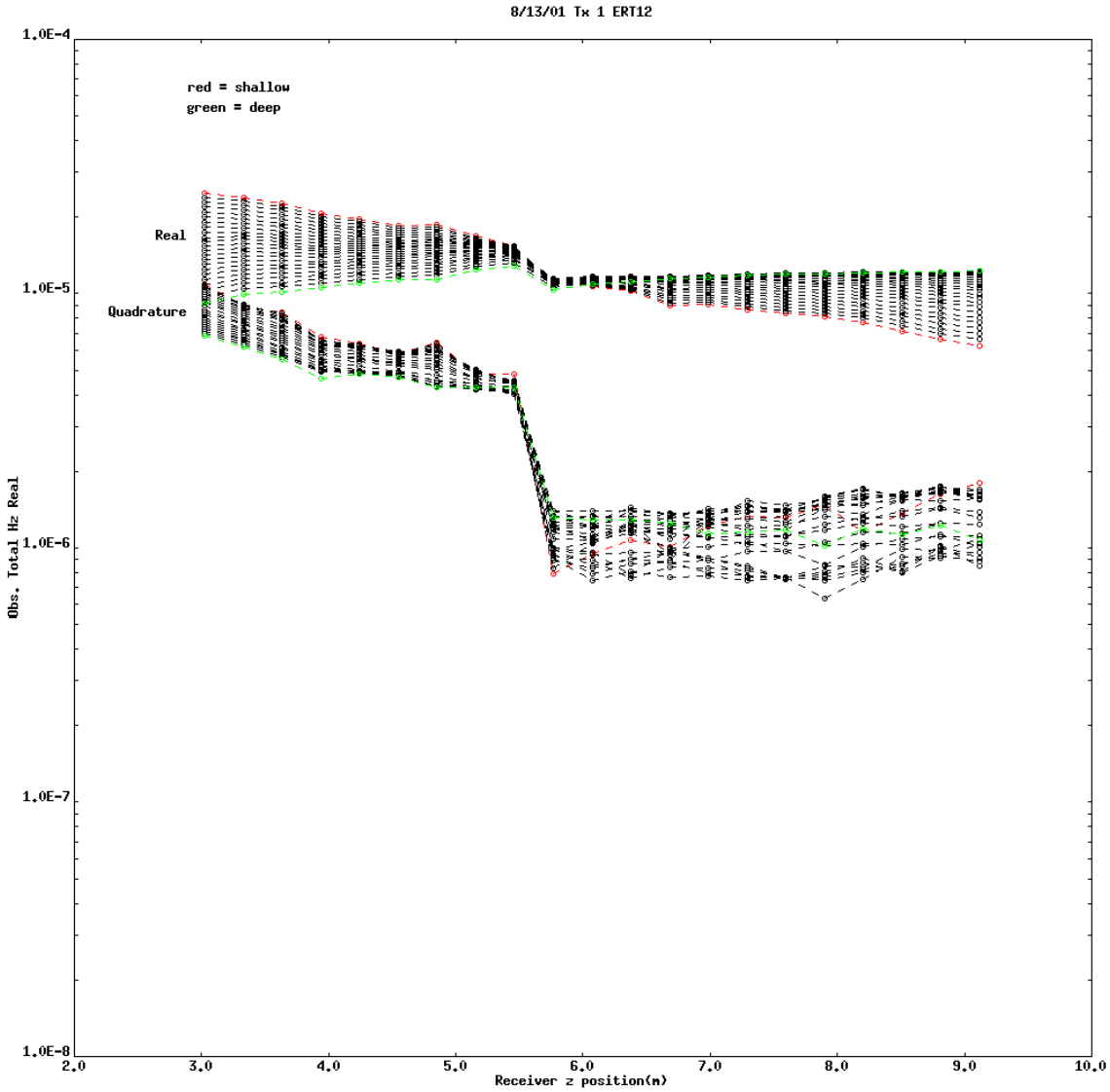

Figure 11: *Real and quadrature magnetic field strengths. Upper set of curves is the real component and lower set is the quadrature component. Horizontal axis is depth in the receiver well that is directly opposite to the transmitter well. Above panel is on August 13 between tx1 and the opposite ERT-14. Subsequent panels (pages C-12 through C-14) are for August 14-17.*

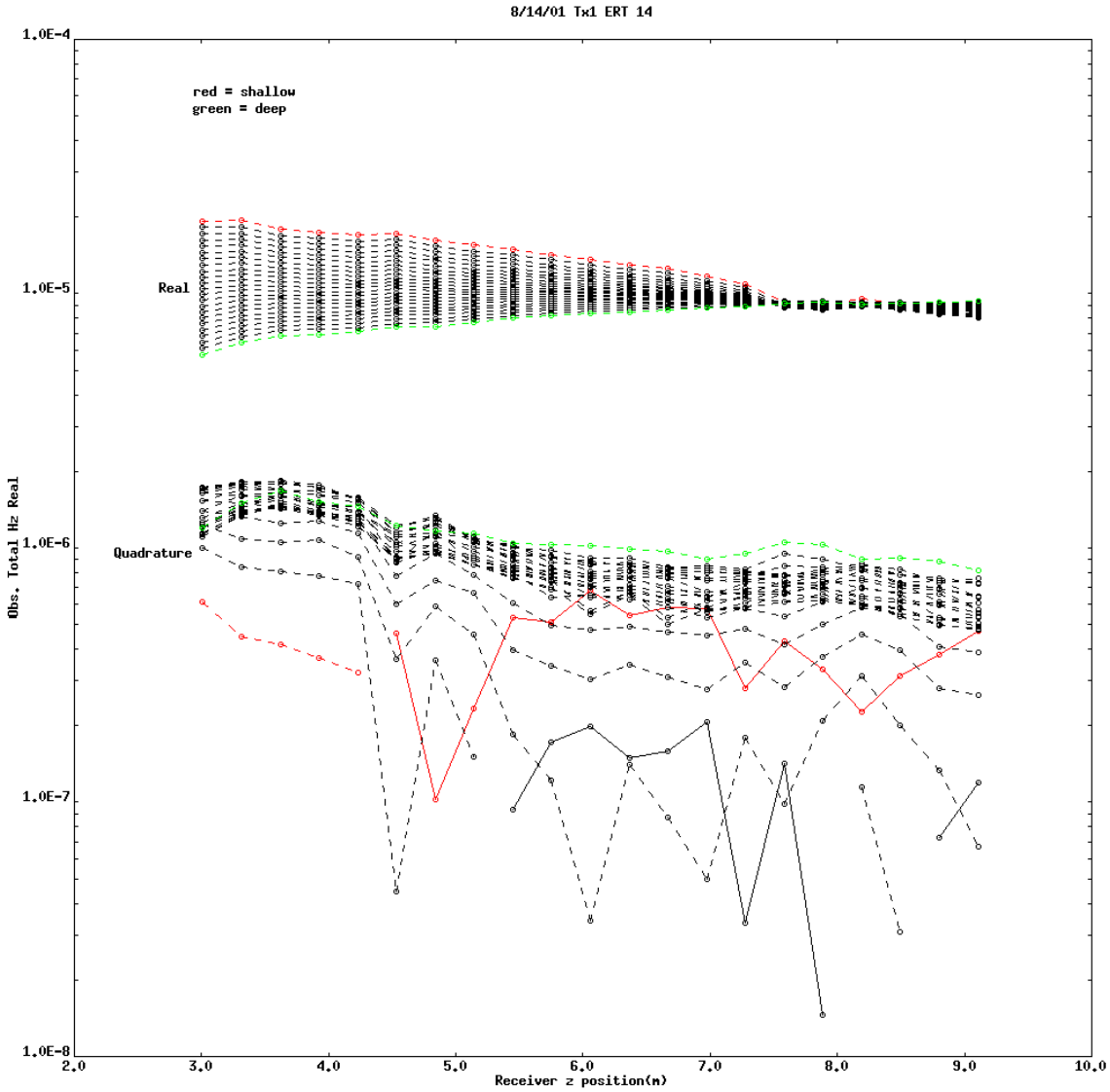

Figure 11: (contd) *August 14 between tx1 and ERT 14.*

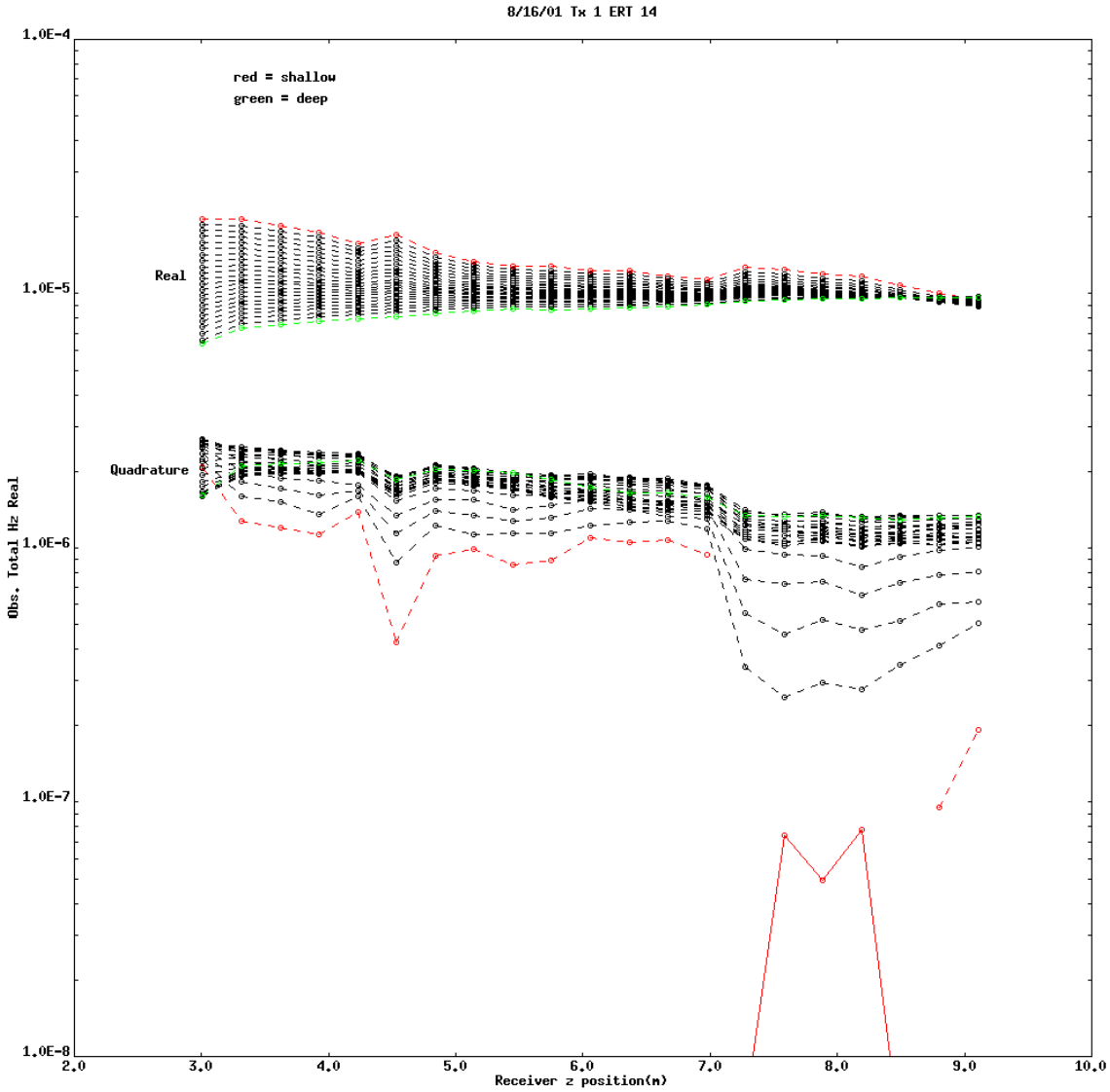

Figure 11: (contd) *August 16 between tx1 and ERT 14.*

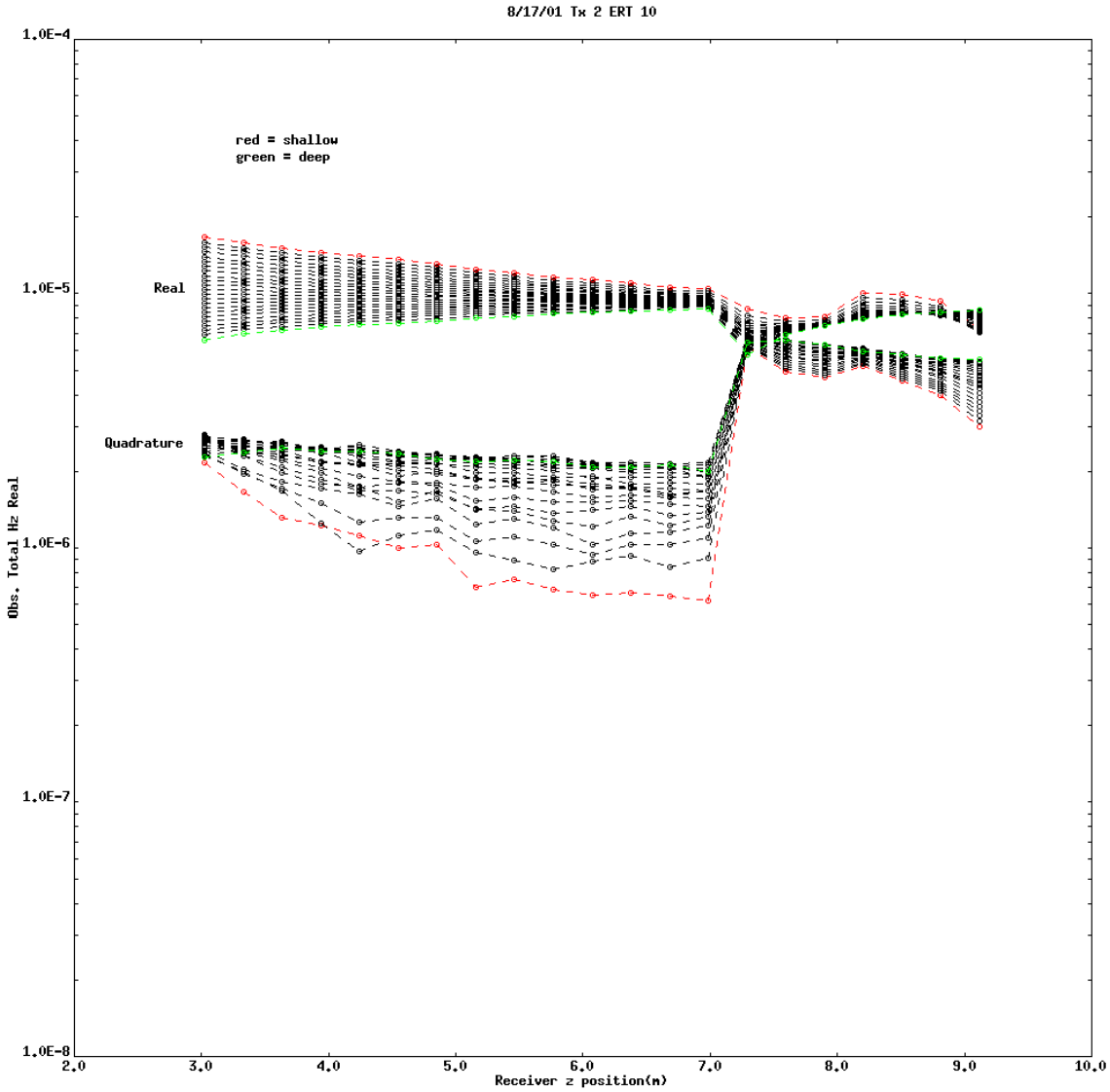

Figure 11: (contd) *August 17 between tx2 and ERT 10.*

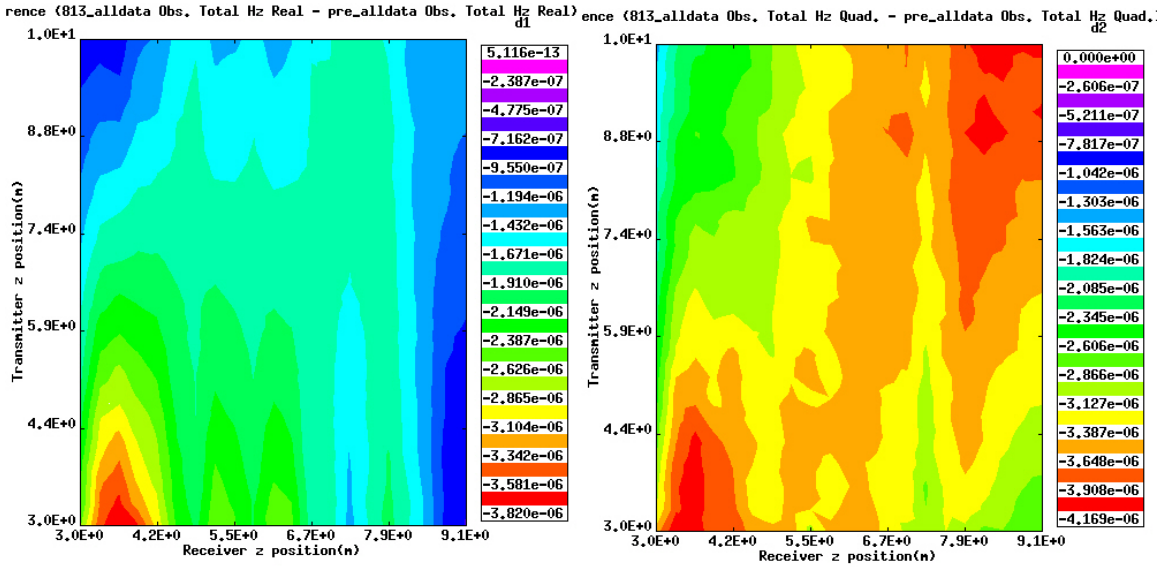

Figure 12: *Time-lapse changes in real (left) and quadrature (right) vertical magnetic field for transmitter Tx2 and receiver well ERT-10between July 23 (pre-injection) and August 13. Largest changes occur for transmitter and receivers near the surface, with peaks in change at 3.6, 5.2, 6 and 8 m depth for the receivers.*

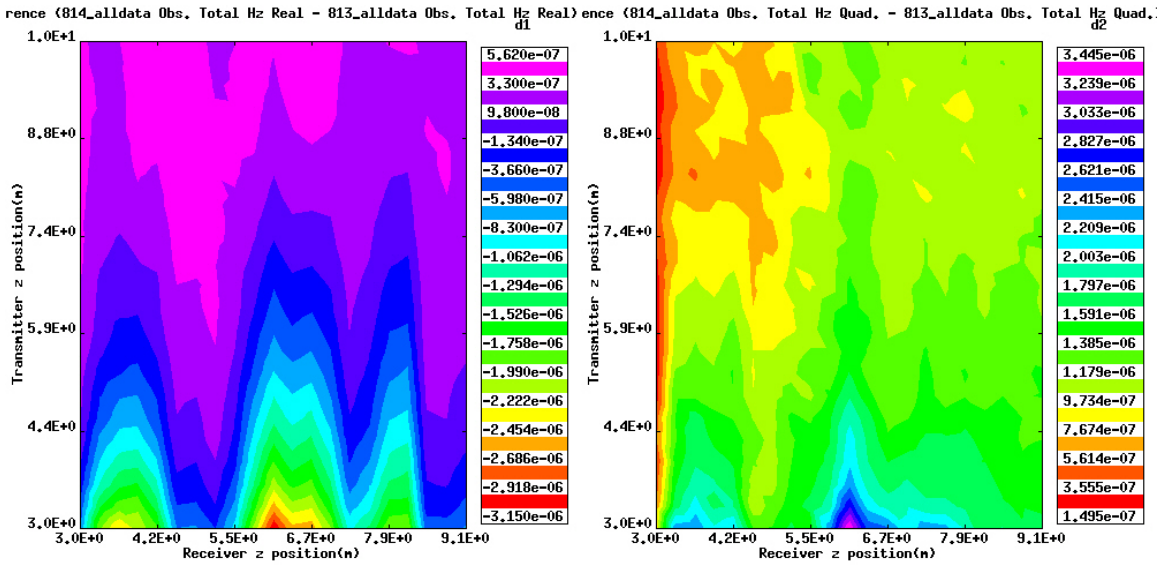

Figure 13: *Time-lapse changes in real (left) and quadrature (right) vertical magnetic field for transmitter Tx2 and receiver well ERT-10 between August 14 and August 13.*

Figure 13 shows the changes between August 14 and August 13 for transmitter well Tx2 and receiver well ERT10. The incremental changes are clearly located in the low resistivity layers shown in the Pitt-10 well log. Changes over a single day are occurring down to a depth of 8.5 meters, indicating rapid transport.

Parameters controlling the EM signal

The parameters controlling the strength and sensitivity of the EM signal in the crosswell configuration are 1) the average earth conductivity (σ), 2) the separation between source and receiver (R), and 3) the operation frequency (f). For significant induction to occur without too much loss these parameters must fall in a range so that the induction number, $(1/R)*500*(1/(\sigma*f))^{0.5}$, should be between 2 and 5.

At the Mock Tank site the background earth conductivity is between 0.001 and 0.002 with a well separation near 22m. The operating frequency of the LLNL system is 74KHz resulting in an induction number near 0.5. This means that we are working with very small amounts of induction. This will be ameliorated to some extent by the increased conductivity caused by the leaks.

Release & measurement schedule

As is listed in Appendix A three wells were used as transmitter wells. The data acquisition from each transmitter well to receivers in three opposing ERT wells used for our EM receivers took approximately 2 hours. Figure 14 shows the leak release schedule along with our measurement times for the week of August 13. The EM measurements took longer than the leaks. If the fluid is moving rapidly, as we suspect, in the subsurface then inverting the data from all three transmitters will cause significant time averaging to occur. It may be better in future work to use only data from a single transmitter well to get a better snap shop in time. In the results presented in this report all three transmitters were used to get better spatial coverage at the expense of averaging the conductivity distribution over time.

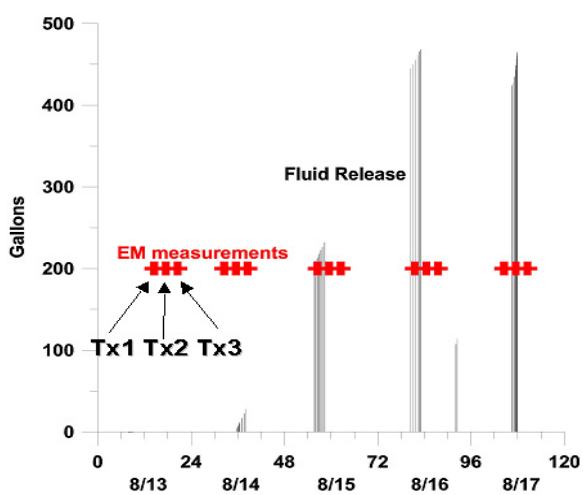

Figure 14: *Leak release schedule and EM measurement times. Each red cross represents measurements from a separate EM transmitter well.*

Time-lapse conductivity changes from inversion

The crosswell EM data for the 5 days August 13 through August 17 were inverted for a three-dimensional conductivity distribution that would fit the observed data. These

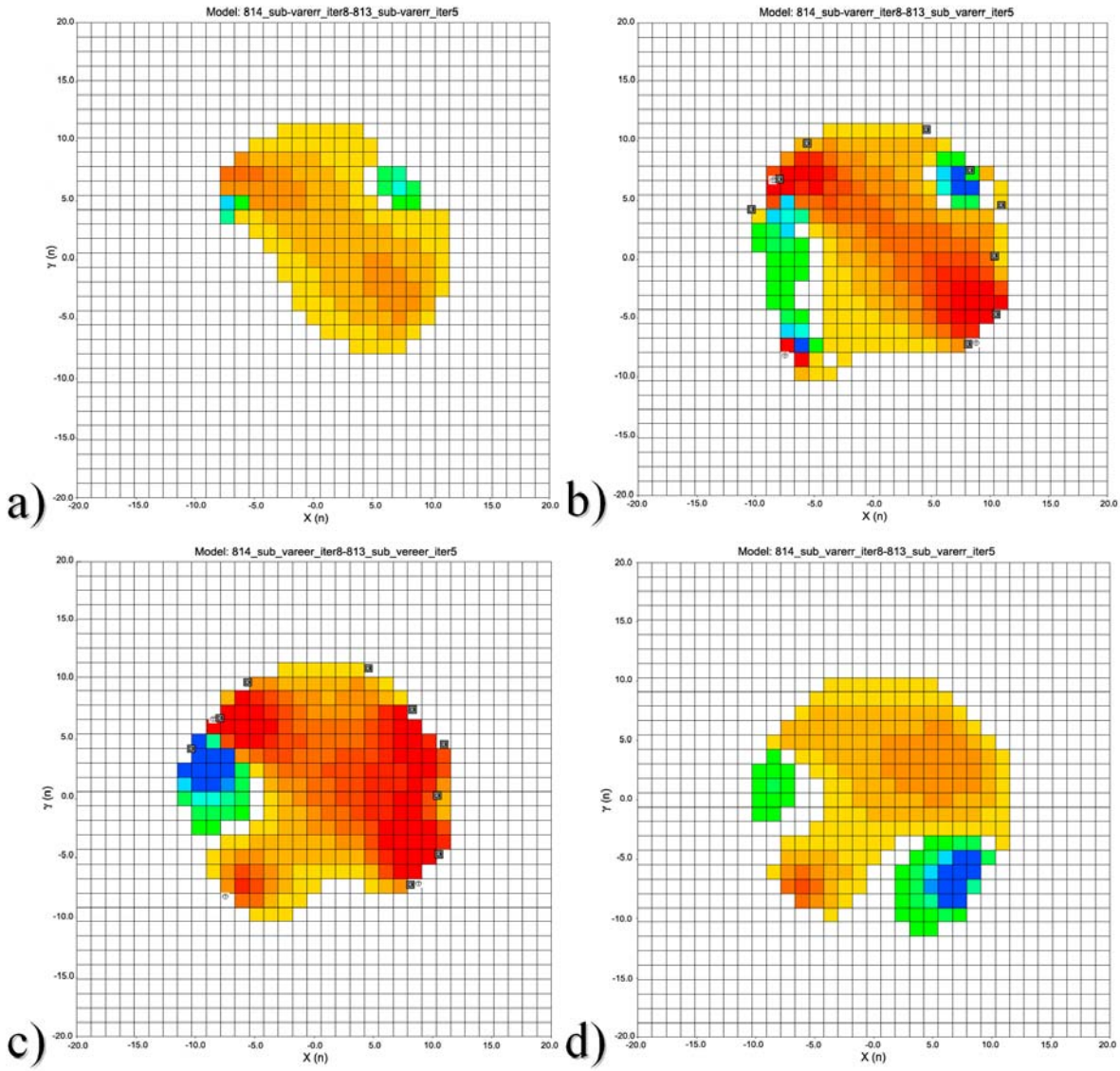

Figure 15: *Time-lapse conductivity difference between August 14 and 13. a) depth 1.2m, b) depth 3.6m, c) depth 7.0m, d) depth 10m. Red= +0.001 S/m, Blue = -0.001S/m. Note the large increase in* σ *to the east and southeast. The horizontal scales are from –10 to +10 meters, with the tank centered on (0,0).*

inversions were differenced between successive days to produce conductivity change volumes. The maximum sensitivity of the data occurs between the source and receiver wells, with very little sensitivity outside of the crosswell region. Figure 15 shows the conductivity difference between August 14 and 13. The maximum changes represented in the figure are +- 0.001 S/m with red representing an increase in conductivity and blue a decrease.

The maximum changes occur to the east and southeast at a depth slice at 7m. Smaller changes occur above and below a depth of 7 m. Figure 16 shows a vertical slice at

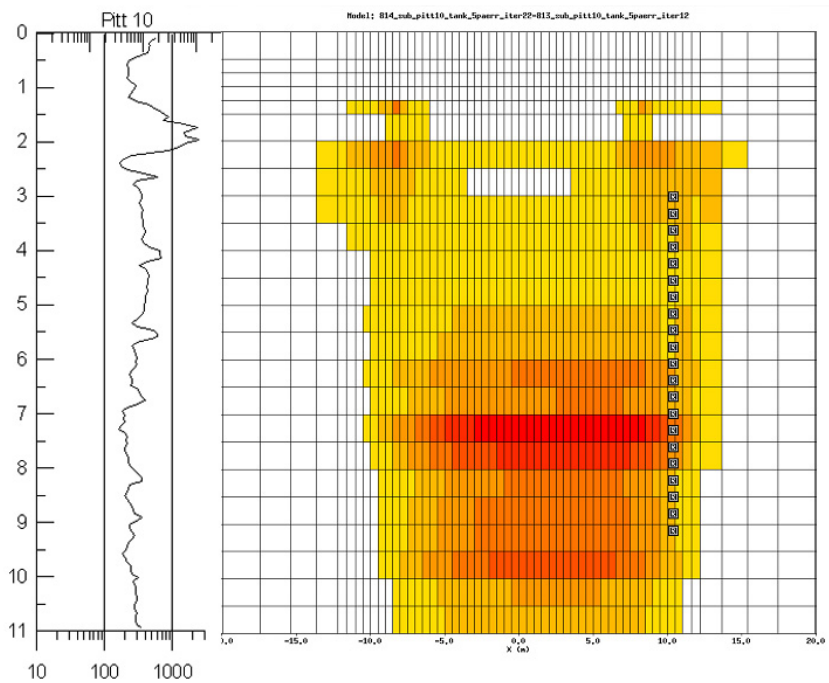

Figure 16: *Vertical cross section at Y=0m through the conductivity difference model for August 14 – August 13. The zones of maximum change at 7 and 9.5 m correspond to low resistivity (high permeability) layers in the Pitt-10 log.*

Y = 0m through the conductivity difference volume. The areas of maximum increase at 7 and 9.5 m correspond to low resistivity (indicating higher permeability) layers in the Pitt-10 resistivity logs.

One of the problems encountered in the interpretation of the time-lapse data was calibration of the EM instruments. The procedure called for pulling the transmitter and receivers from the wells at the end of each day and measuring the response of the system above ground. This provided values of the real and quadrature fields from the system for a known separation. These are used to compute an amplitude and phase value that is used to calibrate the data taken that day. Figure 17 below shows the amplitude values for the week of August 13 – 17. The first two days are relatively constant so we feel the difference of August 14 and 13 as shown above is valid. However, beyond the 14 the amplitude values vary day to day so we are not confident of difference those days.

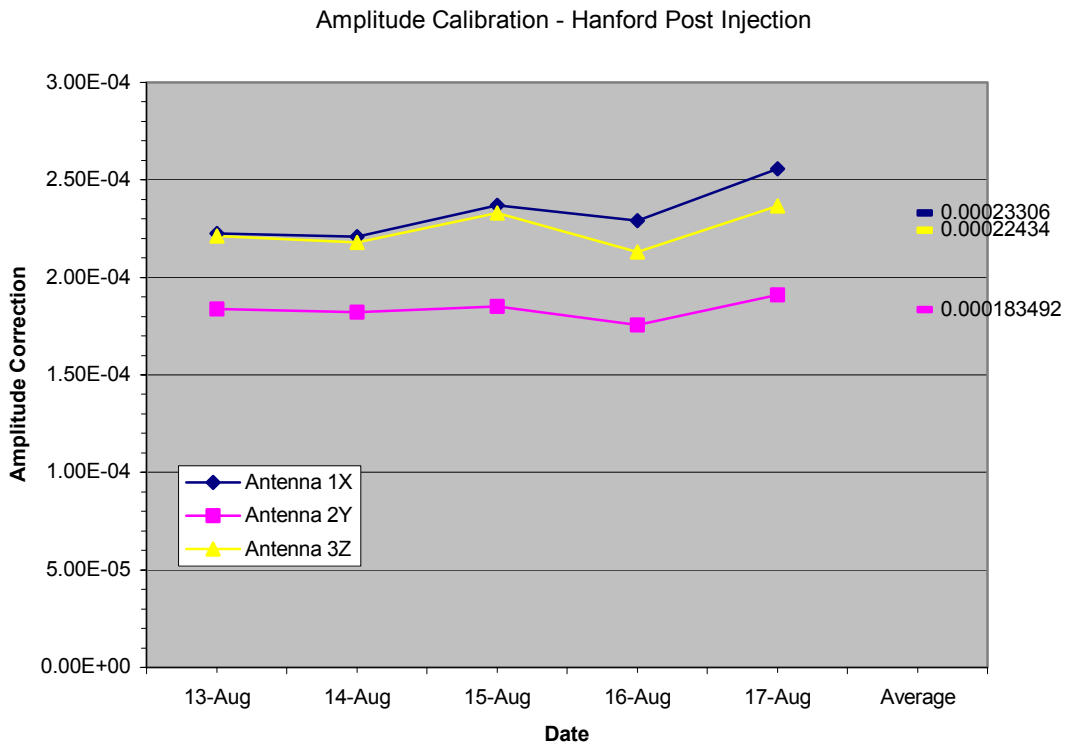

Figure 17: *System amplitude calibration curves. Three receiver coils, 1X, 2Y and 3Z are shown.*

We have calculated an average calibration factor and applied it to all of the data sets.

Discussion

A number of problems in the survey were identified along with limitations of the current system. These can be summaries in the table below.

- NW PVC transmitter (TX1) well
  - Water for seismic source leaked into the formation prior to pre-injection monitoring. This disturbed the conductivity structure around one of our three transmitters and caused it to change over time as the fluid migrated. This led us to not use the pre-leak data as a baseline because of limited data coverage.

- ERT electrodes in wells used for EM receivers produce time variable coupling as the subsurface conductivity distribution changed.

  –Artifacts at many ERT wells at various depths

- 5 hour data acquisition time for all 3 transmitters causes the $\Delta\sigma$ distribution to be different between the different TX acquisitions

– Imaged conductivity distribution is averaged over time
– Re-doing the inversions for individual transmitters and differencing those images will provide a sharper time focus but will have limited spatial coverage.

• Inversion of low-induction number data requires considerable run time

– Ongoing research
– Higher operating frequencies are needed in the low conductivity soils of Hanford.

• Daily calibration of system showed considerable variation

– Using average value will help
– Modifying inversion codes to use ratios of adjacent receiver values will eliminate the calibration problem

Continuing Work

• Inversion work was not complete
–Finer, more stable meshes need to be investigated

• Considerable parallel computing resources are needed
–Different data weighting schemes need to be investigated

• Current research at EMI indicates low-induction number schemes are needed (down-weight the primary component)

• Additional forward modeling to determine optimum EM configuration for maximum sensitivity
–Minimize time-variable EM coupling into tank and other nearby steel

• This experiment will be the background for an upcoming joint Sandia-LBNL EMSP proposal on tank farm EM monitoring.

Conclusions

This experiment has demonstrated a number of limitations of using cross-well EM imaging for leak detection. Chief amount them are the time required for data acquisition and the computing resources required to image the data. Another issue is the dependence of the conductivity images on the inversion algorithms employed. The limitations of time and computing resources can be addressed in the future through better system design and faster codes and computers.

The issue if image, and hence the interpretation, dependence on algorithms is a very serious problem. This is not restricted to crosswell EM but is common to all imaging of geophysical data. Relatively little attention has been paid to how different algorithms and data weighting affect the resulting conductivity images. Experience with crosswell seismic and EM suggest that the un-wary user of geophysical technology will be in for

some nasty surprises if images are used in mission critical decisions without a significant amount of up front testing and verification of the algorithms used.

Even with the problems and limitations of the experiment we are able to conclude that the fluid plume moves rapidly laterally. The day-to-day EM response changes at receiver wells shows that the fluid passed some receiver wells in less than one day. The plume initially moves to the southeast in the shallow sub-surface and later moves more easterly at greater depth.

The interpretation of this data set is at present incomplete and unsatisfactory. Indeed, the ability to infer fluid movement is based entirely on a short-duration sampling window and subsequent numerical modeling; other interpretations of this data are possible. Work will continue both in the development of the inversion algorithms and in the interpretation of the future results.

Appendix A
Pre-injection crosswell EM data acquisition

File nomenclature:

Take for example the file directory **Bt1r161514**.

- "B" is baseline. Subsequent data sets will have the letter of the month and the day (i.e. A05 for August 5th)
- "t1" means the transmitter is in well T1; "t2" means transmitter is in well T2; ...
- The next character is "r" standing for receiver position. Where Antenna 1 (Hx1) is in the first two digit ERT well location, antenna 2 (Hy2) is in the third and fourth digit ERT well number, and so on. (For example r161514 means antenna 1 is in ERT well # 16, antenna 2 is in well ERT-15, and antenna 3 is in ERT-14)

Another example, file directory **Bt1rt31312**:

- This is the baseline survey
- Transmitter is in well T1
- Receiver 1 is in well T3 (or transmit well #3)
- Receiver 2 is in well 13 (or ERT-13)
- Receiver 3 is in well 12 (or ERT-12)

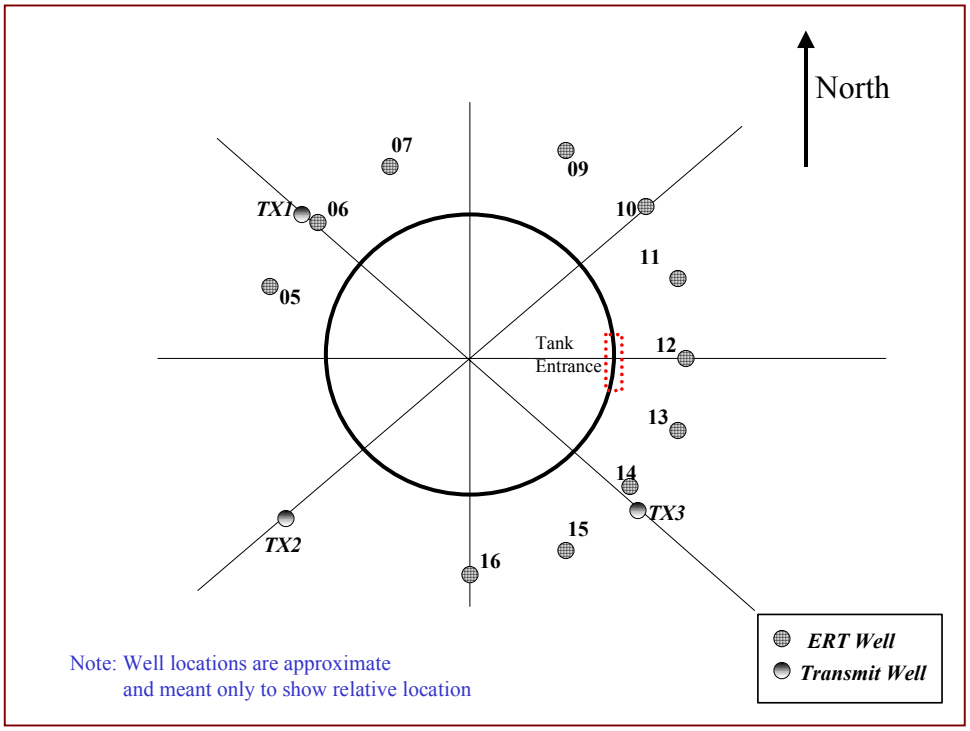

Figure A-1: *Transmitter-receiver well location map*

Data Acquisition:

Filename	Date Acquired	Transmitter Velocity (ft/sec)	Receiver spacing (feet)	Notes
Bt1r161514	July 23, 2001	5	1	
Bt1141312	July 24, 2001	5	1	
Bt1rt31312	July 24, 2001	5	1	Try using receiver well t3 (no electrodes) instead of receiver well ERT-14 (with electrodes). The other two receiver wells ERT-13 and ERT-12 are duplicates of above data set Bt1141312
Bt2r111009	July 25, 2001	10	1	
Bt3r050607	July 25, 2001	10	1	

Appendix B
Post-injection crosswell EM data acquisition summary

Nomenclature is as follows:
"channel"+"prefix letter"+"date"+"transmit station"+"receive stations"

Channel:	ch1 = EMI antenna #0101 ch2 = EMI antenna #0102 ch3 = EMI antenna #0103
Prefix letter:	B "baseline" P "post injection"
Date:	In Month/Day format (i.e. 0816 is August 16)
Transmit station	T1 "NW PVC" T2 "SW PVC" T3 "SE PVC"
Receive stations	i.e. R050607 = antenna ch1 in ERT-05, antenna ch2 in ERT-06, antenna ch3 in ERT-07
File name:	i.e. ch1_p0814t2r091011 is the post injection file acquired on August 14, with a receive antenna in well ERT-09, transmitter antenna in SW PVC i.e. ch3_p0814t2r091011 is the same as above except the receiver antenna is in ERT-11.

Every day, three surveys were acquired:

Survey Name	Transmitter Well	Receive Well **ch1** (distance)	Receive Well **ch2** (distance)	Receive well **ch3** (distance)
01 …T1R141312	NW PVC ("t1")	ERT14 (21.6455)	ERT-13 (22.1549)	ERT-12 (19.9528)
02 …T2R091011	SW PVC ("t2")	ERT-09 (22.6687)	ERT-10 (22.2675)	ERT-11 (22.4321)
03 …T3R050607	SE PVC ("t3")	ERT-05 (22.2361)	ERT-06 (21.7439)	ERT-07 (22.2189)

Data Acquisition Schedule					
Time(hr)	Mon(8/13)	Tues(8/14)	Wed(8/15)	Thurs(8/16)	Fri(08/17)
0600					
0700					
0800		SURVEY 01	SURVEY 01		SURVEY 01
0900		SURVEY 01	SURVEY 01	SURVEY 01	SURVEY 01
1000				SURVEY 01	

1100		SURVEY 02	SURVEY 02		SURVEY 02
1200		SURVEY 02	SURVEY 02	SURVEY 02	SURVEY 02
1300				SURVEY 02	
1400	SURVEY 01	SURVEY 03	SURVEY 03		SURVEY 03
1500	SURVEY 01	SURVEY 03	SURVEY 03	SURVEY 03	SURVEY 03
1600				SURVEY 03	
1700	SURVEY 02				
1800	SURVEY 02				
1900					
2000	SURVEY 03				
2100	SURVEY 03				

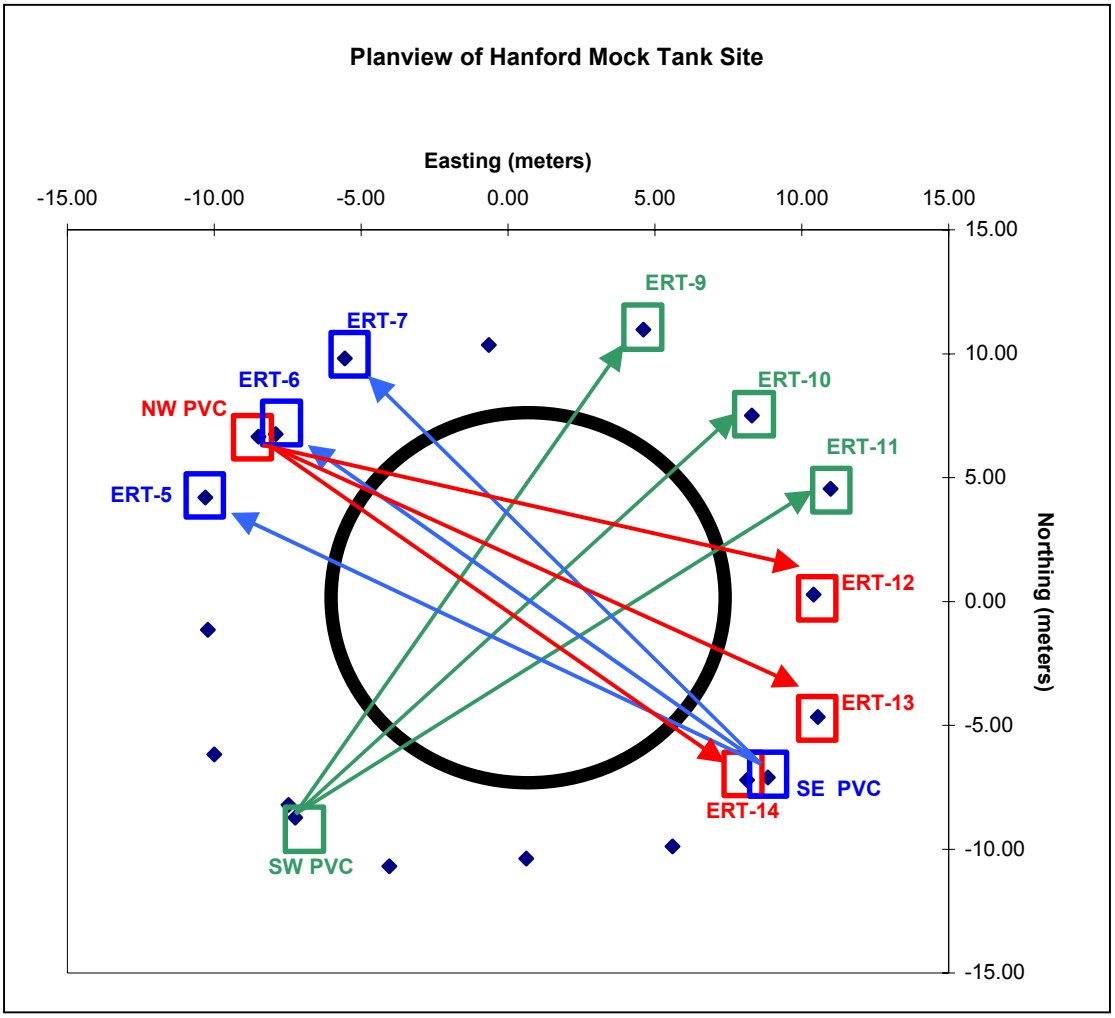

Figure B-1: *Post injection crosswell EM survey configurations. Each combination of transmitter and receiver wells is shown by a distinct color.*

Appendix D

Electrical HRR-SCRT Measurements Completed for the 2001 LDMM Study, Mock Tank Site

James B. Fink, Marc T. Levitt, and Chris Baldyga

Appendix D: Electrical HRR-SCRT Measurements Completed for the 2001 LDMM Study, Mock Tank Site

TABLE of CONTENTS

DESCRIPTION	PAGE
1.0 EXECUTIVE SUMMARY	1
2.0 INTRODUCTION	4
2.1 Objective of Investigation	6
2.2 Site Location	7
2.3 Survey Area & Logistics	7
2.4 Casing and Wire Arrangement	8
2.5 Equipment	9
2.6 Data Acquisition	11
2.7 Data Processing	12
3.0 METHODOLOGY	14
3.1 Electrical Resistance and Resistivity	14
4.0 RESULTS & INTERPRETATION	16
4.1 Measurements Between Steel Casings and the Steel Tank	16
4.1.1 Potential Slope Analysis	18
4.1.2 Perturbation Analysis	20
4.2 Measurements Between Steel Casings and the Injection Electrode	22
4.3 Surface Measurements	23
4.3.1 Measurements Between Surface Electrodes and the Steel Tank or Injection Well	24
4.3.2 Measurements Between Surface Electrodes and the Steel Casings	27
4.4 Measurements Between Pseudo-Casings (fused ERT arrays)	29
4.5 Measurements along Individual Vertical ERT arrays	32
4.6 Measurements at Three ERT array levels (fixed depth)	35
4.7 Measurements Between ERT arrays (full ERT)	35
4.8 1-D Modeling using surface electrode array	35
5.0 SELECTION CRITERIA	30
5.1 Gate Selection Criteria	38
5.2 Matrix Approach Selection	39
6.0 TANK SITE IMPLEMENTATION	41
6.1 Proposed Work Plan	41
6.2 Points of Concern	42
7.0 SUMMARY & RECOMMENDATIONS	44
7.1 Development of New Equipment	45
7.1.1 Problems with the McOhm-21	46
7.1.2 Problems with the SuperSting R8	46
7.1.3 Overcoming Equipment Problems	47
8.0 FUTURE CONSIDERATIONS	48

8.1 Further Processing 48
8.2 Additional Injections 48
9.0 ACKNOWLEDGEMENTS 49
10.0 SIGNATURE PAGE 50

LIST of FIGURES

FIGURE NO.	DESCRIPTION	PAGE
1	Location and Feature Map - Mock Tank Site	8
2	Geophysical Equipment Connection Schematic	10
2a	Time Graph of Data Acquisition Periods (first third of injection period)	11
2b	Time Graph of Data Acquisition Periods (second third of injection period)	12
2c	Time Graph of Data Acquisition Periods (last third of injection period)	12
3	Potential Time Series Plots for Steel Casings and Steel Tank	17
4	Flow Rates vs. Injection Slopes	19
5	Calculation of Flow Rate and Volume for Northwest Casing	19
6	Calculation of Flow Rate and Volume for Southwest Casing	20
7	Expanded view of Data Acquisition Period (Injection 3 and 4)	21
8	Potential Time Series Plots for Steel Casings and the Injection Well	23
9/10	Potential Maps for Surface Electrodes - Steel Tank and Injection Well	26
11/12	Potential Maps for SW and SE Steel Casing and the Surface Electrodes	28
13	Potential Maps for NW Steel Casing and the Surface Electrodes	29
14/15	Potential Maps for Steel Tank, Injection Well and the Pseudo-casings	31
16	Comparison 3-D Dynamic Volumetric Potential Maps	32
17/18	Discrete Point Vertical ERT Distribution	34
19	1-D Resistivity Inversion Profile	36

LIST of TABLES

TABLE NO.	DESCRIPTION	PAGE
1	Summary of Calculated vs. Actual Flow Rates and Volumes	20
2	Summary of Interpreted Flow Events	22
3	Summary of Surface Potential Images for Figures 10-13	24
4	Summary of Surface Potential Images for Figures 14-15	30
5	Table of ERT Fusing Combinations	33

1.0 EXECUTIVE SUMMARY

Our contribution to the 2001 Leak Detection Monitoring and Mitigation (LDMM) project was to perform and evaluate dynamic, direct-contact, ultra-low frequency (quasi-DC) electrical measurements using high-resolution resistivity and steel-casing resistivity technology (HRR-SCRT) at the 105-A Mock Tank Site. As sensor networks for data acquisition, we used a combination of various modes of grounding which consisted of a.) surface electrodes; b.) three, newly-installed, steel-cased boreholes; and c.) sixteen, previously installed, electrical-resistance-tomography (ERT) vertical arrays. The results unequivocally demonstrate that HRR technology is capable of highly accurate leak detection and plume monitoring. This report discusses HRR deployment at the 105-A Mock Tank site and the results thus far.

As with year 2000 and 2001 measurements made at the Sisson and Lu Site, measurements at the Mock Tank Site were made in three general phases:

1. prior to the first injection,
2. during injections, and
3. after all injections were completed.

The exception to the previous measurement pattern was an attempt to monitor continuously during the entire injection sequence.

The measurements were made in two "groups." The principal group consisted of using the newly installed steel casings, the steel tank, the central injection electrode, and sixty-one surface electrodes. We used *five primary grounding points* for the casing-related measurements. All grounding points were used for signal reception. The five transmitting "electrodes" were:

1. the "injection" electrode located inside the central leak point within the steel tank,
2. the steel tank shell itself, and
3. the three, recently installed, 6-inch-diameter, steel casings located southeast, southwest, and northwest of the tank at roughly the same distance from the tank as the ERT arrays.

The receiving electrodes consisted of sixty-one surface electrodes, arranged in a radial pattern emanating in eight directions from the tank, as well as the transmitting electrodes (when they weren't being used as transmitters).

The second group of measurements consisted of various configurations of the ERT arrays. There are sixteen pseudo-casings roughly distributed uniformly around the tank. Each ERT array consists of 8 electrodes spaced at 5-foot intervals from the surface to 35 feet. Leads from each electrode were previously routed to a patch panel located on the north side of the tank. We shorted, or "fused", each vertical ERT array at the patch panel and treated each fused ERT array as a "pseudo-casing". We also made conventional ERT measurements between vertical ERT

arrays (2-D panels), three horizontal levels using single electrodes in each ERT array at 10, 20, and 30 foot depths, and one 3-D data set using transmitting electrodes at the three aforementioned depths. The ERT results are not presented in this report.

In both groups of measurements, data were acquired almost continuously from the time of commencement of the initial injection until after the end of the last injection. There were several time gaps due to equipment failure, bad data, and standby periods during which other groups made their measurements.

Based on the results, the following observations and conclusions have been made.

1. Measurements between the steel casings and using the steel tank as an electrode provided:
    a. Positive and immediate indication of the commencement of injections.
    b. Positive and immediate indication of the cessation of injections.
    c. Good spatial determination of the injection location (somewhat forced because of the algebraic reconstruction used and the central location of the injection point).
    d. Good correlation between the electrical response and changes in the rate of injection.
    e. Good quantitative injection rate estimations.
    f. Good quantitative injected volume estimations.

2. Measurements using the steel casings and the central-injection-electrode provided very similar yet slightly different results (compared to item 1 above) and included:
    a. Positive and immediate indication of the commencement of injections.
    b. Positive and immediate indication of the cessation of injections.
    c. Good spatial determination of the injection location (somewhat forced because of the algebraic reconstruction used and the central location of the injection point).
    d. Good correlation between the electrical response and changes in the rate of injection.
    e. Good quantitative injection rate estimations.
    f. Good quantitative injected volume estimations.

3. Measurements between the steel tank and surface electrodes show that the simple geometry of the grounded tank results in predictable surface potential distributions that can be used for minimizing the signature of such a large signal source.

4. The measurements between the steel casings and the surface electrodes produced the least diagnostic results, primarily due to the limited number of casings.

5. The measurements using various configurations of the ERT arrays were not part of our original work plan. Nevertheless, we took advantage of the opportunity. The preliminary results demonstrate good correlations with the injected volume.

6. The technology can be implemented non-invasively directly on the outer tank shell, although pre-existing invasive structures such as steel well casings can be incorporated and will enhance the results.

7. Deployment of the system is straightforward requiring only simple electrical connections to appropriately grounded metallic structures.

8. Deployment can be made relatively inexpensively and can be adapted to virtually any on-site conditions.

9. Monitoring may be controlled remotely or made autonomous.

10. Results may be telemetered in real-time to a centralized location.

11. The technology can be deployed using existing infrastructure, although site-specific modifications would enhance the performance.

12. Appropriate instrumentation should be built that will eliminate spark hazard and allow operation in the tank farms.

2.0 INTRODUCTION

As part of the Battelle Pacific Northwest National Laboratory's (PNNL) 2001 Leak Detection Monitoring and Mitigation (LDMM), hydroGEOPHYSICS conducted electrical geophysical measurements to dynamically monitor the induced "leak" during August of 2001. Survey efforts were completed at the 105-A Mock Tank injection test site (herein referred to as the Site). The Site is located in the 200 East Area within the Hanford Site.

The electrical data were acquired as continuously as other operations allowed: (1) before any injections were made; (2) during the initial injection; and (3) after the injections were completed. Data acquisition was completed during a single period from August 7 through 25, 2001.

Electrical measurements were made using four types of electrodes, or sensors, for transmitting and receiving. The three types of electrodes used were:

1. 61 stainless-steel receiver electrodes,
2. the carbon-steel tank itself,
3. existing carbon-steel, casings located around the perimeter of the mock tank, and
4. electrical resistance tomography (ERT) vertical arrays previously installed.

All measurements were based on the pole-pole electrode array that was performed using a four-electrode configuration with two internal electrodes, one current electrode at effective infinity and one voltage electrode at effective infinity. One hookup arrangement at the mock tank field setup most closely resembles the mise-a-la-masse approach because we energized one of the internal electrodes as a transmitter by making direct contact with the target body (tank or injection well electrode) and another internal electrode as a receiver (surface electrodes or well casings). Various configurations of this approach were collected.

There were eight configurations of electrical measurements:

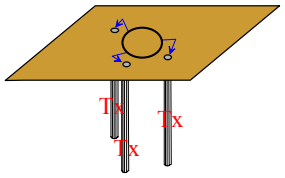

1. Measurements between steel casings and the steel tank. This configuration consisted of energizing the steel casings and measuring potentials at the steel tank. Reciprocal measurements were also made.

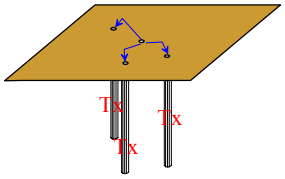

2. Measurements between steel casings and the injection electrode. This configuration consisted of energizing each steel casing and measuring the potential at the injection electrode. Reciprocal measurements were also made.

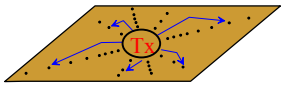

3. Measurements between surface electrodes and the steel tank. This configuration consisted of energizing the steel tank and measuring potentials at the surface electrodes. Reciprocal measurements were not made.

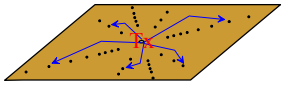

4. Measurements between surface electrodes and the injection electrode. This configuration consisted of electrically energizing the injection electrode and measuring potentials at the surface electrodes. Reciprocal measurements were not made.

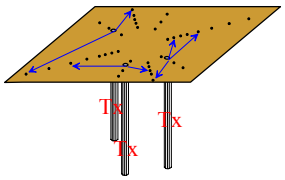

5. Measurements between surface electrodes and the steel casings. This configuration consisted of electrically energizing each steel casing and measuring potentials at the surface electrodes. Reciprocal measurements were not made.

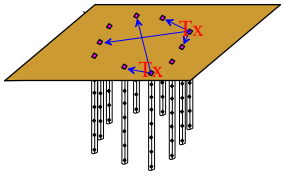

6. Measurements between ERT "pseudo-casings". This configuration consisted of electrically energizing one pseudo-casing and measuring the resultant potentials at all other pseudo-casings.

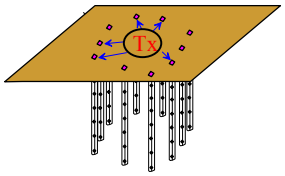

7. Measurements between the steel tank and the ERT "pseudo-casings".

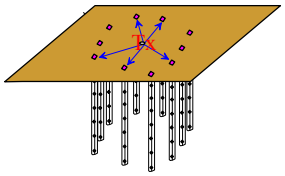

8. Measurements between the central-injection electrode and the ERT "pseudo-casings".

In addition to the above measurement sets we also acquired data using various configurations of the ERT electrode arrays. They are mentioned now because processing is continuing on those data sets for separate publication.

1. Measurements along individual vertical ERT arrays using the pole-pole array. This configuration consisted of electrically energizing various combinations of electrodes in two particular ERT arrays and measuring the potentials at other various combinations of electrodes.
2. Measurements using three depths of ERT electrodes. This configuration consisted of electrically energizing individual electrodes at common depths and measuring the

potentials at the same depths at all the other ERT arrays. Three depth levels were measured.

3. Measurements between proximal ERT arrays. This configuration consisted of making full ERT measurements between the fifteen closest pairs of ERT arrays.

We made different numbers of measurements depending on the length of time to complete a set for all electrode combinations and depending on the relevance of the measurement sets to the overall objectives. We have categorized the data into two basic groups: those data related to or using the tank, central-injection electrode, the three steel casings, and the surface electrodes; and, those data related to the ERT arrays. We acquired approximately 100,000 data points for the first group, and approximately 15,000 data points for the second group. Time to acquire each data set dictated the frequency at which the data sets could be obtained. The first group required approximately 16 minutes per data set. The second group required approximately 35 minutes per data set. During overnight runs we acquired contiguous data sets. During daytime runs, the data sets were acquired as frequently as possible given other group requirements.

We alternated data acquisition periods with other groups during the test. We were able to acquire data while radar measurements were being made while neither interfering nor being interfered with. Preliminary testing suggested some interference between our operations and the crosshole electromagnetics (EM), so, we delayed acquisition during the EM work. The most critical interference was between LLNL's ERT measurements and our own. We were able to work out a compatible schedule to allow both groups to alternate measurement periods effectively. We do not believe that the PITT operation impacted our measurements.

hydroGEOPHYSICS personnel who completed the field data acquisition portion of the survey were Mr. Marc Levitt, Project Engineer, and Dr. James B. Fink, President of hydroGEOPHYSICS. Subsequent processing was performed on-site and in the Tucson office by Mr. Marc Levitt, Mr. Chris Baldyga, and Dr. James B. Fink of hydroGEOPHYSICS.

2.1 Objective of Investigation

The objective of the survey was to characterize the dynamic subsurface hydrogeology of the Site using hydroGEOPHYSICS' proprietary processing procedures on data gathered using three steel well casings, surface electrodes, and a central injection electrode within the tank. Additionally, three-dimensional modeling and associated volumetric estimations of detected injection solution were desired, but not completed due to time constraints during the processing phase.

2.2 Site Location

The U. S. Department of Energy's (DOE) Hanford Site is located approximately twenty miles northwest of the town of Richland, Washington. Access to the Site was by all-weather paved roads and a short dirt road. The surrounding area was relatively flat and fairly densely covered with sagebrush. Remote electrode locations were placed well away from any cordoned-off radiological hazard areas and accessed by walking through the sagebrush.

2.3 Survey Area & Logistics

From a geophysical standpoint, the Site is readily accessible and posed few logistical problems in acquiring data. One complication that is noteworthy for future investigations is that two of the three steel casings installed specifically for this test were covered with a rust-resistant coating. Therefore, although some insulating coating may be removed during the installation process, it is possible that those two casings (the southwest and northwest casings) are only making electrical contact with the ground at welded joints at 10-foot intervals and at other randomly located areas where the insulating coating was scraped off. The southwest casing had a narrow longitudinal strip of the casing insulation abrasively removed prior to installation. We have been unable to determine if there is a difference in the grounding characteristics between the casings. The results thus far are questionable as to whether or not the coating has affected the measurements. Interestingly, the data acquired using the two untreated casings were quite similar in character (for time series analysis) but differed in magnitude. The data from the treated casing differed considerably in the time series analysis, but on a more general amplitude versus location (spatial variation) basis, little difference can be seen. The casings are labeled **SW** for southwest, **SE** for southeast, and **NW** for northwest.

The mock tank differs from the tanks at the tank farms. The mock tank is smaller than the tank-farm tanks (50 feet in diameter versus 75 feet). The mock tank is only buried a few feet compared to the entire tank being buried at the tank farms. And, what may ultimately be a critical difference, the mock tank is not entirely encapsulated in concrete as are the tank-farm tanks. The concrete encapsulation exposed at the base of the outside of the mock tank only extends beneath the mock tank for a few feet. The tank-farm tanks are fully encapsulated in concrete with some rebar and remesh enclosed within the concrete, as best we understand. The mock tank has a relatively large area of the steel bottom in direct contact with the underlying soil. This is substantially different from the tank farms. The relative ease with which the mock tank can be electrically grounded (through its bottom) may not be realized at the tank farms, except in unusual leaking conditions.

Figure 1 is a plan map showing the location of the mock tank, the three steel casings, the surface electrode array, and other features relevant to the electrical survey.

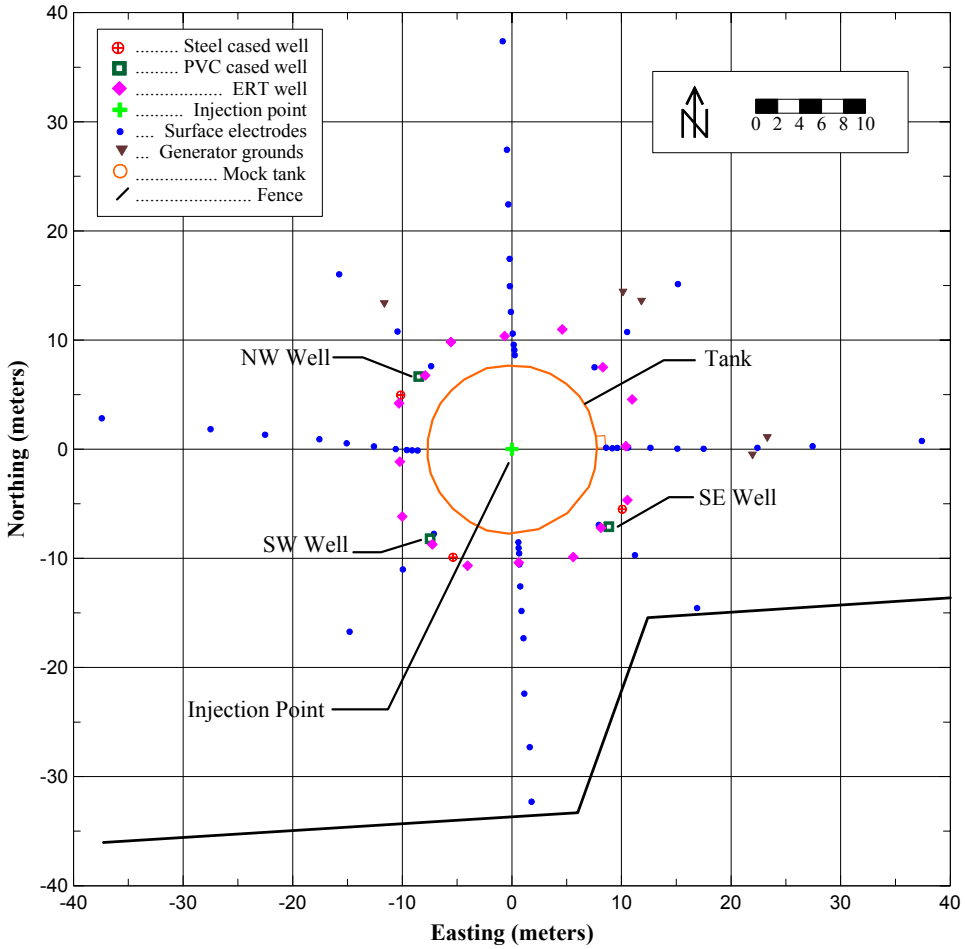

Figure 1: Site Map for Mock Tank Area

2.4 Casing and wire arrangement

All electrical measurements were made using four grounded electrical contacts at any given time; that is, good electrical contact with the subsurface was maintained throughout the experiment. Two contacts were for current injection and two were for potential measurement. Instrument design allowed 8 simultaneous potential measurements for each transmission. All transmitting and potential measuring electrodes had remotely located counterparts.

Approximately 10,000 feet of single conductor, insulated cable has been installed and bundled for the present study and any future studies. The cabling has been left in place. Sufficient "pigtail" remains to allow some flexibility in the location of any future efforts. Remote reference electrodes were approximately 450 meters (1,500 feet) from the tank in two nearly orthogonal directions; west and northeast. The majority of the remainder of the wire connects to the surface electrodes. A very limited amount of wire was necessary to make contact with the tank, central electrode, and the three casings.

Photo 1 – Central injection electrode

Photo 2 – SW Steel casing and ERT sensor

2.5 Equipment

For this round of investigation, the instrument used for the electrical measurements was an Advance Geosciences, Incorporated (AGI) Sting R-8 resistivity and induced polarization (IP) instrument. (AGI website see www.agiusa.com). The Sting R-8 is a recently developed eight-channel, DC-powered, electrical resistivity instrument. The unit we used was the second produced and still suffered from some development problems, but was made available for evaluation under production use. For this investigation, the R-8 was combined with a 54-channel, external, switch box (also built by AGI), and a hydroGEOPHYSICS fabricated patch panel that facilitated control of the different electrode configurations.

Photo 3 – AGI Sting R8, switch box, & patch panel

Photo 4 – Wire loom connected to Sting R8

The Sting R-8 has the capability of automatically switching between electrodes without having to physically move the wire connections after initial set-up. Automatic switching saves physical

labor and time, cuts down on human transcription and tracking errors, and better allows the operator to control array logistics. We took advantage of this capability and programmed the Sting R-8 to make several overnight runs in order to obtain dynamic data while the injections were running. Stacking of the received waveforms ranged from 2 to 15, depending on time available; overnight runs generally used more stacks. Maximum current capability is 500 milliamps (mA), but, typical output was on the order of 200 mA. Each data set acquired was labeled and archived for subsequent processing.

As with the previously used OYO McOhm-21, the advantage the Sting R-8 unit has over other similar resistivity instruments, is the ability to pre-program a survey and repeat the program without operator intervention. While the Sting R-8 had some improvements over the McOhm-21, because of its "newness," it also had its share of difficulties. Twice during injection runs, either the main instrument or the switch-box failed to some degree resulting in either no data or unusable data during those periods. Most unfortunately, the first failure occurred during the initial injection and it had to be sent back to the manufacturer for expedited repair. The second failure was during the latter portion of the injection test. We missed some critical periods of monitoring, but we were able to maintain operation by performing some in-field repairs and "work-arounds."

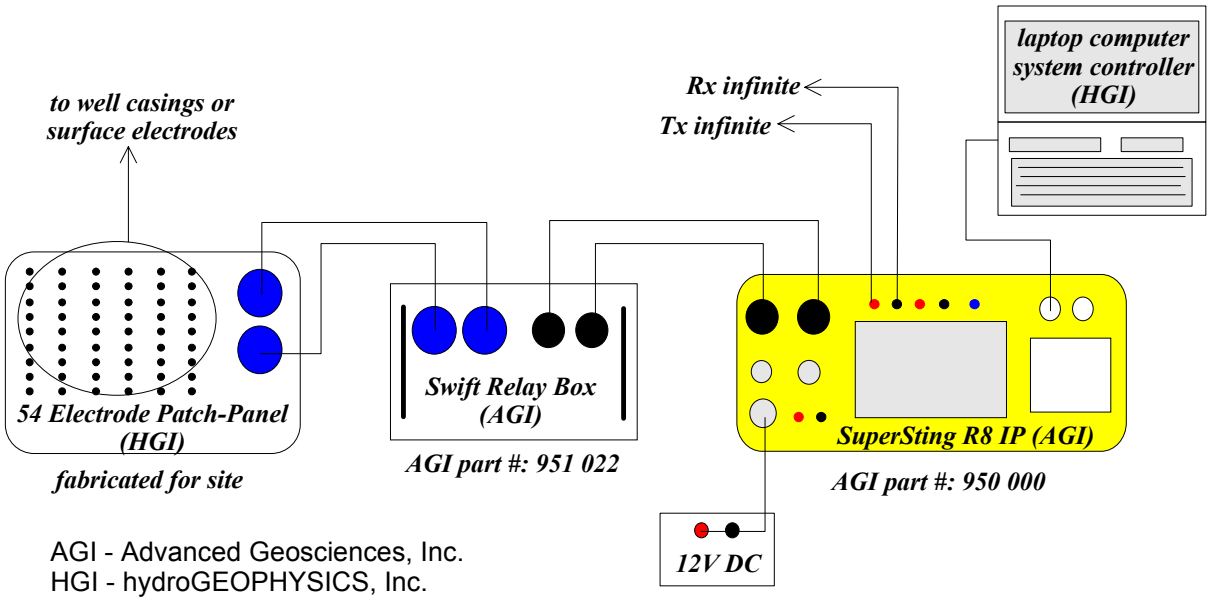

Figure 2: Geophysical equipment connection schematic

Overall, the Sting R-8 was much more thermally stable (relative to the McOhm-21) and provided quality data. We have also worked closely with the manufacturer in an effort to solve the above-mentioned problems. No electrical device is fully immune to failure and we suggest the use of backup units for future testing and implementation.

2.6 Data Acquisition

During the initial setup (background measurements) we tested all combinations and permutations of hookups between the three steel-cased wells, surface electrodes, central injection electrode, and the steel tank. For the background phase only, we acquired reciprocal data for all combinations. Based on the outcome of the initial tests, we focused our efforts on what appeared to be the most diagnostic combinations. We then programmed the system to acquire consecutive, repetitive data sets for each measuring period. The majority of data sets were acquired during overnight runs when other participants were not operating. Data sets acquired during regular working hours were at intervals between equipment changes and downtimes for other participants. Figures 2a, 2b, and 2c show the time-distribution of the data acquisition and injection periods. The purpose for making repetitive measurements after the injection was to dynamically monitor subsequent migration of the induced leak.

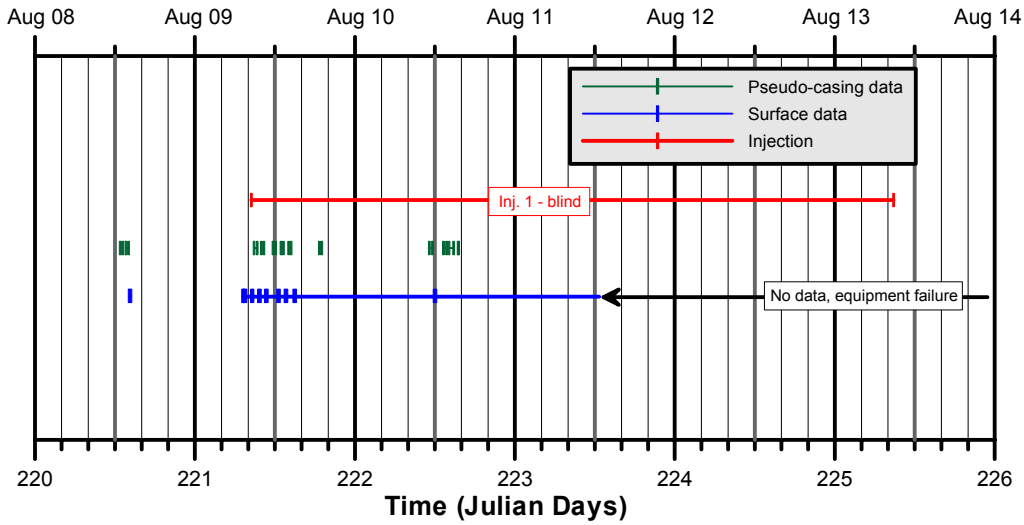

Figure 2a – Time Graph of Data Acquisition and Injection Periods (first third of injection period)

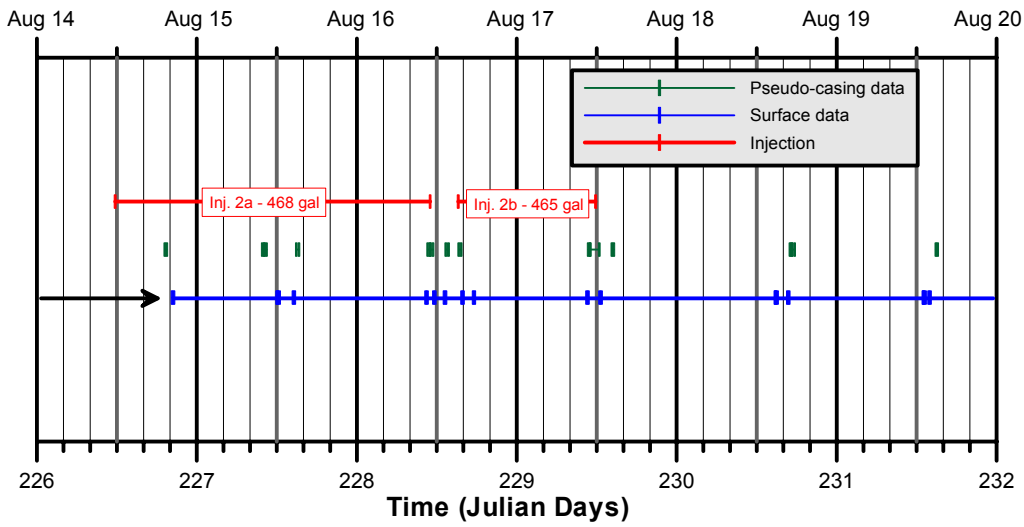

Figure 2b – Time Graph of Data Acquisition and Injection Periods (second third of injection period)

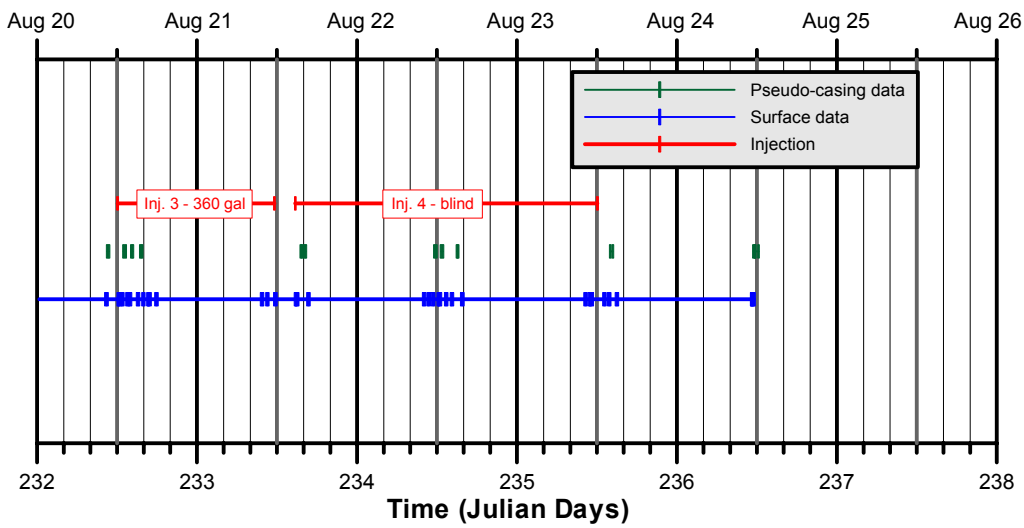

Figure 2c – Time Graph of Data Acquisition and Injection Periods (last third of injection period)

2.7 Data Processing

Data were processed with hydroGEOPHYSICS' proprietary software either on-site, in the Richland area, or in the Tucson office. A large part of the processing to date consists of manual manipulation of the data, primarily to organize the data sets into logical processing units, and secondarily to edit questionable data.

We emphasize the importance of distinguishing between two-electrode *resistance* measurements and four-electrode *electric-field* (e-field) measurements. All data acquired for this study are *electric-field* measurements. The majority of data values presented are voltages normalized to

current and have the units of resistance; i.e. volts divided by amps (V/I). However, they are not "true" resistances that would be measured by a two-electrode system (i.e. a standard voltmeter). In some instances, where the electrode geometry would allow a "point" approximation, apparent resistivities were calculated. Apparent resistivities are presented with units of ohmmeters.

For the difference plots, residual potentials for each repeated data point were determined by subtracting background values from observed data. In some cases, obvious trends, either as a function of time or distance, were removed from the data to enhance more subtle changes. A monotonically increasing or decreasing time series would represent a temporal trend, and continuously decreasing signal amplitude with increasing distance from a signal source would represent a spatial trend. Subtle variations superimposed on such trends can be better viewed when these trends are removed. This is a commonly applied analytical technique practiced by geophysicists.

Two-dimensional contour plots were generated from processed data using Goldensoft's SURFER Version 7 software. Data were initially organized, edited, and partially processed using MicroSoft's EXCEL 2000 spreadsheet software. No three-dimensional volume rendering was performed for this study.

3.0 METHODOLOGY

Leak detection methods have traditionally relied on either: (1) a loss of liquid volume inside a container, or (2) a gain in liquid volume outside a container. We adapted our HRR technology to the Mock Tank environment. This adaptation is referred to as HRR-SCRT to indicate the inclusion of the steel casings and tank/central leak point in contact with the conductive leak solution as key to the measurements. We also incorporated lessons learned at the Sisson and Lu site. In both test locations we demonstrated leak detection, leak location, and initial onset of leakage (binary leak detection, i.e. leak/no leak). We used the steel-cased wells and the tank itself at the Mock Tank site to serve as active and passive electrical sensors (electrodes). We made a variety of measurements to determine which arrangement would be most sensitive to the smallest leak volume and which arrangement would be most accurate in estimating the leak volume. The various arrangements and results are discussed below.

We initially tested all electrode combinations of the three steel-cased wells, the single electrode placed in the center of the tank, and using the tank shell as an electrode. In every configuration we energized one electrode and measured the potential at other electrodes. We again emphasize that all data acquired for this study are four-electrode *electric-field* measurements. At no time did we ever make two-electrode resistance measurements other than as a check for electrical continuity. As with the Sisson and Lu Site, we found that some combinations were very time consuming (because of the large number of combinations) and some went rather quickly (because of the limited number of combinations). For this study, we tried to streamline acquisition for the slowest arrangements by minimizing redundancy. Production deployment would, however, be enhanced by the redundancy. We evaluated various data-stacking options and used the least number of stacks that would produce repeatable data. We eventually discarded a few arrangements, and, in the end, determined that several arrangements have promise. We found that each arrangement produced useful results and where those results were similar, we opted to continue with the more favorable arrangement (based either on time or usefulness of the data).

One of the methods we used during the 2000 and 2001 VZTFS included placing an electrode inside the injection source. We continued this practice at the Mock Tank site. What separates this method from volumetric methods is its high sensitivity to leaks, particularly with electrically conductive solutions. When a leak occurs the liquid pathway provides an electrical pathway. It is essentially a binary indicator; either there is a leak or there isn't. We believe this method of placing an electrode essentially within the container (in the case of the Mock Tank site, an electrode in the injection location) represents an option that may be very helpful within the tank farms. Equivalent results may also be obtained simply by connecting to the steel tank itself.

3.1 Electrical resistance and resistivity

The geophysical resistivity method is based on the capacity of earth materials to conduct an electrical current. The concept behind applying the resistivity method is to detect and map changes or distortions in an imposed electrical field due to heterogeneities in the subsurface. Changes in soil texture and moisture content will cause changes in an imposed electric field. Distortions of the electric field can be measured on the ground surface, in boreholes, or with a combination of the two. Resistivity measurements are made with a minimum of four electrodes in contact with the ground. In conventional resistivity applications these electrodes are always considered to represent point sources. Resistivity calculations depend on the point-source nature of the field measurements. Various electrode arrangements have been used over the decades, most of which involve collinear arrays such as Schlumberger, Wenner, dipole-dipole, three-array, pole-pole (also called "normal" in borehole logging), and many more. Each array shows merit in specific environments and all (ideally) produce useful information. Data acquired for all arrays consists of a current-normalized potential difference. Then, typically, the data are "reduced" to a homogeneous, isotropic half-space by using a geometric factor that takes into account the inter-electrode distances on the half-space surface. Alternatively, current-normalized potentials can be treated independently without invoking half-space constraints.

The data acquired for the VZTFS and LDMM violate the point-source assumption because of the very high aspect ratio of the steel casings that were used as electrodes. Additionally, the casings are not likely equally grounded from top to bottom because of soil moisture variations over the same distance. The steel tank presents itself as a large, flat, circular-plate electrode. It also is not likely equally grounded over its area during the injection tests because of the centrally located point of injection.

The data presented in this report have also been processed with proprietary software that can remove the non-point-source characteristics from the observed measurements. All data are kept in normalized potential form and "apparent resistivity" calculations have been limited to the installed surface electrodes. We believe that this actually allows the data to be presented in a more meaningful manner. We have presented the casing data in various formats; e.g. potential versus time, potential versus distance, potential versus injected volume, and contoured maps of direct and inverted potential distributions.

4.0 RESULTS & INTERPRETATION

The results are presented in a variety of formats that, hopefully, convey the spatial and temporal characteristics most relevant to the objectives of the study.

As with the Sisson and Lu study, all results are presented using normalized potentials. These range from a few milliohms to tens of ohms, a spread of approximately five orders of magnitude. Such a large range of data values, in itself, suggests a high probability of feature recognition and characterization. This large range is due entirely to the high electrical conductivity of the injected solution and its effect on the ground.

We attempted to continuously monitor the injections, but ran into several problems as previously noted. Nevertheless, we observed changes in the amplitude of the electrical signatures, the spatial dependence of the responses, and temporal variations in the responses (related to volume).

On all plots high potentials are expressed in warm (red hued) colors and lower potentials are shown in cool (blue hued) colors.

Several reciprocal measurements were made where the reverse arrangement between energized electrode and sensor was used; i.e. the previously energized electrode became the sensor and the previous sensor became the energized electrode. Whereas a large majority of the Sisson and Lu reciprocal measurements were within one percent of the forward measurements, we encountered many more discrepancies in the Mock Tank reciprocal measurements. We have not yet determined whether this is due to instrumental difficulties (specifically, internal instrument problems), working in this environment (instrument incompatibility with the infrastructure), or if there actually are non-linearities caused by the infrastructure. The concerns are listed in order of their likely occurrence.

4.1 Measurements Between Steel Casings and the Steel Tank

With only three steel casings and one tank, the spatial distribution of data is too limited to create meaningful contour maps. Nevertheless, the data from this configuration contain a wealth of information.

The most useful format for presenting these data is residual-normalized-potential versus time. Residual refers to the removal of “background” or pre-injection data. This processing step removes the majority of the primary field effects that tend to dominate the response. Normalized indicates the measured potentials are divided by the applied current to produce common units of millivolts per milliamps.

NOTE: All potential vs. time plots show an *absolute value* response to make easier visualization of an increasing volume. In reality, all potential responses show a decrease in magnitude over the duration of the injection. Previous presentations of these data erroneously showed a positive increase in residual normalized potential versus time because the data were subtracted from the background instead of the preferred approach to remove the background from the data. Interpreted slopes remain the same but with a sign change. Increases in normalized potential versus time were observed at the Sisson and Lu site and are valid signal changes.

Figure 3 shows a plot of residual-normalized-potentials for all three steel casings using the tank as a source electrode. The abscissa is time in Julian days. The ordinate is the absolute value of the normalized potential in units of millivolts per milliamp (mV/mA or V/A). Note the total range for the entire injection time period is less than one ohm.

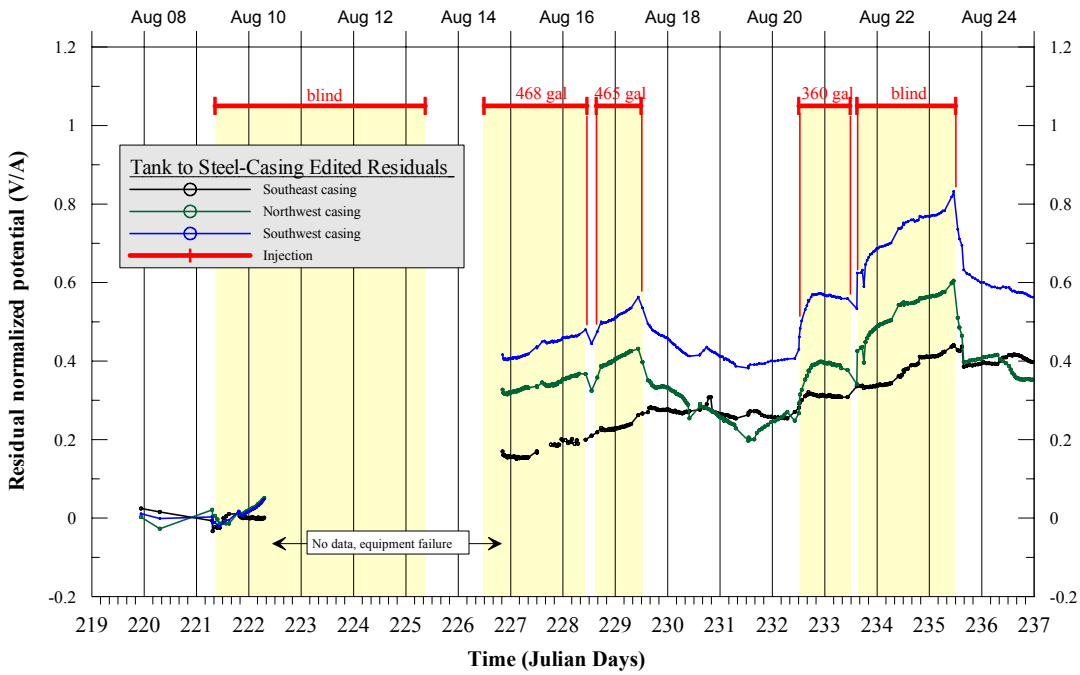

Figure 3 – Residual-normalized potentials versus time using the tank as a transmitter and the steel casings as receivers.

Each injection sequence can be fitted by a linear trend. The trends are obviously averages, but, as trivial as they might be, they offer some interesting insight considering the possible application to the tank farms. The trends show the average rate of injection during the test. For example, we will assume 2000 gallons over a 14-day period. This gives an average injection rate of 143 gallons per day. For the data in Figure 3 this is roughly equivalent to a range of 12 to 25 milliohms per day, depending on which slope you use. In turn, for this particular configuration, we get a pseudo-calibration value of 5 to 10 gallons per milliohm. This, of course, ignores the starts, stops, and changes in injection rate. It simply gives a rough estimate based on a beginning value and an ending value with no regard for intervening variations.

4.1.1 Potential Slope Analysis

However, when we analyzed the data recorded for each individual injection, we saw that the intervening variations suggest a relationship between the trend of the electrical potential and the rate of injection. Figure 4 details this relationship and suggests that we can closely predict flow rates based upon the slopes of electrical potential observed at the casings.

By relating the slope of the potential measurements to known flow volumes, and normalizing to observed time, we derived a linear relationship that appears to allow us to predict a flow rate for a given potential slope. It is interesting to note in Figure 4 that we are plotting the rate of flow, a first derivative, versus the rate of change of potential, another first derivative. The linear fit to the data in Figure 6 is a second derivative relating the two rates of changes. Although the flow is occurring in the unsaturated zone, the analogy between Darcy's Law and Ohm's Law is interesting.

The linear relationship is described by the equation:

Flow Rate = f(slope of potential measurements) – constant

With this equation, we were able to fit a line between any two times along our potential measurement curves. Putting this slope into the "flow rate" equation produces a "calibrated" flow rate for that particular time period based on minimally processed e-field data. This is similar to what we did at the Sisson and Lu site, although at Sisson and Lu we related estimated volume to potential.

Figures 5 and 6 are expanded views of injection 2 for the southwest and northwest casings and demonstrate how close the approximation is, based on the figures available to us at this time. We applied this technique to the blind test to calculate flow rates and total injected volumes.

Table 1 shows a summary of calculated injection rates and volumes for injection releases 2a, 2b, 3 and 4. Unfortunately, due to equipment failure we have no data for the first injection. Note the percent difference between predicted flow rates and volumes and the actual values reported. Note that these figures are based on the data from only one casing, the southwest casing. Calculations on the northwest casing data produced similar results. The southeast casing behaved very differently from the other two and produced virtually unusable results for unknown reasons.

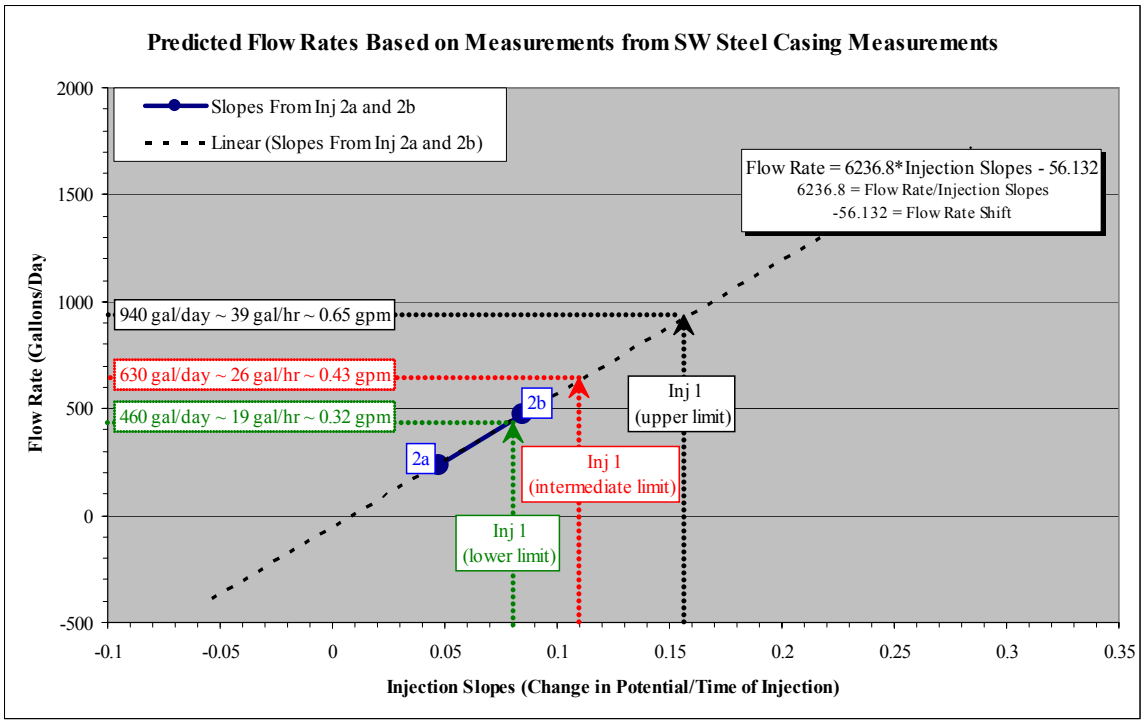

Figure 4 – Flow rates vs. injection slopes

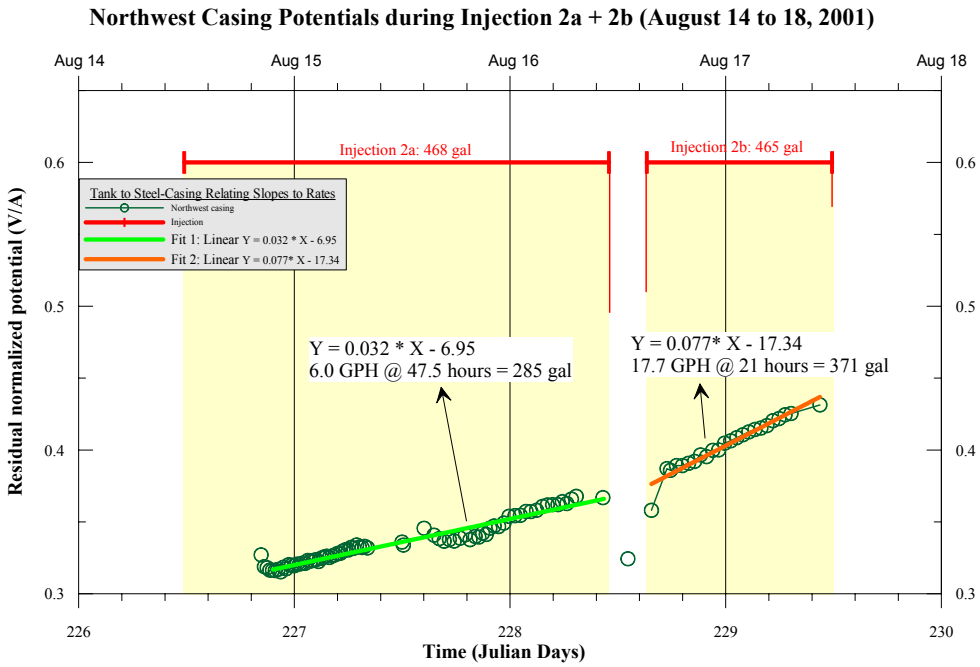

Figure 5 – Calculation of flow rate and volume for potential data using the northwest casing

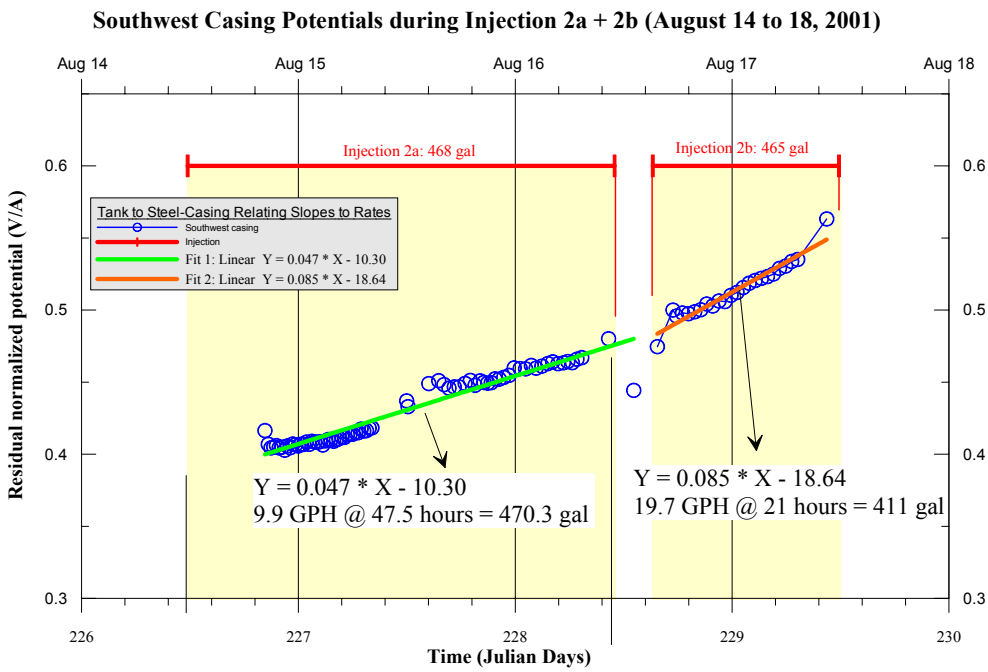

Figure 6 – Calculation of flow rate and volume for potential data using the southwest casing

Inj.	Actual Flow Rate (GPH)	Actual Volume (Gal)	Actual Inj. Time (Hours)	Measuring Electrode	Calculated Flow Rate (GPH)	Calculated Volume (Gal)	Calculated Inj. Time (Hours)	% Diff.
1	blind	blind	96.0	SW casing	N/D	N/D	N/D	N/D
2a	9.9	468	47.3	SW casing	9.9	470	47.5	0
2b	22.5	464	20.6	SW casing	19.7	411	21.0	-11
3	15.3	360	23.6	SW casing	71.9	346	4.8	-4
4	23.9	1080	45.3	SW casing	24.4	1146.8	47.0	6

Table 1 – Summary of calculated flow rates and volumes (actual flow rates and volumes supplied by Vista Engineering)

4.1.2 Perturbation Analysis

Using the electrical data we can readily detect the times at which the injections start and stop. Start and stop indications can be observed in the data within minutes of their occurrence. Commencement of injections is indicated by a rapid increase in potential followed by a rounding of the data and an asymptotic tendency towards a constant slope. Cessation of the injections is similarly indicated by an abrupt decrease in potential followed by a rounding of the data and an asymptotic tendency to a horizontal line, although data were not acquired for a long enough time to confirm this. We suspect that the "rounding" or charging and discharging character of the data may be related to the "time in residence" of the volume of injected solution. To appropriately address this will require further measurements and other supporting data.

The electrical data track the actual injection flow rates so closely that variations in flow are evident within individual injections.

It appears that there may have been a disturbance in flow during injection 3. From the slope of the data there appears to be a gradual failure, i.e. a gradual decrease in flow. Table 2 shows a detailed interpretation of measured potentials and how they describe key events that have been noted on Figure 7 with letters A through E.

Possible injection failure during injections 3 and 4 suggested by electrical data

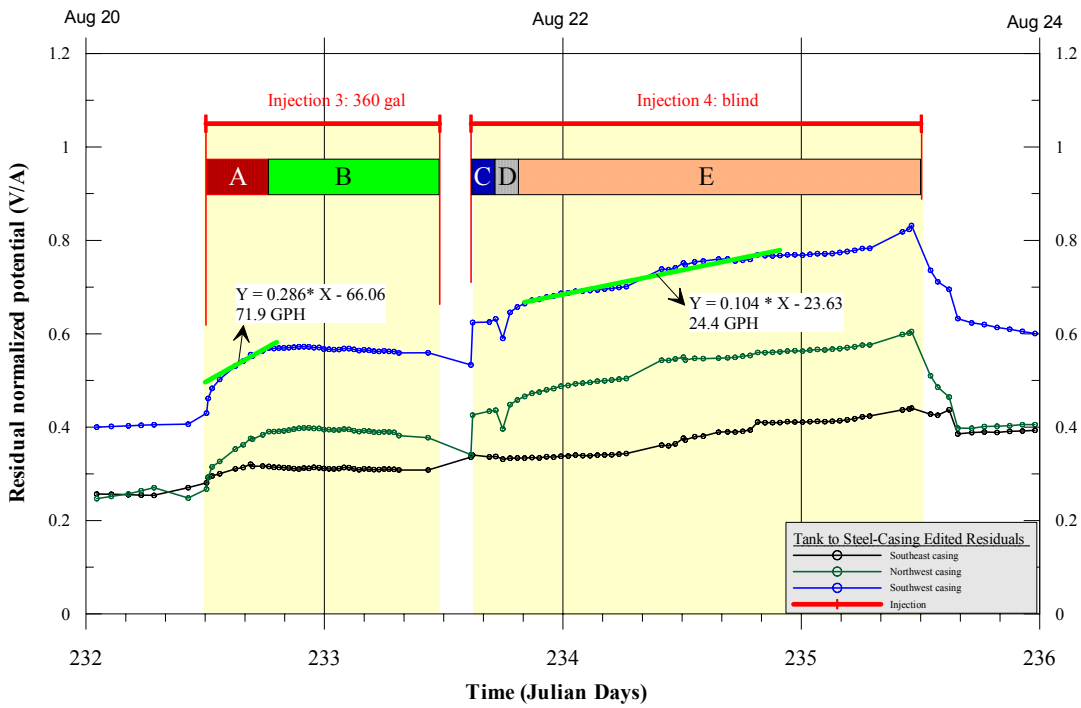

Figure 7 – Expanded view of injections 3 and 4 for all three casings. Residual-normalized potential versus time using the tank as a transmitter and the steel casings as receivers.

A	Injection 3 begins August 20th at 3:15pm, initial flow rate exceeds 100 GPH and slows to approximately 72 GPH by 8:00pm for a total of 300 to 350 gallons.
B	Between 8:00pm and 10:00pm on August 20th, flow begins to slow to under 2 GPH. Injection failure seems to be gradual which may indicate clogging of the flowmeter over time.
C	Injection 4 begins at approximately 6:30pm, initial flow rate exceeds 27 GPH.
D	Flow rate slows dramatically until injection is stopped between 9:00pm and 10:30pm.
E	Injection resumes at 24.4 GPH for a total of 1147 gallons.

Table 2 – Summary of interpreted flow events as depicted by measured potential data

4.2 Measurements Between Steel Casings and the Injection Electrode

As with the previous discussion, there are only three steel casings and one central injection electrode. The spatial distribution of data is too limited to create meaningful contour maps. Nevertheless, and as with the previous discussion, the data from this configuration contain a wealth of information.

The format for presenting these data is residual-normalized-potential versus time. Figure 8 shows a plot of potentials for all three steel casings using the central injection electrode as the source. Note the total range for the entire injection is approximately one ohm.

NOTE: All potential vs. time plots show an absolute value response to make easier visualization of an increasing volume. In reality, all potential responses show a decrease in magnitude over the duration of the injection.

The difference in electrode configuration between this arrangement and that previously discussed is simply a change from the tank as a flat-plate source electrode to the central injection point source electrode. As might be expected, Figure 8 shows a strong similarity to Figure 3. However, upon closer inspection, some gradient characteristics are reversed; that is, when the tank data decrease, the injection electrode data increase. We suspect that the differences are related to injected solution bridging the space between the injection electrode and the tank during injection and absence of this bridge when fluid is not being injected. Each injection commencement and termination is still reflected in the data by gradient changes.

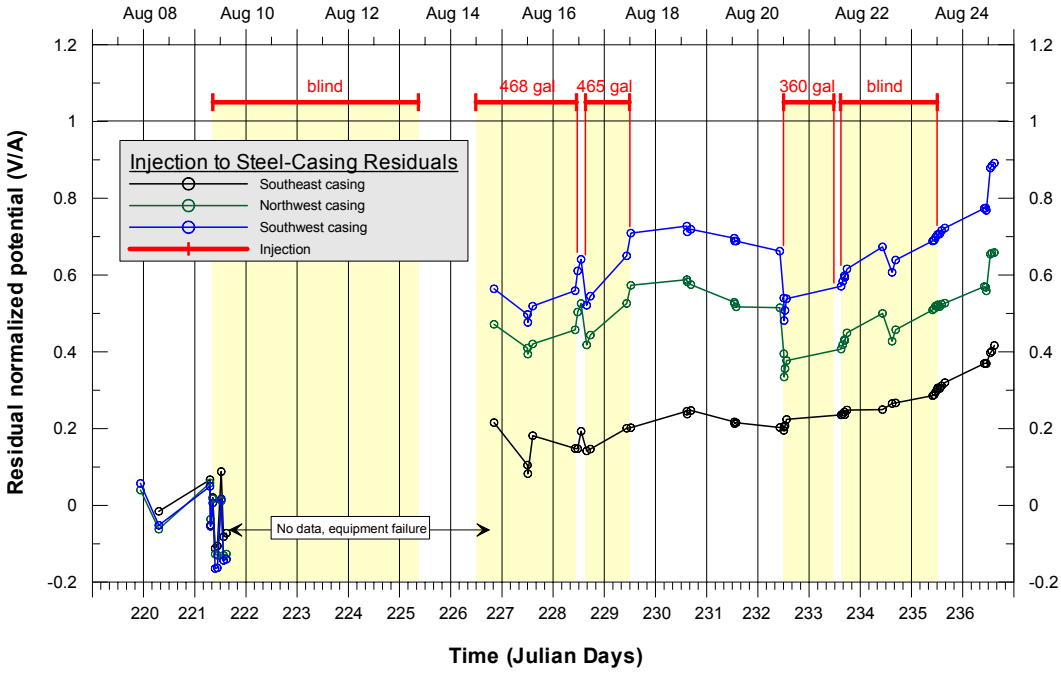

Figure 8 Residual –normalized potential versus time using the three steel casings as receivers and the central injection electrode as a transmitter.

This electrode configuration may be implemented at the tank farms by substituting an electrode in contact with the liquid inside the tanks to function as the electrode in the point of injection for the mock tank study. Again, tank-farm monitoring opportunities should be obvious and the need for additional test studies is apparent.

4.3 Surface Measurements

Figure 9 through 13 show eight images in plan of the distribution of residual potentials as measured by various configurations of surface electrodes, steel casings, injection well, and the tank. The circular shape in the center of the plots is the outline of the tank as surveyed by GPS. The small circles represent surface electrodes. The larger, white circles represent the three steel casings. The single large circle is the outline of the mock tank.

The sequences of images on these figures shows the data gathered at different times during the monitoring process. Going from upper left to lower right in story-board fashion;

Fig.	File Name	Date/Time	Description
A	2-RES	8/08/01 07:09	Pre-injection data set or background
B	6-RES	8/09/01 09:33	Start of Injection 1
C	13-RES	8/14/01 20:18	Start of injection 2a
D	18-RES	8/16/01 10:20	2 days after injection 2a
E	24-RES	8/17/01 12:26	End of injection 2b
F	33-RES	8/20/01 12:26	Start of injection 3
G	50-RES	8/22/01 11:18	Middle of injection 4
H	60-RES	8/23/01 13:43	End of injection 4

Table 3 – Summary of surface potential images for figures 10, 11, 12, 13

Each plot uses the same relative color scale. After sufficient time, the potentials most closely related to the tank decrease with an increase of conductive solution in the ground. This is apparent five days after commencement of the injection. Unfortunately, the minimum volume sensitivity is undetermined because of equipment failure.

4.3.1 Measurements Between Surface Electrodes and the Steel Tank or Injection Well

Figures 9 and 10 shows eight images in plan of the distribution of residual potentials as measured by surface electrodes and using the central-injection-electrode as the transmitting source. The sequence and presentation are explained in the above discussion (4.3).

Plot A shows a background data set and plot B recorded just after the commencement of Injection 1 shows little difference. However, there is a marked increase in response for plots C,

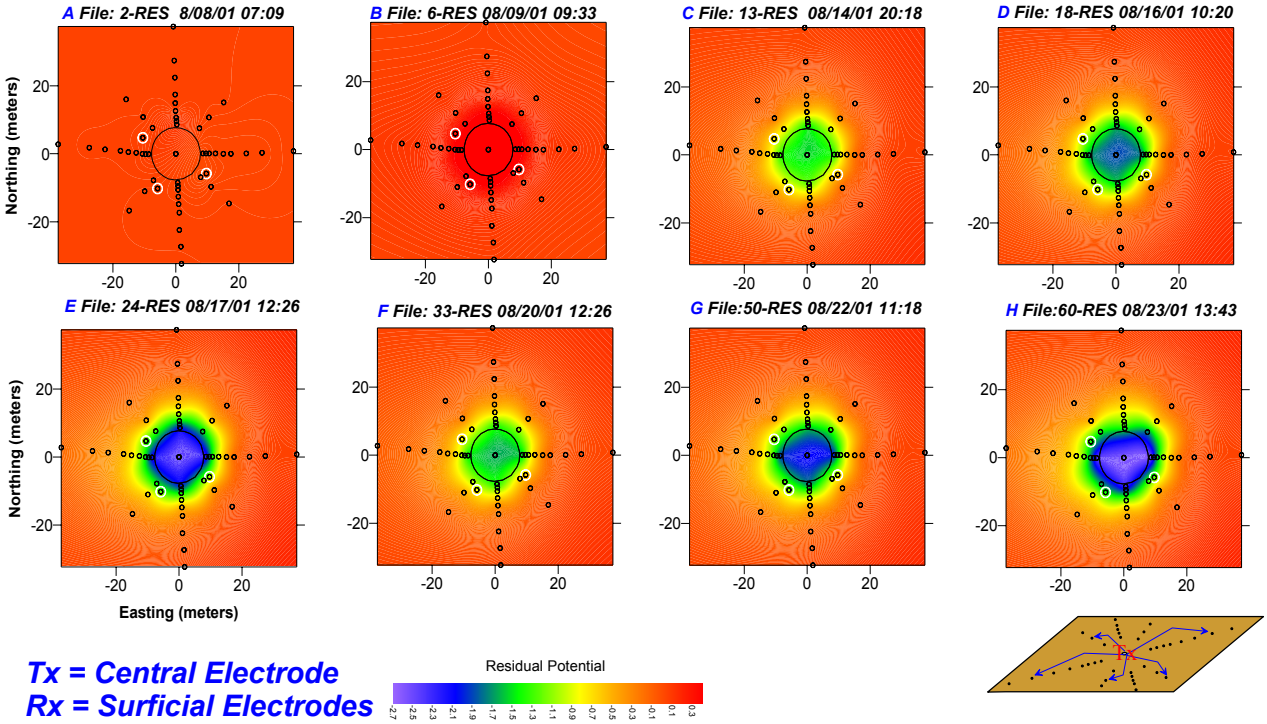

Figure 9 - Residual potential map for different times during the study

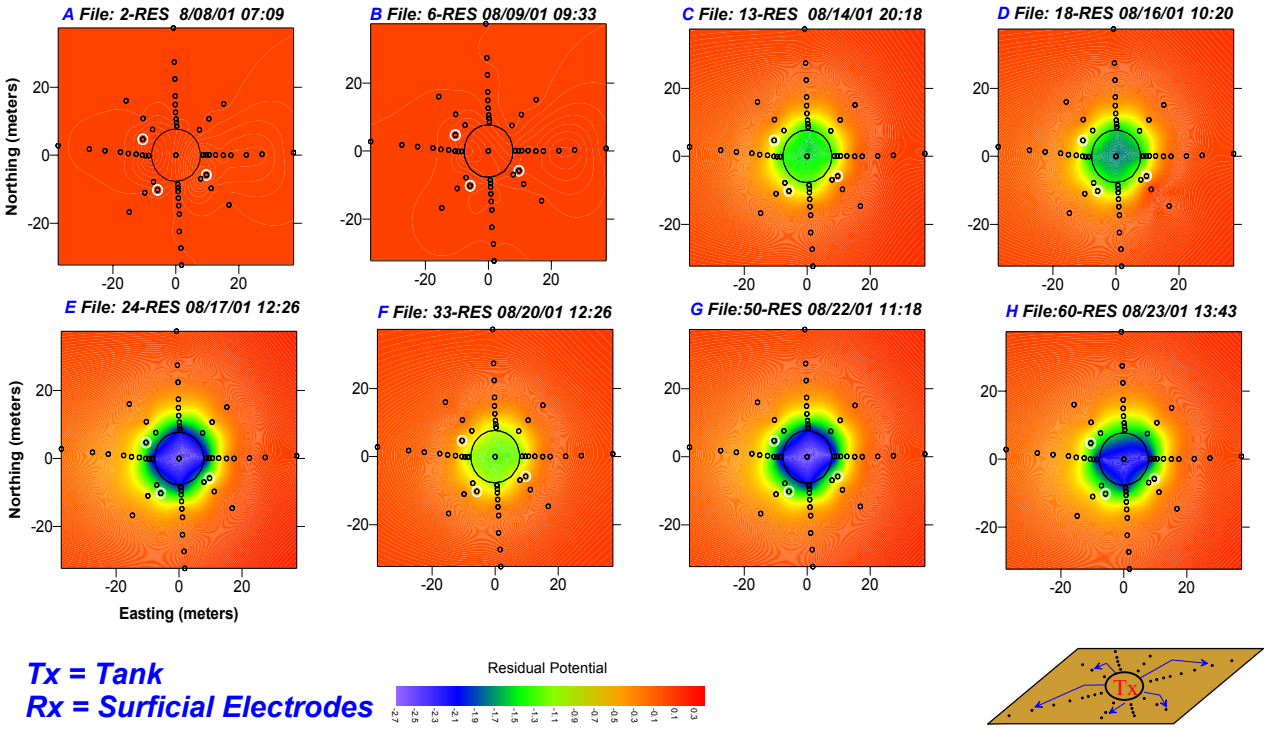

Figure 10 - Residual potential map for different times during the study

D and E, which corresponds well with injection 2a and 2b. Plot F shows a decrease in response that correlates with the 3-day break between injections 2b and 3. Plots G and H again show an increasing response attributed to the increased volume provided by Injection 3 and 4.

The response characteristics between using the tank as a transmitter and using the central injection electrode as a transmitter are quite similar. There are subtle differences that show up in the contoured plots.

The central injection electrode data show an immediate response to the commencement of the injection. At the scales used for the plots, it only shows up as a slight color change in the center of the plot. Subsequent plots appear to show a stronger response in the central injection electrode data compared to the tank electrode data. We actually anticipated less difference because we assumed that once the solution was injected it would immediately short (electrically) to the tank and they would behave as though they were the same. As it turned out, the solution may actually infiltrate more rapidly than expected leaving less solution in direct contact with the tank than anticipated.

This configuration would be desirable for logistical purposes. It is completely non-invasive and there is a lot of flexibility in the location of the surface electrodes. The presence of an electrode in the injection well did allow early detection of the injection, but, the plan map mode of data presentation tends to mask subtle changes.

4.3.2 Measurements Between Surface Electrodes and the Steel Well Casings

This configuration consisted of transmitting on each steel casing and receiving on the surface electrodes. This resulted in three sets of plots, one for each casing. These plots are summarized in Figures 11, 12, and 13. The general spatial trend for all three sets of plots is from a neutral background response to a localized area of low potentials essentially centered on the tank. It is interesting to note that although the steel casings, which were approximately three meters from the tank, were the transmitters, the electrical field was still dominated by the injected solution beneath the tank.

We expected the three plots to display characteristics that would center around each of the respective casings when it was used as a transmitter. They only did so up to a point. All three casing plot sets show a strong response (low normalized potential) in the vicinity of the tank after four days into the test. The SE and SW casings produced peak responses offset in directions towards the tank. The NW casing did not create much of an offset.

The statement above may be interpreted to mean that data results would center on each of the casings used as a transmitter, potentially biasing leak location sensing. In a homogeneous, isotropic, half-space scenario, the iso-potential contours would form perfect circles around the

source, regardless of whether the source was a point or a vertical line (e.g., a casing). In a heterogeneous scenario, a nearby resistive or conductive feature will distort the iso-potential contours providing the basis for an inferred location of a subsurface resistive or conductive feature. The casings, therefore, could be randomly located relative to the tank and would produce the same result. The shape and distribution of the iso-potential lines at the mock tank were determined exclusively by the placement of the surface electrodes.

We are somewhat reluctant to attribute the differences between the casing responses to characteristics of the casings themselves, but we cannot strictly rule that possibility out. As stated elsewhere, the SW and NW casings were installed before the insulating coatings were detected. The SE casing had a one-inch wide strip of insulation ground off to insure continuous electrical contact with the earth for the length of the casing. The other two casings were definitely exposed at the welded joints and randomly exposed wherever the insulation was chipped off.

The interesting result is that the injection can be detected by external grounded structures in combination with non-invasive, surface electrodes. In the case of the mock tank test, a minimum volume of approximately 500 gallons appears to have been detected. This interpretation is based on the earliest positively identifiable change (i.e., distortion of the iso-potential contours) in the observed potentials for the data we acquired using the surface electrodes as receivers and transmitting on the casings. This sensitivity is determined by the frequency of the sampling, which varied due to external factors. With more frequent sampling and more accurate instrumentation, the minimum detectable volume may be less than in the mock tank environment. The implication is that similar results should be anticipated at the tank farms, but that, because of the increased depth of burial, the leaked volume would be have to be greater to produce a detectable response at the surface. This further illustrates how sensitive the overall e-field is to changes.

The most salient feature of Figures 11, 12, and 13 is a dipolar response noted on Plots G and H. Plots G and H show a far larger response but is fairly distorted. The distortions are almost certainly caused by erroneous data, a result of equipment failure. Nevertheless, we have included these plots because, despite the distortions, an increase in response appears to be associated with Injection 4. This is too weak, however, to be of significance.

Early time data show more response located near the transmitting source with a subtle tendency to migrate to the center of the tank with time. We believe that the processing steps might be improved to remove this tendency to have higher residuals around the transmitting casing. Regardless, in a real-tank situation where more casings are available, there may be sufficient information such that this is not a problem.

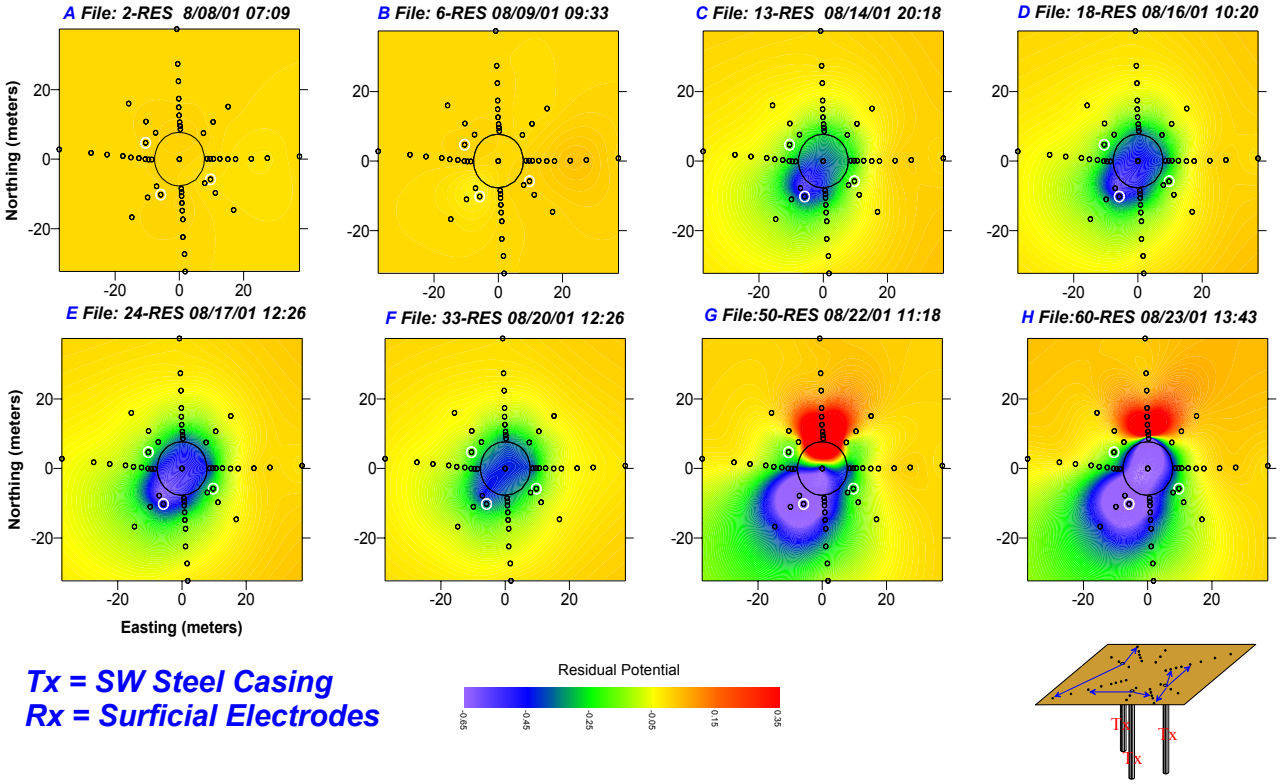

Figure 11 - Residual potential map for different times during the study:

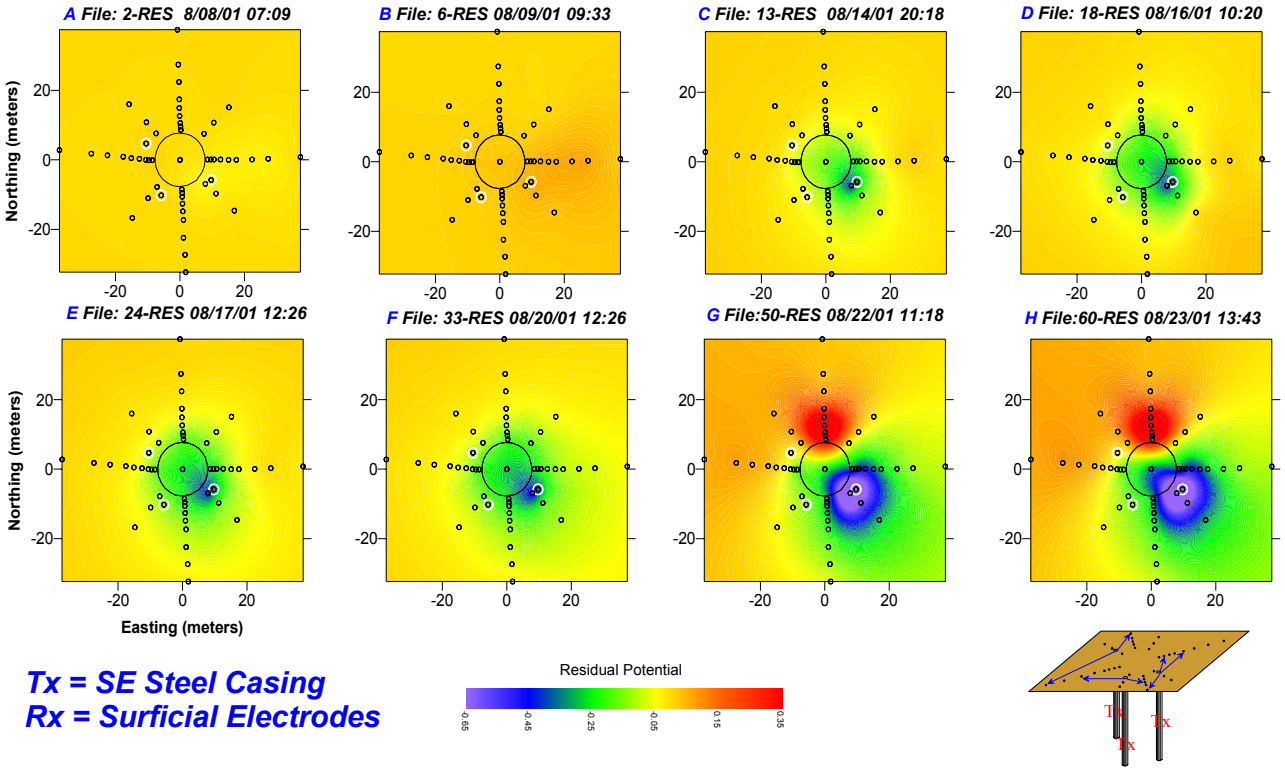

Figure 12 - Residual potential map for different times during the study

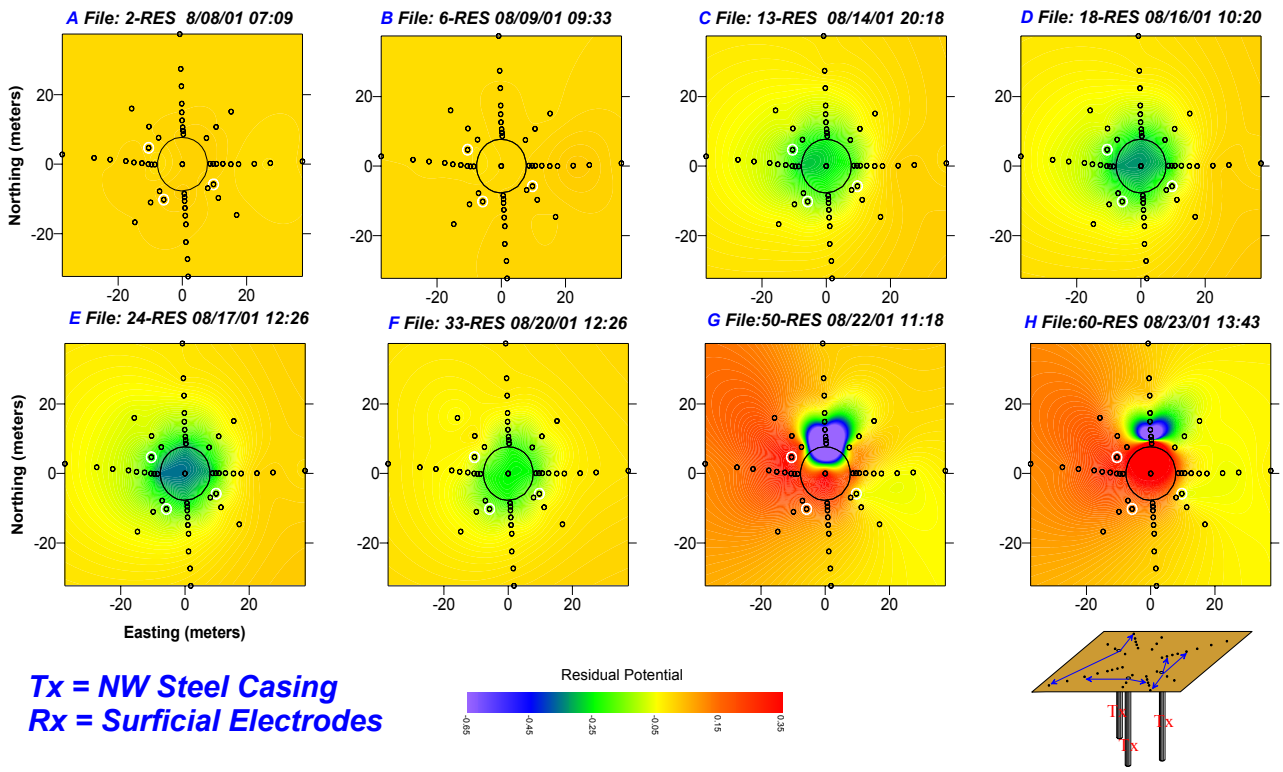

Figure 13 - Residual potential map for different times during the study

4.4 Measurements Between Pseudo-Casings (fused ERT arrays)

We are aware that LLNL personnel have focused on this arrangement using their ERT instrumentation. We were also very interested in acquiring data in this manner, because of the ability to emulate Steel Casing Resistivity Technology (SCRT) and we present some basic results in this report. We made no attempt to do any sophisticated modeling or inversions as those steps were well beyond the original work plan.

One significant difference between our measurements and those of LLNL is that we used both the central injection electrode and the tank for transmitters in addition to cross-array measurements. We developed an algebraic reconstruction technique (ART) specifically for this arrangement. The results are shown in Figures 14 and 15.

Figure 14 and 15 shows eight images in plan of the distribution of residual potentials as measured by various configurations of ERT "pseudo-casings", injection well, and the tank. The circular shape in the center of the plots is the outline of the mock tank and the small circles represent the ERT arrays. The sequences of images on these figures shows the data gathered at different times during the monitoring process. Going from upper left to lower right in storyboard fashion;

Fig.	File Name	Date/Time	Description
A	2-RES	8/08/01 07:09	Pre-injection data set or background
B	6-RES	8/09/01 09:33	Start of injection 1
C	13-RES	8/14/01 20:18	Start of injection 2a
D	17-RES	8/16/01 10:40	2 days after the start of injection 2a
E	22-RES	8/19/01 14:53	1 day before the start of injection 3
F	25-RES	8/20101 15:36	A few hours after the start of injection 3
G	30-RES	8/22/01 12:37	Middle of injection 4
H	634-RES	8/25/01 11:47	2 days after the end of injection 4

Table 4 – Summary of surface potential images for figures 14, 15

Each plot uses the same relative color scale. We developed a short-cut method to simulate an algebraic reconstruction technique (ART) commonly used in resistance tomography to determine if we could use the data in real-time. The radial character of the plots is a result of the short-cut ART. After sufficient time, the potentials most closely related to the tank decrease with an increase of conductive solution in the ground. This is apparent five days after commencement of the injection. Unfortunately, the minimum volume sensitivity is undetermined because of equipment failure.

The pseudo-casing results show temporal results not too different than those of the surface electrodes. However, the spatial distribution is much more focused. Plot 15-B, shows a very weak response near the center of the tank but slightly off center to the southwest. This is not evident in Plot 14-B. Plots 14-C, 15-C, 14-D, and 15-D, were all collected during injection 2a. Plots 14-D and 15-D show an increase in both magnitude and size of response over that of plots 14-C and 15-C acquired one day earlier. Plots 14-E and 15-E show minimal change during the period that corresponds with the 3-day break between injections 2b and 3. Plots 14-F and 15-F show a marked increase in magnitude and response that correlate well with the increase in injected volume from Injection 3. None of the plots from C through F show any evidence of a preferential flow direction.

Plots 14-G, 15-G, 14-H, and 15-H show a far larger response that is fairly distorted. Again, unfortunately, the distortions are caused by missing data as a result of equipment failure. We have included these plots because despite the distortions, one can clearly see the increase in response associated with Injection 4.

It may be noteworthy that the response character between Plots 14-D and 14-E (tank electrode) does not seem to increase either in amplitude or size. However, the same plots generated using the central injection electrode show an increasingly negative amplitude and larger size. The difference in the distribution of the electrical current between the point source (central electrode) and the flat-plate source (tank) may be the cause. Presumably, the point source electrode focuses more current into the plume than the planar tank bottom.

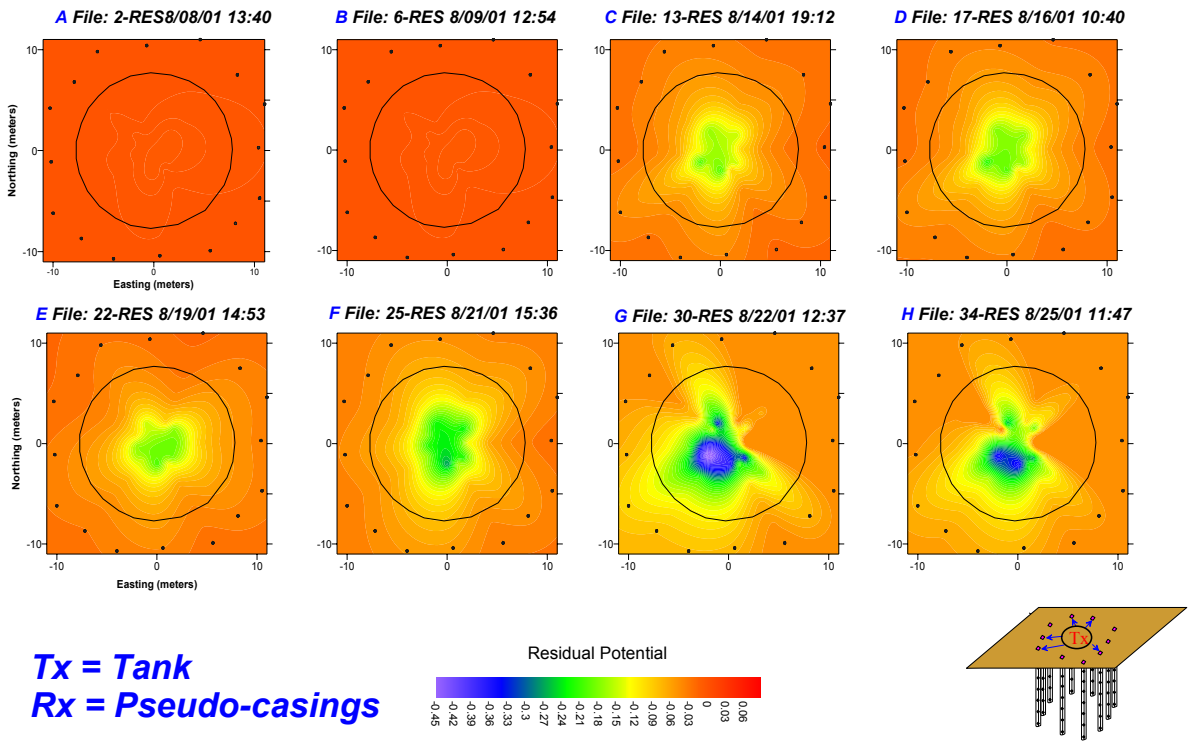

Figure 14 - Residual potential map for different times during the study

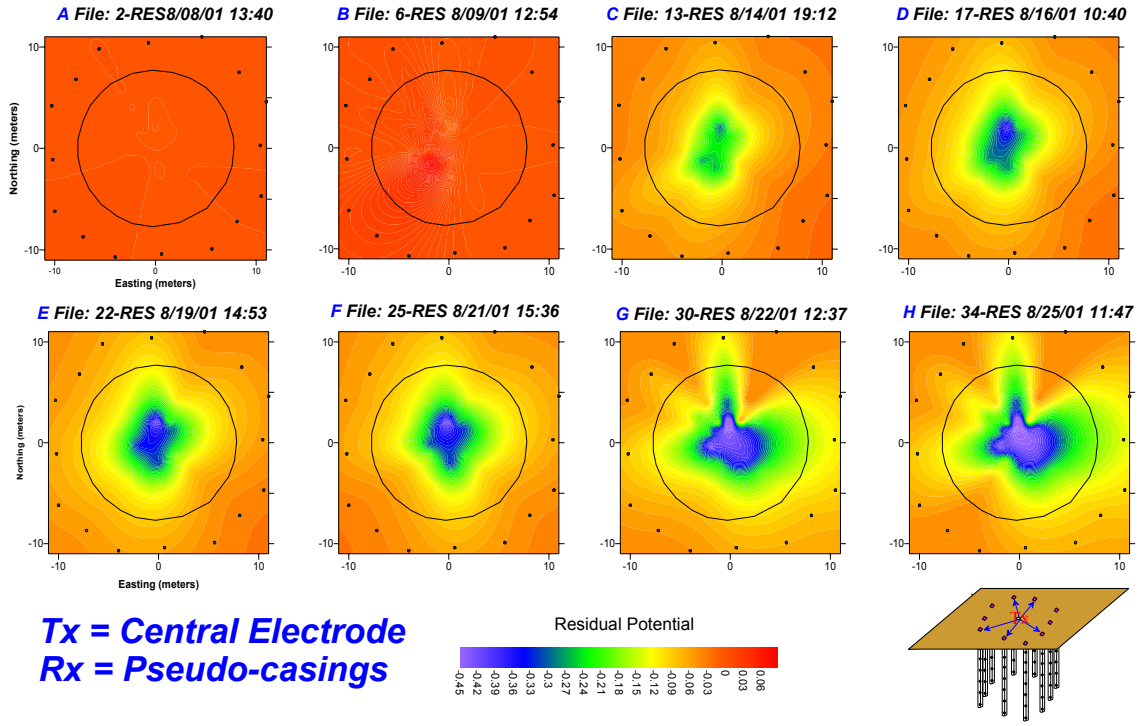

Figure 15 - Residual potential map for different times during the study

4.5 Measurements Along Individual Vertical ERT arrays

A series of tests were performed at the Mock Tank site to approximate the vertical distribution of electrical potential along the length of a casing. This work was a continuation of the processing algorithm that was applied to multiple casing data at the Sisson and Lu site that allowed us to model a three dimensional volume using well-casing potential data.

The measured potential for any given casing is a function of the cumulative transfer impedance between the casing and the hosting media along the length of the casing. The transfer impedance is the frequency-dependent resistance to the flow of electricity between the casing and the surrounding earth. The transfer impedance is affected by the intensity of the oxidation of the outside of the steel casing, the amount of soil moisture in contact with the oxide coating, and the chemical make-up of the moisture. For electricity to flow between the casing and the earth several small steps must occur that change the mode of electrical conduction from electronic in the casing to ionic in the soil moisture and then back again to electronic in the next casing. The vertical distribution of the variations in transfer impedance determines the casing characteristic that will predictably vary from site to site and may even vary from casing to casing within a site.

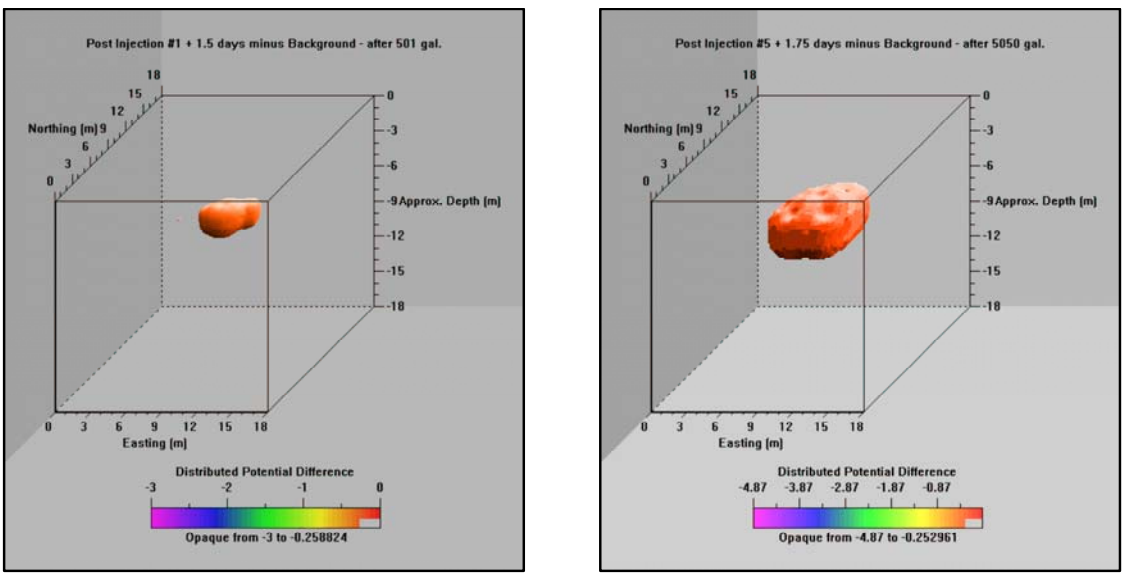

Figure 16 - A comparison of two time-snapshots of dynamic changes in volume produced by distribution function modeling of well-casing electrical measurements. After 501 gallons (left), after 5050 gallons (right).

Although the casings extend to considerable depth (relative to the experiment), the electrical measurements on the casings are essentially two-dimensional data sets. To arrive at three-dimensional models from two-dimensional data we used several methods. The most unusual and interesting one we used was a three-parameter, analytical distribution function. We used the distribution function to effectively spread the scalar potential measured at each casing along that portion of each casing between the depth of injection (approximately 4 meters) and the bottom of

the casing (18 meters). The three parameters allowed for distance from the injection well, dynamic variations (i.e. changes in amplitude with time), and downward progression of the injection with time. There is virtually no potential drop along the casing itself. However, the distribution function chosen should compensate for the non-linear distribution of current flux density along the casings due to variations in the transfer impedance.

The availability of the ERT electrodes at the Mock Tank site has given us the ability to test and refine the distribution function algorithm. To build up a discrete-point, vertical distribution, we energized the southeast casing and measured various combinations of the electrodes on a nearby ERT array. By shorting or fusing together all eight of the ERT nodes we can crudely approximate a vertical well casing. However, because the ERT nodes are separated, we fused various configurations of the ERT nodes to build up a discrete-point, vertical distribution. The table below (Figure 3) illustrates all combinations of fused ERT electrodes that were used to generate a unique distribution function. Each individual column represents one recorded data point with the red "I" denoting which ERT electrodes were fused together. The green numbers group together similar fusing combinations and act as a legend for Figures 17 and 18.

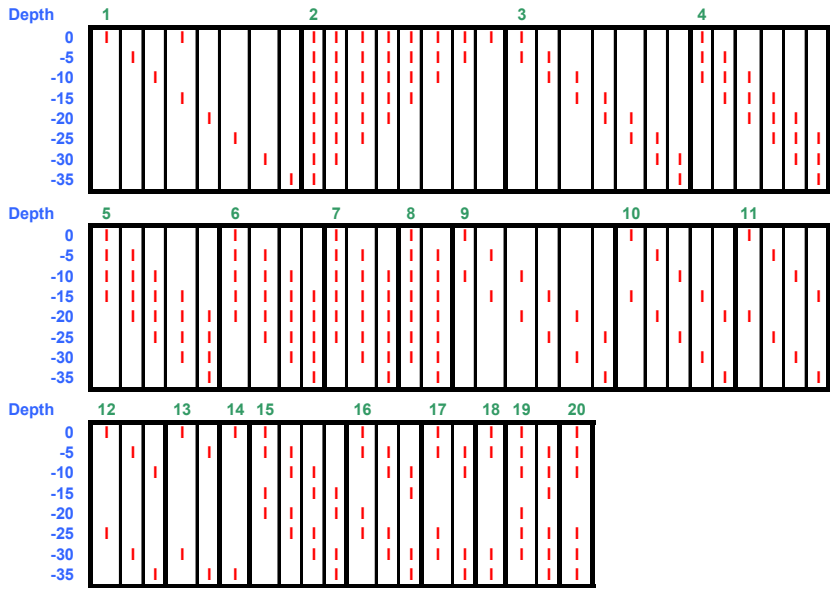

Table 5 – Table of fusing combinations

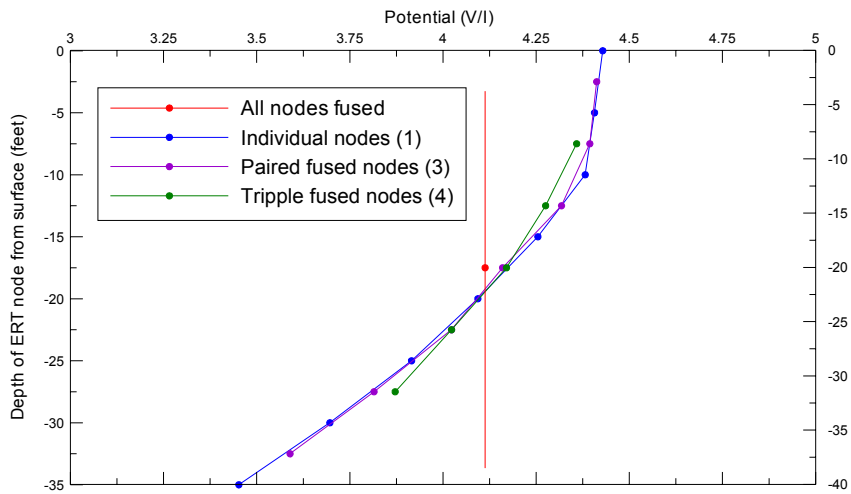

Figure 17 – discrete point vertical distribution of ERT nodes (legend numbers correspond to fused groupings listed on Figure 3)

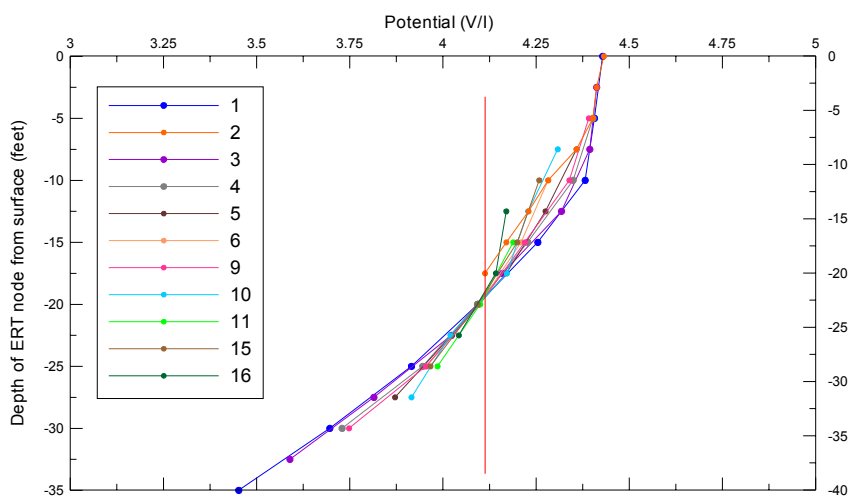

Figure 18 – discrete point vertical distribution of ERT nodes (legend numbers correspond to fused groupings listed on Figure 3)

The results of the fused ERT electrode study clearly show a non-linear variation in observed potential as a function of depth. The vertical red line in both Figures 17 and 18 is the observed potential with all electrodes fused simulating a steel casing. This would be the equivalent to the value observed measuring a single steel casing. The blue data points and blue line represent the values observed at each of the individual ERT electrodes. These two limiting cases; i.e. all electrodes fused and no electrodes fused, show both the variation in potential with depth (for the individual electrodes) and the integrated value (for all electrodes fused). The results were correctly anticipated, but we measured all combinations of electrodes to answer any questions regarding how various combinations of fused electrodes might respond. Those results are shown in Figure 4. Again, as might be expected, the more electrodes that are fused together, the closer

to a singular value is the observed potential. This is graphically indicated by a rotation of the data towards a single value for increasing numbers of shorted electrodes. This study illustrates the utility of the distribution function algorithm for three-dimensional modeling in areas where only casings may exist. This was an independent study separate from the injection test and performed for our own benefit and proof-of-concept.

4.6 Measurements At Three ERT array levels (fixed depth)

These data were acquired late in the injection study. We acquired horizontal ERT data at three levels: 10, 20, and 30 feet. The data were acquired using the pole-pole array. We acquired these data for our own benefit and they were not processed for this report. We report this because the data are available if desired.

4.7 Measurements Between ERT arrays (full ERT)

These data were acquired using the closest pairs of vertical ERT arrays. This is conventional two-dimensional ERT. Each pair of ERT arrays will produce a planar result connecting those two arrays. This will provide a cylinder of information surrounding the mock tank. The data were acquired late in the injection study. We acquired these data for our own benefit and they were not processed for this report. We report this because the data are available if desired.

4.8 1-D modeling using surface electrode array

Figure 1 shows the location of surface electrodes that were placed at approximate logarithmic intervals along eight radials emanating from the mock tank. One of the radials was limited in length by the presence of the cordoned “hot zone” to the south of the site. These surface data were acquired to aide in the understanding and modeling of the shallow electrical properties of the site and to characterize distortion in the e-field caused by the presence of the steel tank. Data were acquired at electrode-to-tank distances of 1, 1.5, 2, 3, 5, 7.5, 10, 15, 20, 30, 50, 75 and 100 meters. Figure 19 shows the results of this phase of testing.

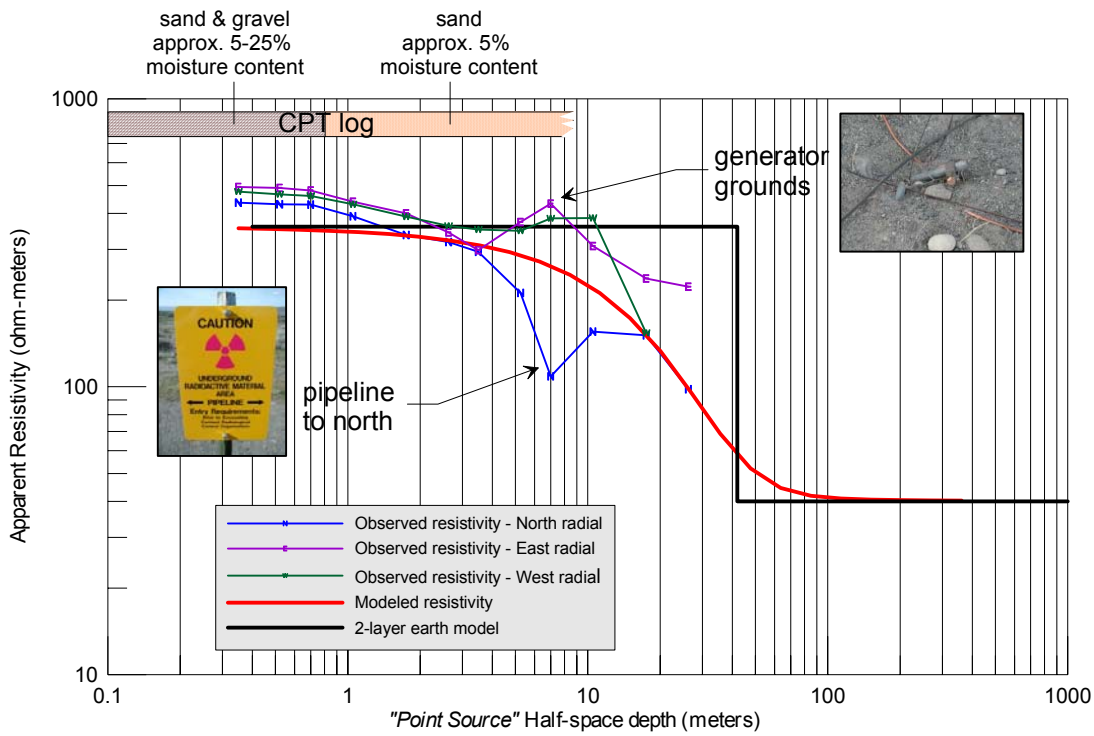

Figure 19 – 1D resistivity inversion

Technically, there are some limitations to the resistivity sounding approach indicated in Figure 1. Resistivity sounding data are based on point sources, point sinks, and point potential measurements. We acknowledge the fact that we are energizing a large, grounded, big steel plate and not a point source. In other sections of this report we discuss potential measurements between cultural features, such as the tank and casings that are also non-point sources. However, in those cases, we discuss raw potential data, not data converted to apparent resistivities as with the data displayed in Figure 19. Again, the transmitting source for the data in Figure 19 is the tank itself. The resultant e-field around the tank can be safely assumed to be different from that of a point source. The point of this discussion is that the inversion of the data to a layered-earth model is not strictly correct and, consequently, we were not overly concerned about carefully fitting the data with a theoretical curve. We were mainly interested in the general behavior of the data. There is a distance from the tank (which we wanted to determine) where the e-field distortion due to the tank is indistinguishable from that of a point source. We estimate that distance to be around 10 meters. This is much closer than we had anticipated and may indicate the limited grounding of the tank. These data were acquired prior to injection.

For the three, long, radials displayed there is good similarity of the data for electrode distances of 1 to 10 meters. This similarity suggests that the shallow manifestation of the e-field due to the tank is uniform in every direction, thereby making possible the removal of this distortion to subsequent data.

The plot also reveals identifiable perturbations in the e-field due to cultural features that include the buried pipeline located to the north of the site and multiple generator grounding locations installed for the PITT test. The 1-D model clearly demonstrates that we have the ability to detect, identify, and segregate undesirable cultural disturbances. This capability will be vital in a real tank environment where there will be an abundance of cultural disturbances. We did not see any other effects due to the pipeline to the north that might have been caused by the cathodic protection system. We made no attempt to determine whether that system was on or off. We assume that it was off.

We fitted a two-layer-earth, model curve to the observed data to estimate quantitative layered depth information. The modeled curve shown in red most closely fits the northern radial data but effects due to the tank and pipelines makes leaves some concern regarding precision of fit. Regardless of how closely the model fits all three radial curves, it does suggest that at least the first 40 meters of earth is consistent in each direction. For our purposes, it suggests that the relevant volume of earth beneath the tank (for the purposes of the study) behaves like a homogeneous, isotropic half-space.

5.0 SELECTION CRITERIA

5.1 Gate Selection Criteria

Gate 1: *Is the technology deployable from both a technical and cost standpoint?*

The HRR/SCRT method involves minimal installation and can make use of existing tank infrastructure. As demonstrated at both Sisson and Lu and the Mock tank site, HRR/SCRT can successfully integrate existing steel casings and tank structures within its sensor network. The method can also be enhanced with the addition of non-invasive surface electrodes that only penetrate to a depth less than 24 inches. Deployment of the system is straightforward requiring only simple electrical connections to appropriately grounded metallic structures. Monitoring may be controlled remotely or made autonomous and results may be telemetered in real-time to a centralized location. The result is a cost effective tool that does not require any expensive permanent deployment of monitoring technology.

Gate 2: *Can the technology detect a 1000-gallon leak with accuracy and reliability?*

HRR/SCRT has demonstrated its ability to readily detect leaks as small as forty liters (ten gallons) and, with the optimal positioning of electrodes, as small as one liter. This result was obtained at the Sisson and Lu site with an electrode in the injection well.

Gate 3: *Can a reliable performance evaluation be developed?*

Reliable performance in the tank farms will depend a great deal on the infrastructure and initial testing. We are confident that procedures can be established in an off-tank-farm situation to evaluate and optimize the performance of the HRR/SCRT system.

Gate 4: *Do the differences between demonstration and deployment affect performance?*

Demonstration is at the mock tank and deployment would be at a real-tank farm. This can be extensively discussed and there is no definitive answer until a tank-farm tank is actually tested. There are many similarities and many differences. The critical factor is the quality and consistency of the concrete and asphalt encapsulation of the full-size tanks, which is difficult to simulate at the mock tank site.

Gate 5: *Can the technology be implemented with operational strategy*?

We are unsure what an "operational strategy" means. If it means can we make the technology an off-the-shelf instrument, then we are not sure at this time. We believe we can simplify the deployment so that a trained technician can operate the system, but, until we actually perform measurements on a full-size tank, it will be difficult to predict where we will encounter problems in the procedurization.

5.2 Matrix Approach Selection

Life Cycle Cost:

<$1M = High, $1M to $3M = Medium, >3M = Low?

Costs for deployment of HRR/SCRT during a 45-day leak detection campaign are estimated to be below $1M. The HRR/SCRT method involves minimal installation and can make use of existing tank infrastructure. Deployment of the system is straightforward requiring only simple electrical connections to appropriately grounded metallic structures. The result is a cost effective tool that does not necessarily require a permanent deployment of monitoring instrumentation. However, for subsequent efforts and more specifically for longer-term benefits, a permanent installation can be made. Telemetry and Internet access are readily available.

Safety Risk:

High = PFA < 5%, Medium = PFA near 5%, Low = PFA > 5%

Current, off-the-shelf instruments are designed to force as much electrical power in the ground as possible to overcome electrical noise problems normally encountered in conventional surveying. The electrode configuration of the HRR/SCRT implementation at the Sisson and Lu site and at the mock tank allows much lower driving current and voltage. We believe that at the full-size tanks low power will also be adequate. We forced the available instrumentation to work in an environment for which they were not designed. In fact, recommended design changes for instrumentation would be to lower the output power for both safety and logistical reasons. Technically, the driving voltage is what would be decreased. Conventional instrumentation operates in the 50 to 500 volt range. The high voltage is needed to overcome the total loop resistance generally encountered due to high electrode-to-ground contact impedance. In the situations that we have seen to date the power requirements have been minimal and the operational aspects optimal (for low power). The key concern is energizing a tank. Low power is obviously desirable. This can readily be achieved with redesigned equipment. Personnel safety is an additional concern, which low power instrumentation favors.

Technical Maturity:

"high" maturity = is one that is being used for plume detection currently by industry and has at least 10 demonstrations of such applications.
"medium" maturity = is one that is an emerging industrial technology and has more than 5 deployments.
"low" maturity = is one that is still in the developmental stage and has been used for less than 3 plume detection applications.

The HRR/SCRT technology is of high technical maturity as a tool for subsurface leak detection, and plume detection, and migration monitoring. However, the basic HRR/SCRT technique has been tailored to allow three-dimensional volumetric detection within a tank farm environment. This derivation of HRR is called "Steel Casing Resistivity Technology" or SCRT; and as such, SCRT is of relatively low technical maturity. We have already observed unsuspected results in the data that will require further study.

Proven Application:

"high" proven application = is one that is or has been deployed at a DOE site and development of the methods and procedures currently exist.
"medium" proven application = has been deployed in industry and development of methods and procedures is easily accomplished in a short time frame.
"low" proven application = is one has only been deployed in development mode and creation and procedures will take considerable time.

HRR/SCRT has been deployed in industry and procedures are well documented. SCRT has been deployed at two DOE sites (Sisson and Lu, mock Tank) but procedures will take a short time to document, therefore SCRT has a medium proven application rating. HydroGEOPHYSICS has performed several single-casing and buried-electrode surveys and has demonstrated advanced capabilities in those areas using HRR/SCRT.

6.0 TANK SITE IMPLEMENTATION

Full-size tank farm implementation would consist of connecting wires to the exposed portion of existing casings (dry wells) and other exposed infrastructure through non-sparking, abrasion contact and an external clamp. Contact with the steel tank liner will vary from tank to tank and may also be through access ports allowing an electrode to be deposited in the sludge or solution. This would best be resolved through review of as-built plans for the various tank farms and discussions with those most closely involved with the physical tank systems.

6.1 Proposed Work Plan

Phase I: Initial site visit & Survey design:

1. Location and Mapping: The first phase of implementing HRR/SCRT within a real tank farm would include designing an electrical network tailored to the specifics of the selected site. This will require an initial site visit to perform a detailed analysis of the on and off-site infrastructure. During such a visit it will be necessary to locate, survey (2nd order accuracy), and generate a map of the following features:
    a. edges of tanks
    b. wells
    c. metallic piping
    d. utility lines (power, water, fire protection, communication, etc.)
    e. cathodic protection systems
    f. generator grounding locations
    g. fence lines
    h. any other grounded metallic structures
2. Training and Permitting: Additionally, we would secure any necessary permits, complete any required training and compile any additional infrastructure/utility maps that may be available.
3. Calibration and Infrastructure Testing: Lastly, we need to check the existence and continuity of reported tank-to-tank piping and cathodic connection. This is crucial in determining how current may flow during actual measurements.

Phase II: Deployment of sensor network:

1. Selecting data acquisition area: All connections to the sensor network will be made using insulated wire run to a central off site location that will serve as a data acquisition center. Such a site would be selected such that:
    a. It is outside the tank far perimeter, but still close enough to prevent lengthy wire connection.
    b. It has unrestricted 24-hour access.
    c. It could house a temporary field trailer.
    d. It has 110-volt AC power (for field computers).

2. Connecting to wells: All steel cased wells would be connected by simply attaching an insulated cable to the well using a metallic hose clamp. This will provide a solid connection without modifying the wells in any way.
3. Connection to the tank: All tanks would be connected by attaching an insulated wire to any metallic junction that connects the metallic tank shell to an access point on the surface. Discussions with PNNL personnel suggest that such a junction does exist. Again we would use a metallic hose clamp to secure the cable in a manner that would prevent a sparking possibility during installation.
4. Installing surface electrodes: To enhance measurements we would install a number of surface electrodes either in radial lines emanating from each tank or in an appropriate grid encompassing the tank/s. Electrodes would consist of 18" stainless steel stakes that would be driven in 2 feet below the ground surface. Each electrode would be connected by insulated cable.
5. Surveying surface electrodes: It will be necessary to survey the location of individual surface electrodes using 2nd order accuracy. This is critical for data processing.
6. Installing infinite electrodes: Based upon the initial infrastructure mapping, we would locate the infinites in an unrestricted location outside the tank farm. It would be desirable to locate them at least 2000 feet from the nearest point of measurement.

Phase III: Deployment of data collection system:

1. Site setup: This would require setting up the following:
    a. unpacking and installing the data acquisition system within field trailer
    b. connecting the system to insulated onsite cabling
    c. performing system tests
    d. performing cable continuity tests
2. Initial calibration and Testing: We would require a short period before tank remediation begins to perform some contact resistance and calibration measurements. We would also record a number of background data sets for use in subsequent processing.

Phase IV: Monitoring of tank remediation:

1. Monitoring preparation: We would require a few days to set up the following:
    a. establish data archiving steps
    b. coordinate with onsite personnel in order to setup an established procedure for notification of possible leaks
2. Record data: We would begin full-time (24hr) monitoring at least a day before remediation efforts begin. Once monitoring commences, we would perform routinely scheduled data downloads and additional processing. We recommend monitoring for at least a few weeks after all remediation efforts have concluded.

6.2 Points of concern

1) Sparking issues: The concern expressed regarding sparking inside the tanks needs to be addressed. Sparking can arise from a variety of sources. The primary concern is whether or not the instrumentation could cause sparking in the tank environment. Conventional equipment definitely poses this problem as that equipment is designed to overcome

typical high grounding resistances and operates at voltages capable of sparking. Our recommendation for low-voltage equipment fabrication is intended to minimize this problem. An inherent safety aspect is that the tank shell itself acts as a potential surface (faraday shield) and will carry the bulk of the current. Sparking can only occur where there is a gap across a dielectric with sufficient potential difference to arc across the gap. All possible precautions would be taken to eliminate this risk. Other possible sources of sparking are static discharges due to low humidity and frictional motion against a suitable dielectric and lightning.

2) Surface electrode issues: Surface electrodes augment the interpretation of the data and enable a better understanding of the impact of the infrastructure on the imposed e-field. We recommend installing sufficient surface electrodes to permit these measurements.
3) Electrical noise 1: Electrical noise is always a problem for electrical methods geophysics. The array normally used for HRR/SCRT has very high signal for minimal current injected. Additionally, the waveform, mode of transmission, data sampling, and processing all allow ULF data to be acquired in severe environments. We have worked effectively within major cities (Phoenix, for example) running across streets, along fences, pipelines, powerlines, etc. and still maintained good signal-to-noise ratio.
4) Electrical noise 2: As an absolute worst-case scenario, in conjunction with LLNL, we performed a test at the Sisson and Lu site to see if we could measure while they were transmitting and vice-versa. They transmitted and received on ERT electrodes and we transmitted and received on casings. Although it slowed data acquisition considerably, we were able to acquire quality data. Because they were operating at a slightly higher frequency, they were unable to acquire data when we were transmitting. This is no way denigrates their system or mode of operation. It only illustrates that the operation parameters for the two systems overlapped. Both systems could easily be configured to operate simultaneously with the other system, but, it would be far from optimal. This was not a carefully performed test, just a quick check to see how severe the effects would be on each other's system.
5) Electrical noise 3: We performed a similar survey using a 1,200 foot long steel casing while an aquifer test was being performed. We used a low current, battery-powered system and mapped surface potentials as was done at both Sisson and Lu and the mock tank site with the surface electrodes. The interesting aspect was that the aquifer test required the 24-hour operation of a 350 horsepower, 480 volt, 3-phase, surface-mounted pump on the well. All data were acquired with the pump running at 1,400 gallons per minute (gpm). We easily read through any associated electrical noise.
6) Equipment problems: For the near term a backup system should be kept available to prevent data loss due to equipment failure. In general, we are using the equipment in a mode of operation for which they were not really intended. Again, appropriate equipment should be developed for the specific application.

7.0 SUMMARY & RECOMMENDATIONS

The specific goals for the LDMM study are ideal for electrical methods. The injected solutions are highly conductive and the vadose-zone host medium is relatively resistive. As a result of the Mock Tank Study, it is further evident that electrical methods should play a role in subsequent studies. We have produced diagnostic results using existing infrastructure, in particular, the steel well casings and the steel tank itself. The lack of additional expensive infrastructure makes HRR/SCRT methods very cost effective and easily deployed.

Two groups of configurations were deployed; 1. various combinations of surface electrodes in conjunction with steel casings and the tank; and, 2. pseudo-casings using the fused ERT arrays. The multiple datasets allow cross-checking (one system versus another) quality control for the data. We have demonstrated that specialized installations of electrodes are not absolutely necessary, but they do provide useful information.

We have demonstrated that our HRR/SCRT methods, as deployed at the Mock Tank site provided:

1. positive and immediate indication of the commencement of injections,
2. positive and immediate indication of the cessation of injections,
3. qualitative volumetric estimations using two different configurations,
4. reasonable location of the leak source using most of the configurations,
5. poor lateral definition of the leaked solution using any of the configurations,
6. a minimum volume detection limit of approximately 500 gals for one method
7. good quantitative injected volume estimates,
8. good quantitative injection rate estimations,
9. no indication or resolution of fingering with any of the methods,
10. good repeatability of data in a complex environment, and
11. poor vertical resolution due to the casing and tank geometry.

These methods can be adapted to a variety of circumstances as shown by the various configurations, each of which produced useful results.

The methods rely on different electrode arrangements and are complementary. Extensive processing has been performed only to realize in some cases that minimal processing can produce highly useful results.

These kinds of electrical measurements are relatively easy to perform and should be able to be done with off-the-shelf equipment for further evaluation, but, not necessarily in the tank farms. We have used relatively sophisticated commercial equipment for all of the electrical studies performed at both the Sisson and Lu site and the mock tank site. We have consistently had problems of some sort that lead us to believe that commercial instruments may not be robust

enough for the particular tasks and the environment. We recommend building a more robust system that can handle some of the unusual problems that seem to continually surface during these studies. Specifications for such a system can be discussed at a future date.

Data acquisition is much simpler than the conceptual understanding required to adequately implement the methods. An understanding of the behavior of electric fields in the vicinity of buried conductors is very beneficial, especially when using those same, grounded structures for data acquisition. We highly recommend further tests in increasingly complicated situations. Continued processing of some of the existing data would also further the understanding of what can be derived from the data. Better shortcuts to faster processing with the aim of real-time results should also be sought.

We would also suggest that future test work should include a more detailed tracking of injected volumes and flow rates. The addition of a continuous data logger would provide real-time correlation with the geophysical features and would greatly aid in testing of geophysical methodology and interpretation of data.

7.1 Development of new equipment

Hardware limitations pose a serious problem for future work. The system used for this test showed great merit in some areas and serious deficiencies in other areas of specific interest for tank farm deployment.

The primary safety concern for future tank farm deployment is the operating voltage when transmitting a signal into the tanks or adjacent wells. Commercially available systems are designed to operate under *exploration* conditions. Such conditions typically require sufficiently high voltage to overcome newly installed small electrodes. Tank farm conditions at Hanford are quite different in that the transmitting structures are very well grounded. Low voltage is necessary to eliminate the environmental safety concerns (spark hazard) and personnel safety concerns (shock hazard). Low humidity (local static discharge) and thunderstorms (regional static discharge, i.e. lightning) pose a greater problem.

Additional equipment limitations include lack of flexibility in operation. The equipment is designed for normal modes of operation typically encountered during conventional surveys. Tank farm applications require considerable additional flexibility. We face a number of data acquisition obstacles many of which are created by site complications (low voltage safety requirements, non-uniform electrode spacing, large ambient temperature range, etc.), but some of which are a direct result of the type of work we are performing. Simply put, the migration of solution within the Hanford Formation vadose zone is so rapid that great attention must be focused upon the ability to record discrete data sets within a very short time period. By contrast, we must also be prepared to sample from an extremely large and varied sensor network that may include hundreds of connections to tanks, steel casings and surface electrodes.

As mentioned in the "Equipment (2.5)" section of this report, we have used two different systems at the Sisson and Lu and Mock Tank sites. The Oyo McOhm-21 was used during the 2000-2001 VZTFS and the AGI SuperSting R8 was used during the 2001 LDMM tests. Detailed in section 7.1.1 and 7.1.2 is a synopsis of the equipment limitations and failures.

7.1.1 Problems with the McOhm-21

We used the McOhm-21 because the combination of PNNL and hydroGEOPHYSICS relay (scanner) boxes and cables provided the ability to simultaneously connect to 96 electrodes. The system was also programmable which allowed us to define different array configurations and to run repeat data sets for a defined time period. Reliability of the unit was excellent; there were no equipment failures during all tests. Unfortunately, the system suffered from a number of design limitations;

1. its design is over 10 years old and there is no longer support or replacement parts,
2. it is only a two channel system requiring multiple hours per data set,
3. it allows limited adjustment to the voltage and current levels,
4. it has a very limited data storage area and transfer of data can only be made using a very dated 720K floppy drive,
5. it draws several amps when sitting idle and therefore requires an extensive array of 12V car batteries when in operation,
6. the most serious of all is an internal thermal problem that causes the data to vary in response to overheating,
7. and the data cannot be remotely accessed or telemetered off-site.

7.1.2 Problems with the SuperSting R8

To overcome the shortcomings of the McOhm-21, we selected the AGI SuperSting R8 because it was a state-of-the-art, 8-channel system manufactured by Advanced Geosciences who has a reputation for building robust resistivity systems. The unit was designed to use a smart electrode cable system that allows all switching to be performed on the cable itself. However, a tank farm environment prohibited us from using such a cable, so a custom fabricated relay box was built by AGI. Simply put, the smart electrodes usually built into the cable were now housed within a relay box that could be located off site. The SuperSting is programmable, used far less power than the McOhm and entire datasets could be collected in one-half hour, rather than multiple hours. AGI provided a solid interface with a laptop computer, which should allow remote or telemetered access and monitoring. However, most seriously, the system failed twice during the LDMM tests that required the return of the unit to the manufacturer. A few months later, we tested another SuperSting on a Los Alamos National Laboratory site and suffered a similar failure and loss of production. We have been working very closely with AGI to resolve these problems, but we cannot confidently deploy the system until we demonstrate that those problems have been resolved on lower priority projects. The present limitations are:

1. it is an 8-channel system which although much faster than the McOhm-21, will require too much time to sample large numbers of electrodes in a real tank farm,

2. it allows only very limited adjustment to the voltage and current levels,
3. it is currently limited to 54 electrode connections.

7.1.3 Overcoming Equipment Problems

hydroGEOPHYSICS personnel have either researched, used, tested or aided in the development of almost all commercially available resistivity instruments since the 1960's. We feel that in order to optimize data collection within a tank farm environment, a new and more tailored resistivity instrument will need to be constructed. Specific recommendations are presented in a separate document.

General characteristics of this new system would include the following:

1. uses a low-voltage signal source
2. faster data acquisition
3. more reliable
4. more flexible
5. provide greater storage
6. requires low power

8.0 FUTURE CONSIDERATIONS

8.1 Further processing

Some ERT data sets were acquired because of the unique opportunity and were not intended to be part of the present study. Those data can be forwarded to PNNL if desired.

We would encourage the consideration of further processing of all existing data sets. Two goals for additional processing would be: (1) to determine the minimum requirement for casings that would still produce an unequivocal result, and (2) to determine if some combination of data sets other than what has been tested might produce even more diagnostic results.

8.2 Additional injections

In our previous report on the Sisson and Lu site we recommended the following. The results we obtained at the mock tank site only reinforce our belief that additional tests should be performed.

It would prove useful to perform a series of variable-rate injections using one method at a time at the mock tank site. This would best be performed using only HRR/SCRT methods to allow continuous data acquisition (i.e. uninterrupted time series). Present results have demonstrated that less than 500 gallons can readily be detected. We recommend considering a series of 1000 gallon, continuous injections, spaced over several months. Each electrode arrangement would be monitored continuously before, during, and after each of the injections. The present data sets were acquired during time windows determined by the various methods used, other participants' needs, long overall injection times, and distance from our own home office. The lack of continuity occurs at critical times for some of the methods. Other methods had no opportunity to operate during the most dynamic periods for the plume. Sufficient time should be allowed to permit the site to recover between injections.

This report is based on our best understanding of the electrical properties of earth materials and is limited to the areas where the surveys were performed. We would appreciate any feedback regarding the interpretation based on additional surveying or invasive characterization.

9.0 ACKNOWLEDGMENTS

We wish to acknowledge all the support provided by PNNL and Vista Engineering personnel. With out their continued efforts this project could not be completed with such success.

1. Glendon W. Gee, Senior Chief Engineer, Hydrology, PNNL.
2. Brent Barnett, Senior Research Scientist I, Applied Geology and Geochemistry, PNNL.
3. Mark D. Sweeney, Research Engineer, Applied Geology and Geochemistry, PNNL.
4. Wesley L. Bratton, Staff Geotechnical Engineer, Vista Engineering.

We would also like to thank Drs. Bill Daily and Abe Ramirez of Lawrence Livermore National Laboratory for their cooperation during simultaneous electrical measurements.

10.0 SIGNATURE PAGE

Respectfully submitted,

James B. Fink, Ph.D., P.E. (geophysical), R.L.S.
President

Marc T. Levitt
Project Engineer

Mr. Chris Baldyga, M.Sc.
Geophysical Engineer

Appendix E

Lithologic and Cone Penetrometer Data from the Mock Tank Site 1996, 2001

Appendix E: Lithologic and Cone Penetrometer Data from the Mock Tank Site 1996, 2001

Lithologic information collected at the Mock Tank Site during 1996 and 2001 is presented in this appendix. The lithologic column of Figure E.1 was derived during drilling activities in 1996 (also see Sections 2.1.2 and 2.3 in the main body of the text). The CPT and neutron probe information was collected prior to the FY 2001 TLDD. Grain size distribution and hydraulic/ pneumatic conductivity analysis were based on 28 samples that were collected from CPT borehole 8 (south of the Mock Tank Structure) at 0.3-m (1-ft) intervals from 2 to 10.7 m (7 to 35 ft) below ground surface. In general, the stratigraphy beneath the Mock Tank Site is dominated by fine-to-medium-grained sand, with minor components of gravel, silt, and clay. Important exceptions to this generality are the gravel layer occurring at ~12 m (~40 ft) and the clay/silt horizon at ~ 4.6 m (15 ft). The CPT log of borehole no. 10 (see Figure E. 4) indicates the presence of a clay/silt horizon at approximately 3.4 m (10 ft) below surface. This latter probably corresponds to the fine layer at 4.6 m (15 ft) shown in Figure E.1, the difference most likely being the result of some inaccuracy in the composite column of Figure E.1.

Description of Sediments from CPT Borehole No. 8

Three grain-size groups were identified based on percentages of each of the four size categories. All 28 samples were composed primarily of sand ranging from 69% to 95% sand by weight. The sand component represents the primary transmissive component, whereas silt and clay reduce the sediments' capability to transmit water under saturated conditions; gravel would hamper flow under unsaturated conditions. The samples were first segregated based on the percentage of gravel by weight. This was done because the permeable materials are basically the sands, and gravels present in sands reduce the total porosity, the effective porosity, and the hydraulic conductivity. All of the samples had some gravel, ranging from 1 to 28% by weight. Samples with 12% or less gravel (approximately pebble size) were considered to have no significant effect on the value selected for hydraulic conductivity; 27 of the 28 samples belong in this category, and only one sample at 8.2 to 8.5 m (27 to 28 ft) had 28% gravel, which was considered significant in selection of hydraulic conductivity values.

The percentage of silt and clay present can have a significant effect on hydraulic conductivity and, because of the way in which it may be deposited, on vertical flow. Out of 28 samples, 24 had 2% or less silt and clay, one had 3%, one 4%, one 5%, and one 6%. Based on work by Khaleel and Freeman (1995), percentages at 5% or less do not have a significant effect on the values for hydraulic conductivity. The percentage of fine sand ranged from 14 to 28%; however, except for three samples, the range was from 14% to 22%. Because of the way basalt sand particles break down rapidly to silt and clay, the three samples (2.4 to 2.7 m [8 to 9 ft], 7.6 to 7.9 m [25 to 26 ft], 10.4 to 10.7 m [34 to 35 ft] bgs) with 4% or more silt and clay also had 24%, 25%, and 28% fine sand, respectively.

One sample (8.2 to 8.5 m [27 to 28 ft] bgs) is a gravel-rich sand or a sandy gravel; three samples (2.4 to 2.7 m [8 to 9 ft], 7.6 to 7.9 m [25 to 26 ft], 10.4 to 10.7 m [34 to 35 ft] bgs) are silty sand with trace amounts of gravel, but contain significant percentages of fine sand, silt and clay. The

remaining 24 samples are basically sand with trace to very minor amounts of gravel, silt and clay. Based on nearby wells and samples from Khaleel and Freeman (1995), the hydraulic conductivity value for the one sandy gravel is estimated to be 1.8 x 10^{-5}cm/s. The hydraulic conductivity for the three silty-sand samples is estimated at 2.8 x 10^{-4}cm/s. Hydraulic conductivity values for the other 24 sand samples are estimated to be 8.7 x 10^{-4}cm/s based on the closest and most similar core-barrel sample 2-1636 from well 299-E24-95.

Neutron Logging Results

Soil-sample analysis and CPT resistivity data collected from both the SDA and the Mock Tank area prior to solution-release tests were correlated with neutron logging tool data from the Infiltration Gallery and from CPT boreholes 8 and 9 (adjacent to the mock-tank structure) to characterize site-wide soil-water saturation (for CPT data, see Figures E.2 through E.4). An overall water-saturation (S_W) value of 0.16 (vol/vol) was obtained from this analysis. This agrees, in general, with other Hanford S_W values in similar soils. The soil-moisture profile indicates that silt layers are located approximately 1 m (3.5 ft) bgs and 10.4 m (34 ft) bgs as suggested by a higher soil moisture content in these zones (Figure E.4).

References

Cameron RJ, JC Evans, MD Johnson, and TL Liikala. 2002. *Summary of Hanford Subsurface Air Flow and Extraction (SAFE) Activities for FY 2001*. PNNL-13820, Pacific Northwest National Laboratory. Richland, Washington.

Khaleel R and EJ Freeman. 1995. *Variability and scaling of hydraulic properties for 200 Area soils, Hanford Site*. WHC-EP-0883, Westinghouse Hanford Company, Richland, Washington.

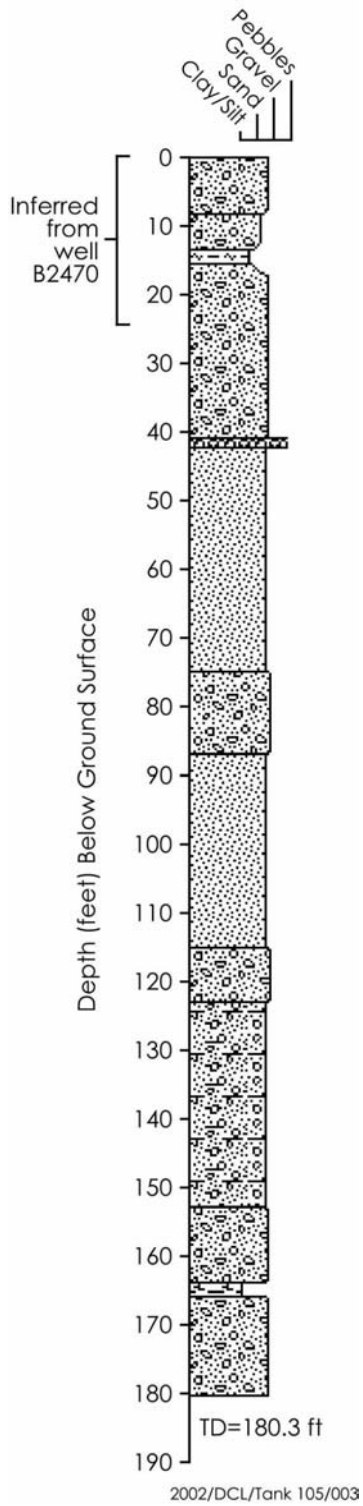

Figure E.1. Stratigraphic Column Derived from 1996 Drilling in what is now the SAFE Development Area (SDA), just East of The Mock Tank

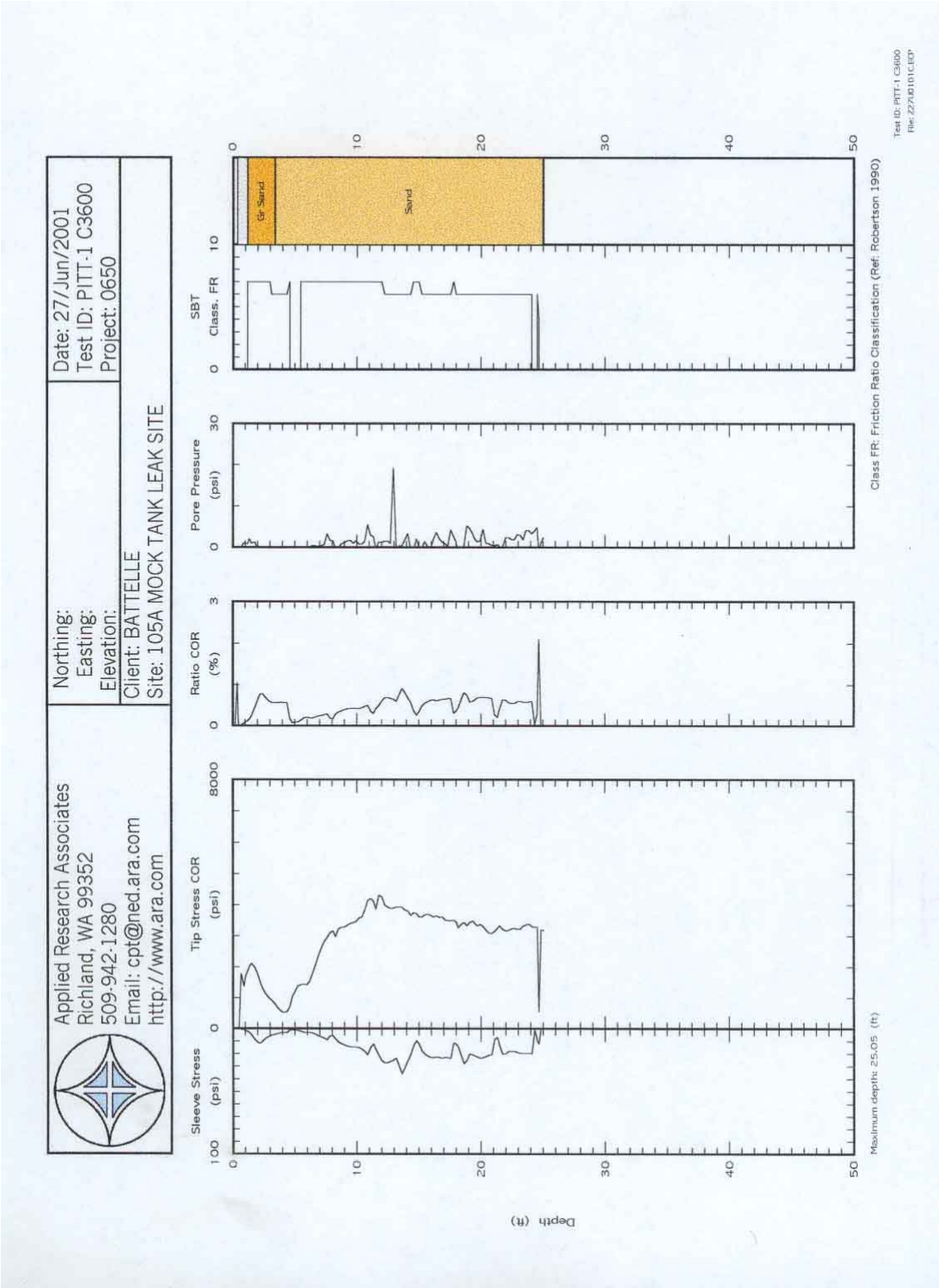

Figure E.2. Cone Penetrometer Characterization Data

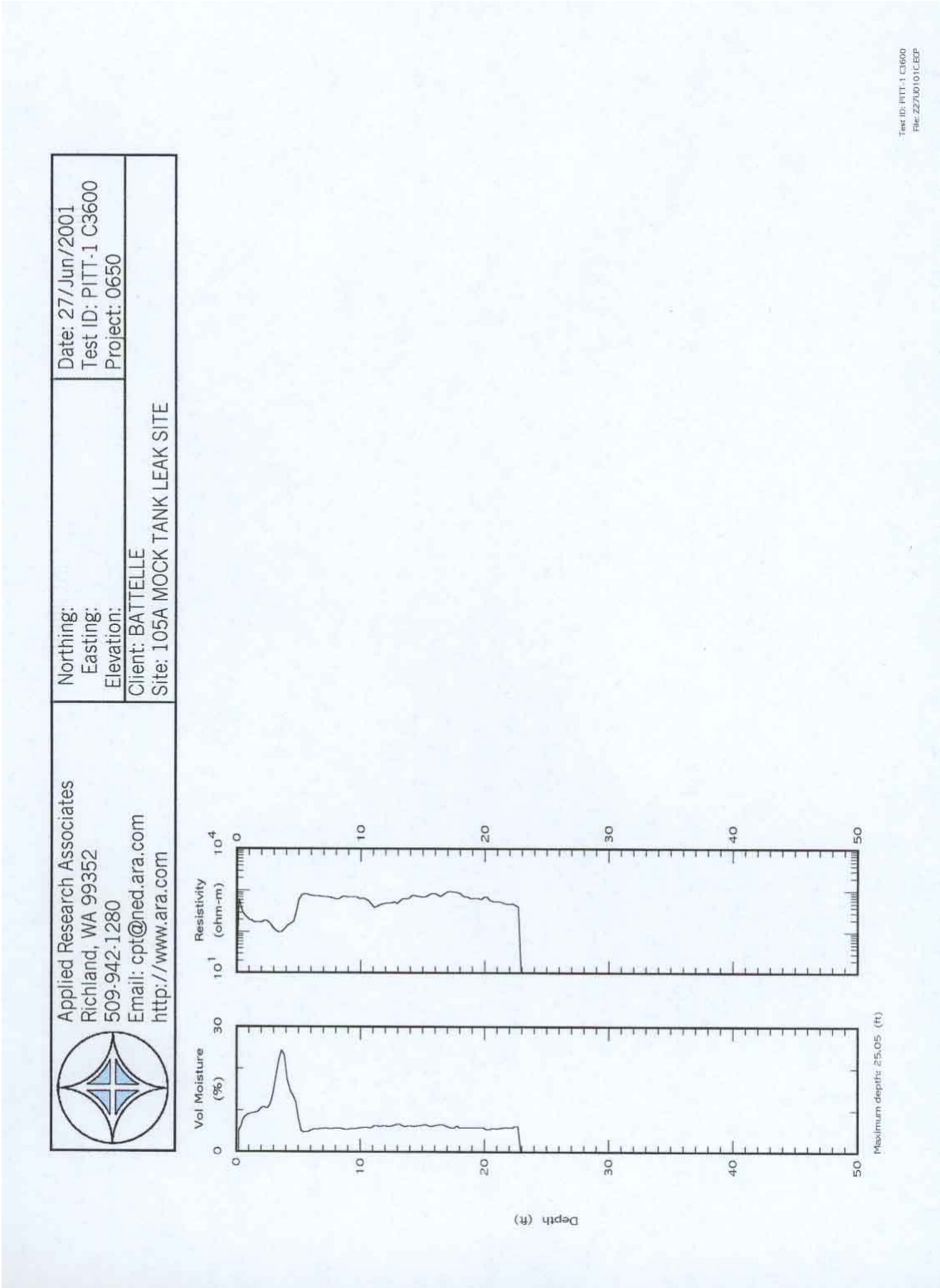

Figure E.2. (contd)

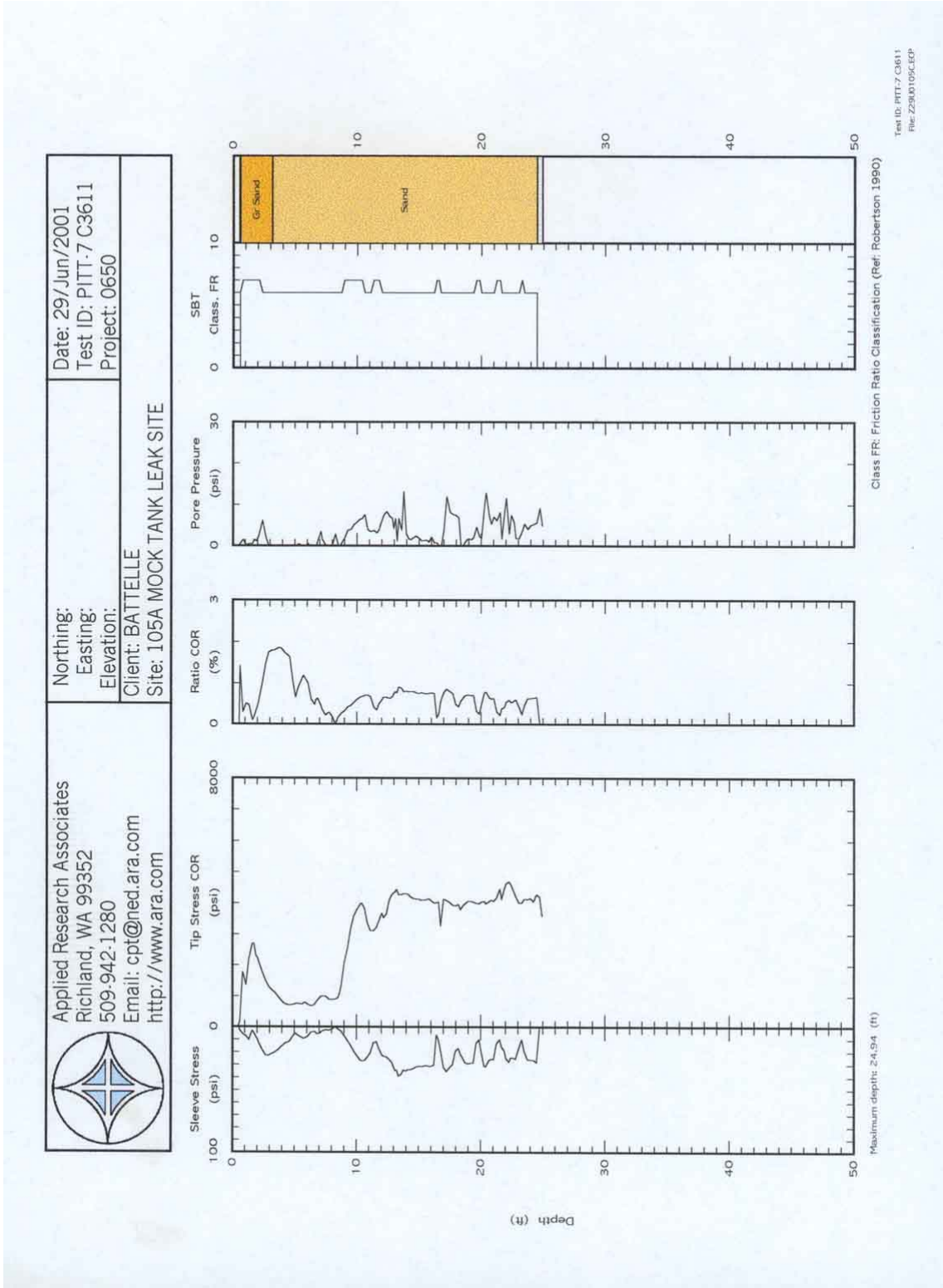
Applied Research Associates
Richland, WA 99352
509-942-1280
Email: cpt@ned.ara.com
http://www.ara.com
Northing:
Easting:
Elevation:
Date: 29/Jun/2001
Test ID: PITT-7 C3611
Project: 0650
Client: BATTELLE
Site: 105A MOCK TANK LEAK SITE
Sleeve Stress (psi)
100
0
Tip Stress COR (psi)
0
8000
Ratio COR (%)
0
3
Pore Pressure (psi)
0
30
SBT
Class. FR
0
10
Gr Sand
Sand
Depth (ft)
0
10
20
30
40
50
Maximum depth: 24.94 (ft)
Class FR: Friction Ratio Classification (Ref: Robertson 1990)
Test ID: PITT-7 C3611
File: Z29J0105C.EP

Figure E.3

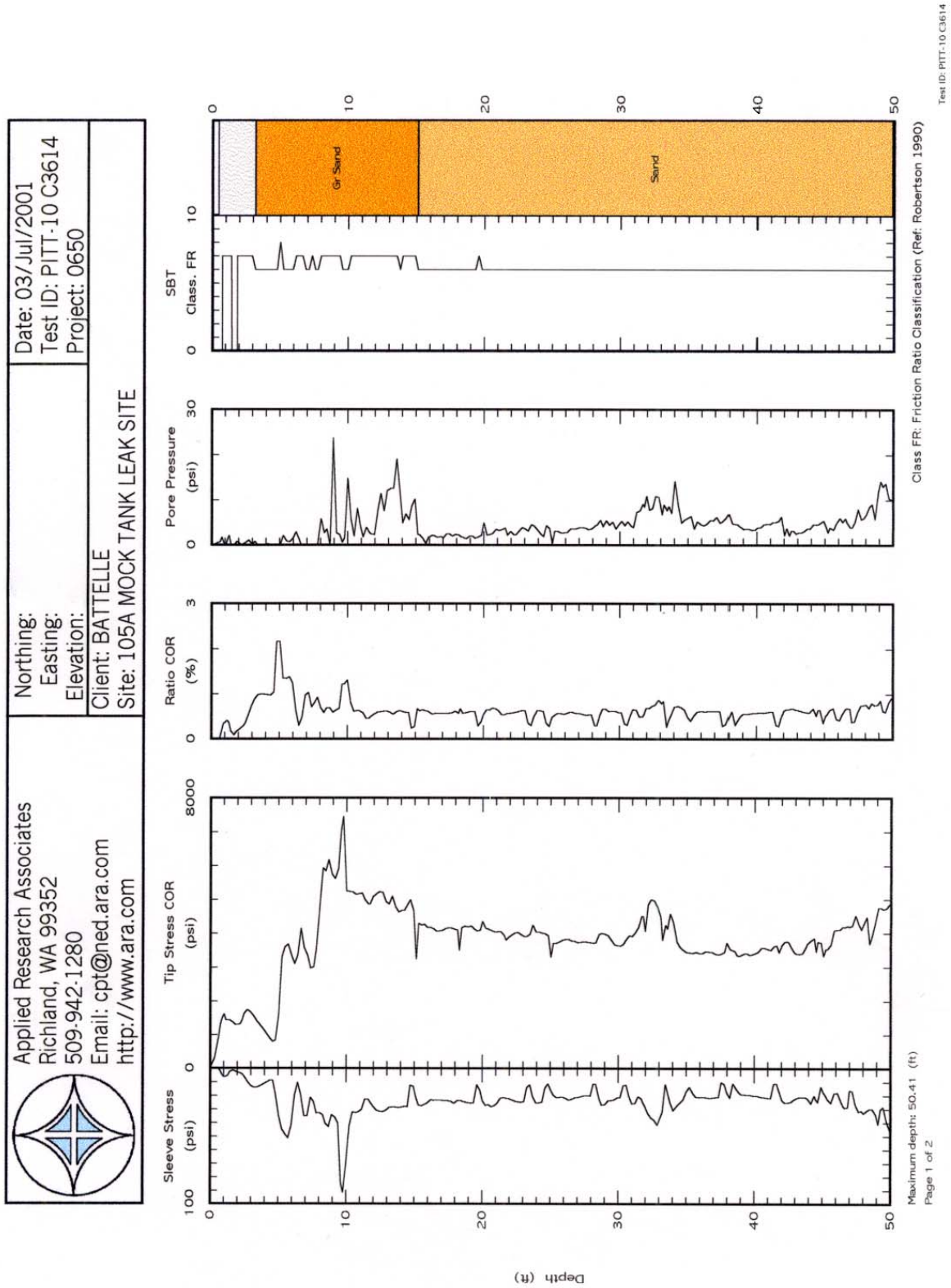
Applied Research Associates
Richland, WA 99352
509-942-1280
Email: cpt@ned.ara.com
http://www.ara.com
Northing:
Easting:
Elevation:
Date: 03/Jul/2001
Test ID: PITT-10 C3614
Project: 0650
Client: BATTELLE
Site: 105A MOCK TANK LEAK SITE
Sleeve Stress (psi)
Tip Stress COR (psi)
Ratio COR (%)
Pore Pressure (psi)
SBT Class. FR
Gr Sand
Sand
Class FR: Friction Ratio Classification (Ref: Robertson 1990)
Test ID: PITT-10 C3614
Maximum depth: 50.41 (ft)
Page 1 of 2
Depth (ft)

Figure E.4

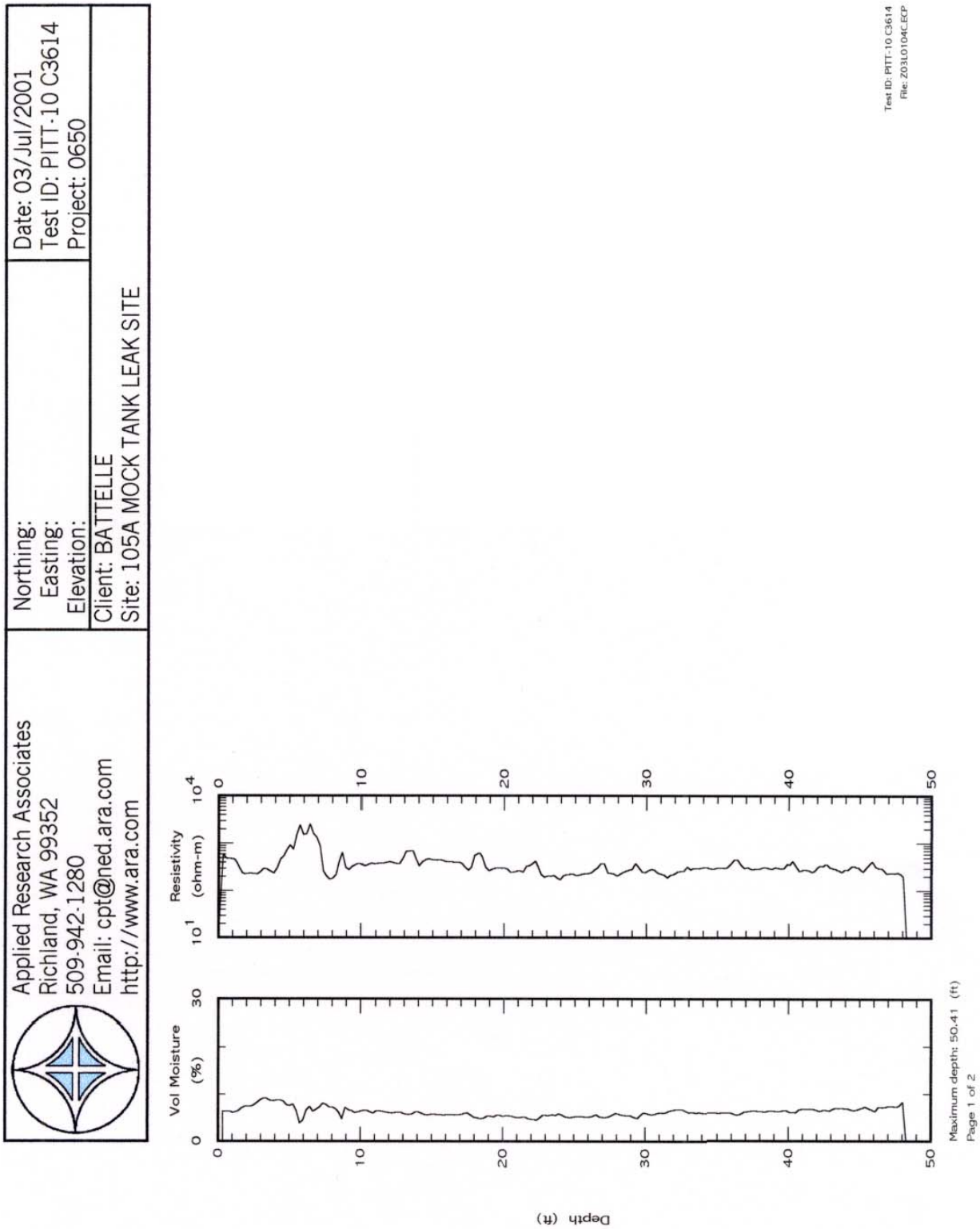

Figure E.4. (contd)

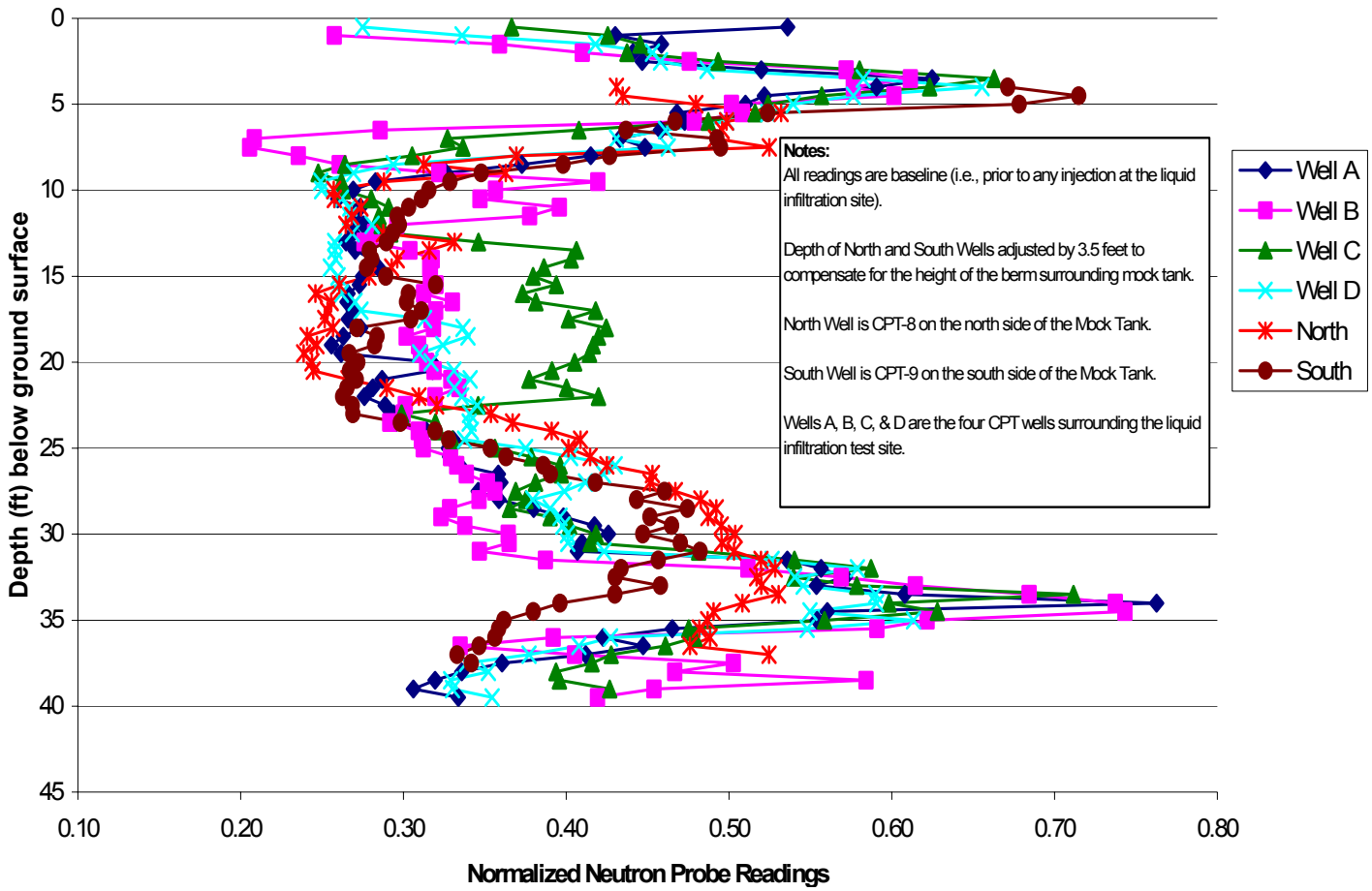

Figure E.5. Baseline Neturon Probe Readings as a Function of Depth Below Ground Surface (Relative Soil Moisture) in the Vicinity of the Mock Tank Site (Cameron et al. 2002)

Appendix F

Log of Physical Parameters for Sodium Thiosulfate Solution During the FY 2001 TLDD

Appendix F: Log of Physical Parameters for Sodium Thiosulfate Solution During the FY 2001 TLDD

Sample Date	Sample Time	Sample	Tare (g)	Wet Solution (g)	Dry Solution (g)	Rel Density	Solids	Soln.	% Solids	Comments	Conductivity (microhmos/cm)
10-Aug-01	9:11 AM	6	164.79	178.21	169.76	1.34	4.97	13.42	37.03%		8.4 * 10000
10-Aug-01	9:11 AM	2	163.56	176.98	168.26	1.34	4.70	13.42	35.02%		
10-Aug-01	9:11 AM	1	161.7	175.11	166.68	1.34	4.98	13.41	37.14%		
										DI conductivity: 0.4*1000	
11-Aug-01	10:25 PM	2	163.55	176.53	168.44	1.30	4.89	12.98	37.67%		8.7*10000
11-Aug-01	10:25 PM	6	164.8	177.72	169.7	1.29	4.90	12.92	37.93%		
11-Aug-01	10:25 PM	1	161.71	174.61	166.59	1.29	4.88	12.9	37.83%		
14-Aug-01	11:55 AM	1	161.7	174.57	166.56	1.29	4.86	12.87	37.76%		8.8*10000
14-Aug-01	11:55 AM	2	163.56	176.5	168.56	1.29	5.00	12.94	38.64%		
14-Aug-01	11:55 AM	6	164.79	177.7	169.76	1.29	4.97	12.91	38.50%		
15-Aug-01	1:00 PM	2	163.56	176.69	168.54	1.31	4.98	13.13	37.93%		8.8*10000
15-Aug-01	1:00 PM	6	164.79	178.03	169.8	1.32	5.01	13.24	37.84%		
15-Aug-01	1:00 PM	1	161.7	174.93	166.72	1.32	5.02	13.23	37.94%		
17-Aug-01	11:17 AM	1	161.7	174.74	166.64	1.30	4.94	13.04	37.88%		8.6*10000
17-Aug-01	11:17 AM	2	163.55	176.47	168.45	1.29	4.90	12.92	37.93%		
17-Aug-01	11:17 AM	6	164.78	177.65	169.62	1.29	4.84	12.87	37.61%		

Sample Date	Sample Time	Sample	Tare (g)	Wet Solution (g)	Dry Solution (g)	Rel Density	Solids	Soln.	% Solids	Comments	Conductivity (microhmos/cm)
20-Aug-01	12:44 PM	1	161.68	174.47	165.9	1.28	4.22	12.79	32.99%		8.8*10000
20-Aug-01	12:44 PM	2	163.53	176.19	167.69	1.27	4.16	12.66	32.86%		
20-Aug-01	12:44 PM	6	164.77	177.48	169.09	1.27	4.32	12.71	33.99%		
21-Aug-01	3:20 PM	1	161.71	174.8	166.69	1.31	4.98	13.09	38.04%		8.9*10000
21-Aug-01	3:20 PM	2	163.56	176.66	168.47	1.31	4.91	13.1	37.48%		
21-Aug-01	3:20 PM	6	164.79	178	169.76	1.32	4.97	13.21	37.62%		
22-Aug-01	9:15 AM	1	161.33	174.48	166.23	1.32	4.90	13.15	37.26%		9.0*10000
22-Aug-01	9:15 AM	2	162.05	175.26	166.89	1.32	4.84	13.21	36.64%		
22-Aug-01	9:15 AM	174	165.83	179.06	170.85	1.32	5.02	13.23	37.94%		
22-Aug-01	3:19 PM	1	162.09	175.23	166.93	1.31	4.84	13.14	36.83%		
22-Aug-01	3:19 PM	3	163.67	176.77	168.47	1.31	4.80	13.1	36.64%		8.9*10000
22-Aug-01	3:19 PM	160	161.56	174.69	166.47	1.31	4.91	13.13	37.40%		
23-Aug-01	11:19 AM	1	161.7	174.94	166.62	1.32	4.92	13.24	37.16%		8.8*10000
23-Aug-01	11:19 AM	2	163.55	176.74	168.44	1.32	4.89	13.19	37.07%		
23-Aug-01	11:19 AM	6	164.78	177.98	169.61	1.32	4.83	13.2	36.59%		
27-Aug-01	1:30 PM	2	163.56	176.78	168.45	1.32	4.89	13.22	36.99%		8.6*10000
27-Aug-01	1:30 PM	6	164.79	178.03	169.67	1.32	4.88	13.24	36.86%		
27-Aug-01	1:30 PM	1	161.7	174.93	166.53	1.32	4.83	13.23	36.51%		

Distribution

No. of Copies

OFFSITE

3 HydroGEOPHYSICS, Inc.
2302 N. Forbes Blvd.
Tucson, AZ 85745
ATTN: C. Baldyga
Dr. J. B. Fink
M. T. Levitt

5 Lawrence Berkeley National Laboratory
1 Cyclotron Road (MS 90-1116)
Berkeley, CA 94720
ATTN: Dr. T. M. Daley
Dr. G. M. Hoversten
Dr. E. L. Majer
Dr. J. E. Peterson
Dr. K. H. Williams

3 Lawrence Livermore National Laboratory
7000 East Avenue
Livermore, CA 94550
ATTN: Dr. W. D. Daily L-130
Dr. B. Kirkendall L-208
Dr. A. Ramirez L-130

3 Vista Engineering Technologies, L.L.C.
8203 W. Quinault, Suite 20
Kennewick, WA 99336
ATTN: W. Bratton
W. Dickerson
J. Maresca

No. of Copies

ONSITE

COGEMA

F. R. Reich H3-28

9 **CH2M HILL Hanford Group**

D. G. Baide S7-65
J. W. Cammann H6-22
J. A. Eacker R2-50
R. E. Raymond R2-50
T. L. Sams H6-22
W. T. Thompson S7-90
R. C. Wilson S7-65
CHG Correspondence Control H6-08
TCSRC R1-10

5 **Numatec Hanford Corporation**

R. M. Boger (5) S7-12

23 **Pacific Northwest National Laboratory**

D. B. Barnett (5) K6-81
J. W. Brothers (3) K7-15
R. J. Cameron K6-96
G. W. Gee (5) K9-33
M. D. Johnson K6-96
T. L. Liikala K6-96
M. D. Sweeney (5) K6-81
Hanford Technical Library (2) P8-55